University of Technology, Sydney

Molecular interactions between *Mycoplasma hyopneumoniae* and host cells

BENJAMIN BERNARD ARMANDO RAYMOND

A thesis submitted in fulfilment of the requirements for the degree of

Doctor of Philosophy: Science

2015

CERTIFICATE OF ORIGINAL AUTHORSHIP

I certify that the work in this thesis has not previously been submitted for a degree nor has it been submitted as part of requirements for a degree except as fully acknowledged within the text.

I also certify that the thesis has been written by me. Any help that I have received in my research work and the preparation of the thesis itself has been acknowledged. In addition, I certify that all information sources and literature used are indicated in the thesis.

Signature of Student:

Date:

Acknowledgements

First and foremost I would like to thank my supervisors Prof Steven Djordjevic and Dr Matthew Padula for their guidance and support throughout my PhD. I can't thank these two people enough for mentoring me and helping me grow as a scientist. Secondly, I would like to thank Prof Ian Charles for the amazing opportunities he has provided me as Director of the ithree institute. For their assistance with all things microscopy-related I would like to thank Dr Michael Johnson, Dr Lynne Turnbull and Assoc Prof Cynthia Whitchurch.

I would like to thank my parents for their unconditional support throughout my long time as a student; I would not be where I am if it were not for the help of you two. I would specifically like to thank my mum, who has been a pillar of support and positivity for me during this time as well as sacrificing so much to get me here. Many thanks go out to the rest of my family; Joshua, Sharon, my grandparents, my aunts and uncles and many cousins for constantly asking me "when can we call you doctor?"

To Dr Cheryl Jenkins, Dr Daniel Bogema, Dr Lisa Seymour, and Dr Ania Deutscher, thank you for collaborative efforts in the early stages of my PhD as well as aiding me in my early experiments. Many thanks go out to the *many* PhD students who have grown to become part of my extended family; having experienced all the highs and lows of being a PhD student together. Special thanks go to Dr Jessica Tacchi, Dr Rita Rapa, Michael Widjaja, Krishneel Singh and Dr Jerran Santos. Jess and Jerran, I cannot thank you both enough for introducing me to the lab and to Jess particularly for being a surrogate supervisor for the first year of my PhD. Rita, thanks for always making me laugh and helping me through the tough times; from Israel and thereafter. Mike and

Krish, thanks for the gains and beating me in Pokemon; you guys have been too awesome. Thank you to Kate Harvey, Jacqueline Melvold, Isabella Hajduk, Veronica Jarocki, Marcelo Moreno, Kayla Madonis, Iain Berry, Samira Aili, Megan Truong, Matthew (George) O'rourke and Dr Joel Barratt for always being there for a laugh. I have made many greats memories with all of you.

I must also thank Prof Andrew Rycroft, Dr Gareth Maglennon and Alannah Deeney for making me feel extremely welcome during my time at the Royal Veterinary College in addition to their help in the lab. Thanks for constantly correcting the way us Aussies say things differently to you.

Finally, I must thank the University of Technology, Sydney, particularly the Science Faculty for their financial support during my PhD.

List of Publications

[Each of these publications has been included on a separate CD and are labelled (e.g. Publication 1) according to their order here]

1. *__Raymond, B. B.__ and S. P. Djordjevic (2015). "Exploitation Of Plasmin(Ogen) By Bacterial Pathogens Of Veterinary Significance." Vet Microbiol. Accepted for publication, doi:10.1016/j.vetmic.2015.04.008, 9th April 2015.

2. O'Rourke, M. B., __B. B. Raymond__, S. P. Djordjevic, and M. P. Padula (2015). "A Versatile Cost Effective Method For The Analysis Of Fresh Frozen Tissue Sections Via Matrix Assisted Laser Desorption Ionisation Imaging Mass Spectrometry (MALDI-IMS)." Rapid Commun Mass SP 29(7): 637-644.

3. Jarocki, V. M., J. Santos, J. L. Tacchi, __B. B. Raymond__, A. T. Deutscher, C. Jenkins, M. P. Padula and S. P. Djordjevic (2015). "MHJ_0461 is a multifunctional leucine aminopeptidase on the surface of Mycoplasma hyopneumoniae." Open Biol 5(1).

4. *__Raymond, B. B.__, C. Jenkins, L. M. Seymour, J. L. Tacchi, M. Widjaja, V. M. Jarocki, A. T. Deutscher, L. Turnbull, C. B. Whitchurch, M. P. Padula and S. P. Djordjevic (2015). "Proteolytic processing of the cilium adhesin MHJ_0194 (P123J) in Mycoplasma hyopneumoniae generates a functionally diverse array of cleavage fragments that bind multiple host molecules." Cell Microbiol 17(3): 425-444.

5. Woolley, L. K., S. A. Fell, J. R. Gonsalves, __B. B. Raymond__, D. Collins, T. A. Kuit, M. J. Walker, S. P. Djordjevic, G. J. Eamens and C. Jenkins (2014). "Evaluation of recombinant Mycoplasma hyopneumoniae P97/P102 paralogs formulated with selected adjuvants as vaccines against mycoplasmal pneumonia in pigs." Vaccine 32(34): 4333-4341.

6. Tacchi, J. L., **B. B. Raymond**, V. M. Jarocki, I. J. Berry, M. P. Padula and S. P. Djordjevic (2014). "Cilium adhesin P216 (MHJ_0493) is a target of ectodomain shedding and aminopeptidase activity on the surface of Mycoplasma hyopneumoniae." J Proteome Res 13(6): 2920-2930.

7. *__Raymond, B. B.__, J. L. Tacchi, V. M. Jarocki, F. C. Minion, M. P. Padula and S. P. Djordjevic (2013). "P159 from Mycoplasma hyopneumoniae binds porcine cilia and heparin and is cleaved in a manner akin to ectodomain shedding." J Proteome Res 12(12): 5891-5903.

8. Robinson, M. W., K. A. Buchtmann, C. Jenkins, J. L. Tacchi, **B. B. Raymond**, J. To, P. Roy Chowdhury, L. K. Woolley, M. Labbate, L. Turnbull, C. B. Whitchurch, M. P. Padula and S. P. Djordjevic (2013). "MHJ_0125 is an M42 glutamyl aminopeptidase that moonlights as a multifunctional adhesin on the surface of Mycoplasma hyopneumoniae." Open Biol 3(4): 130017.

9. Bogema, D. R., A. T. Deutscher, L. K. Woolley, L. M. Seymour, **B. B. Raymond**, J. L. Tacchi, M. P. Padula, N. E. Dixon, F. C. Minion, C. Jenkins, M. J. Walker and S. P. Djordjevic (2012). "Characterization of cleavage events in the multifunctional cilium adhesin Mhp684 (P146) reveals a mechanism by which Mycoplasma hyopneumoniae regulates surface topography." MBio 3(2).

10. Seymour, L. M., C. Jenkins, A. T. Deutscher, **B. B. Raymond**, M. P. Padula, J. L. Tacchi, D. R. Bogema, G. J. Eamens, L. K. Woolley, N. E. Dixon, M. J. Walker and S. P. Djordjevic (2012). "Mhp182 (P102) binds fibronectin and contributes to the recruitment of plasmin(ogen) to the Mycoplasma hyopneumoniae cell surface." Cell Microbiol 14(1): 81-94.

11. Bogema, D. R., N. E. Scott, M. P. Padula, J. L. Tacchi, **B. B. Raymond**, C. Jenkins, S. J. Cordwell, F. C. Minion, M. J. Walker and S. P. Djordjevic (2011).

"Sequence TTKF↓QE defines the site of proteolytic cleavage in Mhp683 protein, a novel glycosaminoglycan and cilium adhesin of Mycoplasma hyopneumoniae." J Biol Chem 286(48): 41217-41229.

[Production note: The list of publications are not included in this digital copy. The CD and print copy of the thesis are available for consultation at UTS Library.]

Conference Presentations

1. The Australian Society for Microbiology, Annual Scientific Meeting, 2015 – **Oral**: "A systems approach for the identification of proteins from *Mycoplasma hyopneumoniae* required for biofilm formation"
2. The 3rd Prato Conference On 'The Pathogenesis Of Bacterial Diseases Of Animals', 2014 – **Poster**: "Proteins involved in the adherence of *Mycoplasma hyopneumoniae* to abiotic surfaces and porcine monolayers which may also play a role in biofilm formation"
    a. Recipient of Best Poster Award
3. The 20th Congress of the International Organisation for Mycoplasmology, 2014 – **Oral**: "*Mycoplasma hyopneumoniae* is an invasive pathogen that invades epithelial cells and forms biofilms"
4. The 19th Lorne Proteomics Symposium, 2014 – **Oral**: "Global analysis of protein-protein interactions important for the virulence of *Mycoplasma hyopneumoniae*"
    a. Recipient of Oral Presentation Award
5. BacPath 12: Molecular Analysis of Bacterial Pathogens, 2013 – **Poster**: "Is *Mycoplasma hyopneumoniae* an invasive pathogen?"
6. Elizabeth Agricultural Macarthur Institute (EMAI) Invited Student Speaker, 2013 – **Oral**: "Using high resolution microscopy and proteomics to investigate host-pathogen interactions in *Mycoplasma hyopneumoniae*"
7. The 18th Lorne Proteomics Symposium, 2013 – **Poster**: "Protein promiscuity in *Mycoplasma hyopneumoniae*: not just for show"

8. The 19th Congress of the International Organisation for Mycoplasmology – **Poster**: "P97 is extensively endoproteolytically processed and a multifunctional adhesin: identification of novel binding domains"
9. "Proteomics and Beyond" Symposium, 2012 – **Oral**: "The surfaceome of *Mycoplasma hyopneumoniae* displays an extensive population of multifunctional endoproteolytic cleavage fragments derived from the P97 & P102 adhesin families"
10. The Australian Society for Microbiology, Annual Scientific Meeting, 2012 – **Poster**: "P97 is extensively endoproteolytically processed and a multifunctional adhesin: identification of novel binding domains"
11. The 17th Lorne Proteomics Symposium, 2012 – **Oral**: "Endoproteolytic cleavage of the *Mycoplasma hyopneumoniae* adhesin MHJ_0494 (P159) reveals a TTKF|QE motif which is also the site of cleavage in other adhesins"
12. UTS Science's Research Day, 2011 – **Poster**: "Elucidating Putative Host-Pathogen Interactions of *Mycoplasma hyopneumoniae* Using Super Resolution Fluorescence Microscopy"
13. Royal North Shore Hospital Scientific Research Meeting, 2011 – **Poster**: "Elucidating Putative Host-Pathogen Interactions of *Mycoplasma hyopneumoniae* Using Super Resolution Fluorescence Microscopy"
14. BacPath 11: Molecular Analysis of Bacterial Pathogens, 2011 – **Poster**: "Extensively processed adhesins, lipoproteins and non-classically secreted molecules dominate the surface topography of *Mycoplasma hyopneumoniae*"
15. The 16th Lorne Proteomics Symposium, 2011 – **Poster**: "Biofilm formation in *Mycoplasma hyopneumoniae*, the causative agent of chronic porcine respiratory disease"

16. Royal North Shore Hospital Scientific Research Meeting, 2010 – **Oral**: "Biofilm formation in *Mycoplasma hyopneumoniae*, the causative agent of chronic porcine respiratory disease: a proteome approach"

Abbreviations

3-Dimensional Structured Illumination Microscopy	3D-SIM
3,3´-diaminobenzidine	DAB
4',6-diamidino-2-phenylindole	DAPI
Base pair	Bp
Bronchoalveolar Lavage Fluid	BALF
Bovine Serum Albumin	BSA
Centimetre	cm
Confocal Laser Scanning Microscope/Microscopy	CLSM
Deoxyribonucleic acid	DNA
Extracellular Matrix	ECM
Extracellular DNA	eDNA
Fibronectin	Fn
Hour	h
Immunofluorescence Microscopy	IFM
Isoelectric Point	pI
Isopropyl β-D-1-thiogalactopyranoside	IPTG
Immobilised pH Gradient	IPG
Kilodalton	kDa
Liquid Chromatography – Tandem Mass Spectrometry	LC-MS/MS
Litre	L
Matrix-Assisted Laser Desorption/Ionization	MALDI
Metre	m
Micro; 10-6	µ

Millilitre	mL
Mycoplasma hyopneumoniae (gene name)	Mhp
Open Reading Frame	ORF
Percent	%
Phosphate Buffered Saline	PBS
Plasminogen	Plg
Polyvinylidene fluoride	PVDF
Porcine Epithelial-like	PK-15
Porcine Reproductive and Respiratory Syndrome Virus	PRRSV
Post-Infection	P.I.
Room Temperature	RT
Scanning Electron Microscopy	SEM
Second	s
Sodium Dodecyl Sulphate-Polyacrylamide Gel Electrophoresis	SDS-PAGE
Time of Flight	TOF
Tributylphosphine	TBP
Wild Type	WT

Abstract

The Mycoplasmas are a group of wall-less bacteria belonging to the Mollicutes that are believed to have diverged from the Gram-positive Firmicutes. Mollicutes have undergone reductive evolution, losing genes for the biosynthesis of essential biomolecules, subsequently having to form parasite relationships with their hosts in order to acquire these nutrients. They form these relationships as both commensals and pathogens, and a number of Mycoplasma species cause significant clinical and agricultural diseases. *Mycoplasma hyopneumoniae* is the causative agent of porcine enzootic pneumonia, a chronic respiratory disease that affects swine populations worldwide. *M. hyopneumoniae* colonises the upper respiratory tract by adhering to the rapidly beating cilia where it causes ciliostasis and eventual cilial death [1]. *M. hyopneumoniae* possesses a family of surface adhesins referred to as the P97 and P102 paralog family that it utilises to adhere to the cilia [2-10]. A hallmark of *M. hyopneumoniae* infection is a potent inflammatory response which is believed to be one of the contributing factors to the gross lung lesions observed in infected swine [11-13].

M. hyopneumoniae is described as a strict extracellular pathogen that only adheres to cilia and knowledge is lacking on additional receptors that *M. hyopneumoniae* binds to. Recent studies have however, shown that viable *M. hyopneumoniae* cells can be cultured from the liver, spleen, kidneys and lymph nodes of infected swine [14-16]. These observations suggest that *M. hyopneumoniae* has the capability to invade through the epithelial barrier and disseminate to distal tissue sites. In addition to this, large microcolonies have been observed in the respiratory tract of swine infected with *M. hyopneumoniae* [17]. These microcolonies are reminiscent of biofilms, and although biofilm formation has never been investigated in *M. hyopneumoniae* it is likely that they play a role in the chronicity of disease. Notably, even when lung lesions in *M.*

hyopneumoniae-infected swine are cleared, bronchial swabs can still test positive for *M. hyopneumoniae* up to 185 days post-infection (P.I.) [18] and pigs can act as convalescent carriers for up to 200 days P.I. [19]. This suggests that *M. hyopneumoniae* possesses mechanisms in which it can remain dormant within its host whilst remaining infectious. Vaccines against *M. hyopneumoniae* can successfully reduce lung lesions but they are unable to prevent transmission in swine herds [20]. In order to create vaccines that inhibit the transmission of *M. hyopneumoniae*, a better understanding of the disease process is required.

This PhD project has thus been devised in order to address the problems outlined above. This work has investigated the ability of adhesins to undergo extensive endoproteolytic processing; demonstrating that proteolytic processing in the P97 and P102 adhesins occurs much more extensively than what has previously been shown. I also show that these adhesins can bind to a myriad of host components such as heparin, fibronectin (Fn) and plasminogen (Plg) and investigate the domains responsible. Additionally, this work presents a number of novel receptors that *M. hyopneumoniae* targets within its host as well as a comprehensive list of putative adhesins that it utilises to do so.

This work has also investigated the ability of *M. hyopneumoniae* to form biofilms on abiotic surfaces, host cells and within the swine respiratory tract and further demonstrate that surface adhesins play a role in biofilm formation. A number of putative biofilm-associated genes have been identified by screening a transposon mutant library, these genes being potential vaccine candidates. Finally, this work has investigated the ability of *M. hyopneumoniae* to become internalised by host cells and reside within the cytoplasm. *M. hyopneumoniae* becomes internalised by vacuole-like structures, and that internalised cells appear to escape from lysosomes to reside free within the cytoplasm.

Overall, this PhD project has contributed significantly to understanding how *M. hyopneumoniae* causes disease. Future work on the novel mechanisms described in this thesis will aid in future vaccine development programs and potentially aid in the control of this important veterinary disease.

Table of Contents

Acknowledgements iii
List of Publications v
Conference Presentations viii
Abbreviations xi
Abstract xiii
Table of Contents xvi
List of Figures xxi
List of Tables xxiv
Chapter One: An introduction to the topics presented in this thesis 1
1.1 An Introduction to the Swine Industry and *Mycoplasma hyopneumoniae* 2
1.2 Host-Pathogen Dynamics in the Respiratory Tract 6
1.3 Interactions between *M. hyopneumoniae* and swine respiratory epithelium 8
1.4 The *M. hyopneumoniae* Cell Surface 12
1.5 Biofilms in Mycoplasma species 17
1.6 Topics and Aims Presented in this Thesis 20
Chapter Two: (Paper I) An introduction to the importance of veterinary pathogens and how they circumvent host defences 23
Declaration 24
2.1 Structure & Function of Plg 25
2.2 How Do Bacteria Exploit Plasmin(ogen)? 28
2.3 The Coagulation and Complement Systems and Plasmin(ogen) 31
2.4 The Mycoplasmas: Innate Immunity and Plasmin 38
2.5 Conclusion 47
Chapter Three: (Paper II) *M. hyopneumoniae* surface adhesins undergo extensive endoproteolytic processing 49
Declaration 50
3.1 Introduction 51
3.2 Materials and Methods 54
3.2.1 Culture Conditions 54
3.2.2 Cell Surface Analyses 54
3.2.3 Preparation of *M. hyopneumoniae* whole cell lysate 55

3.2.4 One- and two-dimensional gel electrophoresis and immunoblotting 56
3.2.5 Affinity chromatography 57
3.2.6 1D LC-MS/MS using QTOF 57
3.2.7 MS/MS Data Analysis 58
3.2.8 Avidin purification of interacting proteins 59
3.2.9 Bioinformatic analyses of P159 60
3.3 Results 61
3.3.1 P159 is an endoproteolytically processed, modular cell surface protein 61
3.3.2 Identification of cleavage sites that generate P27, P110 and P52 63
3.3.3 Identification of cleavage fragments of P159 by 2D SDS-PAGE and LC-MS/MS... 64
3.3.4 Identification of lower abundance cleavage fragments of P159. 68
3.3.5 Identification of regions of P159 that bind to PK-15 cell surface proteins 73
3.3.6 Regions of P159 that bind heparin 73
3.3.7 Regions of P159 that bind to porcine cilia 76
3.4 Discussion 77
3.5 Conclusions 84
Chapter Four: (Paper III) Investigation of the multifunctional adhesin P97 and the co-localisation of Fn with *M. hyopneumoniae* 85
Declaration 86
4.1 Introduction 87
4.2 Materials and Methods 91
4.2.1 Bacterial strains and cultures 91
4.2.2 Enrichment of *M. hyopneumoniae* surface proteins 91
4.2.3 Preparation of *M. hyopneumoniae* whole cell lysates for mass spectrometry 91
4.2.4 One- and two-dimensional gel electrophoresis and immunoblotting 91
4.2.5 Fn and anti-Fn antibodies 92
4.2.6 Protein expression, purification and generation of antisera 92
4.2.7 Plasmids, protein expression and purification 92
4.2.8 Surface plasmon resonance analyses 93
4.2.9 Heparin affinity chromatography 94
4.2.10 Avidin purification of PK-15 interacting proteins 94
4.2.11 Avidin purification of Fn binding proteins 94
4.2.12 1D LC-MS/MS using ion trap 95

4.2.13 Protein extraction and digestion for strong cation exchange chromatography and MudPIT 96
4.2.14 Peptide fractionation by cation-exchange chromatography 96
4.2.15 Multidimensional Protein Identification Technology (MudPIT) 97
4.2.16 1D LC–MS/MS Using QTOF 97
4.2.17 MS/MS Data Analysis 97
4.2.18 Microtitre plate-binding assays 98
4.2.19 Microscale Thermophoresis 99
4.2.20 Cell culture and infection assays 99
4.2.21 Immunofluorescence microscopy 100
4.2.22 Immunohistochemistry 101
4.2.23 Bioinformatic analysis of P123 102
4.3 Results 103
4.3.1 Structural analysis of P123 103
4.3.2 Enrichment of low abundance cleavage fragments 106
4.3.3 Heparin-binding sites in P123 113
4.3.4 The C-terminus of the mature cilium adhesin and the $P28_{232}$ cleavage fragment bind Plg 118
4.3.5 The C-terminus of P28 binds Fn 121
4.3.6 Identifying cleavage fragments of $P123_J$ that adhere to PK-15 cell surface proteins 123
4.3.7 *M. hyopneumoniae* co-localises with Fn when colonising PK-15 cell monolayers 124
4.4 Discussion 128
4.5 Conclusion 133
Chapter Five: (Paper IV) Global analysis of adhesins and host receptors, and biofilm formation in *M. hyopneumoniae* 136
Declaration 137
5.1 Introduction 138
5.2 Materials and Methods 141
5.2.1 Bacterial strains and culturing of biofilms 141
5.2.2 Protein expression, purification and generation of antisera 141
5.2.3 Live-cell imaging 141
5.2.4 Biofilm formation on PK-15 monolayers 141
5.2.5 Immunofluorescence microscopy of infected monolayers 142
5.2.6 Immunofluorescence microscopy of biofilms 143

5.2.7 Processing of immunofluorescence images....144
5.2.8 Ruthenium red (RR) staining....144
5.2.9 Infection experiments for scanning electron microscopy....144
5.2.10 Scanning electron microscopy of tracheal sections....146
5.2.11 Avidin Purification of Interacting Proteins....146
5.2.12 Avidin Purification of Actin-binding Proteins....147
5.2.13 Microscale thermophoresis....148
5.2.14 1D LC–MS/MS Using QTOF....149
5.2.15 MS/MS Data Analysis....149
5.2.16 One- and Two-Dimensional Gel Electrophoresis and Ligand Blotting....149
5.2.17 Biofilm Screening Assay....149
5.2.18 Growth curves of ΔMhpX and ΔMhpY....150
5.3 Results....151
5.3.1 *M. hyopneumoniae* forms biofilms on abiotic surfaces....151
5.3.2 *M. hyopneumoniae* biofilms stain with ruthenium red....155
5.3.3 *M. hyopneumoniae* biofilms contain extracellular DNA....157
5.3.4 Live/dead staining of *M. hyopneumoniae* biofilms....161
5.3.5 *M. hyopneumoniae* adheres to and forms biofilms on PK-15 monolayers....162
5.3.6 *M. hyopneumoniae* forms biofilms in the swine respiratory tract....166
5.3.7 *M. hyopneumoniae* surface adhesins bind PK-15 monolayers....168
5.3.8 Identification of target receptors on the surface of PK-15 monolayers....174
5.3.9 Global analysis of actin-binding proteins....178
5.3.10 Domains within P97 bind actin....185
5.3.11 Screening for Biofilm-Deficient Mutants....186
5.3.12 Growth Curve of ΔMhpX, ΔMhpY and WT....188
5.4 Discussion....190
5.5 Conclusion....199
Chapter Six: (Paper V) *M. hyopneumoniae* is an invasive pathogen that escapes lysosomes....200
Declaration....201
6.1 Introduction....202
6.2 Materials and Methods....204
6.2.1 Bacterial strains....204
6.2.2 Infection of PK-15 monolayers....204
6.2.3 Immunofluorescence microscopy....204

6.2.4 Processing of immunofluorescence images.....205
6.2.5 Transmission electron microscopy.....205
6.2.6 Field emission scanning electron microscopy.....206
6.3 Results.....207
6.3.1 Scanning Electron Microscopy of *M. hyopneumoniae* cells adhering to, and invading PK-15 monolayers.....207
6.3.2 Immunofluorescence microscopy of *M. hyopneumoniae* cells adhering to and invading PK-15 monolayers.....211
6.3.3 Transmission Electron Microscopy of *M. hyopneumoniae* invading PK-15 monolayers and porcine tracheal epithelia.....213
6.3.4 Co-localisation LAMP1 with *M. hyopneumoniae* cells.....217
6.4 Discussion.....224
6.5 Conclusion.....228
Chapter Seven: Final Summary and Future Directions.....229
7.1. The extent of proteolytic processing in the adhesins P159 and P97 and the cleavage sites present in these molecules.....231
7.2. The interaction of *M. hyopneumoniae* with host molecules such as Fn and actin and the cellular responses the interaction elicits in its host.....233
7.3. The ability of *M. hyopneumoniae* to form biofilms on abiotic and host cells.....235
7.4 Internalisation and cytoplasmic life of *M. hyopneumoniae*.....236
7.5 Concluding remarks.....238
Appendix.....240
Chapter 3 (Paper II).....240
Chapter 4 (Paper III).....246
Chapter 5 (Paper IV).....253
References.....256

List of Figures

Figure 1.1: Scanning Electron Microscopy (SEM) of the respiratory tract of swine infected with *M. hyopneumoniae*……5

Figure 1.2: Diagram depicting Fn-mediated endocytosis……11

Figure 1.3: Proteomic analysis of Mhp683 and its cleavage products……16

Figure 2.1: Amino acid sequence alignment of Plg……26

Figure 2.2: Diagram demonstrating the multitude of Plg functions……33

Figure 2.3: Cartoon depicting the interaction of *M. hyopneumoniae* with the fibrinolytic system……46

Figure 3.1: Structural analysis of P159……62

Figure 3.2: Mock 2D gel indicating locations of spots containing peptides mapping to P159. ……65

Figure 3.3: 2D Immunoblots probed with F1P159 – F4P159. ……67

Figure 3.4: Biotinylated *M. hyopneumoniae* surface proteins captured by avidin chromatography resolved by 2D PAGE……70

Figure 3.5: Schematic representation of P159 heparin-binding domain motifs and heparin-binding fragments……74

Figure 3.6: Dominant, major and minor cleavage sites within P159……75

Figure 3.7: Binding of P159 fragments to porcine cilia……76

Figure 3.8: Schematic representation of cleavage fragments……79

Figure 4.1: Structural analysis of P123J (MHJ_0194)……105

Figure 4.2: Tryptic peptides of biotinylated cleavage fragments of P123J identified by LC-MS/MS……110

Figure 4.3: Cartoon depicting a summary of the cleavage fragments derived from P123J……112

Figure 4.4: Heparin binding regions within P123J……114

Figure 4.5: Comparative sequence analysis of the C-terminal region of P123J and P125232 and recombinant fragments used to characterize the function of the C-terminus……117

Figure 4.6: Surface plasmon resonance……120

Figure 4.7: The C-terminus of P123J and P125232 binds Fn……122

Figure 4.8: Fluorescence micrographs showing the distribution of Fn in *M. hyopneumoniae*-infected PK-15 monolayers……125

Figure 4.9: Mycoplasma cells and Fn co-localise in infected lung tissue……127

Figure 5.1: Biofilm formation of *M. hyopneumoniae* cells on glass over a time period of 15 days……152

Figure 5.2: CLSM maximum intensity projections of 30 day *M. hyopneumoniae* biofilms forming on glass and stained with F2P97 (A), P65 (B), PdhB (C), and rpL3 (D) antisera……154

Figure 5.3: RR staining of *M. hyopneumoniae* biofilms……156

Figure 5.4: eDNA (A-F) and live/dead (G-L) staining of 30 day *M. hyopneumoniae* biofilms growing on glass coverslips……158

Figure 5.5: 3D-SIM images of *M. hyopneumoniae* biofilms grown on glass for 30 days……160

Figure 5.6: *M. hyopneumoniae* cells forming biofilms on PK-15 monolayers after 6 days. ……164

Figure 5.7: IFM and SEM of *M. hyopneumoniae*-infected PK-15 cell monolayers……165

Figure 5.8: Scanning electron micrograph of tracheal epithelium from pigs experimentally infected with the Hillcrest strain of *M. hyopneumoniae*……167

Figure 5.9: 2D ligand blot of *M. hyopneumoniae* proteins that bind to PK-15 cell surface receptors……169

Figure 5.10: *M. hyopneumoniae* interacts with actin……179

Figure 5.11: Biofilm screen of *M. hyopneumoniae* transposon mutants……187

Figure 5.12: Growth Curve of ΔMhpX, ΔMhpY and WT……189

Figure 6.1: Scanning electron micrograph of *M. hyopneumoniae* cells interacting with and invading PK-15 monolayers……208

Figure 6.2: *M. hyopneumoniae* cells adhering to PK-15 monolayers with what appear to be caveolin-like structures……210

Figure 6.3: *M. hyopneumoniae* cells internalised within PK-15 cells……212

Figure 6.4: Transmission electron micrograph of *M. hyopneumoniae* cells becoming internalised by PK-15 monolayers……214

Figure 6.5: Transmission electron micrograph of tracheal sections taken from the respiratory tract of a pig infected with *M. hyopneumoniae*……216

Figure 6.6: Association of intracellular *M. hyopneumoniae* cells with lysosomes……219

Figure 6.7: 3D-SIM images of intracellular *M. hyopneumoniae* cells associating with lysosomes……..……..……..……..……..……...221

Figure 6.8: Super-resolution microscopy of intracellular *M. hyopneumoniae* cells that appear to have escaped from lysosomes……..……..……..……223

List of Tables

Table 1.1: Accession and gene numbers of P97 and P102 paralogs from five *M. hyopneumoniae* strains whose genomes have been sequenced……..13

Table 5.1: *M. hyopneumoniae* proteins purified from Biotinylated PK-15 affinity column……171

Table 5.2: Porcine proteins purified by the biotinylated *M. hyopneumoniae* affinity column……175

Table 5.3: Putative actin-binding proteins of *M. hyopneumoniae*……182

Chapter One: An introduction to the topics presented in this thesis

1.1 An Introduction to the Swine Industry and *Mycoplasma hyopneumoniae*

Pork represents one of the largest components of the meat production industry and many nations are heavily reliant on the exportation of pork products for their annual revenue. Australia alone produces approximately 30, 000 tonnes (carcass weight) of pig meat per month. Annual Australian pig exports are valued at approximately 100 million AUD, with annual imports valued at approximately $500 million AUD (Australian Pork Limited; 2012-2013 Annual Report). Bacterial, parasitic and viral infections are easily transmitted through commercial swine herds and cause significant reductions to the output of these farms. Therapeutic practices have improved in recent times with vaccines being the preferred method of prevention over antibiotics (NSW Department of Primary Industries). Antibiotic treatment strategies are still implemented, with chlortetracycline, tiamulin and tilmicosin being the preferred therapeutics (NSW Department of Primary Industries). According to the NSW Department of Primary Industries; *Actinobacillus pleuropneumoniae* (APP), *Brucella suis*, *Mycoplasma hyopneumoniae*, *Haemophilus parasuis*, *Streptococcus suis* and porcine parvovirus are some of the major diseases affecting commercial swine herds in Australia (NSW Department of Primary Industries). Due to the crowded nature of factory farms where animals are housed, it is hard to prevent the dissemination of these infectious agents. Depopulation strategies involve the removal of diseased and young pigs prone to infection from the herd, storing healthy pigs in a holding area while pens are cleared and disinfected, and re-introducing high-health status pigs into the herd. These strategies although effective, are cumbersome and expensive.

Regardless of geographic origin, *M. hyopneumoniae* is one of the most significant swine pathogens. The Mycoplasmas are a distinct genus of bacteria that belong to the

Mollicutes and are characterised by their lack of a cell wall, small low G+C content genomes, and inability to synthesise essential biomolecules [21]. *M. hyopneumoniae* is the causative agent of porcine enzootic pneumonia which although not fatal, is a chronic respiratory disease that contributes to significant economic losses to the commercial swine production industry.

M. hyopneumoniae associates closely with the cilia that line the swine respiratory tract [22-24] and causes the cilia to become entangled and clumped (Figure 1.1) and leads to distress in the infected host [22-24]. In tracheal organ cultures it has been found that low passage *M. hyopneumoniae* can reduce the percentage of the epithelium with cilia to 20% within five days P.I. [1]. This same low passage *M. hyopneumoniae* also significantly reduced the vigour of cilial beating over the same period [1]. A reduction in the efficacy of the mucociliary escalator contributes to the symptoms displayed by pigs infected with *M. hyopneumoniae*, such as coughing and wheezing. Although it is a mild respiratory disease, *M. hyopneumoniae*-infected pigs are at a greater risk of acquiring secondary infections such as Porcine Reproductive and Respiratory Syndrome Virus (PRRSV) and swine influenza virus [25,26]. Pigs infected with *M. hyopneumoniae* and subsequently with PRRSV display more severe microscopic and macroscopic lesions than pigs that were infected with PRRSV alone [25]. Pigs still exhibited lung lesions 38 days P.I. with both *M. hyopneumoniae* and PRRSV compared with pigs infected with PRRSV alone which appeared normal [25]. This suggests that the joint infection by these two pathogens increases the chronicity of pneumonia in pigs [25]. Interestingly, even when the *M. hyopneumoniae* induced lesions were minimal, once PRRSV was introduced, lesions were significantly increased suggesting that there is a synergistic effect in this particular disease complex [25].

It has been shown that pathogenic *M. hyopneumoniae* cells can increase intracellular calcium levels by 250 nM within 100 seconds of being added to porcine ciliated tracheal cells [27]. Interestingly, a non-pathogenic strain of *M. hyopneumoniae* as well as a strain of *Mycoplasma flocculare*, a commensal of the swine respiratory tract, did not elicit a rise in intracellular Ca^{2+} [27]. Increased intracellular Ca^{2+} has been linked to the cilial loss observed in *M. hyopneumoniae*-infected swine [27]. There is evidence suggesting intracellular Ca^{2+} levels are directly correlated with cilial beat frequency in mammalian cells such that an increase in intracellular Ca^{2+} levels is proportional to an increase in cilial beat frequency [28,29]. One mechanism in which intracellular Ca^{2+} levels in cilia become elevated is due to the binding of Fn to β_1-integrins [30]. *M. hyopneumoniae* possesses a number of Fn-binding proteins on its cell surface (described in section 1.3) [5,7-9]. It could thus be hypothesised that Fn-binding proteins on the surface of *M. hyopneumoniae* bind to β_1-integrins via Fn on the cilial surface and cause intracellular Ca^{2+} levels to increase; causing a sharp increase in cilial beat frequency which if sustained may cause cilial damage.

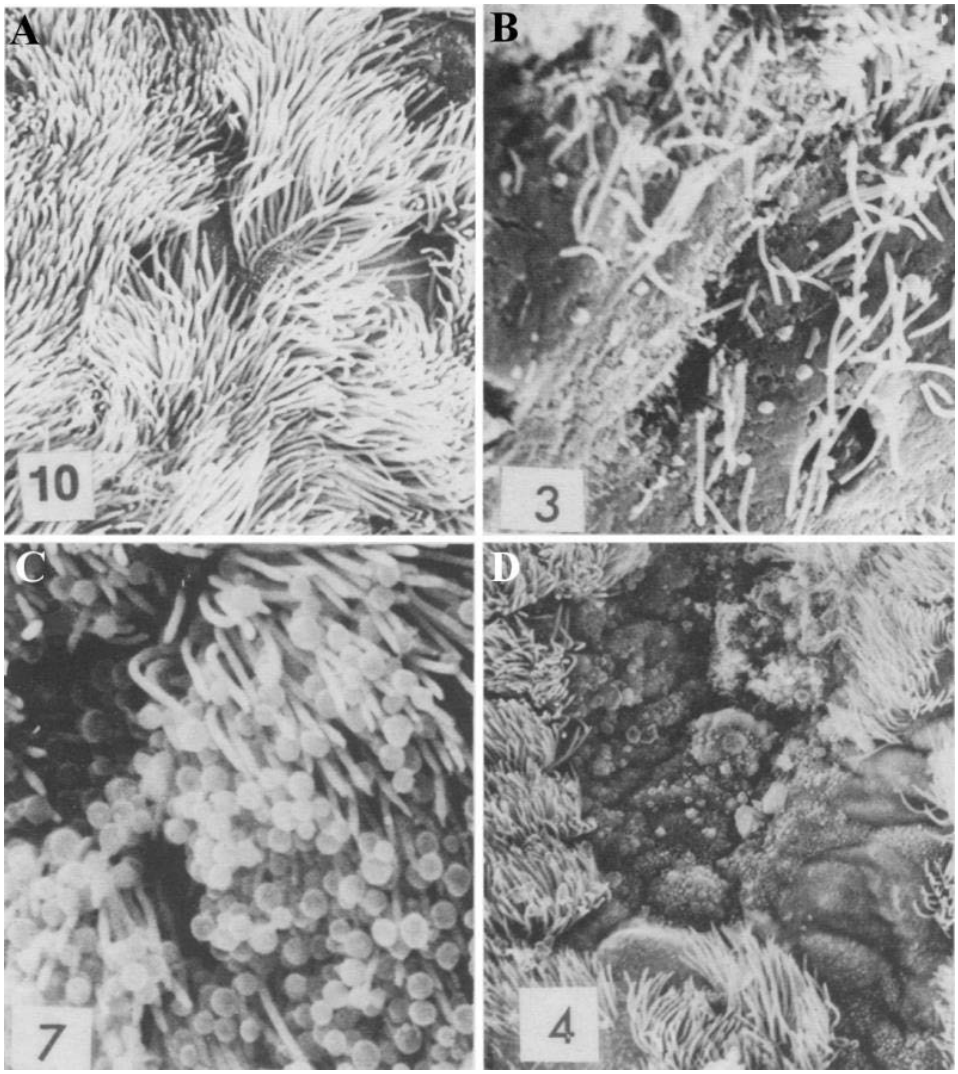

Figure 1.1: Scanning Electron Microscopy (SEM) of the respiratory tract of swine infected with *M. hyopneumoniae*.

A) Healthy cilia of the lower bronchus. The entire epithelium can be seen completely covered in cilia. B) Ten weeks PI; the underlying tracheal epithelium can be seen which significant damage to the cilia. C) Fourteen weeks PI; numerous *M. hyopneumoniae* cells can be seen forming biofilms that adhere to the remaining cilia of the midtrachea. D) Thirteen weeks PI: large areas of the epithelium are denuded of cilia. Adapted from [22].

1.2 Host-Pathogen Dynamics in the Respiratory Tract

The swine respiratory tract is a harsh environment for bacterial pathogens to colonise. The mucociliary escalator shifts mucosal secretions produced by goblet cells. The ciliated epithelium drives the mucus and microbial pathogens that are trapped in the mucus out of the respiratory tract and forms one of the major defences that protects against infection. Porcine cilia generate beat frequencies that range from 11.3 – 15.8 Hz depending on where in the respiratory tract they reside [31]. The mechanisms by which *M. hyopneumoniae* circumvents the mucociliary escalator, binds to cilia, and persists within the swine respiratory tract is not fully understood. As will be discussed in section 1.3, numerous bacterial pathogens such as *M. hyopneumoniae* bind to glycoconjugates and Extracellular Matrix (ECM) components. Mucins are heavily glycosylated proteins that constitute the mucus that bathes the respiratory tract. *M. hyopneumoniae* has been shown to bind to porcine mucin, and it has been demonstrated that pre-incubation of *M. hyopneumoniae* cells with mucin significantly reduced their ability to bind to intact ciliated cells [32]. Infection with *M. hyopneumoniae* seems to alter the mucins expressed in the swine respiratory tract; total goblet cells with mucin are reduced at all stages of infection with the exception of sulfated mucins that are significantly increased [24]. The reasons for the increase in sulfomucins is believed to be a response to *M. hyopneumoniae* colonisation [24]. The bronchiolar epithelium stained intensively for the mucins MUC2, MUC5AC, MUC5B and MUC4 21 days P.I. with *M. hyopneumoniae,* correlating with peribronchial and peribronchiolar lymphoid hyperplasia as well as the presence of gross lung lesions [33]. Mucin staining decreased to the same levels as uninfected control pigs at 35 days P.I., once again correlating with the decrease in the presence of lung lesions [33]. The correlation between *M. hyopneumoniae* cells and the subsequent lung pathology and mucin production may be due to direct or indirect

damage to the ciliated epithelium [1,33]. Increases in proinflammatory cytokines such as TNF-α, IL-1β and IL-6 are a hallmark of *M. hyopneumoniae* infection and are thought to be the main cause of the observed lung lesions in infected swine populations [11-13,34]. Lymphoid hyperplasia of the bronchus-associated lymphoid tissue is a common observation in the airway of infected swine, with macrophages and B lymphocytes being the most dominant [35]. These cells are capable of inducing the expression of proinflammatory cytokines such as TNF-α and IL-1β which further promotes the infiltrations of immune cells [36]. The interplay between proinflammatory cytokines, lungs lesions and the serine protease plasmin are described in detail in Chapter II.

In addition to interacting with the ciliated epithelium, *M. hyopneumoniae* is influenced by the fluid that bathes this environment. This fluid is referred to as the epithelial lining fluid and is sampled in a procedure referred to as bronchoalveolar lavage [37]. The proteome profiles of the bronchoalveolar lavage fluid (BALF) as well as the airway surface liquid from newborn pigs have been investigated in an effort to better understand the microenvironment within the swine respiratory tract [38]. A large number of the proteins identified were found to be secreted host defence molecules such as complement components, cathepsins, and ECM proteins [38]. The presence of these components as well as the constant beating of the mucociliary escalator presents a formidable challenge for a genome-reduced pathogen such as *M. hyopneumoniae* to overcome; yet it successfully manages to colonise this niche and induce chronic infection.

1.3 Interactions between *M. hyopneumoniae* and swine respiratory epithelium

The repertoire of host-derived receptors that are targeted by *M. hyopneumoniae* are not well understood. Microtitre plate assays using immobilised cilia demonstrated that *M. hyopneumoniae* bound cilia in a dose-dependent and saturable matter [32]. This interaction is significantly reduced when *M. hyopneumoniae* cells are pre-incubated with heparin [39]. The surface of porcine respiratory cilia is known to display glycosaminoglycans that are sensitive to heparinase [40]. Heparin is a highly sulfated glycosaminoglycan used to mimic glycosaminoglycans in binding studies [2-10,41-44]. Pre-incubation of *M. hyopneumoniae* cells with heparin blocks their adherence to porcine epithelial-like (PK-15) monolayers and ligand blotting studies have shown that *M. hyopneumoniae* possesses numerous heparin-binding proteins [4]. To date, all published members of the P97 and P102 adhesin family have been shown to bind heparin and most directly bind porcine cilia [2-10,41-44]. Domains within these adhesion families enriched with positively charged amino acid residues such as lysine and arginine are thought to bind the negatively charged heparin/glycosaminoglycans [41]. The ability to bind the glycosaminoglycans that are expressed on the surface of cilia is considered crucial to the ability of *M. hyopneumoniae* to colonise the swine respiratory tract in the early stages of infection [41].

To determine how *M. hyopneumoniae* causes disease the receptors that are targeted by adhesion molecules must be characterised. In addition to binding glycosaminoglycans *M. hyopneumoniae* binds the ECM components laminin [32], Fn [5,7-9], Plg [2,7-9] and La, Lb and Lc glycolipids [45]. No further work has been performed to investigate the interaction between *M. hyopneumoniae* and glycolipids. Fn is a glycoprotein found

ubiquitously in mammalian cells where it acts as a major constituent of the ECM as well as a signalling molecule [46]. The ECM is the space that separates the epithelial surface from the underlying endothelium and vasculature, and is comprised of molecules such as Fn, proteoglycans, collagen, elastin and laminin. Fn exists as a ~440 kDa heterodimer that consists of a number of binding domains for heparin, integrin, collagen, gelatin and fibrin [46]. Fn exists as 2 forms: soluble Fn that circulates in blood, and insoluble Fn that comprises part of the ECM [46]. There are three Fn domains termed FnI, FnII and FnIII which contains repeats regions that bind these molecules. It is for this reason that pathogens and commensal bacteria target Fn as it can be hijacked as a bridging molecule to a number of host molecules [46]. The P97 paralog Mhp271 was the first *M. hyopneumoniae* adhesin shown to bind Fn [5]. Mhp271 is the only P97 paralog to contain both R1 and R2 repeats (explained in detail in Chapter IV) and binds heparin with nanomolar affinity (8.1 ± 0.4 nM) [5]. The recombinant fragment $F2_{271}$ that encompasses the $R2_{271}$ and $R1B_{271}$ repeat regions bound Fn with a K_D of 174 ± 13 nM [5]. Notable, the $R1B_{271}$ and $R2_{271}$ regions share sequence identity with collagen VI and ribosomal binding protein 1 respectively [5]. Collagen VI is itself a Fn-binding protein [47], which suggests that *M. hyopneumoniae* utilises host molecular mimicry in order to gain an advantage when colonising the swine respiratory tract. In the context of the swine respiratory tract, Fn is restricted to the underlying basement membrane as well as the epithelial lining fluid [38]. It is not known for what purpose *M. hyopneumoniae* binds Fn to its cell surface and whether or not Fn is present on the cilial surface. Other bacterial pathogens such as *Campylobacter jejuni* commandeer host Fn as a bridging molecule to adhere to host cells [48] and aid in invasion [49,50]. Fn has an affinity for β_1 integrins and it is this interaction that allows the ECM to interact with the intracellular cytoskeleton and modulate intracellular signalling pathways for apoptosis,

endocytosis and cytoskeletal rearrangements. In addition to Fn, integrins act as receptors for the ECM components laminin, vitronectin and collagen. *C. jejuni* invades host cells by binding Fn and interacting with integrin β_1 that initiates downstream signalling cascades that cause cytoskeletal rearrangements; facilitating the uptake of the bacteria into host cells (Figure 1.2) [49,50]. *Staphylococcus aureus* employs a similar mechanism by using Fn as bridging molecule to bind integrin $\alpha_5\beta_1$ and become internalised by host cells [51]. When deletions were made in *S. aureus* Fn-binding proteins, invasiveness was lost but could be restored when these genes were overexpressed in double knock-out mutants [51]; underpinning the importance of Fn-binding proteins to this process. It is not known if *M. hyopneumoniae* has an intracellular life stage and whether or not Fn-binding proteins play a role. It has been shown however that viable cells can be cultured from the liver, spleen, kidneys and lymph nodes of pigs infected with *M. hyopneumoniae* [14-16]. The ability to invade host cells and replicate within this niche offers protection from the host immune response and antimicrobial therapy. In order to better understand the way in which *M. hyopneumoniae* persists within its host, an investigation into alternative lifestyles as well as the host receptors that it interacts with is required. As will be described in Chapter II, there is evidence to suggest that *M. hyopneumoniae* invades epithelial cells by commandeering the fibrinolytic component Plg to disseminate to distal tissue sites.

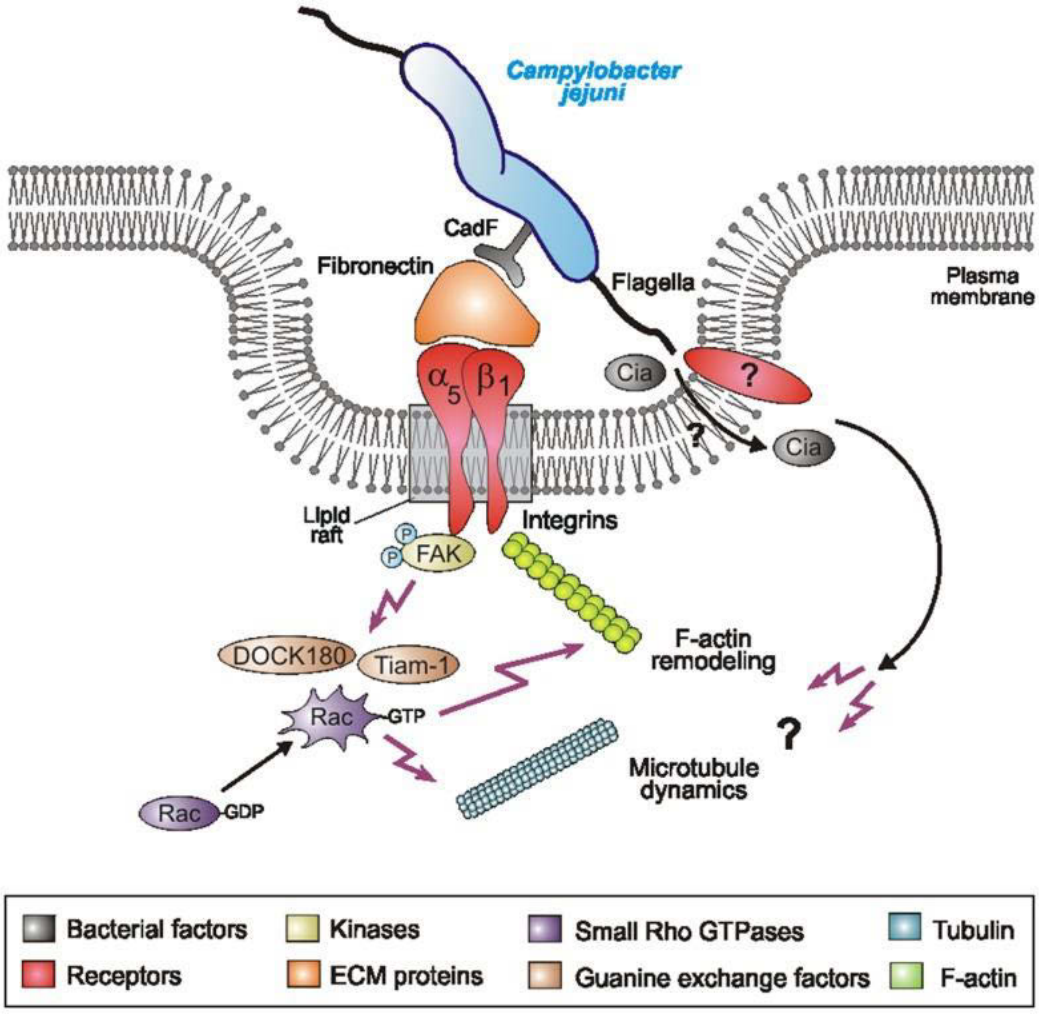

Figure 1.2: Diagram depicting Fn-mediated endocytosis.

Fn bound to surface of *C. jejuni* acts a bridging molecule to $\alpha_5\beta_1$ integrins that are imbedded in the host cell membrane. This causes a signalling cascade that activates Rac1 GTPase which leads to cytoskeletal rearrangements at the site of attachment. This action causes the membrane ruffling and eventual uptake of *C. jejuni* cells. Adapted from [49].

1.4 The *M. hyopneumoniae* Cell Surface

M. hyopneumoniae possesses two families of surface adhesins referred to as the P97 and P102 paralog families that it uses to interface with its host. There are six and seven paralogs of P97 and P102 (Table 1.1) respectively and mRNA transcripts for all of these genes have been found except for Mhp280 [52]. Although they share similarity to P102; Mhp494 and Mhp275 are not considered members of the P102 family as they fall under the sequence homology threshold for being considered paralogs [52]. P97 was the first *M. hyopneumoniae* adhesin to be characterised and will be described in detail in Chapter IV. Proteogenomic investigation of *M. hyopneumoniae* strain 232 by our lab supported the findings of Adams *et al.* by confirming the presence of all members of the P97 and P102 adhesin families [53]. This study was also able to find peptides matching to Mhp280 [53] where no mRNA transcript was previously found [52].

Table 1.1: Accession and gene numbers of P97 and P102 paralogs from five *M. hyopneumoniae* strains whose genomes have been sequenced.

		Strains				
	Protein Name	232	J	7448	7442	168
P97 Paralogs	P97	Mhp183 Q601L9	MHJ_0194 Q4AAD6	MHP_0198 Q4A8G7	MHL_3220 S5FXB0	MHP168_110 E4QSB0
	P216	Mhp493 Q600G2	MHJ_0493 Q4A9J2	MHP_0496 Q4A7M7	MHL_3210 S5G761	MHP168_503 E4QTF2
	P146	Mhp684 Q5ZZM3	MHJ_0063 Q4A925	MHP_0663 Q4A764	MHL_2965 S5GAG9	MHP168_676 E4QTX2
	Mhp385	Mhp385 Q600R9	MHJ_0369 Q4A9W4	MHP_0373 Q4A7Z5	MHL_3119 S5FZ95	MHP168_423 E4QT75
	Mhp107	Mhp107 Q601U4	MHJ_0264 Q4AA66	MHP_0272 Q4A893	MHL_3225 S5G9G7	MHP168_293 E4QSU5
	Mhp271	Mhp271 Q601D1	MHJ_0105 Q4AAM4	MHP_0108 Q4A8Q6	MHL_3142 S5G648	MHP168_195 E4QSJ9
	P95	Mhp280 Q601C2	MHJ_0096 Q4AAN1	MHP_0099 Q4A8 R3	MHL_3042 S5FZP4	MHP168_103 E4QSA5
P102 Paralogs	P102	Mhp182 Q601M0	MHJ_0195 Q4AAD5	MHP_0199 Q4A8G6	MHL_3601 S5G9B0	MHP168_198 E4QSK2
	P159	Mhp494 Q600G1	MHJ_0494 Q4A9J1	MHP_0497 Q4A7M6	MHL_3203 S5FXY1	MHP168_504 E4QTF3
	P135	Mhp683 Q5ZZM4	MHJ_0662 Q4A926	MHP_0662 Q4A765	MHL_3001 S5G7M6	MHP168_675 E4QTX1
	Mhp384	Mhp384 Q600S0	MHJ_0368 Q4A9W5	MHP_0372 Q4A7Z6	MHL_3108 S5G0C9	MHP168_424 E4QT76
	Mhp108	Mhp108 Q601U3	MHJ_0263 Q4AA67	MHP_0271 Q4A894	MHL_3415 S5FXE7	MHP168_292 E4QSU4
	Mhp272	Mhp272 Q601D0	MHJ_0104 Q4AAM5	MHP_0107 Q4A8Q6	MHL_3312 S5FYK8	MHP168_196 E4QSK0
	Mhp274	Mhp274 Q601C8	No J homolog	No 7448 homolog	No 7442 homolog	No 168 homolog
	Mhp275	Mhp275 Q601C7	No J homolog	No 7448 homolog	MHL_3599 S5G628	No 168 homolog

Proteomic analyses of *M. hyopneumoniae* whole-cell lysates rarely identify full length adhesins at their predicted molecular masses [2-4,10,54]. Extensive work has shown that these adhesins are cleaved generating a series of cleavage fragments that retain adhesive functions [2-10,54]. The prevailing hypothesis is that these cleavage events are performed by endoproteases but the enzymes responsible for endoproteolysis remain unidentified [2-10,54]. However, defined cleavage sites have been mapped (see below). Due to the mass context needed to identify these cleavage fragments, methodologies that do not retain such information such as shotgun proteomics will not identify proteolytic activity. This was made evident during studies of the P102 paralog Mhp683, a molecule with a predicted mass of ~135 kDa. The pre-protein undergoes two cleavage events generating three fragments that resolve at ~50 kDa on 1-Dimensional Sodium Dodecyl Sulfate-Polyacrylamide Gel Electrophoresis (SDS-PAGE) [3]. These fragments were resolved by 2-Dimensional SDS-PAGE (2D SDS-PAGE) due to their differences in isoelectric point (pI) (Figure 1.3) [3]. Notably, recombinant proteins spanning these cleavage fragments were able to bind to porcine epithelial cilia, suggesting that each of the three cleavage fragments are cilium adhesins [3]. Adhesion is critical to the survival of *M. hyopneumoniae* as it is dependent on swine to provide the essential nutrients for growth. As such despite having undergone significant genome reduction, functional redundancy is essential for the successful colonisation of the ciliated epithelium. Functional redundancy may i) aid in immune evasion by creating decoy molecules, ii) create variation to the cell surface architecture, and iii) maximise coding capacity by creating multiple functional proteins from the translation of a single open reading frame (ORF). Processing occurs at the cleavage motif S/T-X-F↓X-D/E, where ↓ denotes the point of cleavage, and although the protease responsible is unknown, it has been shown to occur in a number of other P97 and P102 adhesins

[2,3,9,44]. P97 and P102 paralogs are subjected to both efficient (minimal trace of the pre-protein) or inefficient cleavage where cleavage that creates low abundance cleavage fragments [2,3,5-9]. Given that the full length pre-proteins are not present on the cell surface and that the products of processing are the functional molecules that interact with the host, it is crucial to investigate how these molecules are processed and the functional domains that are retained thereafter. As will be discussed in Chapters III and IV; additional cleavage motifs have been identified in P97 and P102 paralogs and provide an insight into how *M. hyopneumoniae* processes and presents these molecules on its cell surface. Other Mycoplasma species such as *Mycoplasma pulmonis* have mechanisms with which they create surface diversity and modulate interactions with their host. For example, *M. pulmonis* can alter the length and order of repeat regions in the Vsa protein that plays a role in biofilm formation, immune evasion and adherence to host cells [55-59].

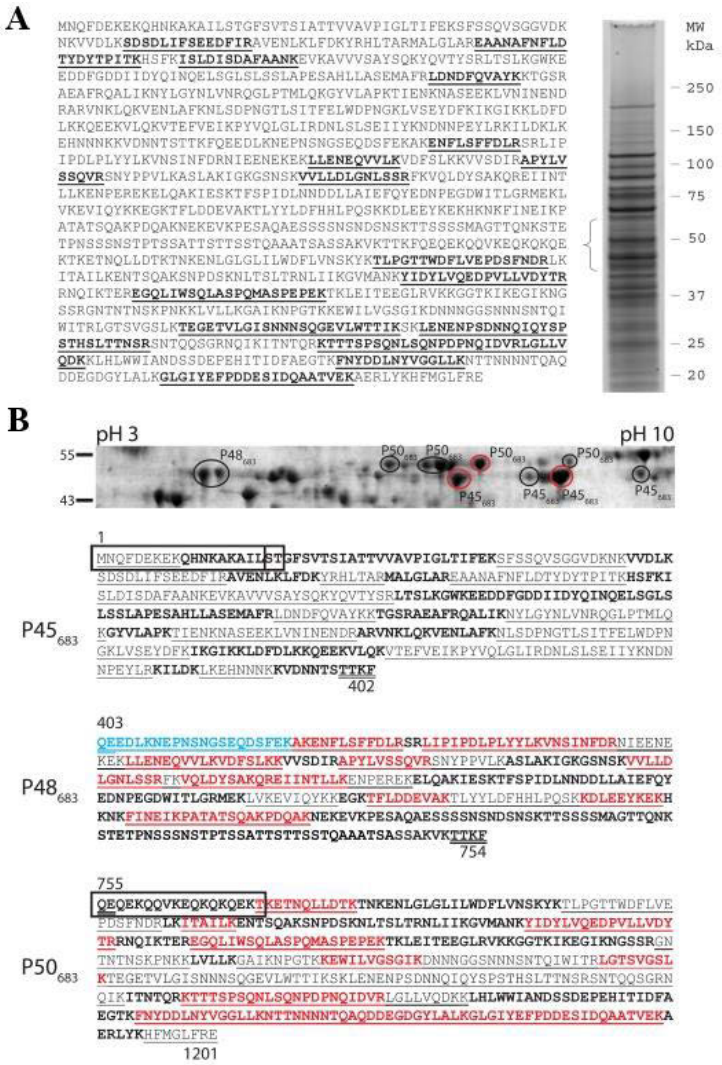

Figure 1.3: Proteomic analysis of Mhp683 and its cleavage products.

A) Peptides identified by Liquid-Chromatography, Tandem Mass Spectrometry (LC-MS/MS) from 1D SDS-PAGE at an apparent molecular mass of ~50 kDa. Peptides identified from this region matched to the N-terminus, middle region and C-terminus of Mhp683. B) Peptides identified by LC-MS/MS and Matrix-Assisted Laser Desorption/Ionization – Time of Flight (MALDI-TOF)-MS from individual spots resolved by 2D SDS-PAGE. $P45_{683}$, $P48_{683}$ and $P50_{683}$ can be seen resolving at different points from pI 3 to 10. Peptides from these spots matched to discrete regions within the N-terminus, middle region and C-terminus of Mhp683; conforming to the proteolytic cleavage site TTKF↓QE at amino acid positions 402 and 754. Adapted from [3].

1.5 Biofilms in Mycoplasma species

Biofilms are adherent communities of bacteria that are encased in an extrapolymeric matrix composed of DNA, protein, lipid and polysaccharide and offer protection from the lytic effects of antimicrobials and the host immune system [60]. The ability of *M. hyopneumoniae* to form biofilms has not been investigated. A number of pathogenic mycoplasma species such as *Mycoplasma putrefaciens*, *Mycoplasma cottewii*, *Mycoplasma yeatsii*, *Mycoplasma agalactiae*, *Mycoplasma bovis*, *M. pulmonis, Mycoplasma gallisepticum*, *Mycoplasma mycoides subsp. mycoides capri, LC and SC* and *Mycoplasma pneumoniae* have been shown to form persistent biofilms on abiotic surfaces [61-67]. *M. bovis* biofilms have been shown to be more resistant to heat and desiccation than its planktonic counterparts [61] while *M. gallisepticum* biofilms are more resistant than planktonic cells to antibiotics such as gentamicin and tetracycline [66]. Biofilms of other bacteria are known to provide up to 1000 times increased resistance to environmental stressors such as antibiotics [68]. Given their strict requirements for host-derived molecules for growth, the ability to form biofilms may allow Mycoplasma species to persist outside of their host for prolonged periods of time.

Variable surface antigen (Vsa) plays a significant role in the ability of *M. pulmonis* to form biofilms [62]. *M. pulmonis* is used as a model to study the pathogenesis of human respiratory Mycoplasmas. The Vsa protein is a size and phase variable protein. Stochastic processes generated by slip-strand mispairing during replication regulate how cells in a population express the Vsp (phase variation) and the number of tandem repeats (size variation) [57,69-71]. Cells expressing longer forms of the Vsa protein have been found to have reduced adherence to polystyrene and erthyrocytes but an enhanced resistance to complement killing [58,72]. The reverse is also true; cells

expressing a shorter Vsa protein adhere to polystyrene and erythrocytes but are susceptible to killing by complement [58,72]. Furthermore, cells producing a longer Vsa protein adhere poorly to murine cells compared to those with shorter repeats [55]. The length of tandem repeats within the Vsa protein has also been linked to biofilm formation [62]. Cells expressing a Vsa protein with shorter tandem repeats adhered to glass and polystyrene and formed prolific biofilms, whereas those with longer repeats could not form adherent biofilms [71]. Cells residing within these structures were found to be more resistant to complement and gramicidin compared with those cells that had dispersed from the biofilm [73]. It appears that even though cells producing a shorter Vsa are susceptible to killing by complement, their ability to form biofilms may be a mechanism to compensate. It has also been shown that *M. pulmonis* cells producing a long Vsa protein are resistant to killing by macrophages [56]. The ability to stochastically modulate the Vsa protein and hence the ability to adhere, form biofilms, and resist killing by complement and macrophages is thought to be a mechanism in which *M. pulmonis* persists within its host.

The Vsa protein has also been linked to the binding of exopolysaccharide-I (EPS-I) to the cell surface [39]. Cells expressing a short Vsa protein could more readily bind EPS-I and hence form a glycocalyx which enhances complement resistance [39]. However, mutants that do not produce EPS-I but still produce a long Vsa protein were susceptible to killing by complement [39]. This suggests that both Vsa length and EPS-I production are important for complement resistance. Notably and regardless of Vsa length, mutants that do not produce EPS-I have an enhanced ability to form biofilms; suggesting that EPS-I may hinder biofilm production [39].

The ability of *M. hyopneumoniae* to form biofilms has been hypothesised but never investigated. SEM images of the swine respiratory tract, show *M. hyopneumoniae* cells forming large aggregates in between cilia which are reminiscent of biofilms (Figure 1.1) [22]. Experimental infections with *M. hyopneumoniae* have demonstrated that cells are recoverable from bronchial swabs up to 185 days P.I. [18], and 100% of experimental infections are cleared by 254 days P.I. [19]. Pigs can remain infectious up to 200 days P.I. in the absence of any discernible lesions [19]. These observations suggest that *M. hyopneumoniae* has the capability to reside within its host in a dormant state. In this state it remains transmissible, indicative of it forming persistent biofilms in the swine respiratory tract. To effectively design vaccines against *M. hyopneumoniae* we need to determine if it is capable of forming biofilms and which genes play a critical role in biofilm formation.

1.6 Topics and Aims Presented in this Thesis

- **AIM ONE:** To determine the extent of proteolytic processing in the adhesins P159 and P97 and the cleavage sites present in these molecules (Chapters III & IV).
- **AIM TWO**: To examine the interaction of *M. hyopneumoniae* with host molecules such as Fn and actin and the cellular responses it elicits in its host (Chapters IV & V).
- **AIM THREE**: To examine the ability of *M. hyopneumoniae* to form biofilms on abiotic and host cells (Chapter V).
- **AIM FOUR**: To determine if *M. hyopneumoniae* can invade porcine epithelial cells and exist intracellularly (Chapter VI).

Evidence is lacking as to how *M. hyopneumoniae* colonises the swine respiratory tract and causes chronic disease. To date, it is known that *M. hyopneumoniae* utilises the surface exposed P97 and P102 adhesin paralogs to interact with glycosaminoglycans, Fn and Plg. There is additional, albeit limited, data that suggests *M. hyopneumoniae* binds laminin and glycolipids. In order to better understand the disease process, we need to identify additional receptors that *M. hyopneumoniae* targets (**AIM TWO)**. This was investigated using a novel-affinity chromatography methodology where the surface of *M. hyopneumoniae* cells were labelled with biotin and loaded onto to avidin agarose beads as bait proteins. These agarose beads were exposed to native PK-15 lysates in order to capture those proteins that are recognised by *M. hyopneumoniae* surface proteins. PK-15 proteins that bound were collected and analysed by LC-MS/MS. This methodology identified a number of putative receptors of *M. hyopneumoniae* such as

actin. The ability of *M. hyopneumoniae* proteins to bind actin was further investigated and it was found that the P97 adhesin binds actin with nanomolar affinity. *M hyopneumoniae* cells were also found to adhere to PK-15 monolayers where actin was most pronounced. In addition to actin, we show that *M. hyopneumoniae* co-localises with Fn at the site of infection and that Fn is not present at the ciliary border of uninfected pigs. This suggests that *M. hyopneumoniae*-induced tissue damage makes Fn available at the ciliary border.

One of the focuses of this PhD was the characterization of the surface proteome of *M hyopneumoniae* using surface biotinylation to purify those proteins that are present on the cell surface. From this work it was found that a number of P97 and 102 paralogs undergo endoproteolytic processing to a greater extent to which was previously published. Manuscripts focusing on the paralogs P159 and P97 and how they are processed were each published (**AIM ONE)**.

Infection with *M. hyopneumoniae* is chronic; however there is no evidence as to how *M. hyopneumoniae* evades the immune response and persists despite this response. We investigated two novel lifestyles of *M. hyopneumoniae*: biofilms and invasion of host cells (**AIMS THREE & FOUR**). We demonstrated that *M. hyopneumoniae* forms biofilms on abiotic surfaces and PK-15 monolayers, as well as on the denuded epithelium of the swine respiratory tract. We linked genotype to phenotype by identifying three novel biofilm-associated proteins MhpX, MhpY and MhpZ that appear to have a profound effect on biofilm formation (gene names have been altered for intellectual property purposes). Using SEM and TEM we observed *M. hyopneumoniae* cells invading PK-15 monolayers (Figure 6.4). TEM studies demonstrated *M.*

hyopneumoniae cells residing within vacuole-like structures within the cytosol of PK-15 cells. Using antibodies that recognise the lysosomal marker LAMP1 and 3-Dimensional Structured Illumination Microscopy (3D-SIM) we showed that i) internalised *M. hyopneumoniae* cells associated closely with lysosomes but never within them and ii) *M. hyopneumoniae* cells escape lysosomes and persist within the cytosol.

Chapter Two: (Paper I) An introduction to the importance of veterinary pathogens and how they circumvent host defences

Declaration

I declare that the following publication included in this thesis in lieu of a chapter meets the following:

- More than 50% of the content in the following publication included in this chapter has been planned, executed and prepared for publication by me
- The work presented here has been peer-reviewed and accepted for publication
- I have obtained approval to include the publication in this thesis from the Publisher
- The initial draft of the work has been written by me and any subsequent changes in response to co-authors and editors reviews was performed by me
- The publication is not subject to any obligations or contractual agreements with a third party that would constrain its inclusion in the thesis.

Publication title: Exploitation Of Plasmin(Ogen) By Bacterial Pathogens Of Veterinary Significance

Authors: Benjamin B. A. Raymond and Steven Djordjevic

Candidate's contribution (%): above 50 %

Journal name: Veterinary Microbiology

Volume/ page numbers: 178(1-2):1-13

Status: Accept for publication doi:10.1016/j.vetmic.2015.04.008

I declare that the publication above meets the requirements to be included in the thesis.

Candidate's name: Candidate's signature: Date (dd/mm/yy):

2.1 Structure & Function of Plg

Plg (Plg) is a single chain glycoprotein which circulates in mammals in two dominant forms; Glu- and Lys-Plg. Human Plg is approximately 90 kDa in size, comprising 810 amino acids. The molecule comprises seven domains including an N-terminal domain where critical processing events take place, 5 kringle domains and a C-terminal protease domain (Figure 2.1). The kringle domains mediate substrate binding, specifically kringle domains 1 and 4 that contain lysine binding sites responsible for binding fibrin and other cell surface receptors that will be discussed later [74,75]. The C-terminal domain of Plg, accessible only in the active form plasmin contains the catalytic site which is comprised of the key amino acids His^{603}, Asp^{646} and Ser^{741} [76]. The native circulating form of Plg is Glu-Plg. Glutamic acid constitutes the first residue in the protein after removal of the signal peptide. Further processing events which remove 62-77 amino acid residues (known as the pre-activation peptide) from the N-terminus generate what is referred to as Lys- Plg. This cleavage event can occur at Lys^{62}, Arg^{68} or Lys^{77} and is performed by plasmin [77-79]. tPA (tissue-specific Plg activator) or uPA (urokinase Plg activator) are Plg activating proteases that cleave Glu-Plg and Lys-Plg to the active serine endoprotease plasmin at the Arg^{561}-Val^{562} peptide bond (Figure 2.1) [80,81]. The activation site targeted by tPA and uPA is more readily accessible in Lys-Plg than in Glu-Plg which makes Lys-Plg much more susceptible to activation than Glu-Plg; an important regulator of the plasmin cascade that will be described below [80,81]. Two interchain disulfide bonds link the N-terminal heavy chain to the C-terminal light chain that houses the binding and peptidase domains respectively. For a detailed description of the structural features of Plg see reviews by Sanderson-Smith et al., 2012 and Fulde et al., 2011.

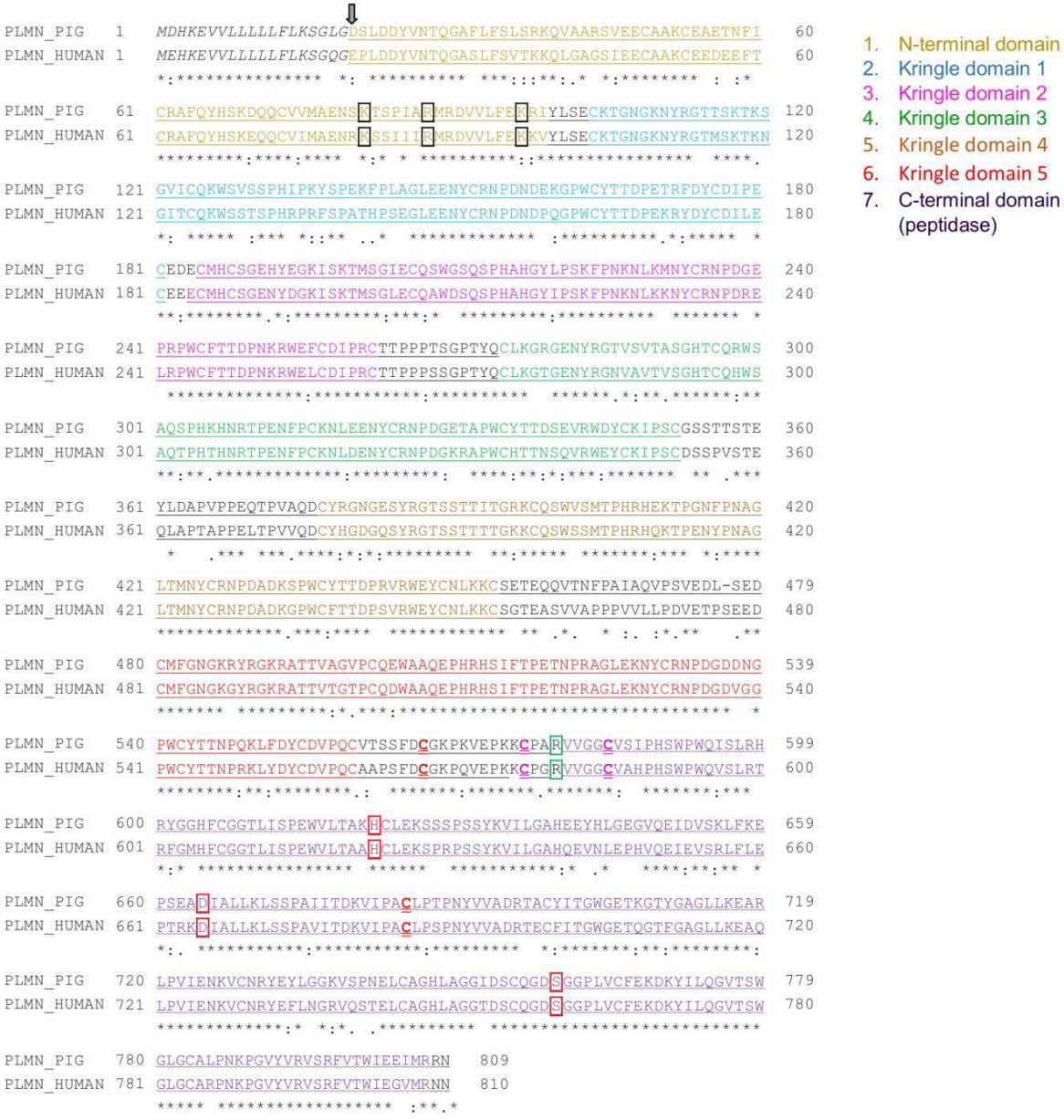

Figure 2.1: Amino acid sequence alignment of Plg.

(*Sus scrofa*, accession number; P06867 and *Homo sapiens*, accession number; P00747). The domains of Plg are described in the key and amino acid numbers are indicated on the right of the sequence. The arrow indicates the beginning of Glu-Plg after the removal of the signal peptide. Italics from amino acids 1-19 indicate the signal peptide; underlined regions indicate the Plg heavy chain; wave underlined regions indicate the Plg light chain. Black boxed amino acid residues highlight the site where plasmin cleaves Glu-Plg to Lys-Plg. Green boxed amino acid is the cleavage site that generates

plasmin. Red boxed amino acid residues are responsible for the catalytic activity of plasmin. Light chain and heavy chains are held together by two disulphide bonds indicated by red and pink double underlined cysteine residues respectively. Asterisks indicate amino acid residues that are identical between human and swine, double dots indicate strong similarity, single dots indicate weak similarity and no mark indicates a dissimilar amino acid substitution. Functional domains of Plg are highly conserved between human and swine and it is only the regions between these domains that display significant differences in their sequences. It is important to note that the 19 amino acid signal peptide is typically ignored when referring to amino acid numbers in Plg and this is why published amino acid numbers do not match with database sequences.

Plasmin degrades fibrin clots and as such is the key homeostatic component of the fibrinolytic system. Circulating Glu-Plg is non-enzymatic and typically becomes activated to plasmin in the presence of clots or cell surfaces; fibrin being one of its main cofactors. During coagulation, thrombin cleaves fibrinogen to fibrin and activates coagulation Factor XIII which subsequently crosslinks fibrin monomers forming an adhesive matrix/clot. Factor XIIIa also plays a role in cross-linking the N terminus of circulating plasma Fn (pFn) to the C terminus of the fibrin α chain [82,83]. As such pFn has been shown to control the lateral aggregation of fibrin fibers and is recognized to play an important role in the final steps of the coagulation cascade [83]. The kringle 1 domain of Plg contains a fibrin binding region that allows Plg to be incorporated into the fibrin clot. Damaged endothelium at the site of injury allows tPA to disseminate from the endothelial cells to the fibrin clot where it activates Plg to plasmin [75]. Fibrin

enhances the ability of tPA to activate Plg by 2 orders of magnitude and is thus an effective mechanism for recruiting and localising plasmin activity at the site of injury.

The proteolytic activity of plasmin degrades the fibrin clot and maintains homeostasis. Plasmin is a potent serine endoprotease that degrades a variety of substrates such as fibrin, ECM components and junction proteins [84], as well as activates matrix metalloproteinases (MMP). The ability to cleave ECM and junction proteins is crucial to cell migration as well as the removal of apoptotic cells. Plg has been implicated in a number of pathological processes such as inflammation, malignancy, autoimmunity and microbial infection.

2.2 How Do Bacteria Exploit Plasmin(ogen)?

The interaction of bacterial surface adhesins with Plg has been well documented [84]. Group A *Streptococci* was the first pathogen shown to bind Plg [85]. Both Gram-positive and Gram-negative bacteria exploit the fibrinolytic system to promote their adherence to host cells and to hijack the proteolytic activity of plasmin as a means to degrade ECM and disseminate to distal tissue sites [84]. Proteolytic fragments of the ECM, particularly Fn have cell signaling and immunomodulatory roles that influence inflammatory disease states [46] that are only now being fully appreciated. pFn also plays an important role in regulating thrombosis, independent of fibrinogen, and can be observed integrating with fibrin at the site of injury [83].

Bacterial cell surfaces contain receptors that bind Plg. The binding event induces a conformational change in Plg that enables plg activators greater access to key activation sites. Cleavage at these sites converts Plg to plasmin and arms the bacteria with an

active, broad-spectrum serine endoprotease on its cell surface. Surface bound plasmin is exploited to degrade host junction proteins and initiate signaling events that facilitate bacterial uptake and invasion [84]. Plasmin(ogen) mediated invasion has been shown to occur via multiple pathways; reinforcing the importance of Plg-binding proteins on the surface of bacteria. Integrin α5β1 is the main Fn receptor on eukaryote cells and has been shown to bind and increase the activation of Plg [86]. Integrins are transmembrane adhesins that react to extracellular stimuli; acting as receptors to various ECM components and initiating downstream signaling events that can regulate cell shape and motility. These interactions trigger integrin-linked kinase (ILK) which activates Rac1 GTPase and influences cytoskeletal function [87-89]. This has been shown to be particularly important to phagocytosis by both professional and non-professional cells, as cytoskeletal rearrangements give rise to pseudopods that engulf particles for uptake [90]. Pathogenic bacteria target integrins and subsequently become engulfed by target cells. *Campylobacter jejuni* and *Staphylococcus aureus* utilise Fn as a bridging molecule to bind α5β1 to promote their uptake into host cells [50,51,91] and the exploitation of integrins by Fn-binding proteins in Group B *Streptococcus* is crucial to their ability to cross the blood brain-barrier and cause meningitis [92,93]. Plg-binding in *Streptococcus pyogenes* has been shown to promote integrin-mediated invasion via ILK-signaling events [94]. Cytochalasin D, an inhibitor of actin polymerisation inhibited the internalisation of *S. pyogenes* cells, further supporting the hypothesis that Plg binding triggers integrin-related signaling pathways that cause cytoskeletal rearrangement [94]. Plg can therefore function as a bridging molecule similar to Fn, initiating signaling events that promote bacterial uptake and warrants further investigation.

Another mechanism that bacteria exploit to invade host tissue involves the direct degradation of junction proteins such as VE-cadherin. Cadherins link the intracellular cytoskeletal network of adjacent cells and form the junctions that act as the main barrier to bacterial cells. *Streptococcus pneumoniae* can sequester Plg onto its cell surface, convert it to plasmin and cleave VE-cadherin. *S. pneumoniae* incubated without Plg or with a plasmin inhibitor were unable to cleave VE-cadherin [95]. *S. pneumoniae* cells incubated with Plg were more effective at transmigrating across epithelial and endothelial monolayers as well as disrupting cellular junctions compared with those incubated without Plg or with a plasmin inhibitor [95]. Notably, *S. pneumoniae* cells incubated with Plg adhered strongly to epithelial monolayers whereas *S. pneumoniae* cells incubated with plasmin adhered poorly [95]. Differences in adherence were attributed to the increased proteolytic activity on the *S. pneumoniae* surface and suggest that the initial interaction of bacteria with Plg promotes adherence to host cells followed by the activation of Plg to plasmin which promotes internalisation and invasion [95].

Knowledge that has been garnered on interactions between bacterial surface proteins and Plg has been derived from studies of human pathogens with little focus on its role in veterinary microbiology. *Streptococcus suis* is an emerging zoonotic pathogen that has been shown to bind and activate Plg on its cell surface; allowing it to degrade the ECM component Fn [96]. *S. suis* can cause significant disease in humans ranging from meningitis to septicaemia, endocarditis or deafness and can be fatal [96]. Therefore significant attention needs to be paid to veterinary pathogens that are not only zoonotic but contribute to the use of antibiotics in the commercial livestock industry. Globally, the commercial livestock industry is the biggest user of antibiotics and currently uses all major classes of antibiotics that are of clinical importance to humans [97,98]. These

antibiotics are often used at sub-therapeutic doses that increase the likelihood of creating antibiotic-resistant bacteria. Antibiotic-resistant bacteria can be readily transmitted to humans, adding to their prevalence in the environment [97,98]. Advocates of antibiotic use in the commercial livestock industry argue that antibiotic use reduces economic loss and improves animal welfare. Therefore novel therapeutic targets are required if we are to lower the use of antibiotics in agriculture. The development of efficacious vaccines is one approach to achieve reduced dependence on antibiotics. Here we have chosen to focus on two pathogenic bacteria whose interactions with Plg are well characterised in order to assess this interaction in the broader scope of veterinary and zoonotic disease.

2.3 The Coagulation and Complement Systems and Plasmin(ogen)

The coagulation and complement systems are both part of the innate immune system and play important roles in the early response to tissue injury [99,100]. The complement system is one of the most important components of the innate immune system. It is comprised of over 30 proteins which mobilise to form the Membrane Attack Complex (MAC); a protein complex that lyses targets cells such as bacteria by creating a transmembrane channel in the lipid bilayer. In addition to forming the MAC, the complement system is also responsible for chemotaxis and opsonisation and agglutination of target cells. There are three major pathways of the complement system; classical, alternative and lectin. The three pathways intersect through the production of C3 convertase that cleaves C3 to C3a and C3b [101,102]. C3b binds to and opsonises bacterial cell surfaces and initiates the formation of the MAC. C3b also binds to C5 and aids in its cleavage by C5 convertase to C5a and C5b; C5b being crucial to the formation of the MAC. C3a and C5a are both chemoattractants that trigger

degranulation of mast cells and an increase in proinflammatory cytokines. This cascade of events causes a potent inflammatory response that opsonises and removes foreign material. Plg influences how these key events unfold.

Plasmin binds C3, C3b, C3d and C5 and directly cleaves C3b and C5 [99,100]. Cleavage of C3b and C5 renders them non-functional and inhibits the activity of the complement system [100]and reduces the ability of immune cells to migrate to the site of infection to engulf opsonised cells and initiate the MAC (Figure 2.2). These events represent a mechanism to reduce inflammation at the site of injury P.I. Plasmin is therefore a regulator of the coagulation and complement systems; both of which maintain homeostasis and are the first line of defense against foreign agents.

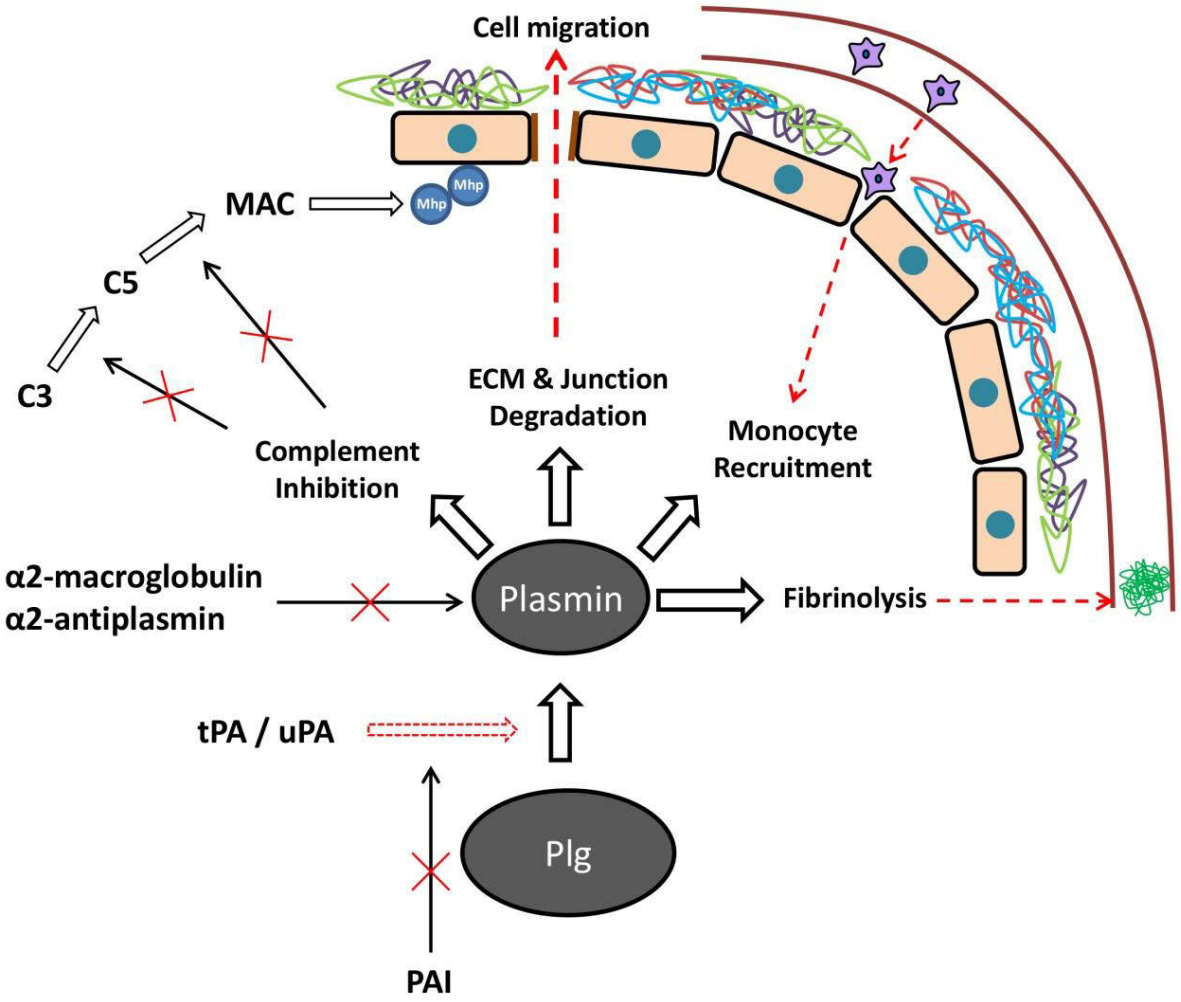

Figure 2.2: Diagram demonstrating the multitude of Plg functions.

Plg is activated to plasmin by tPA or uPA, and its activation is inhibited by Plg activator inhibitors (PAI). The activity of plasmin is inhibited by α2-macroglobulin and α2-antiplasmin. In addition to degrading blood clots (fibrinolysis) plasmin can also degrade ECM and junction proteins, which in turn promotes cellular migration. When bound to the surface of mononuclear cells, plasmin has a dual role in chemotaxis and upregulating the expression of proinflammatory cytokines. Plasmin also degrades complement components C3 and C5, effectively inhibiting the formation of the Membrane Attack Complex (MAC).

The Leptospira are one of the most important emerging zoonotic pathogens that infect a wide range of animals. Mortality rates associated with Leptospira infections in humans is thought to exceed 10% [103]. Rats are the main carriers although all mammals are thought to play a role in transmission. In mammals the kidneys are the main site of colonisation; facilitating the shedding of bacteria via urination. Upon contact with contaminated urine, leptospires penetrate the skin and cause systemic infection, utilizing the circulatory system to travel to body sites. Symptoms of leptospirosis can vary from a mild headache and fever to severe manifestations such as leptospirosis-associated pulmonary hemorrhagic syndrome (LPHS) and Weil's syndrome, which is characterized by jaundice, meningitis, hemorrhage and multiple organ failure. Leptospirosis is endemic to tropical and sub-tropical areas of the globe and there are approximately half a million new cases reported yearly [104]. Although epidemiological data is lacking, leptospirosis is a leading cause of concern in the food animal industry as it is thought to be responsible for a large percentage of reproductive failure in cattle and other ruminants [105]. Although disease-causing mechanisms of leptospires are largely unknown, a hallmark of pathogenic leptospires is their ability to circumvent the innate immune system via complement pathways enabling the infection to disseminate within their respective hosts largely unabated [106,107].

Leptospira are not thought to be facultative intracellular pathogens although they do seem to exploit the ability to internalise within host cells. Both pathogenic and non-pathogenic strains have been shown to resist killing by macrophages and replicate after internalisation [108]. However, when incubated with homologous IgG, macrophages are able to internalise and kill both pathogenic and non-pathogenic Leptospiral strains [109]. Serum complement alone was unable to assist in the killing of pathogenic strains

suggesting that specific IgG is required for opsonisation of virulent strains. It is thought that *L. interrogans* utilises Fn as a bridging molecule to bind CR3 receptors on neutrophils and macrophages promoting its uptake into these cells [110]. The ability to become internalised by immune cells may be one of the mechanisms in which pathogenic Leptospiral species disseminate and cause systemic infection. Highly virulent strains of *L. interrogans* become internalised by macrophages, escape phagosomes and invade the nucleus [111]. Less virulent strains of *L. interrogans* reside within phagosomes suggesting that the ability to escape and invade the host nuclei is important to the disease process [111]. The ability to invade the nucleus is thought to provide protection from cytoplasmic defenses [112]. *L. interrogans* also has the ability to translocate through MDCK epithelial monolayers and does so more effectively when compared with non-pathogenic *L. biflexa* [113]. The ability to bind VE-cadherin is important in the transmigration of bacterial pathogens [114]. *L. interrogans* has been shown to bind to VE-cadherin and disrupt cell layer integrity [114] while non-pathogenic *L. biflexa* improves cell layer integrity [114,115]. Together these observations suggest that pathogenic Leptospira species have the ability to invade immune cells and transmigrate across epithelial barriers. The mechanisms employed by pathogenic Leptospira to achieve this remains unknown.

Little is known about how pathogenic *Leptospira* species are able to evade the innate immune system and cause systemic infection although numerous studies have focused on interactions with the complement system [116]. There is a distinct difference in the deposition of complement components onto the surface of serum-sensitive and serum-resistant strains of Leptospira [107]. Non-pathogenic, serum-sensitive strains are more sensitive to killing by human serum and have complement components C3, C5, C6 and

C8 in addition to components of the MAC deposited on their cell surface [107]. Serum-resistant strains of Leptospira only have C3 deposited on the cell surface suggesting that the complement cascade is halted at the C3 level [107]. Factor H is a cofactor to Factor I that promotes C3b cleavage to its inactive form iC3b; a process which is crucial to halting the progression of the alternative complement pathway that ultimately ends in the formation of the MAC [117]. It was found that serum-resistant strains of Leptospira bind Factor H whereas serum-sensitive strains fail to do so [107] and explains why the full repertoire of the alternative pathway is found on the surface of non-pathogenic strains that cannot bind Factor H. The ability to bind Factor H is a redundant process among Leptospira species [118-123]. Leptospiral surface adhesins also bind C4bp, an inhibitor of the lectin and classical complement pathways that inactivates C4b [123-125].

Leptospira species possess a large number of functionally redundant adhesins that bind to a wide range of ECM components as well as cellular receptors [122,126-132]. Both *L. biflexa* and *L. interrogans* bind human Plg [133]. Recombinant fragments representing different Leptospira surface proteins bind Plg and facilitate its activation in the presence of specific activators [134]. In the presence of uPA, cell surface Plg is activated to plasmin resulting in a markedly increased ability to transmigrate across endothelial cells and degrade Fn [132,133,135]. Interestingly, both pathogenic and non-pathogenic strains are able to facilitate the conversion of Plg to plasmin on their cell surface in the presence of uPA [133]. 24 h after infection with *L. interrogans*, MMP-9, and uPA levels are significantly elevated when compared with uninfected controls [135]. A similar observation was made using uPA- and tPA-specific ELISA kits as well as metalloprotease activity tests for serum samples of patients with leptospirosis;

suggesting that the utilisation of Plg by Leptospira species is an important pathological event [135]. Total serum plasmin and MMP-9 levels were significantly higher in individuals in the initial stages of leptospirosis compared with those in convalescent stages suggesting that the sequestration and activation of proteolytic activity, followed by bacterial invasion occurs at the early stages of infection [135].

In addition to degrading Fn, plasmin on the surface of *L. interrogans* is a source of proteolytic activity that is capable of destroying components of the complement pathway such as C3b that have key roles in opsonisation and MAC formation [136]. Similar observations have been reported for *Staphylococcus aureus* and *S. pneumoniae* [137,138]. Leptospires treated with Plg and uPA survive incubation with normal human sera for up to 4 days while untreated Leptospires were quickly killed [136]. Elongation Factor Tu (EF-Tu) moonlights on the Leptospira cell surface and binds Plg and complement Factor H [121]. Immobilised recombinant EF-Tu from Leptospira incubated with Plg and uPA degrades fibrinogen and complement component C3b [121]. Leptospira surface adhesins bind plasmin and Factor H to their cell surface to degrade and inhibit components of the innate immune system. Functional redundancy is a mechanism that ensures simultaneous binding of different host components. *L. interrogans* can concomitantly bind Plg and Factor H without either of these blocking the other [136]. *L. interrogans* can bind Factor H and retain the ability to bind and activate Plg in the presence of uPA [136]. Collectively, these studies suggest that Leptospira spp. utilise Plg to transmigrate through host cells and to evade the innate immune system.

2.4 The Mycoplasmas: Innate Immunity and Plasmin

The mycoplasmas are a specialized group of genome-reduced bacteria that are phylogenetically related to the low G+C Firmicutes. The process of degenerative evolution has resulted in the shedding of genes required for cell wall biosynthesis, the tricarboxylic acid cycle, cholesterol biosynthesis and many other anabolic pathways including the ability to synthesise amino acids and nucleotides. As such, most mycoplasma species are host-specific pathogens or commensals that have evolved mechanisms to regulate the immune response and form chronic infectious states with their respective hosts.

A number of mycoplasma species including *Mycoplasma bovis, Mycoplasma leachii, Mycoplasma fermentans, Mycoplasma gallisepticum, Mycoplasma synoviae, Mycoplasma hyopneumoniae* and *Mycoplasma pneumoniae* have been shown to bind Plg on their cell surface and activate it to plasmin in the presence of tPA or uPA [9,139-147]. In cattle, *Mycoplasma bovis* and *Mycoplasma leachii* are part of the *Mycoplasma mycoides* cluster that cause mastitis, pneumonia and polyarthritis in cattle [148]. *M. bovis* cells have been shown to reside within the cytosol of phagocytic cells [149], erythrocytes, and in vacuole-like structures within a number of peripheral blood mononuclear cells [150]. The mechanism of invasion has not been established but it is thought that this mechanism allows *M. bovis* cells to disseminate from the lung to distal tissue sites.

α-enolase is a highly conserved and well known glycolytic enzyme that moonlights on the surface of eukaryote cells where it binds Plg as well as regulating a number of cellular processes [151]. It is also one of the main bacterial proteins involved in Plg

binding [152]. α-enolase resides on the surface of *M. bovis* and binds Plg [140]. Antisera raised against recombinant α-enolase identified α-enolase in both cytosolic and membrane fractions of *M. bovis* [152]. When *M. bovis* cells were pre-incubated with bovine Plg their ability to adhere to embryonic bovine lung cells was enhanced. Anti α-enolase antibodies did not significantly inhibit adherence [152] suggesting that α-enolase is not solely responsible for binding Plg. Clearly, functional redundancy ensures that pathogenic Mycoplasmas retain a number of proteins on their cell surface that can bind and activate Plg. Recombinant α-enolase cloned from *M. gallisepticum* was also shown to bind Plg. α-enolase antibodies labelled the surface of *M. gallisepticum* and detected the protein in membrane fractions [153]. In contrast to studies in *M. bovis*, α-enolase antibodies were able to significantly inhibit the ability of *M. gallisepticum* to adhere to chicken embryo fibroblasts [153]. Notably antisera raised against α-enolase significantly inhibited adherence of *M. synoviae* to chicken embryo fibroblasts [146]. These data suggest that Plg binding proteins, particularly α-enolase are important for attachment of Mycoplasmal pathogens of veterinary origin to target epithelial cells.

M. hyopneumoniae is a porcine-specific pathogen that displays an affinity for the negatively charged glycosaminoglycans exposed on the surface of ciliated epithelial cells that line the upper airways of the respiratory tract [4,40,154]. *M. hyopneumoniae* is an economically-significant and globally-dispersed pathogen that causes growth rate retardation and reduced feed conversion efficiency in affected pigs. *M. hyopneumoniae* destroys the mucociliary escalator by causing ciliostasis, cilial shedding and epithelial cell death and creates a microenvironment in the lungs of pigs that is conducive to secondary infections by bacteria and viruses [25,26]. Adherence to cilia is in large part facilitated by the presence of two large adhesin families known as the P97 and P102

adhesin families [2-5,7-10,41-44]. To date, seven adhesins (Mhp108, Q601U3; Mhp107, Q601U4; Mhp183, Q601L9; Mhp684, Q5ZZM3; MHJ_0461, Q4A9M4; MHJ_0125, Q4AAK4) have been shown to bind Plg [2,7-9,42,145,155]. Members of the P97 and P102 adhesin families are processed by endoproteolytic enzymes generating a multitude of functional cleavage fragments and represent the functional effector proteins that define the key functions of these adhesin families [54]. Mhp683, Mhp684, Mhp183, Mhp493 and Mhp494 are highly expressed efficiently processed adhesins [2-4,10,42-44,54] while adhesins Mhp107, Mhp182, Mhp108, Mhp271, Mhp385 and Mhp384 [5-9] are targets of relatively limited and less efficient cleavage events and as such it is possible to detect small quantities of the parent preprotein. Over 90 functional effector proteins derived from processing events targeting the P97 and P102 adhesin families have been characterized or are inferred from known cleavage events. Cleavage is not confined to the adhesin families. Members of the lipoprotein family and several moonlighting proteins that are known to reside on the cell surface of *M. hyopneumoniae* are also targets of posttranslational cleavage (Tacchi et al., unpublished results). Thus processing substantially increases the functional repertoire of proteins that can be generated from 692 ORFS predicted from the genome sequence of *M. hyopneumoniae* strain 232 [156]. To our knowledge there is no other bacterial pathogen known to process surface molecules to the extent observed in *M. hyopneumoniae*.

An extensive body of research indicates that the ability of *M. hyopneumoniae* to engage with the host Plg system is critical for pathogenesis. *M. hyopneumoniae* bind Plg in a dose-dependent manner [7]. Mhp108, a 116 kDa paralog of the cilium adhesin P102 [7] displays a C-terminal lysine residue that plays a key role in binding Plg. A C-terminal

recombinant fragment of Mhp108 ($F4_{P116}$) bound to Plg with nanomolar affinity (K_D = 44.5 nM). Surface plasmon resonance studies showed that removal of the C-terminal lysine residue by site-directed mutagenesis abolished the ability of recombinant fragment $F4_{P116}$ to bind Plg [7]. Since these initial experiments we have shown that cleavage fragments derived from different members of the P97 and P102 paralog families bind Plg and promote its activation to plasmin. Mhp684 is a 146 kDa P97 paralog that is highly expressed on the surface of *M. hyopneumoniae*. Mhp684 from pathogenic 232 strain and its homologue in non-pathogenic strain J displays C-terminal arginine and lysines residue respectively [2]. Recombinant proteins spanning the C-terminal region of P146 from both strains bound Plg indicating that a positively charged C-terminal amino acid residue is necessary for binding [2]. When the C-terminal lysine/arginine residue was removed from these recombinant fragments, binding was reduced 5-fold [2] highlighting the importance of C-terminal lysine/arginine residues for Plg binding in this molecule. The C-terminal lysine and positively charged arginine and histidine residues that reside near the C-terminus facilitates binding to Plg by the Group A Streptococcal adhesin Prp [157]. Mutagenesis of the C-terminal lysine to alanine reduced but did not abolish binding to Plg whereas the replacement of arginine and histidine residues with alanine completely abolished binding [157]. While C-terminal lysine residues in *M. hyopneumoniae* have been shown to play a crucial role in binding Plg, several adhesin cleavage fragments that lack C-terminal lysine, arginine or histidine residues can effectively bind Plg and promote activation of Plg to plasmin. One such example is in the C-terminal P28 cleavage fragment of the cilium adhesin P97 (Mhp183). Plg bound comparably with recombinant C-terminal fragments with and without a C-terminal lysine residue [43]. This phenomenon is likely due to their being a large number of lysine residues in the C-terminus of P97 which are accessible to the

kringle domains of Plg. Based on these studies it appears that even though there is a high level of redundancy in relation to Plg-binding, the presence of a C-terminal lysine is not critical for binding Plg.

Glycosaminoglycans (GAGs) decorate the surface of the ciliated epithelium in the porcine respiratory tract [40]. While the structure of GAGs is highly variable many display regions that are highly sulfated and are sensitive to heparinase [40]. *M. hyopneumoniae* has an affinity for highly sulfated glycosaminoglycans on ciliated epithelium. Heparin and the highly sulfated GAG fucoidan have been used to effectively block attachment of *M. hyopneumoniae* to cilia [32]. Notably, high molecular mass heparin is known to bind Plg and tPA [158]. Heparin stimulates the release of tPA from vessel walls [159] and enhances activation of Plg by binding to and potentially causing a conformational change to tPA [160]. In addition to Plg almost all members of the P97 and P102 adhesin families bind heparin [2-8,10,41] and many also bind Fn [5,7-9,42]. Thus the process of colonizing the ciliated epithelial lining of the porcine respiratory tract by *M. hyopneumoniae* brings plasmin, Fn and GAGs in close proximity to one another. The P97 and P102 adhesin families are multifunctional proteins that carry binding domains for heparin, Fn and Plg. We recently showed that i) Fn colocalises to the site where *M. hyopneumoniae* adheres to porcine epithelial cells and ii) colocalises on the ciliated epithelial border in the lungs of infected but not healthy pigs [42]. *M. hyopneumoniae* has evolved a sophisticated mechanism of generating a complex repertoire of cleavage fragments specialized in the ability to bind heparin, Fn and Plg as a means of colonizing the porcine respiratory tract. The binding of these host components bestows *M. hyopneumoniae* cells with a powerful tool with which they can interact with and influence a large subset of cellular systems. Given the

recent developments in the successful mutagenesis of *M. hyopneumoniae* [161], we can now begin to assess the importance of these heparin, Fn, and Plg-binding proteins.

We have recently characterized two aminopeptidases MHJ_0125 and MHJ_0461 on the surface of *M. hyopneumoniae* that encode a glutamyl-aminopeptidase and a leucyl-aminopeptidase respectively. Both aminopeptidases moonlight as surface assessable proteases and can bind to and enhance the activation of Plg [145,155]. Both proteins are functional as aminopeptidases and are thought to provide *M. hyopneumoniae* with a supply of amino acids for growth. We also hypothesise that the ability of these aminopeptidases to facilitate the production of plasmin, a broad spectrum serine protease that degrades ECM and activates matrix metalloproteinases with widespread proteolytic activity represents a mechanism to generate free N-termini that are substrates for these aminopeptidases [145,155]. As a genome-reduced pathogen that has lost the ability to synthesize amino acids *M. hyopneumoniae* is able to elicit proteolytic cascades in the lungs of pigs to ensure a supply of amino acids for growth [43,44,145]. To our knowledge MHJ_0125 and MHJ_0461 represent the first examples of aminopeptidases that moonlight as adhesins and plasmin(ogen) binding proteins on the surface of a bacterial pathogen.

M. hyopneumoniae is described as an extracellar pathogen with an affinity for ciliated epithelium in the porcine respiratory tract. It is not widely appreciated that *M. hyopneumoniae* has been isolated from the liver, spleen, kidneys and lymph nodes of infected pigs [14-16]. Isolation of viable *M. hyopneumoniae* from extrapulmonary sites suggests that it possesses the ability to invade lung tissue and disseminate systemically. We have previously shown that Plg is readily detectable in the bronchoalveolar lavage

(BAL) fluids that bath the ciliated airways in both healthy and *M. hyopneumoniae*-infected pigs [9]. Plasmin levels in BAL are significantly elevated in most pigs after experimental challenge with *M. hyopneumoniae* [9]. *M. hyopneumoniae* cells bind Plg and facilitate its conversion to plasmin by tPA (Seymour et al., 2012). Notably, surface bound plasmin was shown to degrade fibrinogen [9]. Subsequent studies found that there was a correlation between plasmin activity in the lung of experimentally challenged pigs and the host inflammatory response [34]. At 21 days post infection when plasmin levels were highest, the proinflammatory cytokines TNF-α, IL-1β and IL-6 were also elevated [34]. Increases in proinflammatory cytokines are a hallmark of infections caused by *M. hyopneumoniae* and are likely to be responsible for the lung pathology initiated by this pathogen [11-13]. Lymphoid hyperplasia of the bronchus-associated lymphoid tissue is common in the airways of *M. hyopneumoniae*-infected swine with macrophages and B lymphocytes being the most dominant [35]. These cells induce the expression of proinflammatory cytokines such as TNF-α and IL-1β which further promotes the infiltration of immune cells [36]. Transcriptome analysis of porcine alveolar macrophages infected with *M. hyopneumoniae* showed that proinflammatory cytokines IL-1β and TNF-α were up-regulated 41-fold and 6-fold respectively, further supporting previous findings [162]. Notably, pigs that received the commercial bacterin formulation Suvaxyn™ did not exhibit an increase in plasmin activity or proinflammatory cytokines in the BAL fluid compared to unvaccinated animals [34]. Vaccinated pigs developed less severe lung lesions suggesting that upregulation of plasmin activity and proinflammatory cytokines are major contributors of lung pathology [20,34]. Plasmin is a known chemo-attractant and activator of mononuclear cells [163,164]. Chemo-attraction is mediated via a cyclic guanosine monophosphate–dependent pathway. Activation of the pathway occurs via the Annexin II-S100a10

complex which stimulates Janus kinase JAK1/TYK2 signaling [163,165,166]. Annexin II-S100a10 is known to increase the activation of Plg to plasmin [167,168]. Plasmin cleaves the Annexin II-S100a10 heterotetramer which causes the stimulation of the Janus kinase JAK1/TYK2 signaling pathway in human macrophages; a process that leads to proinflammatory cytokine expression [111,163,166].

In summary, Plg is present along the ciliary borders of the porcine lung of healthy pigs and is readily available to be sequestered to the *M. hyopneumoniae* cell surface [9]. In the presence of tPA, *M. hyopneumoniae* promotes a localised increase in plasmin activity in the respiratory tract [9,34]. Plasmin activity correlates with an increase in proinflammatory cytokines, likely as a result of infiltration of mononuclear cells and the subsequent exploitation of the Annexin II-S100a10 complex and Janus kinase JAK1/TYK2 signaling pathway [34,111,163,164,166]. The airways of *M. hyopneumoniae*-infected pigs are known to become infiltrated by a large number of inflammatory cells; a likely effect of this positive feedback loop [9]. Stimulation of expression of proinflammatory cytokines is likely to play an important role in the development of the characteristic lung pathology known to be associated with *M. hyopneumoniae* infection [169]. This process is depicted in Figure 2.3.

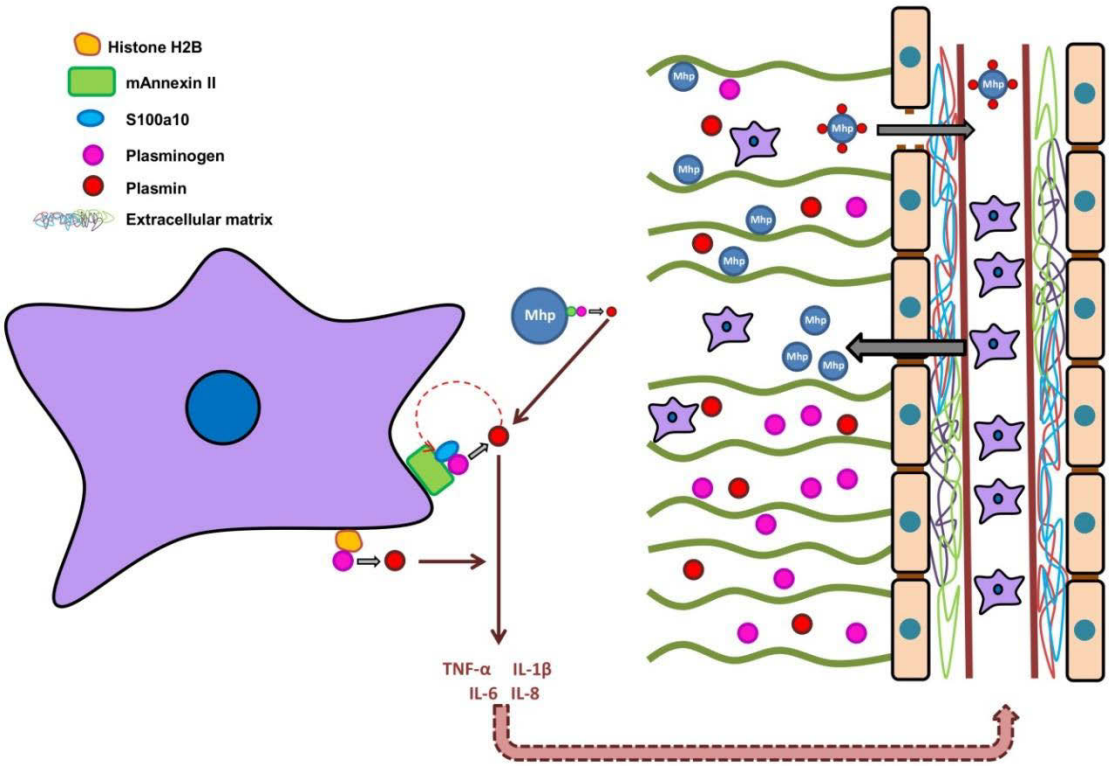

Figure 2.3: Cartoon depicting the interaction of *M. hyopneumoniae* with the fibrinolytic system.

At the site of infection *M. hyopneumoniae* cells adhere to the rapidly beating cilia and recruit Plg to their cell surface where it is activated to plasmin. Macrophages and other immune cells such as neutrophils infiltrate the site of infection, and due to the localised increase in plasmin activity, secrete proinflammatory cytokines. Proinflammatory cells induce the activation of Plg to plasmin through the annexin II-S100a10 complex and histone H2B. This initiates a cascade that attracts more immune cells to the site of infection.

2.5 Conclusion

Gram negative, Gram positive and genome reduced bacterial pathogens (Mollicutes) have all evolved strategies to commandeer host plasmin(ogen). Bacteria that colonize a wide variety of mucosal surfaces including the respiratory, genital and gastrointestinal tracts seem to deploy Plg-binding proteins as a means of colonizing these niche environments. In addition, bacteria also utilize the Plg system as a means to disseminate from their initial site of colonization and gain entry to distal tissue sites [84]. Highly specialized, species-specific surface proteins that bind Plg are expressed by most pathogenic bacteria. A feature that stands out is the multifunctional nature of these specialized proteins that bind Plg as many also bind key ECM molecules including Fn and various glycosaminoglycans. This is exemplified by studies in *M. hyopneumoniae*. Cleavage fragments derived from members of the P97 and P102 adhesin families are capable of binding Fn, heparin and Plg [2-10,41-44]. We recently identified an amino acid motif with the sequence KKSSLKVKITVK in the C-terminus of the cilium adhesion P123J that plays a central role in binding to Fn and heparin (Raymond et al., 2015). In addition to highly specialized Plg-binding adhesins, bacteria also employ multifunctional, highly conserved proteins to capture Plg onto their cell surface. These so called moonlighting proteins are described as anchorless because they lack signal secretion sequences. The precise mechanism by which moonlighting proteins localize to the cell surface has not been elucidated. Plg-binding moonlighting proteins are often members of the glycolytic pathway, chaperones and other metabolic enzymes and have been isolated from phylogenetically diverse bacteria [170-172]. While most Plg binding proteins have been characterized from pathogenic bacteria, commensal bacterial also display proteins that bind and activate Plg and play important roles in establishing interactions with their host [173-175]. These studies clearly show that the ability to

commandeer the plasmin(ogen) system arms both pathogenic and commensal bacteria with the ability to interface with and persist in the host environment.

Chapter Three: (Paper II) *M. hyopneumoniae* surface adhesins undergo extensive endoproteolytic processing

Declaration

I declare that the following publication included in this thesis in lieu of a chapter meets the following:

- More than 50% of the content in the following publication included in this chapter has been planned, executed and prepared for publication by me
- The work presented here has been peer-reviewed and accepted for publication
- I have obtained approval to include the publication in this thesis from the Publisher
- The initial draft of the work has been written by me and any subsequent changes in response to co-authors and editors reviews was performed by me
- The publication is not subject to any obligations or contractual agreements with a third party that would constrain its inclusion in the thesis.

Publication title: P159 from *Mycoplasma hyopneumoniae* binds porcine cilia and heparin and is cleaved in a manner akin to ectodomain shedding

Authors: Benjamin B.A. Raymond, Jessica L. Tacchi, Veronica M. Jarocki, F. Chris Minion, Matthew P. Padula and Steven P. Djordjevic

Candidate's contribution (%): above 50 %

Journal name: Journal of Proteome Research

Volume/ page numbers: 12(12):5891-903

Status: Published

I declare that the publication above meets the requirements to be included in the thesis.

Candidate's name: Candidate's signature: Date (dd/mm/yy):

3.1 Introduction

Mycoplasma hyopneumoniae remains an economically significant threat to the health of swine despite widespread vaccination with bacterin formulations. Vaccination reduces lung pathology and improves weight gain but fails to prevent colonisation of the respiratory tract by *M. hyopneumoniae* [25,176-179]. *M. hyopneumoniae* is a genome-reduced, swine-specific bacterial pathogen and the number of predicted ORFs determined by *in silico* analysis of the genome sequences of four geographically diverse strains (232, J, 7448, 168) is approximately 700 [156].

M. hyopneumoniae preferentially colonises the surface of cilia and microvilli on porcine respiratory epithelium [17,180]. Cilium and epithelial cell adhesion is a complex process involving a number of cell surface proteins, many of which belong to the P97 and P102 paralog adhesin families. The P97 and P102 adhesin families each share 30% sequence identity [156] and display redundant functions as cilium, Fn, Plg and glycosaminoglycan-binding proteins. Genes encoding six paralogs of the archetype cilium adhesin P97 (MHJ_0369/Mhp385, MHJ_0264/Mhp107, MHJ_0663/Mhp684, MHJ_0096/Mhp280, MHJ_0105/Mhp271, MHJ_0493/Mhp493) and six paralogs of P102 (MHJ_0368/Mhp384, MHJ_0263/Mhp108, MHJ_0662/Mhp683, MHJ_0104/Mhp272, Mhp274 and Mhp275) from strains J and 232 respectively are conserved.

While P97 and P102 and their paralogs are heavily expressed during broth culture they are presented on the membrane surface of *M. hyopneumoniae* as cleavage fragments derived by endoproteolytic processing [3,5-10,54]. Dominant processing events are typically confined to the carboxyl side of phenylalanine residues within the motif S/T-

X-F↓X-D/E [3]. Other cleavage motifs are believed to play a role in shaping the surface protein topography of *M. hyopneumoniae*, but some of these have not been experimentally verified [5,6,54]. Members of the P97 and P102 families often carry coiled-coil motifs and expansive regions of protein disorder spanning more than 40 consecutive amino acids [2,3,5,6]. Dominant cleavage sites that adhere to the S/T-X-F↓X-D/E motif typically reside within disordered regions [2,3,5,6] suggesting that disorder can influence the accessibility of cleavage motifs in the pre-protein to proteolytic cleavage. The most abundant cleavage fragments derived from P97 and P102 paralog families are multifunctional cilium adhesins that bind glycosaminoglycans [2-6,8,10,41], Fn [5,7-9], and Plg [2,7-9]. The ability to bind highly sulphated glycosaminoglycans is considered significant during the early stages of colonisation because heparin effectively blocks binding of *M. hyopneumoniae* to porcine respiratory tract cilia [4,5,32]. Surface proteins of *M. hyopneumoniae* that do not belong to the P97 and P102 paralog families also bind glycosaminoglycans and Plg, underscoring the importance of these interactions to the survival of the species [145].

P159 (Mhp494) is not a member of the P97 and P102 paralog families yet it is known to be a cellular adhesin [4]. The P159 homolog from strain 232 comprises 1410 amino acids and is processed to form N-terminal, central and C-terminal fragments of 27 kDa (P27), 110 kDa (P110) and 52 kDa (P52) respectively, and these cleavage fragments are presented on the surface of *M. hyopneumoniae*. Previously, we examined the functions of these three dominant cleavage products by expressing four polyhistidine-tagged proteins ($F1_{P159}$-$F4_{P159}$ spanning amino acids 31-264, 265-519, 558-909 and 958-1405 respectively) in *Escherichia coli*. P159 is not detectable by SDS-PAGE or by immunoblotting using serum against F2-$F4_{P159}$. C-terminal recombinant fragments

$F3_{P159}$ and $F4_{P159}$ bound heparin and latex beads coated with recombinant fragments $F2_{P159}$ - $F4_{P159}$ displayed the ability to adhere to porcine kidney epithelial-like (PK-15) cells [4]. P159 is subject to further cleavage events because western blots exposed to antiserum raised against $F2_{P159}$ and $F3_{P159}$ identified 76 kDa (P76) and 35 kDa (P35) cleavage fragments and numerous less abundant fragments [4]. We were unable to determine the precise cleavage sites that generate P27, P52 or P110 in our earlier study, but showed that cleavage events were confined to regions spanning amino acids 219-303 and 841-978 [4].

Our proteome data indicates that P159 is abundantly expressed. Here we have characterised the precise endoproteolytic cleavage events that define the dominant (P27, P110, P52) and major (P76, P35) cleavage fragments, and assessed the ability of recombinant fragments $F1_{P159}$ – $F4_{P159}$ spanning P159 to bind to porcine respiratory tract cilia. We also provide compelling evidence that P159 is extensively processed, generating numerous surface-accessible cleavage fragments, many of which retain the ability to bind glycosaminoglycans. Processing requires the activity of different proteases and generates a large combinatorial library of cleavage fragments that create functional diversity on the surface of *M. hyopneumoniae*.

3.2 Materials and Methods

3.2.1 Culture Conditions

M. hyopneumoniae (strain J) was grown in modified Friis broth [181] and harvested as described previously [182]. The recipe for Friis medium is shown in Table S3.1. The yeast extract detailed in this recipe was made by diluting 167g Baker's yeast type (II) in 1L MilliQ water and incubating at 37°C for 20 minutes followed by heating at 100°C for 5 minutes. Once cool, the debris was removed by centrifuging at 2,000 x g 30 min at RT, retaining the supernatant and centrifuging again until the supernatant was clear. The supernatant was filtered through a 0.2 μm filter and aliquoted.

Cells were grown in Friis broth for approximately 48 h at 37°C until the medium turned a light orange colour at which point they were centrifuged at 11, 000 × g for 10 min and washed with PBS 3 times. Washed pellets were stored at – 20°C until required.

3.2.2 Cell Surface Analyses

Cell surface biotinylation was carried out as described previously [3] on intact cells using EZ-link sulfo-NHS-biotin (Thermo Fischer Scientific), combined with avidin column purification and/or blotting to purify or identify biotinylated surface proteins [3,183]. Described ad verbum from [3]: for surface biotinylation experiments, freshly harvested *M. hyopneumoniae* cells were washed extensively (>3 times) in PBS (4000 × g, 30 min, 4 °C) and pelleted by centrifugation (9000 × g, 10 min, 4 °C). Cells were resuspended in PBS (pH 7.8) and biotinylated with sulfo-NHS-LC biotin (Thermo Scientific) for 30 s on ice. The reaction was then quenched with the addition of a final concentration of 50 mm Tris-HCl, pH 7.4 and incubated for 15 min. Cells were washed in three changes of PBS and pelleted by centrifugation. A 0.1 g pellet of M. hyopneumoniae cells was resuspended in solubilisation buffer (7 m urea, 2 m thiourea,

40 mm Tris (pH 8.8), 1% (w/v) C7bZ0) and disrupted with four rounds of sonication at 50% power for 30 s bursts on ice. Proteins were reduced and alkylated with 20 mm acrylamide monomers, 5 mm TBP for 90 min. Insoluble material was pelleted by centrifugation. Soluble proteins were precipitated in 5 volumes of ice-cold acetone for 30 min, and the pellet was air-dried and then resuspended in 7 m urea, 2 m thiourea, 1% (w/v) C7bZ0. Biotinylated proteins were purified by avidin column affinity chromatography by incubating the lysate with avidin agarose (Thermo Scientific), collecting the flow through and washing extensively using 100 mM NH_4HCO_3. Biotinylated proteins were recovered by eluting in 30% acetonitrile and 0.4% trifluoroacetic acid. Biotinylated proteins were separated by two-dimensional gel electrophoresis and identified by Western blotting. Spots corresponding to biotinylated proteins were cut from simultaneously run two-dimensional gels and examined using LC-MS/MS.

Enzymatic cell surface shaving with trypsin was also used as described previously [5]. Washed *M. hyopneumoniae* cells were incubated in PBS or 50 μg/ ml trypsin in PBS for 5 min at 37°C. Liberated surface proteins were collected, reduced and alkylated, and further digested to peptides with trypsin for LC-MS/MS analysis as described previously and in section 3.2.6 [184].

3.2.3 Preparation of *M. hyopneumoniae* whole cell lysate

Procedures used to generate whole cell lysates of *M. hyopneumoniae* have been described earlier [9]. Briefly, a 0.1 g pellet of *M. hyopneumoniae* cells was resuspended in solubilisation buffer (7M urea, 2M thiourea, 40mM Tris-Hcl pH 8.8, 1% (w/v) C7BzO) and disrupted with four rounds of sonication at 50% power for 30 second (s)

bursts on ice. Proteins were reduced and alkylated with 20 mM acrylamide monomers and 5 mM tributylphosphine (TBP) for 90 minutes. Insoluble material was pelleted by centrifugation. Protein was precipitated in five volumes ice cold acetone for 30 minutes and the pellet air dried. Protein pellet was resolubilised in 7M urea, 2M thiourea, 1% (w/v) C7BzO, supplemented with 0.2% 3-10 BioLyte ampholytes (BioRad) for 2D separation.

3.2.4 One- and two-dimensional gel electrophoresis and immunoblotting

A detailed protocol for performing 1D and 2D gel electrophoresis and immunoblotting has been described previously [6]. For 1D gel electrophoresis proteins were separated by SDS-PAGE and gels were fixed and visualized by staining with either Flamingo™ fluorescent gel stain (BioRad) or colloidal Coomassie Blue G-250. For 2D gel analyses, 250 µg of protein was cup-loaded onto partially rehydrated 11 cm pH 4-7 immobilised pH gradient (IPG) strips (BioRad) or 6-11 Immobiline drystrips (GE Healthcare). Focusing was performed in a BioRad Protean IEF cell at a constant 20˚C and 50 µA current limit per strip with a 3-step program: slow ramp to 4000 V for 4 hours, linear ramp to 10000 V for 4 hours, then 10000 V until 120 kVh was reached. Following IEF, the strips were equilibrated with 5 mL equilibration solution (2% SDS, 6 M urea, 250 mM Tris-HCl pH 8.5, 0.0025% (w/v) bromophenol blue) for 20 minutes before the second dimension SDS-PAGE. *M. hyopneumoniae* proteins separated by 1D or 2D SDS-PAGE were blotted onto PDVF membrane using a semi-dry transfer method [185]. Membranes were blocked with 5% (w/v) skim milk powder in phosphate buffered saline (PBS) with 0.1% Tween 20 (v/v) (PBS-T) at room temperature (RT) for one hour and incubated with $F1_{P159}$ - $F4_{P159}$ polyclonal antisera (diluted 1:100 in PBS-T) for 1 h at RT. Blots were washed and exposed to peroxidase conjugated anti-pig

antibodies (diluted 1:3000 in PBS-T) for 1 hour. Membranes were routinely washed in three changes of PBS-T and developed with SIGMA*FAST*™ 3,3′-diaminobenzidine (DAB) tablets (Sigma-Aldrich) as per manufacturer's instructions.

3.2.5 Affinity chromatography

M. hyopneumoniae whole cell lysates were prepared by sonicating washed cell pellets in 10 mM sodium phosphate, pH 7 on ice for 3 rounds of 30 s bursts. Insoluble material was pelleted by centrifugation at 16000 *g* for 10 minutes. *M. hyopneumoniae* soluble protein (300 µg) was loaded into an autosampler vial on a Waters 2690 Alliance LC separations module and loaded at 0.5 ml min^{-1} onto a 1 mL HiTrap™ Heparin HP column (GE healthcare) in binding buffer (10 mM sodium phosphate, pH 7). The standard elution program was run at 0.5 ml min^{-1} with continuous gradients as follows: Sample was loaded and washed with 100% binding buffer (20 min) followed by 0-50% elution buffer (10 mM sodium phosphate, 2 M sodium chloride, pH 7) (25 min), 50-100% elution buffer (10 min), 100% elution buffer (5 min), before returning to 100% binding buffer. The elution profile was monitored at *A* 210 – 400 nm with a Waters 996 photodiode array detector and fractions were collected in 3 min intervals using a Waters fraction collector III.

3.2.6 1D LC-MS/MS using QTOF

Sample (10 µl) was loaded at 20 µl min^{-1} with MS buffer A (2% Acetonitrile + 0.2% Formic Acid) onto a C8 Cap Trap column (Michrom, USA) using an Eksigent AS-1 autosampler connected to a Tempo nanoLC system (Eksigent, USA). After washing the trap for 180 s the peptides were washed off the trap (300 nL min^{-1}) onto an IntegraFrit column (75 µm x 100 mm) packed with ProteoPep II C18 resin (New Objective,

Woburn, MA). Peptides were eluted from the column and into the source of a QSTAR Elite hybrid quadrupole-time-of-flight mass spectrometer (Applied Biosystems/MDS Sciex) using the following program: 5-50% MS buffer B (98% Acetonitrile + 0.2% Formic Acid) over 30 minutes for gel slices or 15 minutes for gel spots, 50-80% MS buffer B over 5 minutes, 80% MS buffer B for 2 minutes, 80-5% for 3 minutes. The eluting peptides were ionized with a 75 μm ID emitter tip that tapered to 15 μm (New Objective) at 2300 V. An Intelligent Data Acquisition (IDA) experiment was performed, with a mass range of 375-1500 Da continuously scanned for peptides of charge state 2+ - 5+ with an intensity of more than 30 counts/scan and a resolution >12000. Selected peptides were fragmented, and the product ion fragment masses measured over a mass range of 100-1500 Da. The mass of the precursor peptide was then excluded for 120 s for gel slices or 15 s for gel spots.

3.2.7 MS/MS Data Analysis

The MS/MS data files were searched using Mascot (provided by the Australian Proteomics Computational Facility, hosted by the Walter and Eliza Hall Institute for Medical Research Systems Biology Mascot Server) against the LudwigNR database (comprised of the UniProt, plasmoDB and Ensembl databases (vQ312. 19375804 sequences; 6797271065 residues)) with the following parameter settings. Fixed modifications: none. Variable modifications: propionamide, oxidised methionine. Enzyme: semitrypsin. Number of allowed missed cleavages: 3. Peptide mass tolerance: 100 ppm. MS/MS mass tolerance: 0.2 Da. Charge state: 2+ and 3+. For biotinylated samples, variable modifications also included biotinylated lysine and N-terminal biotinylation.

3.2.8 Avidin purification of interacting proteins

To identify *M. hyopneumoniae* proteins that bind to surface proteins on porcine kidney (PK15) epithelial cells, a protocol adapted from [186] was used. One 175 cm^2 culture flask containing semi-confluent PK-15 cells was washed 3 times with ice cold PBS (pH 8.0) to remove medium components. Cells were detached by incubating with TrypLE™ Express (Life Technologies) for 10 minutes at RT. Cells were washed twice with PBS by centrifugation to remove any excess reagent. Cells were then labeled with 2 mM EZ-link sulfo-NHS-biotin (4˚C for 30 minutes) with gentle inversion. PBS with 100 mM glycine was added to quench the reaction and remove excess biotin (10 minutes at RT). Glycine was removed by washing twice in PBS. Cells were lysed in 1.0% Triton X-100 in Tris-HCl pH 7.6, 150 mM NaCl with protease inhibitors on ice (30 minutes) with vortexing. After insoluble material was removed by centrifugation, the cleared lysate was added to avidin agarose (Thermo Scientific) and incubated (1 hour at RT) on a rotating wheel. The slurry was then packed into a column and the flow through was collected for monitoring by SDS-PAGE. Unbound proteins were removed by 6 washes with PBS.

M. hyopneumoniae cells from a 250 ml culture were pelleted, washed with PBS and gently lysed in 0.5% Triton X-100 in Tris-HCl pH 7.6, 150 mM NaCl with protease inhibitors on ice with vortexing and water bath sonication. Insoluble material was removed by centrifugation at 16000 *g* for 10 minutes, and the cleared lysate incubated with the biotinylated PK-15-avidin agarose mixture overnight at 4˚C on a rotating wheel. The mixture was packed into a column, the flow through collected, and non-interacting proteins were removed by washing 6 times with 25 mM Tris-HCl in 150 mM NaCl, pH 7.4. Interacting proteins were collected by eluting 5 times with 100 mM Tris-HCl in 2 M NaCl, pH 7.4. A secondary elution in 30% acetonitrile and 0.4%

trifluoroacetic acid was performed in order to collect the biotinylated PK-15 proteins and any strongly bound *M. hyopneumoniae* proteins which were not eluted by 2M NaCl. The salt and acidic elutions were concentrated separately through 3000 dalton cut-off filters and then acetone precipitated at -20°C for 30 minutes and finally pelleted by centrifugation at 25000 *g* at 4°C for 30 minutes. Protein was resuspended in SDS sample buffer and separated by 1D SDS-PAGE. Proteins were in-gel trypsin digested and analysed by LC-MS/MS.

3.2.9 Bioinformatic analyses of P159

Bioinformatic analysis of P159 used online resources: ProtParam [187], COILS [188] and PONDR VSL1 [189].

3.3 Results

3.3.1 P159 is an endoproteolytically processed, modular cell surface protein

The J strain homolog of P159 MHJ_0494 (Swiss-Prot: Q4A9J1) comprises 1427 amino acids and has a predicted p*I* of 8.05. P159 carries almost identical numbers of positively charged (198 K/R residues) and negatively charged (195 D/E residues) amino acids but their arrangement in the sequence is unevenly distributed. Analysis of charge distribution shows P159 is a modular protein that contains three acidic domains, approximately 200 amino acids in length, that are enriched in aspartic acid (D) and glutamic acid (E) residues spanning amino acids 200-370 (acidic domain 1; p*I* 5.7), 820-1000 (acidic domain 2; p*I* 4.8) and 1230-1427 (acidic domain 3; p*I* 5.8). Four regions spanning a minimum of 40 amino acids that display protein disorder were identified in P159 using PONDR and PrDOS algorithms and four coiled coil regions were identified using EMBnet COILS (Figure 3.1). Of four regions displaying protein disorder, domains 1, 3 and 4 align closely with acidic domains (Figure 3.1).

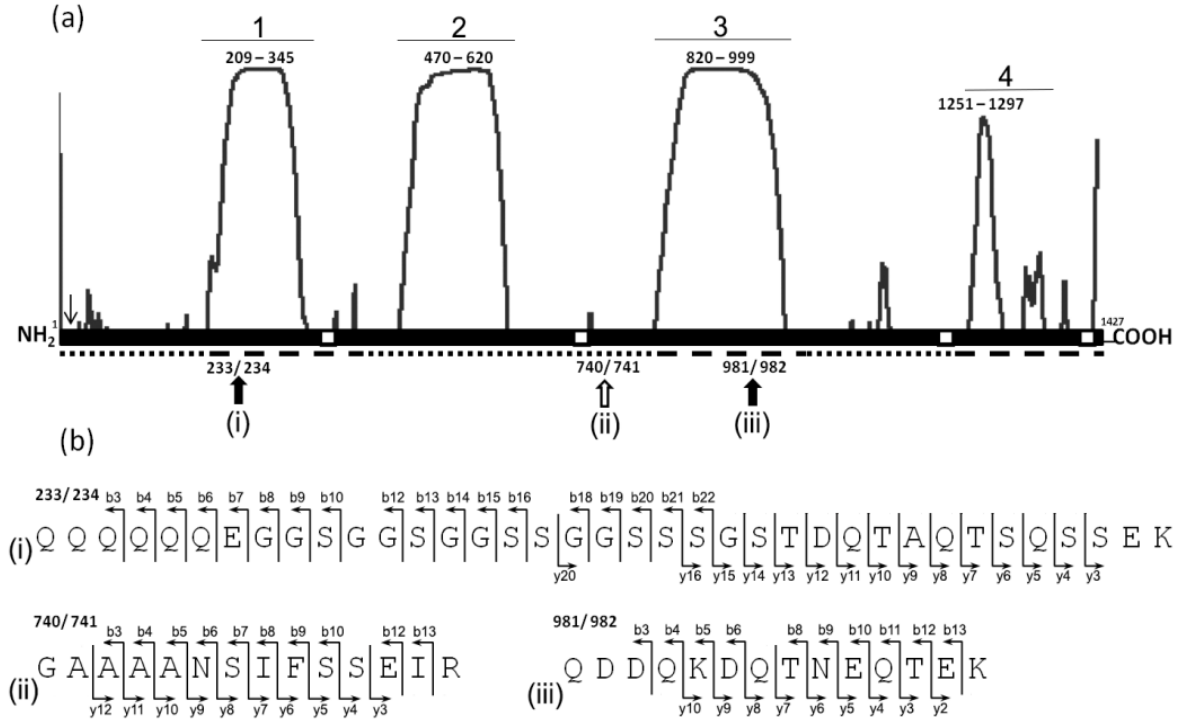

Figure 3.1: Structural analysis of P159.

A) regions of disorder within P159 (black bar) as peaks above the molecule, labeled 1, 2, 3 and 4, predicted by PONDR VSL1 [189]. Dominant cleavage sites are shown by solid black arrows (i and iii) and a major cleavage site is represented by a hollow arrow (ii). Coiled coil regions as predicted by COILS [188] are shown by white boxes. Small dashed lines represent regions within P159 that are rich in basic amino acids and larger dashed lines represent those rich in acidic amino acids. B) shows sequences of semi-tryptic peptides identified at positions i-iii as indicated in panel a, denoting the N-terminus of cleavage fragments. Spectra shown in Figure S3.1.

3.3.2 Identification of cleavage sites that generate P27, P110 and P52

Recently we reported the location of dominant endoproteolytic cleavage sites bearing an S/T-X-F↓X-D/E motif within regions of protein disorder in members of the P97 and P102 paralog families [2,3,6]. P159 is not a member of the P97 and P102 paralog families but it is a target of endoproteolytic processing so much so that P159 is undetectable by SDS-PAGE. These cleavage events generate N-terminal 27 kDa (P27), central 110 kDa (P110) and C-terminal 52 kDa (P52) fragments, representing the major effector molecules of P159 [4]. While we were previously unable to define the precise cleavage sites that created these fragments, cleavage sites were localized to regions spanning amino acids 219-303 and 841-978 in the P159 homolog in *M. hyopneumoniae* strain 232 [4] which shares 95.6% sequence identity at the amino acid level with the strain J homolog. LC-MS/MS analysis of whole cell lysates described in Seymour [9] identified a large semi-tryptic peptide spanning 37 amino acids (position 234-270) which defined the cleavage site that generated P27 to reside within the sequence ^{231}T-E-F↓Q-Q-Q-Q-Q-Q^{239} with cleavage occurring at position 233 after the phenylalanine reside (Figure 3.1). Dominant cleavage sites in P97 and P102 paralog family members have been known to follow a phenylalanine (F) residue that precedes a short run of glutamine residues (Q) [3,6]. The same approach was used to identify the cleavage site that generates P52 in the sequence ^{979}T-T-F↓Q-D-D^{984} with cleavage occurring at the phenylalanine residues at position 981. Spectra that confirm the identities of these cleavage site peptides are shown in Figure S3.1.

3.3.3 Identification of cleavage fragments of P159 by 2D SDS-PAGE and LC-MS/MS

We previously constructed four recombinant polyhistidine fusion proteins ($F1_{P159}$-$F4_{P159}$) spanning regions along P159 and generated polyclonal antisera against each of these proteins [4]. To identify processing events in P159, LC-MS/MS analysis was performed on all *M. hyopneumoniae* strain J protein spots separated by 2D SDS-PAGE using immobilized pH gradients from 4-7 and 6-11 (Figure 3.2). The identities of P27, P110 and P52 in strain J were confirmed by LC-MS/MS of tryptic peptides generated from protein spots shown in Figure 3.2. In addition, four cleavage fragments within the central 110 kDa fragment of P159 (P110) were identified, two of which represent N-terminal 76 kDa (P76) and C-terminal 35 kDa (P35) fragments (Figure 3.2). P35 (Fragment 7) comprises 240 amino acids (position 741-981), spans most of acidic domain 2 and migrates with a p*I* of 5.25. P35 was identified in a short spot train with a mass of 35 kDa and p*I* of 5.3 in 2D immunoblots probed only with anti-$F3_{P159}$ serum (Figure 3.3). Loss of P35 from the C-terminus of P110 generates P76 which comprises amino acids 234-740 and migrates with a p*I* of 8.48 (Figure 3.2). This is consistent with a ~75 kDa spot train (Fragment 3) on 2D immunoblots probed separately with anti-$F2_{P159}$ and anti-$F3_{P159}$ (Figure 3.3). Both P35 and P76 migrate abnormally during SDS-PAGE because their predicted masses are 28 kDa and 56 kDa respectively. We attribute the abnormal migration during SDS-PAGE to the pockets of acidic residues found in the N-terminus of P76 and most of P35. Consistent with these data, a semi-tryptic cleavage peptide ^{741}GAAAANSIFSSEIR^{754} (Figure 3.1) which delineates the N-terminus of P35 was identified by LC-MS/MS. We also identified the sequence GAAAANSIFSS by Edman degradation of a protein eluted from a protein spot containing P35 (data not shown).

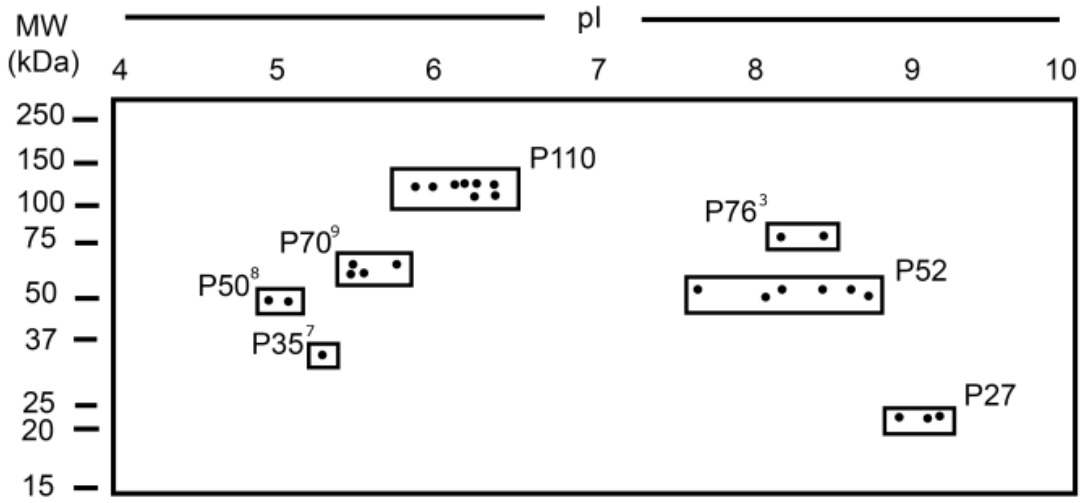

Figure 3.2: Mock 2D gel indicating locations of spots containing peptides mapping to P159.

Seven distinct fragments of P159 were identified from 2D gels. Superscript numbers correspond to fragments described in Figure 3.8.

Two novel cleavage fragments with p*I* between 4.9 and 6.0 with masses of 50 kDa (P50; Fragment 8) and 70 kDa (P70; Fragment 9) respectively were also observed. These cleavage fragments span regions within P159 lacking K and R residues, and tryptic peptides generated from protein spots representative of these two cleavage fragments do not provide comprehensive coverage to accurately map their identities. Nonetheless, P50 has its N-terminus at the same position as P35 as we also identified the N-terminal semi-tryptic peptide ^{741}GAAAANSIFSSEIR^{754} by LC-MS/MS of P50-containing spots (Figure S3.1). Thus, the P50 sequence must extend past the ^{979}T-T-F↓Q-D-D^{984} cleavage site into the N-terminus of P52 but by how many amino acids cannot be determined at this time. P50 is present as a ~50 kDa spot train on 2D immunoblots (Fragment 8; Figure 3.3) probed separately with anti-F3$_{P159}$ and anti-

$F4_{P159}$ serum. LC-MS/MS analysis of spots containing P70 generated almost identical tryptic peptide coverage as P35 except that we identified the tryptic peptide ^{740}VGAAAASNIFSSEIR^{754} (Figure S3.1). These data suggest that P70 encompasses all of P35 but contains sequences that overlap with P76 at its N-terminus and P52 at its C-terminus. Proteins of 35 kDa (P35), 50 kDa (Fragment 8) and 70 kDa (Fragment 9) were all detected by anti-$F3_{P159}$ serum on 2D immunoblots with p*I* from 5.3-6.2. Unlike P35, Fragments 8 (P50) and 9 (P70) also reacted with anti-$F4_{P159}$ on 2D immunoblots (Figure 3.3) indicating that they both contain sequences within P52.

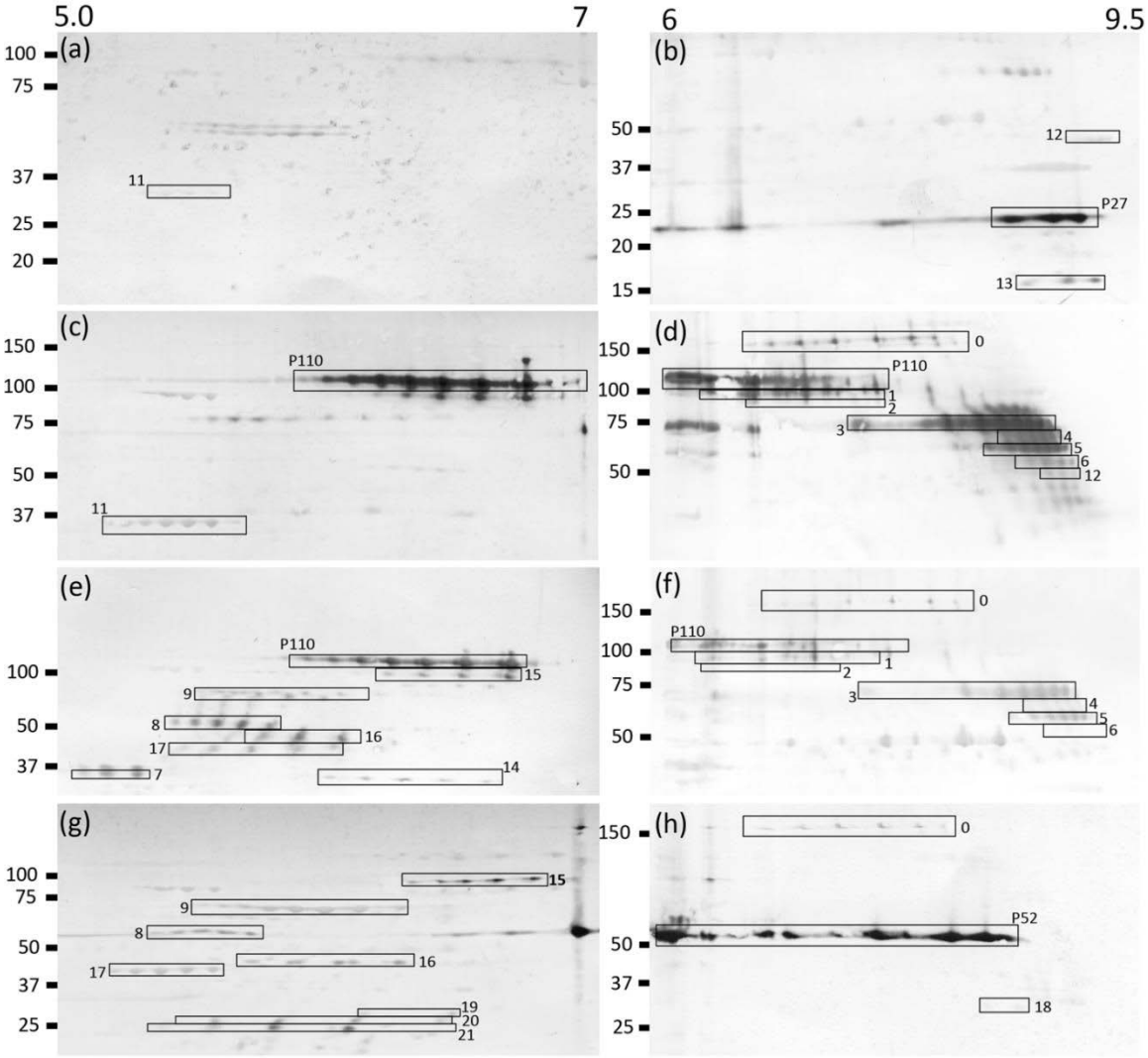

Figure 3.3: 2D Immunoblots probed with $F1_{P159}$ – $F4_{P159}$.

The left column of gels represents proteins that were separated in the pH 4-7 range and the right column are those which were separated in the pH 6-11 range. Blots were probed with anti-$F1_{P159}$ (panels a and b), anti-$F2_{P195}$ (panels c and d), anti-$F3_{P159}$ (panels e and f), anti-$F4_{P159}$ (panels g and h). Cleavage fragments reported by Burnett *et al.* [4] are labeled and novel cleavage fragments are boxed and numbered.

The majority of fragments were identified to occur in spot trains, comprising proteoforms of varying isoelectric point. Previous studies have indicated post-translational modifications such as phosphorylation occur in *M. hyopneumoniae* and other Mycoplasma species in proteins that resolve as spot trains during 2D SDS-PAGE [190,191]. Spot trains could be due to various modifications reflecting bona fide post-translational modifications that alter the pI or are an artefact generated during sample preparation [192].

3.3.4 Identification of lower abundance cleavage fragments of P159.

We employed several approaches to identify low abundance cleavage fragments. *M. hyopneumoniae* cells were briefly exposed to sulfo-NHS-biotin. Biotinylated proteins were recovered by affinity chromatography and characterized by LC-MS/MS. Tryptic fragments that carry a biotin adduct on the N-terminal amine group represent bona fide neo N-termini. 2D immunoblots of whole cell protein preparations using p*I* gradients from 4-7 and 6-11 were probed with F1-F4$_{P159}$ antisera to determine if cleavage was consistent with the location of these N-termini. We identified approximately 60 unique spots on 2D blots indicating that P159 is a target of multiple processing events (Figure 3.3). Enrichment protocols where LC-MS/MS was used to characterize P159 fragments recovered from heparin agarose proved useful to identify peptides mapping to low abundance cleavage fragments.

Blots probed with anti-F1$_{P159}$ reacted strongly with P27 as expected and identified a 17 kDa fragment (Fragment 13) with a p*I* of ~9 (Figure 3.3). LC-MS/MS analysis of *M. hyopneumoniae* proteins that bound heparin agarose identified tryptic peptides of P159

spanning amino acids 47-208 and 128-198 in gel slices from 20-25 kDa (Fragment 27) and 15-20 kDa (Fragment 28), respectively (Figure 3.5).

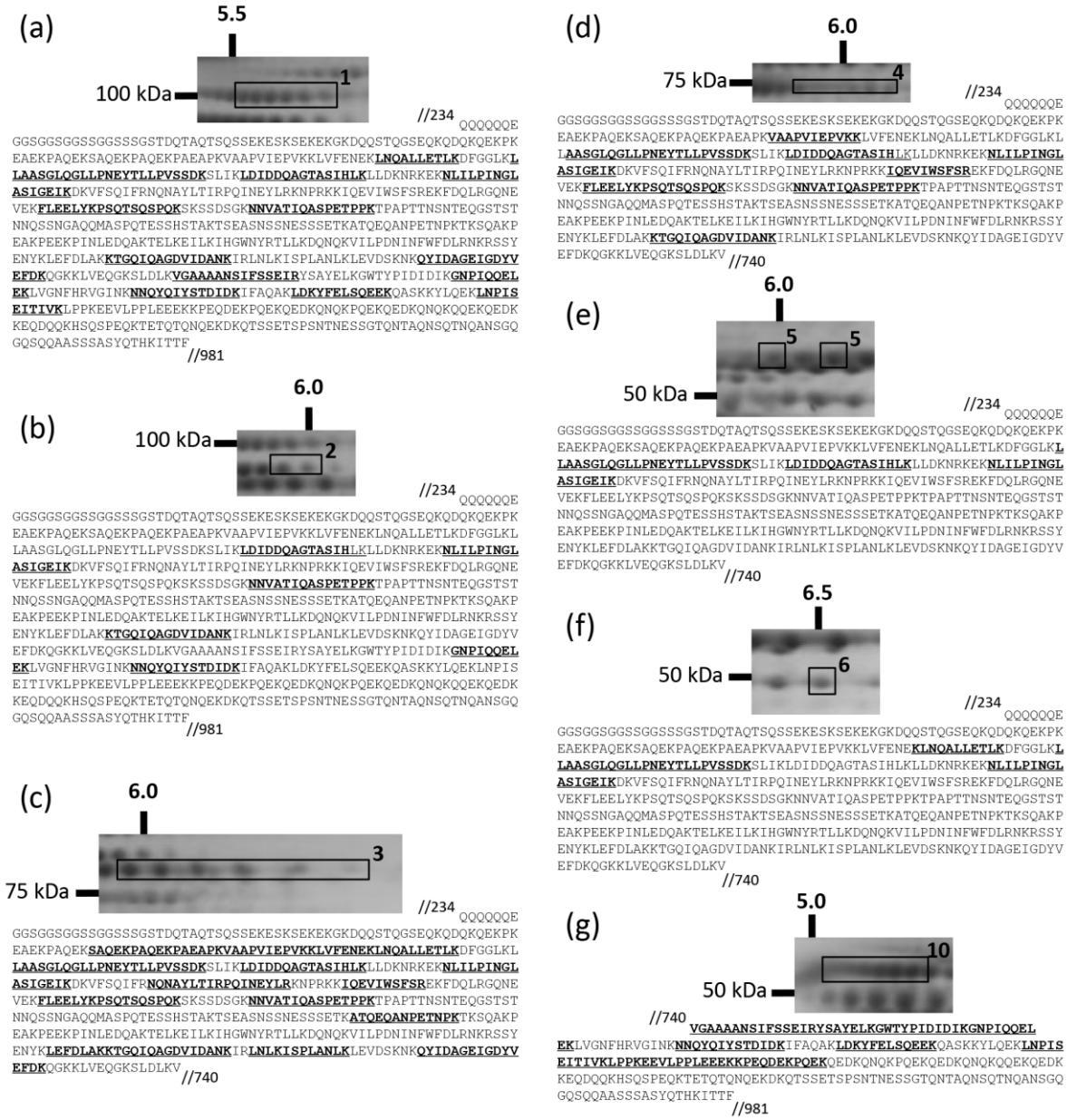

Figure 3.4: Biotinylated *M. hyopneumoniae* surface proteins captured by avidin chromatography resolved by 2D PAGE.

Peptides spanning P159 are underlined in each panel and were identified by LC-MS/MS from single spots or a train of spots in the corresponding gel image. Spot numbers correspond to Figure 3.8.

P27 has a p*I* of ~9.0 (Figure 3.2). However, anti-$F1_{P159}$ and anti-$F2_{P159}$ sera (Fragment 11) both recognized protein spots, which contain portions of P27 of 35 kDa with p*I* of 5.2-5.5. To accommodate the large shift in p*I*, we propose that Fragment 11 spans amino acids 42-361 containing acidic domain 1, generating a protein with a theoretical mass and p*I* of 35.4 kDa and 6.0 respectively. A tryptic peptide carrying a biotinylated N-terminus with the sequence ^{362}AASGLQGLLPNEYTLLPVSSDK^{383} (Figure S3.2c) within P110 was detected supporting this hypothesis.

Anti-$F2_{P159}$ and anti-$F3_{P159}$ sera detected many fragments of P159. Proteins marked as P110 generated tryptic peptides (data not shown) spanning amino acids 234-981, have a predicted p*I* of 6.16 (Figure 3.3) and, as expected, are recognized by anti-$F2_{P159}$ and anti-$F3_{P159}$ sera (Figure 3.3 panels c and e). A 100 kDa fragment (Fragment 1) generated tryptic peptides that mapped to all but the C-terminal 10 kDa of P110 (Figure 3.4). Fragment 1 has a predicted p*I* of 6.4 consistent with where it resides in Figure 3.3. LC-MS/MS analysis of fragments 2, 3, 4, 5 and 6 identified tryptic peptides spanning different regions of P110 that have progressively lost part of the C-terminus, react with anti-$F2_{P159}$ and anti-$F3_{P159}$ sera and display a basic p*I* (Figure 3.4). Two peptides, ^{594}TKSQAKPEAK^{603} and ^{672}KTGQIQAGDVIDANK^{686} carrying biotinylated N-termini (Figure S3.2d and e) reside within P76 (Figure 3.6). Fragment 3 generated tryptic fragments spanning amino acids 234–740, migrates with a p*I* of 7.5–8.5 and reacts with anti-$F2_{P159}$ and anti-$F3_{P159}$ sera consistent with it representing P76. Fragment 10 has an almost identical mass and p*I* to Fragment 8 (Figure 3.4) but we identified the tryptic peptide ^{740}VGAAAASNIFSSEIR^{754} instead of the semi-tryptic peptide ^{741}GAAAANSIFSSEIR^{754}. This suggests that Fragment 10 is a slightly larger minor variant of Fragment 8 which cannot be distinguished from one another on 2D

immunoblots. Fragments 8, 9, 15, 16 and 17 are recognized by anti-$F3_{P159}$ and anti-$F4_{P159}$ on 2D immunoblots. We hypothesize that fragment 10 spans amino acids 672-1093, generating a protein with a predicted mass and p*I* of 48.2 kDa and 5.17, respectively. This fragment is generated by two cleavage events at $K{\downarrow}K^{672}$ (^{672}KTGQIQAGDVIDANK^{686}) and $K{\downarrow}T^{1094}$ (^{1094}TGDKPYLQGR^{1103}). Fragment 9 has a mass of 70 kDa and p*I* of 5.7 and was identified by LC-MS/MS analysis of protein spots cut from 2D gels (Figure 3.2). Fragment 9 is likely to span amino acids 594-1170, and such a fragment would display a predicted mass of 66.2 kDa and p*I* of 5.95. Fragment 15 spans amino acids 594-1427 generating a protein with a mass of 95.6 kDa and a p*I* of 6.80. Fragment 16 has a mass of 43.6 kDa and a p*I* of 5.71. A protein that spans amino acids 672-1093 would display a mass of 48 kDa and a p*I* of 5.2. Fragment 17 has a mass of 40 kDa and a p*I* of 5.2. We predict that Fragment 17 spans amino acids 741-1093 generating a protein with a mass of 40.6 kDa and a p*I* of 5.05. There appeared to be three cleavage fragments (Fragments 19-21) residing within P52 (Figure 3.3). We identified two N-terminal biotinylated peptides within P52 (Figure S3.2a and b). These cleavage sites are capable of generating numerous combinations of cleavage fragments consistent with Fragments 19-21 shown in Figure 3.3. These data suggest that other, as of yet uncharacterized cleavage sites reside within P52.

Biotinylated *M. hyopneumoniae* proteins recovered by avidin chromatography were also resolved using 1D SDS-PAGE and characterized by LC-MS/MS analysis. Using this approach we identified Fragment 0 with a mass of about 160 kDa that is recognized with anti-$F2_{P159}$, anti-$F3_{P159}$ and anti-$F4_{P159}$ sera (Figure 3.3, panels d, f and h). Tryptic peptides identified by LC-MS/MS spanned P110 and P52 (amino acids 234 – 1427, data not shown) generating a protein with a predicted mass of 135 kDa and a p*I* of 6.98.

3.3.5 Identification of regions of P159 that bind to PK-15 cell surface proteins

We applied a systems wide strategy to identify *M. hyopneumoniae* proteins that interact with proteins that are displayed on the cell surface of porcine kidney epithelial-like cell monolayers (PK-15 cells). This approach recovered P27, P110 and P52 (data not shown) indicating that these three dominant cleavage fragments retain the ability to bind to PK-15 cells.

3.3.6 Regions of P159 that bind heparin

Heparin-binding P159 proteins displayed masses from 73-92 kDa (band 1, Fragment 22), 60-72 kDa (band 2, Fragment 23), 48-59 kDa (band 3, Fragment 24), 38-47 kDa (band 4, Fragment 25), 32-37 kDa (band 5, Fragment 26), 20-26 kDa (band 6, Fragment 27), and 15-19 kDa (band 7, Fragment 28) (Figure 3.5). Tryptic peptides generated by digesting *M. hyopneumoniae* proteins that are retained during heparin-agarose chromatography span most regions of P159, including the dominant cleavage fragments P27, P110 and P52 at their correct masses when resolved by SDS-PAGE. Consistent with these observations, the P159 protein sequence carries a wide array of putative heparin-binding motifs that span the entire molecule (Figure 3.5).

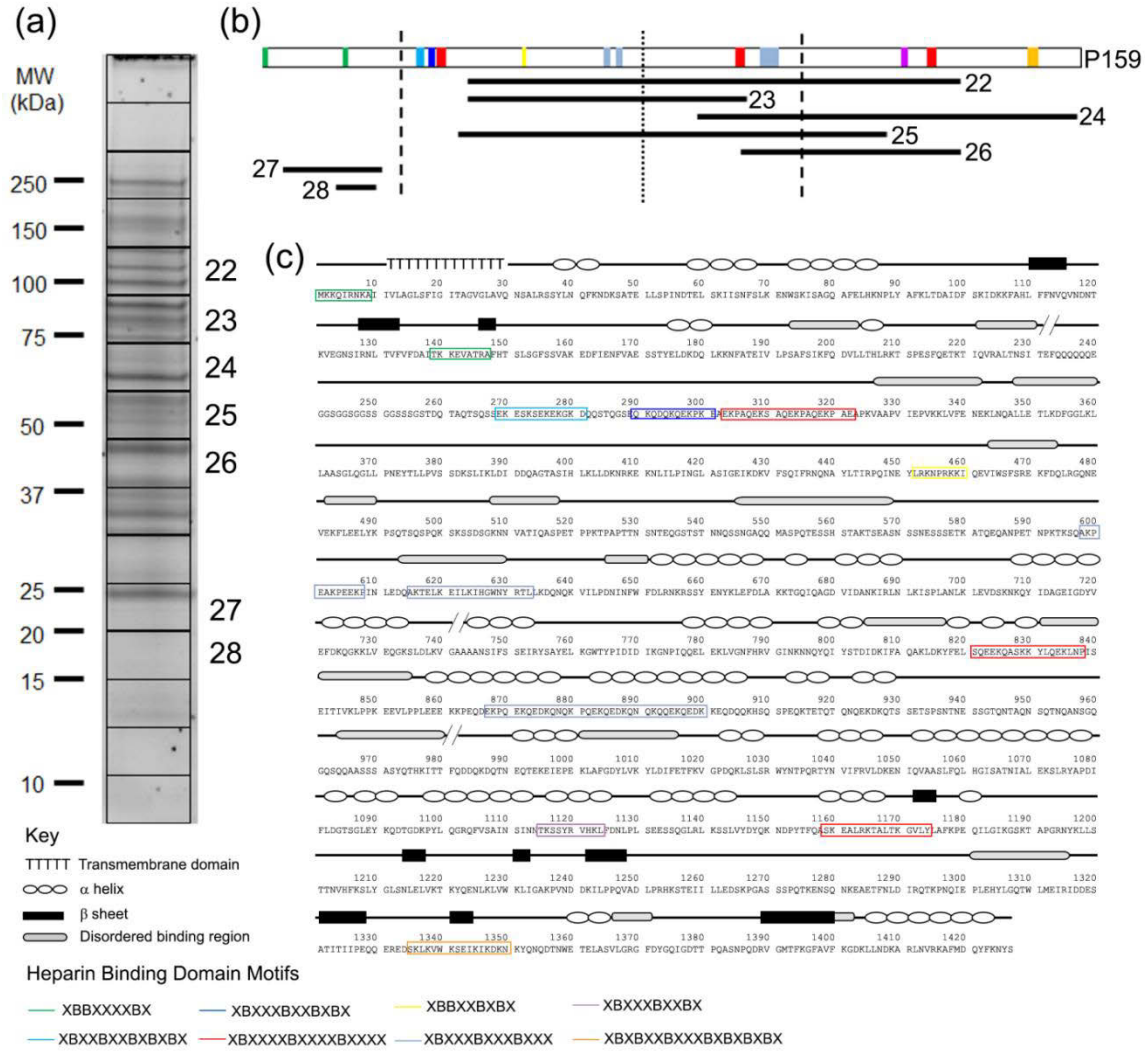

Figure 3.5: Schematic representation of P159 heparin-binding domain motifs and heparin-binding fragments.

A) 1D gel of *Mycoplasma hyopneumoniae* heparin-binding proteins with slices containing peptides matching to P159 fragments (see also Figure 3.8). B) shows locations of heparin-binding motifs in the box (colour-coded to positions indicated in panel c) and identified fragments of P159 from the most N-terminal to most C-terminal peptide matched. Fragments may extend beyond these boundaries. Heavy dashed vertical lines represent dominant cleavage sites and the light dashed line represents the major, less efficient cleavage site. C) Schematically depicts P159 with heparin-binding domain motifs boxed and colour-coded and structural features as indicated in the key.

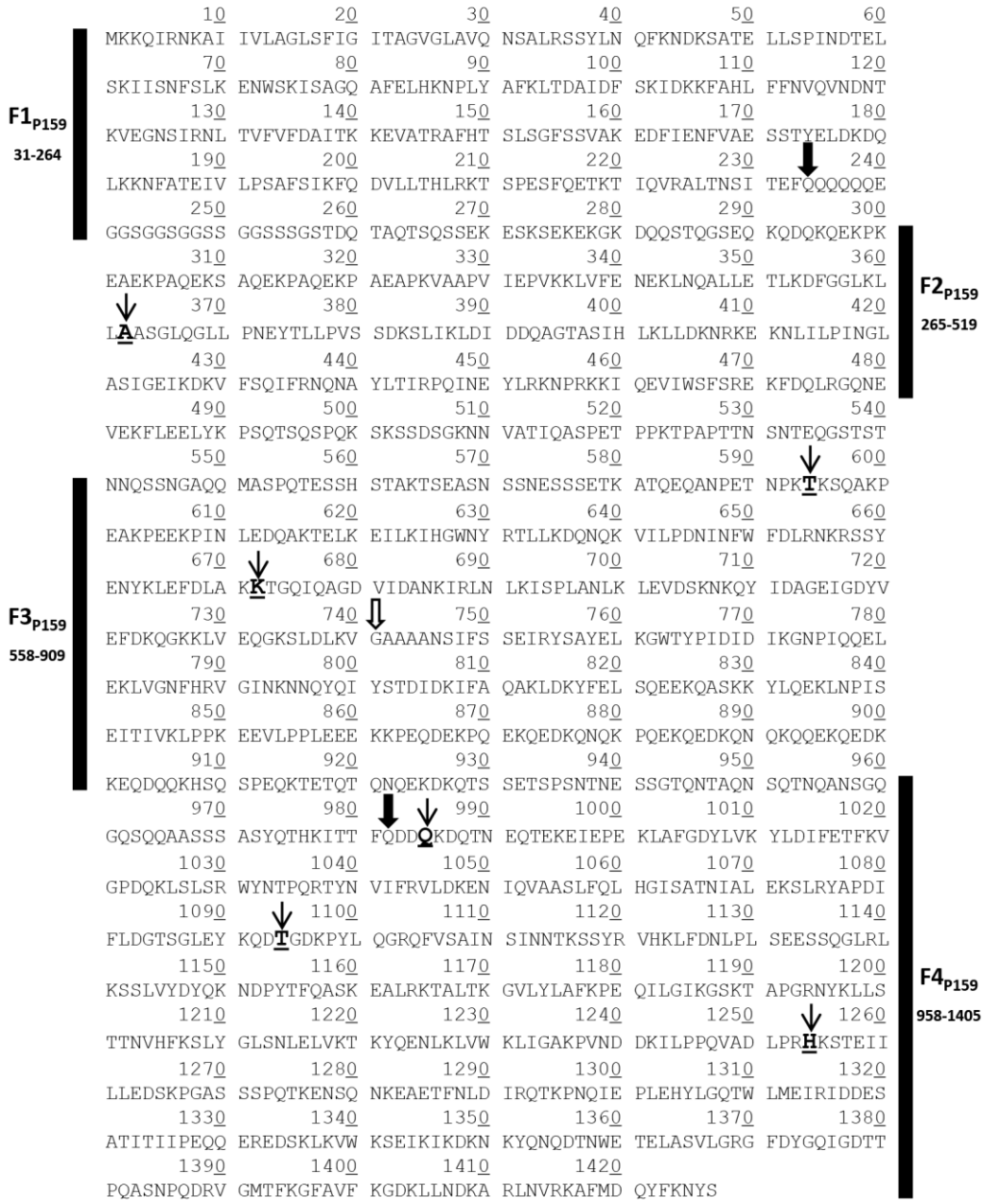

Figure 3.6: Dominant, major and minor cleavage sites within P159.

Solid black arrows indicate major cleavage sites which produce P27, P110 and P52; the most readily identifiable cleavage fragments of P159. The major cleavage site generating P76 and P35 is shown by a hollow arrow. The first (biotinylated) amino acid of biotinylated N-terminal peptides is shown with narrow arrows in enlarged, bold and underlined text.

3.3.7 Regions of P159 that bind to porcine cilia

We tested the ability of recombinant fragments $F1_{P159}$ – $F4_{P159}$ to bind to porcine cilia using an established cilium-binding assay [10]. We show that $F2_{P159}$ and $F4_{P159}$ retain the capacity to bind cilia. $F1_{P159}$ and $F3_{P159}$ do not bind cilia (Figure 3.7).

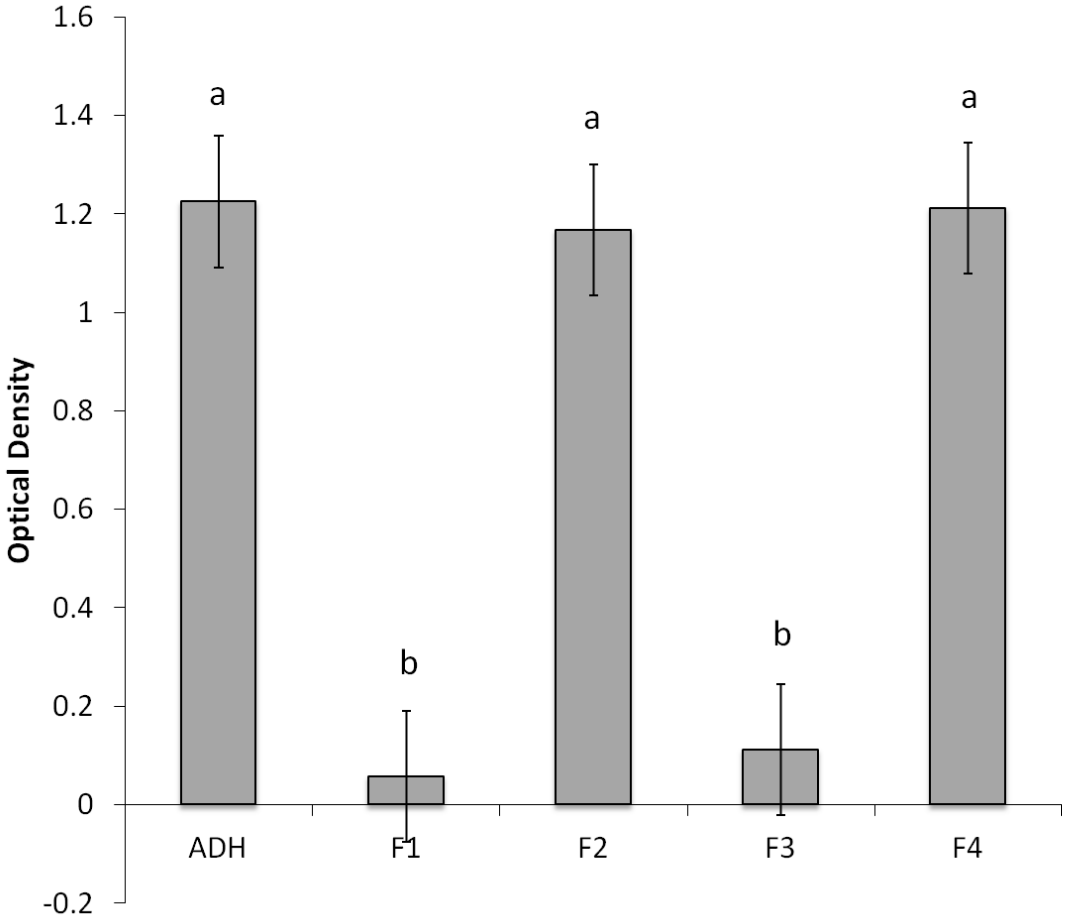

Figure 3.7: Binding of P159 fragments to porcine cilia.

Data represents the mean ± standard error of two independent experiments as determined by a one-way ANOVA. Data with the same labels are the same statistically ($p<0.0001$). ADH is a positive control and represents the C-terminal fragment of P97 that contains the cilium-binding domain [5].

3.4 Discussion

P159 is one of the most highly expressed proteins in the *M. hyopneumoniae* proteome. We show that it is a target of multiple processing events that generate an extensive repertoire of fragments on the cell surface. Previously we described three cell surface cleavage products comprising N-terminal 27 kDa, central 110 kDa and C-terminal 52 kDa fragments, but we were unable to define the precise cleavage sites that produced them. LC-MS/MS analyses of tryptic peptides of fragments of P159 resolved by 2D SDS-PAGE identified the peptides ^{234}QQQQQQEGG/24/SSEK^{270} and ^{982}QDDQKDQTNEQTEK^{995} confirming that cleavage occurred at the C-terminal side of the phenylalanine residue in the motifs ^{230}I-T-E-F↓Q-Q-Q^{237} and ^{978}I-T-T-F↓Q-D-D^{984}. The ^{230}I-T-E-F↓Q-Q-Q^{237} cleavage site defines P27 as a protein that commences at position 1 and ends at position 234. The ^{978}I-T-T-F↓Q-D-D^{984} cleavage site shows that P110 spans amino acids 235–981 and P52 spans amino acids 982–1427. These cleavage sites are consistent with our earlier study where we broadly mapped P27, P110 and P52 by MALDI TOF-MS [4].

P159 is a modular protein. Domains residing within P27, P110 and P52 are flanked by large regions of protein disorder spanning more than 200 amino acids. S/T-X-F↓X-D/E cleavage sites reside within disordered regions which are enriched in glutamine and aspartic acid residues. The disproportionate concentration of D/E residues imparts an acidic p*I* to cleavage fragments that span these domains. In contrast, regions of P159 lying outside these expansive disordered regions are enriched in K and R residues that impart a basic p*I* to endoproteolytic fragments. As a result, endoproteolytic fragments display isoelectric points ranging from 5 - 10. We were able to provide robust data to characterise a subset of 28 proteins from a much larger pool of cleavage fragments that

were produced at concentrations too low for LC-MS/MS but were detectable by immunoblotting with anti-$F1_{P159}$-$F4_{P159}$ sera or enrichment protocols including avidin chromatography of biotinylated surface proteins and heparin-agarose chromatography. This remarkable observation indicates that endoproteolytic processing creates considerable surface protein diversity. Figure 3.8 provides a summary of cleavage fragments we found in P159.

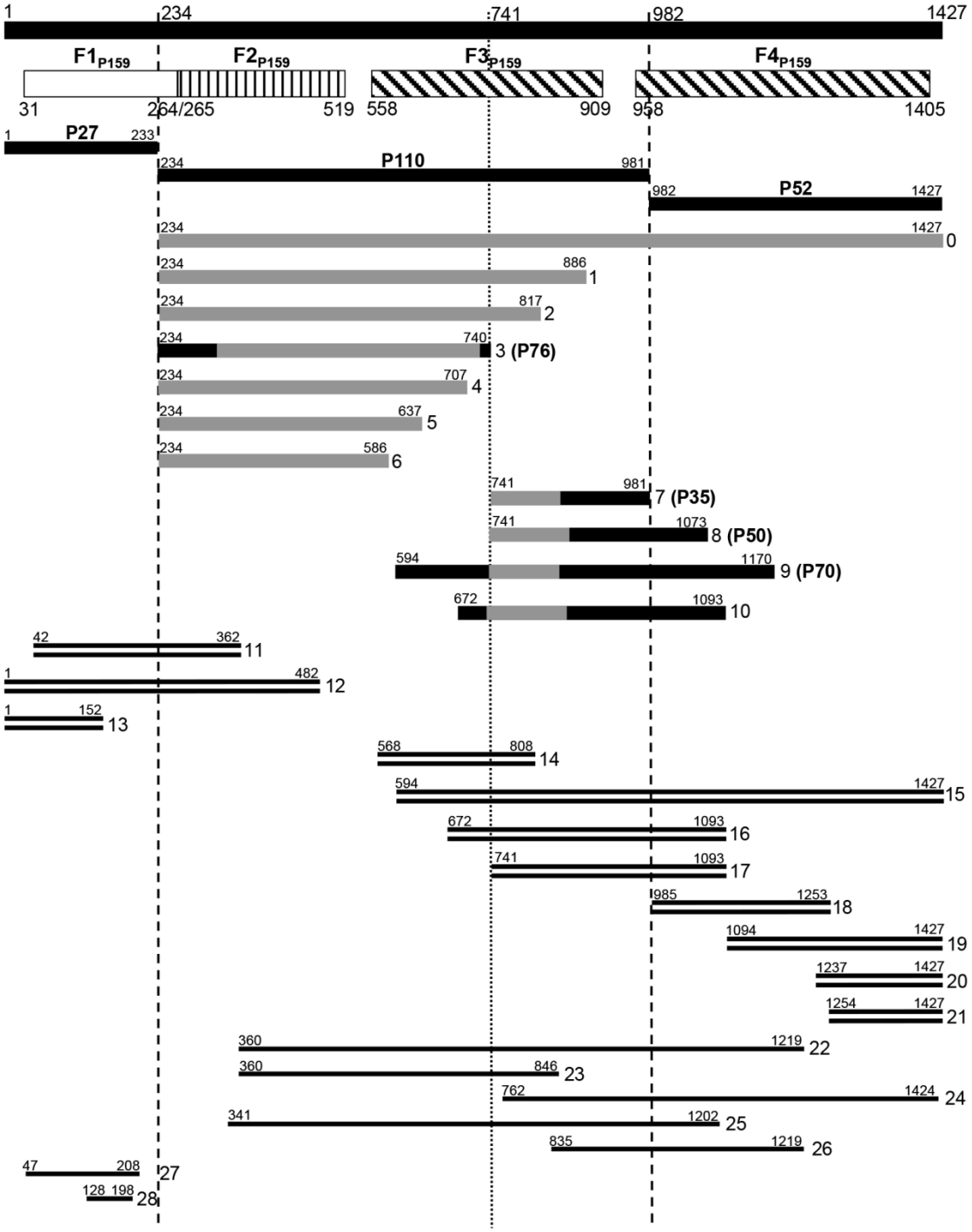

Figure 3.8: Schematic representation of cleavage fragments.

Full length P159 is represented by a solid black line, marked with amino acid numbers. Proteolytic cleavage sites occurring at ^{233}F↓Q^{234} and ^{981}F↓Q^{982} motif are shown by dashed vertical lines and the cleavage site occurring at ^{738}L-K-V↓G-A-A^{743} is shown by a dotted vertical line. Recombinant proteins (F1-F4$_{P159}$).

A single heparin binding consensus motif XBBXBX (where B represents a basic residue and X is any amino acid) [193] is located between amino acids 407-412 of P159 sequence. However, numerous putative heparin-binding motifs, including XBBXXBXBX (452-460), XBBXXXXBX (1-9, 139-147), XBXXBXXBXBXBX (269-281), XBXXXBXXBX (1115-1124), XBXXXBXXBXBX (290-301, 401-412), XBXXXXBXXXXBXXXX (303-323, 824-839, 1159-1174), XBXXXBXXXBXXX (594-608, 615-625, 867-901) and XBXBXXBXXXBXBXBXBX (1335-1350), are distributed across the P159 protein sequence and are likely to contribute to the ability of cleavage fragments to interact with mucins and epithelial cell and cilial receptors. The widespread distribution of putative heparin-binding motifs ensures that cleaved ectodomains retain an ability to bind to glycosaminoglycans that decorate the surface of porcine cilia and microvilli [40].

We also mapped the precise cleavage event in P110 that generates P76 and P35 within the sequence ^{738}L-K-V↓G-A-A^{743} by identifying the semi-tryptic fragment ^{741}GAAAANSIFSSEIR^{754} by LC-MS/MS. Unlike S/T-X-F↓X-D/E sites, this cleavage site does not reside within a disordered region of P159. We previously identified a cleavage site in Mhp385, a heparin-binding paralog of P97 that showed sequence similarity with ^{738}L-K-V↓G-A-A^{743}. This cleavage event occurred at the sequence L-N-V↓A-V-S and like ^{738}L-K-V↓G-A-A^{743} it did not reside within a region of protein disorder. The peptide ^{359}K-L-L↓A-A-S^{364} retains similar amino acids in key positions in the motif L-X-V↓X-V/A-X. Cleavage sites L-N-V↓A-V-S from Mhp385, ^{359}K-L-L↓A-A-S^{364} and ^{738}L-K-V↓G-A-A^{743} from this study all conform to a motif L-X-V↓X-V/A-X suggesting that cleavage at these sites is performed by a protease that is different to the one that recognises S/T-X-F↓X-D/E sites. Six N-terminal tryptic peptides that were

biotinylated on their N-termini were identified by LC-MS/MS confirming that numerous, less-abundant cleavage events occur within P159. Many P159 cleavage fragments are retained on heparin-agarose columns and span regions that bind to porcine cilia indicating that processing releases functionally active fragments in a manner akin to ectodomain shedding in eukaryote cells [194].

Unlike the S/T-X-F↓X-D/E cleavage motif we were not able to decipher the sequence of motifs that produced low abundance cleavage fragments. Nonetheless, three of the six N-terminal fragments were bona fide tryptic peptides suggesting that a trypsin-like protease may be functionally active on the surface of *M. hyopneumoniae*. Our data suggest that once the major cleavage fragments have been generated, they become susceptible to further proteolytic cleavage. Alternatively, the N-termini of the major cleavage fragments may be targeted by aminopeptidases that recover amino acids essential for growth. Recently we showed that MHJ_0125 is a multifunctional protein that displays glutamyl-aminopeptidase activity and moonlights as a Plg-binding protein on the cell surface of *M. hyopneumoniae* [145]. However, we have not shown that the MHJ_0125 targets *M. hyopneumoniae* proteins. In the current study, the peptide ^{985}QKDQTNEQTEKEIEPEK^{1001} was identified as a biotinylated N-terminal peptide (Figure S3.3). This peptide sequence commences two amino acids downstream of the N-terminal fragment ^{982}↓QDDQKDQTNEQTEK^{995} that separates P52 from P110. The ^{985}QKDQTNEQTEKEIEPEK^{1001} peptide is unusual because it is semi-tryptic and may be the product of aminopeptidase activity.

P159 encodes a single transmembrane domain spanning amino acids 9–29 (TmPred score 2050). We previously showed that transmembrane domains found in members of

the P97 and P102 paralog families are not removed during secretion to the cell surface. Consequently, P27 and larger low-abundance N-terminal fragments that include parts of P110 are expected to remain embedded in the *M. hyopneumoniae* cell membrane. Many P159 fragments do not carry a transmembrane sequence. It is remarkable that we were able to detect evidence of most cleavage fragments as many are expected to be shed into the extracellular milieu where conceivably they i) bind target cell receptors, ii) act as decoys for effector molecules of the porcine immune response and iii) represent docking sites that promote homopolymeric interactions for cell-cell contact and biofilm formation. The high serum content found in *M. hyopneumoniae* medium precludes studies that seek to detect shed cleavage fragments. Several host molecules including Fn and Plg are known to be sequestered onto the surface of *M. hyopneumoniae* and these may provide a scaffold for retaining cleavage fragments [2,3,5-9,145].

Surface accessible membrane proteins in eukaryotes are known to be released into the extracellular milieu via a process known as ectodomain shedding [194]. Ectodomain shedding is now recognised as a widespread process in eukaryotes and algorithms have been developed to identify membrane proteins that are targeted by sheddases [135]. Earlier studies in eukaryote systems suggested that approximately 4% of surface associated proteins are targets for ectodomain shedding [195]. Shed proteins regulate neuron migration, osteoclast development, the differentiation and proliferation of hematopoietic precursor cells, cell fate and the presentation of CD44 [196-198] underscoring the biological utility of this process. These data are consistent with the notion that many, if not all proteins are multifunctional and highlights the informational content of proteins is likely to be significantly underestimated.

The S/T-X-F↓X-D/E motif is now firmly established as a site where dominant cleavage occurs in major adhesin families of *M. hyopneumoniae*. Our initial surfaceome studies show that approximately 150 ORFs can be detected on the surface of *M. hyopneumoniae* using biotinylation and trypsin shaving strategies (data not shown). Our studies with members of the P97 and P102 paralog families [2-10,54] and P159 presented here indicate that cleavage may be a complex, sophisticated mechanism to generate surface protein diversity in a manner akin to ectodomain shedding. We are now determining how many proteins on the surface of *M. hyopneumoniae* are targets of endoproteolytic activity. Previously we provided evidence that abundantly expressed surface proteins in Gram negative gastrointestinal pathogen *Campylobacter jejuni* [199], Gram positive pathogen *Streptococcus pyogenes* [200] and the avian pathogen *Mycoplasma gallisepticum* [184] are presented on the cell surface as protein fragments indicating that they are targets of endoproteolytic processing. Further studies are needed to examine the role of endoproteolysis of surface proteins in pathogenesis and prokaryote biology more broadly.

3.5 Conclusions

P159 (MHJ_0494) is a highly expressed, extensively processed, surface accessible molecule that shares functional similarities with members of the P97 and P102 paralog families. Cleavage fragments of P159 display a remarkable capacity to bind to glycosaminoglycans and function as epithelial cell [4] and cilium adhesins. It is now clear that proteolytic processing represents the principal means by which *M. hyopneumoniae* generates surface protein diversity and functional redundancy in glycosaminoglycan- and cilium-binding [2-10,41,54,145]. Processing events presumably have evolved to ensure *M. hyopneumoniae* is adept at colonising and persisting within the porcine respiratory tract and potentially at other organ sites in the face of an immunological assault from the host. Endoproteolysis of adhesin families in the genome-reduced microbial pathogen *M. hyopneumoniae* displays all the hallmarks of ectodomain shedding; a process that has evolved to generate functional diversity in eukaryotes.

Chapter Four: (Paper III) Investigation of the multifunctional adhesin P97 and the co-localisation of Fn with *M. hyopneumoniae*

Declaration

I declare that the following publication included in this thesis in lieu of a chapter meets the following:

- More than 50% of the content in the following publication included in this chapter has been planned, executed and prepared for publication by me
- The work presented here has been peer-reviewed and accepted for publication
- I have obtained approval to include the publication in this thesis from the Publisher
- The initial draft of the work has been written by me and any subsequent changes in response to co-authors and editors reviews was performed by me
- The publication is not subject to any obligations or contractual agreements with a third party that would constrain its inclusion in the thesis.

Publication title: Proteolytic processing of the cilium adhesin MHJ_0194 (P123J) in *Mycoplasma hyopneumoniae* generates a functionally diverse array of cleavage fragments that bind multiple host molecules

Authors: Benjamin B.A. Raymond, Cheryl Jenkins, Lisa M. Seymour, Jessica L. Tacchi, Michael Widjaja, Veronica M. Jarocki, Ania T. Deutscher, Lynne Turnbull, Cynthia B. Whitchurch, Matthew P. Padula and Steven P. Djordjevic

Candidate's contribution (%): above 50 %

Journal name: Cellular Microbiology

Volume/ page numbers: 17(3):425-44

Status: Published

I declare that the publication above meets the requirements to be included in the thesis.

Candidate's name: Candidate's signature: Date (dd/mm/yy):

4.1 Introduction

Mycoplasma hyopneumoniae is a significant cause of economic loss to swine production worldwide. Colonisation of the porcine respiratory epithelium by *Mycoplasma hyopneumoniae* elicits a sustained inflammatory response that produces characteristic lung pathology defining clinical presentation of porcine mycoplasmal pneumonia [201,202]. In colonising, *M. hyopneumoniae* adheres strongly to the ciliated epithelial lining in the upper airways destroying cilial function and limiting mucociliary clearance. Attempts to develop bacterin vaccine formulations to control *M. hyopneumoniae* have failed to reduce colonisation of the lung epithelium [203] and the need for an effective vaccine remains.

An attractive target for vaccine development is the cilium adhesin P97 of *M. hyopneumoniae*, a dominant cleavage fragment derived from the gene encoding Mhp183 in virulent strain 232. For clarity, subscripts will be used when distinguishing proteins or adhesin fragments from different *M. hyopneumoniae* strains, for example, $P97_{232}$ designates the P97 cilium adhesin fragment of strain 232 and the subscript J will be used to designate fragments of the homologous protein from the laboratory-adapted strain J. P97 is expressed as a preprotein ($P125_{232}$ and $P123_{J}$ in strains 232 and J, respectively) that is a target of a highly efficient processing event at amino acid 195 at an S/T-X-F↓X-D/E motif of ^{193}T-N-F↓A-D^{197}. This cleavage releases a 22 kDa N-terminal fragment ($P22_{232/J}$) and the mature adhesin which has a variable mass in different *M. hyopneumoniae* strains according to differences in the number of tandem repeats located in the R1 and R2 domains in the C-terminal region of the molecule [3,54]. The mature adhesin in strains J ($P94_{J}$) and 232 ($P97_{232}$) contains 9 and 15 copies, respectively, of the cilium-binding pentapeptide repeat A-A-K-P-V/E in R1, while in R2

there are 5 and 4 copies, respectively, of the decapeptide repeat G-T-P-N-Q-G-K-K-A-E [54,204]. A second cleavage event at position ^{860}T-N-T↓N-T-N^{865} in P94$_J$ separates the C-terminal 230 amino acids (P28$_J$) from P66$_J$ but the function of P28 remains unknown [54]. Both cleavage sites have been confirmed by Edman degradation [54,154] and are conserved in homologs of P123 in geographically diverse strains of *M. hyopneumoniae* underscoring their importance to the function of the molecule. A minimum of 8 tandem copies of the pentapeptide repeat in R1 is required to bind cilia [205-207]. The number of tandem repeats within R1 and R2 in homologs of P123 varies considerably, despite which most field strains carry the requisite 8 copies of the A-A-K-P-V/E repeat in R1 [204,206].

Many of the key features of P97$_{232}$ were identified using the monoclonal antibodies (mAbs) F1B6 and F2G5 [54,154,204]. Both antibodies recognise three tandem copies of the A-A-K-P-V/E repeat [207] in the R1 domain and partially block attachment (60-70% inhibition) of *M. hyopneumoniae* to porcine cilia [154]. Affinity chromatography using F2G5 recovered proteins of 125, 97, 81 and 72 kDa, and several with masses less than 72 kDa [154], but, P97 was the most prominent protein. F2G5 reactive proteins purified by affinity chromatography partially blocked binding of *M. hyopneumoniae* to cilia in a dose-dependent manner, indicating that cleavage fragments containing the R1 domain play a key role in binding cilial receptors [154]. While proteins with these masses were observed by Western blots of *M. hyopneumoniae* lysates probed with F1B6 or F2G5, many other F1B6-reactive proteins are evident [54]. Analyses of genome sequences of *M. hyopneumoniae* reveal that only Mhp183 (P97$_{232}$) and P97 paralogs Mhp385 and Mhp271 display R1-like repeats [156,208]. While Mhp385 contains a C-terminal R1-like domain with four tandem A-A-K-P-V/E-like repeats [6], Mhp271

displays two R1 regions known as $R1A_{271}$ (3 copies of the pentapeptide repeat) and $R1B_{271}$ (6 copies of the pentapeptide repeat), and an R2 region containing almost two complete copies of the decapeptide repeat, $R2_{271}$ in the C-terminus of Mhp271. Both Mhp271 [5] and Mhp385 [6] do not appear to be extensively processed by endoproteolysis and the cleavage fragments identified by 2D SDS-PAGE and LC-MS/MS analysis were insufficient to explain the complex banding profiles observed when *M. hyopneumoniae* lysates are probed with F1B6 [54]. A thorough understanding of the processing events that shape how regions of the P123 cilium adhesin reside on the surface of *M. hyopneumoniae* is yet to be elucidated.

P97 is a heparin-binding protein [41,205] that contains a minimum of two heparin-binding domains. Recombinant fragments spanning the N-terminal amino acids 106-758 of $P94_J$ and C-terminal amino acids 768-1069, which includes R1 and R2, bound heparin in a dose-dependent manner, with binding to heparin inhibited by fucoidan and mucin [41]. *M. hyopneumoniae* sequesters Fn and Plg onto its cell surface in a dose-dependent manner and several paralogs of Mhp183 ($P125_{232}$), Mhp182 (P102) and paralogs of Mhp182 have been shown to bind Plg and Fn [2,5,7-9]. The challenge has been to determine the critical regions within these molecules that function as adhesins of key host molecules. Cleavage events define how regions within cilium adhesins are presented on the cell surface of *M. hyopneumoniae*. An understanding of the structure of the cleavage fragments provides an opportunity to identify regions within these molecules that bind to proteoglycan receptors and ECM components on the surface of target host tissues [2-10,43,44,204] and the fibrinolytic system component Plg [2,5,7-9]. Here we use 2D SDS-PAGE and LC-MS/MS to identify a series of novel cleavage sites in $P123_J$. These events explain the complex processing events that underpin immunoblot

profiles previously observed when cell lysates of *M. hyopneumoniae* are probed with mAbs F1B6 / F2G5 [54,154]. In addition, we identify novel binding functions for the C-terminus of P28 and reveal multifunctional binding capabilities of the P97 adhesin.

4.2 Materials and Methods

4.2.1 Bacterial strains and cultures

M. hyopneumoniae strains were cultured in modified Friis medium as previously described [182,209].

4.2.2 Enrichment of *M. hyopneumoniae* surface proteins

Cell-surface biotinylation was carried out as previously described [3] on intact *M. hyopneumoniae* cells using EZ-link sulfo-NHS-biotin (Thermo Fisher Scientific), combined with avidin column purification or blotting to purify or identify biotinylated surface proteins.

4.2.3 Preparation of *M. hyopneumoniae* whole cell lysates for mass spectrometry

M. hyopneumoniae whole cell lysates were prepared as previously described [5]. Briefly, cells were lysed in 7 M urea, 2 M thiourea, 40 mM tris, 1% (w/v) C7BzO detergent (Sigma-Aldrich), followed by three rounds of sonication at 50% power on ice. Proteins were reduced and alkylated with 20 mM acrylamide monomers and 5 mM TBP for 90 min. Insoluble material was removed by centrifugation and the protein present in supernatant precipitated by adding five volumes of acetone. After centrifugation, the protein pellet was solubilised in 7 M urea, 2 M thiourea, 1% (w/v) C7BzO.

4.2.4 One- and two-dimensional gel electrophoresis and immunoblotting

The separation of proteins by 1D and 2D SDS-PAGE has been described in detail previously [5,54]. For 1D SDS-PAGE, after separation, gels were fixed and visualised by staining with either Flamingo fluorescent gel stain (Bio-Rad) or Coomassie Blue G-250. For 2D SDS-PAGE, ~250 µg of protein was cup-loaded onto partially rehydrated 11 cm pH 4−7 IPG strips (BioRad) or 6−11 Immobiline drystrips (GE Healthcare).

Focusing was performed in a Bio-Rad Protean IEF cell as per Raymond *et al.,* (2013). Following IEF, the strips were equilibrated with 2% (w/v) SDS, 6 M urea, 250 mM tris-HCl pH 8.5, 0.0025% (w/v) bromophenol blue for 20 min before the second-dimension SDS-PAGE. *M. hyopneumoniae* proteins separated by 2D SDS-PAGE were blotted onto PDVF membrane using a semi-dry transfer method. Membranes were blocked with 5% (w/v) skim milk powder in PBS with 0.1% (v/v) tween 20 (PBS-T) at RT for 1 h and incubated with P97 N-termB [54] R1 or R2 [41] polyclonal antisera (diluted 1 in 100 in PBS-T) for 1 h at RT.

4.2.5 Fn and anti-Fn antibodies

Purified Fn (440 kDa) was supplied by Calbiochem. Rabbit anti-Fn antibody was supplied by MP Biomedicals, Inc. Horseradish peroxidase (HRP)-labeled sheep anti-rabbit conjugate was obtained from Chemicon.

4.2.6 Protein expression, purification and generation of antisera

Purified cilium adhesin fragments ($F4_{P94\text{-}J/\Delta23}$) were expressed and purified as previously described [41]. Antisera against $F1_{P94\text{-}J}$ – $F3_{P94\text{-}J}$ and $F4_{P94\text{-}J/\Delta23}$ were generated in a previous study and with titres determined empirically [41].

4.2.7 Plasmids, protein expression and purification

Polymerase chain reaction was performed in a Cooled Mastercycler ep gradient S (Eppendorf, Germany) using PfuUltra™ High-Fidelity II DNA polymerase (Stratagene, USA). *M. hyopneumoniae* strains 232 and J chromosomal DNA were used to amplify *mhp183* and *MHJ_0194*, respectively. *Mhp183* (Genbank accession number AE017332) was amplified using an overlap extension mutagenesis method to change in-frame TGA

codons to TGG codons. The *mhp183* and *MHJ_0194* genes were separately cloned into pET151/D-TOPO® (Invitrogen) according to the manufacturer's instructions. The pET151:mhp183 and pET151:MHJ_0194 constructs were used as templates to amplify regions of the genes, which were then cloned into pET151/D-TOPO® (Invitrogen). All plasmid constructs were sequenced to check fidelity to the original *mhp183/MHJ_0194* gene. *E. coli* BL21 star (DE3) was used as the expression strain for the plasmid constructs. When the *E. coli* cultures reached an OD_{600} of 0.8, 1 mM IPTG was added to induce protein expression. Protein purification was performed under native and denaturing conditions using Ni-NTA agarose resin according to the manufacturer's instructions (Qiagen, USA). Purified proteins were dialysed into phosphate buffered saline (PBS; 10 mM sodium phosphate, 137 mM sodium chloride, 2 mM potassium phosphate, 2.7 mM potassium chloride; pH 7.4). SDS-PAGE of purified proteins was performed. Electrospray Ionisation Mass spectrometry (ESI-MS) was undertaken to determine the size of the expression product. Protein was dialysed into 50 mM ammonium acetate in Milli-Q water and analysed with a Waters Synapt HDMS mass spectrometer (Waters, UK), using a conventional ESI source.

4.2.8 Surface plasmon resonance analyses

A Biacore T100 instrument (Biacore AB, Sweden) was used to analyse real-time interactions of P123 recombinant proteins with Plg. Porcine Plg was purified from plasma by affinity chromatography [197,210], with further purification performed using gel filtration and ultrafiltration [7]. The activity and purity of purified Plg was assessed with Spectrozyme PL (American Diagnostica, USA) [7]. Buffer exchange of recombinant proteins into HBS-EP+ (10 mM HEPES, 150 mM NaCl, 3 mM EDTA, 0.05% (v/v) Surfactant P20; Biacore AB), immobilisation of ligands and subsequent

kinetics assays have been described previously [7]. Binding kinetics were measured with recombinant proteins over a range of concentrations (0 – 200 nM) at 20˚C. Analysis of association rates was performed using the 1:1 Langmuir binding model with BiaEvaluation software 3.1 (Biacore AB) and Graphpad Prism version 4 (Graphpad Software, USA).

4.2.9 Heparin affinity chromatography

Affinity purification of heparin binding proteins from *M. hyopneumoniae* was performed as described in Raymond *et al.,* (2013) with no modifications.

4.2.10 Avidin purification of PK-15 interacting proteins

The purification of *M. hyopneumoniae* proteins that bind PK-15 proteins was performed as described in Raymond *et al.,* (2013) with no modifications. *M. hyopneumoniae* lysates were incubated with avidin agarose in the absence of biotinylated proteins to demonstrate that *M. hyopneumoniae* proteins do not bind to avidin agarose. No naturally occurring biotinylated proteins or non-specifically bound proteins were detected by SDS-PAGE when avidin agarose loaded with *M. hyopneumoniae* proteins was treated with 30% acetonitrile/ 0.4% trifluoroacetic acid.

4.2.11 Avidin purification of Fn binding proteins

1 mg of human Fn (Calbiochem) was biotinylated with EZ-link sulfo-NHS-biotin (Thermo Fisher Scientific) and then bound to avidin agarose (Thermo Scientific) overnight at 4°C on a rotating wheel. The slurry was then packed into a column, and the flowthrough was collected for monitoring by SDS-PAGE. Unbound biotinylated Fn was removed with 4 × 5 ml sequential washes with PBS. Freshly harvested *M.*

hyopneumoniae cells were washed extensively (>3 times) in PBS and pelleted by centrifugation (1,1000 × *g*, 10 min). Cells were resuspended in 10 ml of 1% (w/v) C7BzO (Sigma-Aldrich) in PBS (pH 7.8) and disrupted with three rounds of sonication at 80% power for 30 s bursts whilst on ice. After insoluble material was removed by centrifugation, the cleared lysate was added to the slurry and incubated again overnight at 4°C on a rotating wheel. The mixture was again packed into a column, the flow through collected, and non-binding proteins were removed by washing with 4 × 5 ml sequential washes with PBS. Fn binding proteins were collected by eluting with 7 M urea, 2 M thiourea, 40 mM tris and 1% (w/v) C7BzO. The elution was concentrated through 3,000 Da cut-off filters, then acetone precipitated at −20°C overnight, and finally pelleted by centrifugation at 25,000 × *g* at 4°C for 30 min. Protein was resuspended in SDS sample buffer and separated by 1D SDS-PAGE. Proteins were in-gel trypsin digested with trypsin and analysed by LC–MS/MS.

4.2.12 1D LC-MS/MS using ion trap

Each of the 16 SDS-PAGE fractions of triplicate sets were analysed by nanoflow LC-MS/MS (nanoLC-MS/MS) using a LTQ-XL linear ion trap mass spectrometer (Thermo Fisher Scientific). In a fused silica capillary with an integrated electrospray tip, reversed-phase columns were packed in-house to approximately 7 cm (100 µm ID) using 100 Å, 5 µm Zorbax C18 resin (Agilent Technologies). An electrospray voltage of 1.8 kV was applied *via* a liquid junction upstream of the C18 column. Samples were injected onto the column using a Surveyor autosampler, which was followed by an initial wash step with buffer A (5% v/v ACN, 0.1% v/v formic acid) for 10 min at 1 µL/min. Then, peptides were eluted from the column with 0–50% buffer B (95% v/v ACN, 0.1% v/v formic acid) for 58 min at 500 nL/min. The column eluate was directed

into a nanospray ionization source of the mass spectrometer. Spectra were scanned over the range of 400–1,500 amu and, using Xcalibur software (Version 2.06, Thermo) automated peak recognition, dynamic exclusion and MS/MS of the top six most intense precursor ions at 35% normalization collision energy were performed.

4.2.13 Protein extraction and digestion for strong cation exchange chromatography and MudPIT

To extract and alkylate proteins, lyophilised cells were resuspended in 8 M urea, 100 mM ammonium bicarbonate, pH 9 and sonicated with an ultrasonic probe at 80% power for 3 × 30 sec on ice. Reduction and alkylation of cysteine and precipitation was carried out as described above. The protein was resuspended in 8 M urea, 100 mM ammonium bicarbonate, pH 9 and digested to peptides firstly by addition of 2.5 µg of Endoproteinase LysC (Roche) and incubating overnight at 37 °C. The sample was then diluted to 1 M urea by adding 100 mM ammonium bicarbonate prior to the addition of 2.5 µg of trypsin (Promega) and incubated at 37 °C for 16 h. Formic acid was added to a concentration of 1% and the peptides desalted and concentrated using an OASIS HLB SPE column (Waters, 1cc) as per manufacturer's instructions. Bound peptides were eluted with 75% acetonitrile, 0.2% formic acid. The acetonitrile was removed by vacuum centrifugation to a volume of 50 µl and 5 µl removed for 1DLC-MS/MS using QTOF as described.

4.2.14 Peptide fractionation by cation-exchange chromatography

After addition of 20 mM monopotassium phosphate, 20% acetonitrile, pH 3 (SCX buffer A), the complex peptide sample was separated using a PolyLC PolySULFOETHYL™ A column (2.1 mmID × 100 mmL) pre-equilibrated in SCX buffer A while connected to an Agilent 1200 HPLC system. After sample injection and

collection of unbound peptides, retained peptides were fractionated by an increasing gradient (0-50% B in 50 min) of 20 mM monopotassium phosphate, 20% acetonitrile, pH 3 + 0.5 M KCl (SCX buffer B). Eluting peptides were monitored at 214 nm and collected in a 96 well plate by peak detection mode. Peptide fractions were then transferred to microtubes and lyophilised to approximately 10 µl. The peptide fractions were desalted using OMIX C18 SPE pipette tips as per manufacturer's instructions. Desalted peptide fractions were briefly (2 min) lyophilised to remove acetonitrile and 10 µl of MS solvent A (2% acetonitrile, 0.2% formic acid) added prior to analysis by 1DLC-MS/MS on the QTOF as described.

4.2.15 Multidimensional Protein Identification Technology (MudPIT)

Methods for two-dimensional chromatography were performed as described previously with no modifications [53].

4.2.16 1D LC−MS/MS Using QTOF

Methods were performed as described previously with no modifications [43].

4.2.17 MS/MS Data Analysis

MS/MS data files were searched using Mascot as previously described [43] with slight modifications. Data files from avidin purification of interacting proteins were searched for both bacterial and mammalian proteins in order to identify the biotinylated "bait" proteins eluted in their respective experiments. Mascot and E-scores generated by Matrix Science were interrogated for each peptide identified. The Mascot score for a peptide is a measure of how much evidence in the way of fragment ions there is to match an ion's raw fragmentation data to the theoretical fragment data generated from a

sequence in the database. The E-value indicates whether or not the match could be due to random chance and should be less than 0.05. For peptides with an E-value greater than 0.05, the spectra were manually interrogated to confirm that all major peaks correspond to a fragment ion of the peptide sequence.

4.2.18 Microtitre plate-binding assays

Fn-binding assays were performed as above and previously described [5], except binding was detected using the TMB Substrate Reagent Set (BD Biosciences OptEIA™) for approximately 5 minutes. The reaction was stopped with an equal volume of sulphuric acid and read at 450 nm on a PowerWave HT Microplate Spectrophotometer (Bio-Tek). Background binding observed in wells without recombinant protein were subtracted from all readings.

The peptide binding assays followed the same protocol with the following modifications: 2.5 μg of each peptide was added to microtitre plate wells and incubated overnight at RT. Wells were blocked in 2% (w/v) bovine serum albumin (BSA) in PBS. 50 μg/mL of biotinylated heparin, biotinylated Plg or Fn in 1% skim milk powder was added to each well. Rabbit anti-human Fn antibody (1:3,000) was added to wells for detecting Fn, followed by HRP conjugated sheep, anti-rabbit IgG (1:1,000). ExtrAvidin (1:3,000) (Sigma-Aldrich) was added to wells for detecting biotinylated heparin and biotinylated Plg. The presence of each ligand was detected by TMB substrate as described above. Controls were performed to confirm that protein adhered to the microtitre plate and that proteins (and peptides) did not bind primary or secondary antibodies and produce a colour reaction in the absence of ligand.

4.2.19 Microscale Thermophoresis

For heparin binding assays, $F4_{P94\text{-}J}$ and $F4_{P94\text{-}J/\Delta23}$, were fluorescently labelled with amine reactive NT-647 dye (NanoTemper) in a 3-fold molar excess for 30 min. Excess dye was removed using a desalting column (NanoTemper). Tween-20 (0.5%) was added to prevent aggregation of sample. The non-fluorescent heparin was titrated against $F4_{P94\text{-}J}$ and $F4_{P94\text{-}J/\Delta23}$ (constant concentrations of 600 nM and 850 nM respectively) in a 1:1 serial dilution starting from 10 μM. Samples were loaded into a Monolith NT.115™ (NanoTemper) in hydrophilic capillaries. Capillary scans were performed to confirm that no sample aggregation was occurring and that the fluorescence intensity was within the range of 80-1500 counts. The data presented here was generated at 80% and 100% MST laser power for $F4_{P94\text{-}J}$ and $F4_{P94\text{-}J/\Delta23}$ respectively, measuring the thermophoretic movement after the MST laser is switched off for 30 s. Experiments were performed in triplicate over 3 different days. NanoTemper analysis software was used to analyse and generate the K_D values.

4.2.20 Cell culture and infection assays

Porcine kidney epithelial-like monolayers (PK-15) were grown to semi-confluency and seeded onto glass coverslips (13 mm, no. 1.5 thickness; Gerhard Menzel GmbH) placed in the wells of microtitre plates at approximately 10^4 cells/ well and allowed to adhere overnight. A 48 h *M. hyopneumoniae* culture was washed 2 times in PBS and resuspended in 25 mM HEPES in DMEM containing 5% fetal bovine serum (Life Technologies) (infection medium) and incubated at 37 °C for 2 h. *M. hyopneumoniae* cells were added to PK-15 cells so that 0.5 mL of the original 48 h *M. hyopneumoniae* culture was added to each well. *M. hyopneumoniae* cells were allowed to adhere for 16 h. Following infection samples were washed 3 × in PBS and fixed in 2%

paraformaldehyde for 30 min at 4 °C. Uninfected PK-15 monolayers were set up in parallel with infected samples.

4.2.21 Immunofluorescence microscopy

Triple immunofluorescence microscopy (IFM) of infected PK15 monolayers was achieved by sequential staining. Uninfected PK-15 monolayers were treated in the same way as infected samples to insure that no *M. hyopneumoniae* cells were present. Cells were blocked in 2% (w/v) BSA in PBS for 1 h at RT. Coverslips were washed and then incubated in 1:100 goat anti-Fn for 1 h at RT. Samples were washed and incubated with 1:1,000 donkey anti-goat Alexa Fluor® 488 for 1 h at RT. Anti-$F2_{P97}$ antiserum [41] was incubated at a dilution of 1:100 for 1 h at RT. Samples were then incubated with 1:1,000 goat anti-rabbit Alexa Fluor® 568 for 1 h at RT. Following further PBS washes, monolayers were incubated in 4',6-diamidino-2-phenylindole (DAPI) nucleic acid stain (Life Technologies). Coverslips were washed, mounted in VECTASHIELD® medium and viewed with a Nikon A1 Confocal Laser Scanning Microscope (CLSM) under a 100 × oil immersion objective. Super-resolution 3D-SIM was used to image these same slides on a V3 DeltaVision OMX 3D-SIM Imaging System (Applied Precision, GE Healthcare) as previously described [211]. Infected PK-15 monolayers were incubated with goat anti-rabbit Alexa Fluor® 568 and anti-goat Alexa Fluor® 488 in the absence of primary antibody to confirm that there was no cross-reactivity between our cells and these secondary antibodies.

4.2.22 Immunohistochemistry

Porcine lung tissue was derived from experimentally infected swine. Animals (9 pigs) were derived from a high-health herd at 8 weeks of age. Three uninoculated pigs represented the negative control group, while 6 pigs were inoculated intratracheally with *M. hyopneumoniae* at 16 weeks of age. Material for inoculation was derived from a Hillcrest pig displaying lung lesions and testing positive for *M. hyopneumoniae*, and consisted of either lung homogenate (4 pigs) or thrice-passaged cultures of the Hillcrest strain (2 pigs). All swine were slaughtered 8-10 weeks P.I. Porcine lung tissue was collected at slaughter and were fixed in neutral-buffered formalin and embedded in paraffin blocks. Serial tissue sections (5 µm thickness) were cut, mounted on glass slides and dried for 20 min. Sections were de-waxed with 2 × 3 min incubations in xylene followed by 2 × 3 min incubation in absolute alcohol. Endogenous peroxides were then blocked with a 1.8% solution of peroxide in methanol for 20 min. Slides were agitated in 2 changes of distilled water until sections were fully de-waxed. Antigens were unmasked at 37 ºC for 30 min in 0.2% trypsin-0.1% CaCl2. Sections were washed twice with distilled water and once with PBS before being blocked for 20 min with 0.5% BSA-1% goat serum. Primary antisera (1:500 anti-$F2_{P97}$, 1:500 anti-Fn or 1:500 irrelevant rabbit serum) were then added to the sections which were incubated for 1 h at 37 ºC. Cross-reactivity between anti-Fn and *M. hyopneumoniae* was ruled out using a Western blot performed as described previously [4], but using a 1:200 dilution of anti-Fn as primary antibody. The sections were washed twice in PBS and incubated in EnVision™ goat anti-rabbit serum (Dako) at 37 ºC for 1 h. Following two PBS washes, the sections were developed for 5 min. Chromogenic solution was prepared by adding a 200 µL aliquot of 0.1% aminoethylcarbazole in dimethylformamide to 10 mL acetate buffer, pH 5. Prior to addition to the slides, the chromogen was activated with 5 µL of 30% H_2O_2. Slides were rinsed in distilled water to stop the colour reaction,

counterstained with haematoxylin and mounted with Faramount aqueous mounting medium (Dako). Slides were examined with an Olympus BX50 microscope and imaged with an Olympus DP70 cooled digital camera.

4.2.23 Bioinformatic analysis of P123

Bioinformatic analysis of P123 used online resources: ProtParam, COILS, and PONDR® VSL2 [212]. The secondary structures for P123 were predicted using PROF, which has an expected average accuracy of > 72% for helix, strand and loop states [213]. Protein binding sections in disordered regions were predicted using ANCHOR [214]. Using ScanProsite additional basic residue clusters [193] were uncovered using the search parameters B-X(0-2)-B-X(0-2)-B and B-X(1-4)-B-X(1-4)-B.

4.3 Results

4.3.1 Structural analysis of P123

The cilium adhesin preprotein (MHJ_0194) in strain J ($P123_J$) comprises 1092 amino acids (123 kDa) and has a p*I* of 8.99. The homolog (Mhp183) in strain 232 ($P125_{232}$) is slightly larger with 1108 amino acids (p*I* 8.92), largely due to three extra pentapeptide repeats in the R1 region [204]. PROF and ANCHOR algorithms were used to predict protein secondary structure and protein binding sections in disordered regions, respectively. These analyses indicate that the $P123_J$ preprotein is chimeric in nature with beta-strands and alpha-helices the dominant features in the 755 N-terminal amino acids and loops and disordered regions predominating from amino acids 756-1092 in the C-terminus where R1 and R2 are found (Figure 4.1). The PONDR® VSL2 algorithm identified four major regions of disorder spanning a minimum of 30 consecutive amino acids between amino acids 175-208 (D1, p*I* = 4.94), 381-420 (D2, p*I* = 8.22), 780-878 (D3, p*I* = 9.70) and 934-1034 (D4, p*I* =9.30) (Figure 4.1). Previously, we showed that the cilium adhesin preproteins $P123_J$ and $P125_{232}$ in strains J and 232 respectively are targets of two dominant endoproteolytic cleavage events [54]. One of these events generates the mature cilium adhesin $P94_J$ ($P97_{232}$ in strain 232) and an N-terminal 22 kDa fragment known as $P22_J$ (amino acids 1-194). The ^{192}T-N-F↓A-D^{196} cleavage motif where the preprotein in strains J ($P123_J$) and 232 ($P125_{232}$) is cleaved is located within the first region of disorder, D1. Following cleavage at this site, Western blots show that only a small percentage of the preprotein remains, indicating that cleavage between F and A residues in the sequence ^{192}T-N-F↓A-D^{196}, an event that conforms strictly to cleavage at S/T-X-F↓-X-D/E sites in *M. hyopneumoniae* [2,3], is an efficient process. Consistent with efficient cleavage at S/T-X-F↓-X-D/E sites occurring in other members of the P97 and P102 adhesins, the S/T-X-F↓-X-D/E motif ^{192}T-N-F↓A-D^{196} resides

within a disordered region enriched in D/E residues (p*I* of 4.94) [2,3,9,43]. An analysis of the charge distribution in the $P123_J$ preprotein reveals 5 regions enriched in D/E residues spanning amino acids amino acids 61 – 360 (acidic region 1, p*I* = 5.23), 401-540 (acidic region 2, p*I* = 5.29), 601 – 660 (acidic region 3, p*I* = 5.25), 721 – 780 (acidic region 4, pI = 4.72) and 863 – 960 (acidic region 5, p*I* = 4.96) (Figure 4.1).

The second dominant cleavage event previously studied creates $P66_J$ and $P28_J$ and occurs at position 862 in the sequence ^{861}N-T↓N-T-N-T^{866}, removing a 28 kDa fragment from the C-terminus of the mature adhesin. An identical cleavage event also occurs in P97 in strain 232 generating $P72_{232}$ and $P28_{232}$ [54]. The cleavage event at position 862 is significant because it: (i) separates the R1 region containing the cilium binding pentapeptide repeats from R2, which comprises tandem copies of decapeptide repeats of unknown function and (ii) destroys a glycosaminoglycan-binding domain [41]. The ^{861}N-T↓N-T-N-T^{866} cleavage motif where $P94_J$ is cleaved into $P66_J$ and $P28_J$ is located in D3. R1 (814-858) and R2 (961-1010) domains are located within D3 and D4, respectively.

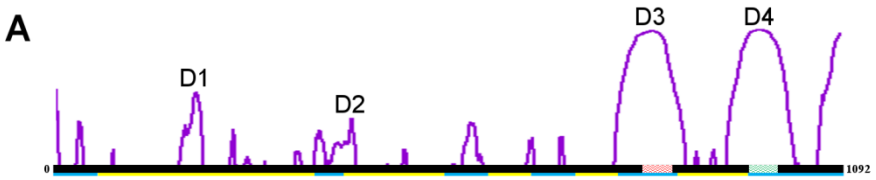

B

```
         10         20         30         40         50         60
MSKKSKTFKI GLTAGIVGLG VFGLTVGLSS LAKYRSESPR KIANDFAAKV STLAFSPYAF
DDDDDDD                          DDDDDDDD DDD
         70         80         90        100        110        120
ETDSDYKIVK RWLVDSNNNI RNKEKVIDSF SFFTKNGDQL EKINFQDPEY TKAKITFEIL
                        DDDD
        130        140        150        160        170        180
EIIPDDVNQN FKVKFQALQK LHNGDIAKSD IYEQTVAFAK QSNLLVAEFN FSLKKITEKL
                                                           DDDDDD
        190        200        210        220        230        240
NQQIENLSTK ITNFADEKTS SQKDPSTLRA IDFQYDLNTA RNAEDLDIKL ANYFPVLKNL
DDDDDDDDDD DDDDDDDDD DDDDDDDD
        250        260        270        280        290        300
INRLNNAPEN KLPNNLGNIF EFSFAKDSST NQYVSIQNQI PSLFLKADLS QSAREILASP
     DDDDD DDD
        310        320        330        340        350        360
DEVQPVINIL RLMKKDNSSY FLNFEDFVNN LTLKNMQKED LNAKGQNLSA YEFLADIKSG
                                   DDDDD DDDDD
        370        380        390        400        410        420
FFPGDKRSSH TKAEISNLLN KKENIYDFGK YNGKFNDRLN SPNLEYSLDA ASASLDKKDK
  DDDDDDDD DDDDDDDDD  DDDDDDDDDD DDDDDDDDDD DDDDDDDDDD DDDDDDDDDD
        430        440        450        460        470        480
SIILIPYRLE IKDKFFADDL YPDTKDNILV KEGILKLTGF KKGPKIDLPN INQQIFKTEY
                                                  DDD
        490        500        510        520        530        540
LPFFEKGKEE QAKLDYGNIL NPYNTQLAKV EVEALFKGNK NQEIYQALDG NYAYEFGAFK
     DDDDD D
        550        560        570        580        590        600
SVLNSWTGKI QHPEKADIQR FTRHLEQVKL GSNSVLNQPQ TTKEQVISSL KSNNFFKNGH
             D  D           DDD DDDDDDDDDD DDDDDDDDDD DDDDDD
        610        620        630        640        650        660
QVASYFQDLL TKDKLTVLET LYDLAKKWGL ETNRAQFPKE VFQYTKDIFA EADKLKFLEG
                                                           DDD
        670        680        690        700        710        720
KKKDPYNQIK EIHQLSFNIL ARNDVIKSDG FYGVLLLPQS VKTELEGKNE AQIFEALKKY
DDDDDDDD                                    DDDDDDDD
        730        740        750        760        770        780
SLIENSAFKT TILDKNLLEG TDFKTFGDFL KAFFLKAAQF NNFAPWAKLD DNLQYSFEAI
                                                             D
        790        800        810        820        830        840
KKGETTKEGK REEVDKKVKE LDNKIKGILP QPPAAKPEAA KPVAAKPEAA KPETTKPVAA
DDDDDDDDDD DDDDDDDDDD DDDDDDDDDD DDDDDDDDDD DDDDDDDDDD DDDDDDDDDD
        850        860        870        880        890        900
KPEAAKPVAA KPVAAKPVAT NTNTNTGFSL TNKPKEDYFP MAFSYKLEYT DENKLSLKTP
DDDDDDDDDD DDDDDDDDDD DDDDDDDDDD DDDDDDDD             D DDDDD
        910        920        930        940        950        960
EINVFLELVH QSEYEEQKII KELDKTVLNL QYQFQEVKVT SEQYQKLSHP MMTEGSPNQG
              DDDDDDD                 DDDDDDD DDDDDDDDDD DDDDDDDDDD
        970        980        990       1000       1010       1020
KKAEGAPNQG KKAEGAPSQG KKAEGAPNQG KKAEGAPSQG KKAEGASNQQ STTTELTNYL
DDDDDDDDDD DDDDDDDDDD DDDDDDDDDD DDDDDDDDDD DDDDDDDDDD DDDDDDDDDD
        1030       1040       1050       1060       1070       1080
PELGKKIDEI IKKQGKNWKT EVELIEDNIA GDAKLLYFVL RDDSKSGDPK KSSLKVKITV
DDDDDDDDDD DDDD                             DDDDDDDDD DDDDDDDDDD
        1090
KQSNNNQELK SK
DDDDDDDDDD DD
```

Figure 4.1: Structural analysis of P123$_J$ (MHJ_0194).

A) P123$_J$ is represented by a black bar. Regions of disorder predicted by PONDR® are shown in purple as D1, D2, D3 and D4. The height of the peaks corresponds to the level

of disorder represented as a PONDR® score. R1 and R2 are represented by red and green hatched boxes at amino acid positions 814-858 and 961-1010 respectively. Yellow and blue lines depict regions enriched in acidic and basic amino acids in P123$_J$ respectively. B) P123$_J$ sequence depicting semi-tryptic peptides (bold) identified by LC-MS/MS (Table S4.1). Underlined regions within peptides depict evidence of aminopeptidase activity. Amino acids highlighted in yellow and blue indicate regions enriched in acidic and basic amino acids in P123$_J$ respectively. S/T-X-F↓X-D/E motifs and the cleavage site generating P28 (amino acid 863) are double underlined. Neo N-termini resulting from cleavage are boxed. D denotes amino acids predicted by PONDR® that generate regions of protein disorder. R1 and R2 are boxed in red and green respectively.

4.3.2 Enrichment of low abundance cleavage fragments

Immunoblotting studies using antisera raised against recombinant fragments spanning different regions of P123$_J$ indicated that numerous endoproteolytic events occur [54]. Prior to this study, only the ^{861}N-T↓N-T-N-T^{866} cleavage site in the C-terminus of P94$_J$ strain had been mapped precisely [54]. LC-MS/MS analysis of protein spots derived from *M. hyopneumoniae* strains J and 232 cell lysates resolved by 2D SDS-PAGE gels separated on p*I* gradients from 4-7 and 6-11 did not identify new P123$_J$ cleavage fragments (data not shown). Based on this observation we concluded that the remaining cleavage fragments are of lower abundance compared to the dominant cleavage fragments already described.

To characterise low abundance cleavage fragments we employed several enrichment protocols that enabled us to recover fragments that retained the ability to bind to host

molecules. One approach relied on the recovery and characterisation of *M. hyopneumoniae* cell surface proteins labeled with biotin as described previously [3]. Peptide coverage from protein spots was obtained for the previously reported cleavage fragments $P22_J$, $P28_J$, $P66_J$ and $P94_J$ [54], confirming these fragments to be present on the surface of *M. hyopneumoniae* (Figure 4.2, Fragments 1, 2, 4 and 5, respectively). A full schematic representation of the semi-tryptic peptides that we believe to be true N-termini of a number of the fragments described below are presented in Figure 4.1. These were identified from fractionated and unfractionated *M. hyopneumoniae* lysates mapping to different regions in the cilium adhesin and their respective spectra are supplied in Figure S4.1. Our analysis indicates that many of the dominant cleavage fragments are targets of further endoproteolysis and aminopeptidase activity, albeit at low efficiency. None of these cleavage events occur at S/T-X-F↓X-D/E motifs, but cleavage was detected within regions enriched in hydrophobic amino acids consistent with studies describing cleavage events in P159 [43] and P216 [44]. Furthermore, we have described several surface accessible aminopeptidases in *M. hyopneumoniae* that have preferences for the amino acids that are being targeted in these events [145]. The N-terminal peptide derived from $P28_J$ (spot 5) produced the sequence ^{863}N-T-N-T-G-F-S-L-T-N-K^{873} consistent with the true N-terminus of $P28_J$ as determined previously by Edman sequencing [54]. Our raw LC-MS/MS data were searched against a database of protein sequences theoretically digested to tryptic peptides, in which this peptide was identified on multiple occasions confirming it represents the start site for $P28_J$ (Figure S4.1).

Two novel, biotinylated cleavage fragments of approximately 29 and 27 kDa (Fragments 8 and 9, respectively) mapped to the N-terminal region of $P94_J$ and $P66_J$

(Figure 4.2). While the tryptic peptide ^{295}E-I-L-A-S-P-D-E-V-Q-P-V-I-N-I-L-R^{311} was common to both cleavage fragments, the tryptic peptide ^{345}G-Q-N-L-S-A-Y-E-F-L-A-D-I-K^{358} was detected by LC-MS/MS analysis only of $P29_J$. We identified an S/T-X-F↓X-D/E site (^{434}K-F-F↓A-D-D^{439}) downstream of the second tryptic peptide suggesting that $P29_J$ spans a region from amino acids 195 to 436 (predicted mass of 27.6 kDa; p*I* 6.02). A semi-tryptic peptide with the sequence ^{437}A-D-D-L-Y-P-D-T-K-D-N-I-L-V-K^{451} was identified consistent with a cleavage event at this site (Figure S4.1). A little upstream, we also detected a series of semi-tryptic peptides within the sequence ^{398}R-L↓N↓S-P-N-L-E↓Y-S-L-D-A-A-S-A-S-L-D-K^{417} where arrows indicate the point of cleavage based on the N-termini of peptides identified, indicating that $P27_J$ spans a region of P94 from position 195 to 407. This cleavage fragment has a theoretical mass of 24.2 kDa (p*I* 5.58). Both $P27_J$ and $P29_J$ encompass acidic regions and they migrate with a p*I* that is more acidic than all the dominant cleavage fragments. Consistent with this analysis, both $P29_J$ and $P27_J$ are found on 2D SDS-PAGE gels containing biotinylated surface proteins of *M. hyopneumoniae* at positions that are more acidic than the dominant cleavage fragments $P22_J$, $P28_J$, $P66_J$ and $P94_J$ (Figure 4.2).

A biotinylated N-terminal fragment of $P94_J$, approximately 50 kDa, was identified and has been denoted as P50N (Figure 4.2, Fragments 6a, 6b, 6c). LC-MS/MS analysis of the individual spots belonging to $P50N_J$ identified a number of tryptic peptides spanning amino acids 222-583 commencing with ^{222}N-A-E-D-L-D-I-K^{229} in Fragment 6a and ending with ^{570}L-G-S-N-S-V-L-N-Q-P-Q-T-T-K^{583} in Fragment 6b. PATTINProt identified an S/T-X-F↓X-D/E motif at amino acid positions ^{604}S-Y-F↓Q-D-L^{609}. Consistent with our analysis, cleavage at this site would generate a fragment from 195-606 with a predicted mass of 47 kDa (p*I* 7.85). Fragments 6a and 6b appear to have the

same molecular mass; however, the ^{570}L-G-S-N-S-V-L-N-Q-P-Q-T-T-K^{583} peptide was not identified in Fragment 6a. The semi-tryptic peptide ^{571}G-S-N-S-V-L-N-Q-P-Q-T-T-K^{583} was frequently identified by LC-MS/MS (Figure S4.1) and cleavage at this site in Fragment 6b would result in only a slight shift in mass. The p*I* of Fragments 6a and 6b are 6.46 and 7.85, respectively, consistent with their relative positions on the 2D gel. Fragment 6c is a slightly smaller fragment and peptide coverage was too poor to establish the site of cleavage. The cleavage event that generates Fragment 6c is likely to take place at this position and this hypothesis is supported by the identification of the semitryptic peptide ^{529}D-G-N-Y-A-Y-E-F-G-A-F-K^{540}.

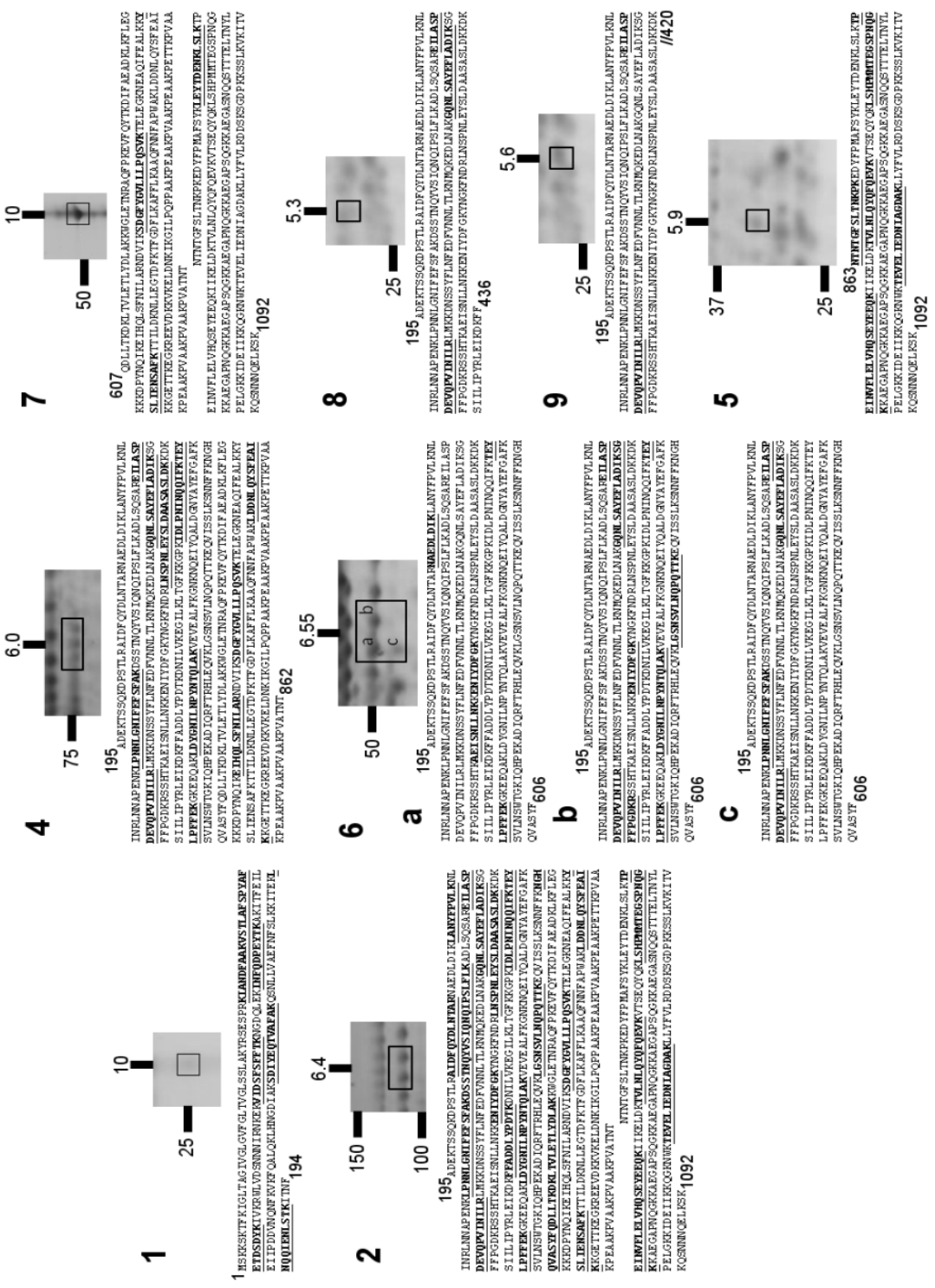

Figure 4.2: Tryptic peptides of biotinylated cleavage fragments of P123$_J$ identified by LC-MS/MS.

Biotinylated proteins were purified using avidin chromatography and separated by 2D SDS-PAGE. Proteins in spots containing fragments of P123$_J$ are designated by numbers

and correspond to cleavage fragments presented in Figure 4.3. Molecular masses (kDa) are indicated on the left of the 2D gel inserts and p*I* on the top.

Three tryptic peptides spanning the C-terminal half of $P94_J$ (P50C) commencing with ^{688}S-D-G-F-Y-G-L-L-L-P-Q-S-V-K^{702} and ending with ^{887}L-E-Y-T-D-E-N-K-L-S-L-K^{898} were also identified (Figure 4.2, Fragment 7). Cleavage at ^{604}S-Y-F↓Q-D-L^{609} generates a fragment from 607-1092 with a predicted mass of 54 kDa (p*I* of 9.05). This fragment is also likely to be cleaved at the ^{861}T-N↓N-T-N-T^{866} site generating an R1 containing fragment of approximately 29 kDa (p*I* 9.17) and the R2-containing $P28_J$ fragment. A summary of all the cleavage fragments identified in our studies is presented in Figure 4.3.

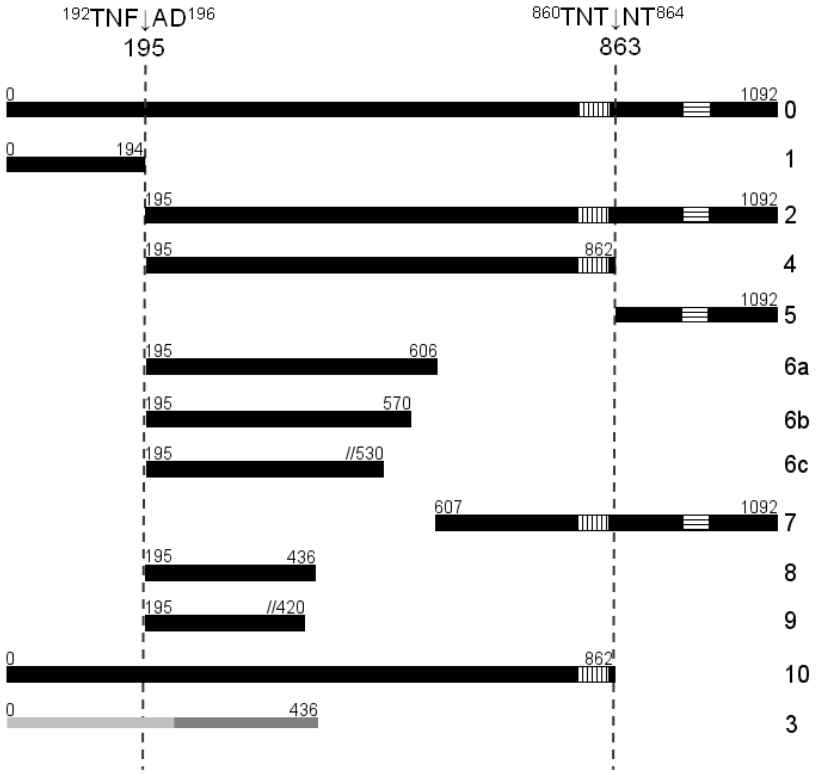

Figure 4.3: Cartoon depicting a summary of the cleavage fragments derived from P123$_J$.

Cleavage fragments presented in this diagram have been compiled from data previously generated by Djordjevic *et al.,* (2004) and data generated from surface biotinylation. Vertically hatched boxes indicate R1 region and horizontally hatched boxes depict R2. Fragment 3 was identified in strain 232 during heparin-agarose chromatography. Light grey bar in Fragment 3 indicates peptide coverage obtained by LC-MS/MS. The dark grey bar in Fragment 3 indicates the estimated mass of the molecule based on gel migration and known cleavage sites. Fragment 10 was recovered from affinity chromatography experiments using biotinylated PK-15 surface proteins as bait. Double slashes indicate estimated C-terminal cleavage sites.

4.3.3 Heparin-binding sites in P123

Highly sulphated glycosaminoglycans (GAGs), such as heparin and fucoidan, can effectively abolish binding of *M. hyopneumoniae* to cilia [205]. We have been interested in characterising surface-accessible heparin-binding proteins because their role is central to the ability of *M. hyopneumoniae* to colonise lung epithelial cilia [40]. Previously we showed that at least two regions within the $P123_J$ cilium adhesin bind heparin [41]. One heparin-binding site resides within amino acids 106-758 and the second is located within amino acids 768-1069, which contains both R1 and R2 regions [41]. To determine if other heparin-binding sites are located within $P123_J$, we used ScanProsite to survey the $P123_J$ sequence for putative glycosaminoglycan-binding sites by identifying regions within the sequence containing periodically repeating lysine (K), arginine (R), and histidine (H) residues. Eight structural motifs between 6 and 14 amino acids in length with sequences of B-X(0-2)-B-X(0-2)-B or B-X(1-4)-B-X(1-4)-B, where B represents K, R, or H residues and X any amino acid, were identified and their locations within $P123_J$ is shown in Figure 4.4. Native *M. hyopneumoniae* protein lysates (strains J and 232 separately) were subjected to heparin-agarose affinity chromatography, eluted using a sodium chloride gradient and bound proteins were separated by 1D SDS-PAGE and characterised by LC-MS/MS. Adhesin fragments corresponding to $P22_{J/232}$, $P28_{J/232}$, $P55_{232}$ (novel), $P66_J$/$P72_{232}$, and $P94_J$ /$P97_{232}$ were identified in native lysates derived from strains J and 232 (Figure 4.4). We hypothesise that each of these cleavage fragments contains one or more putative heparin-binding motifs.

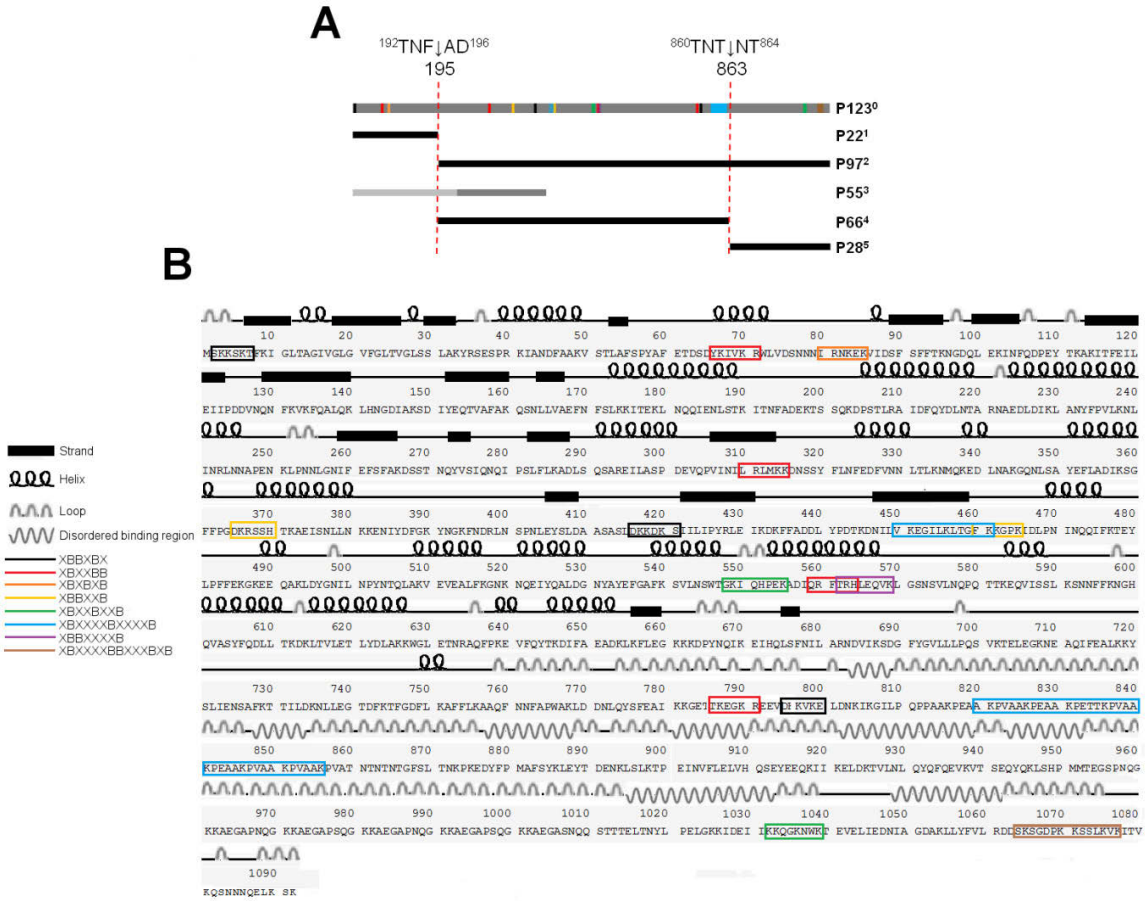

Figure 4.4: Heparin binding regions within P123$_J$.

Cleavage fragments isolated by heparin-agarose chromatography are shown in panel A. Known sites are indicated by broken lines. Fragments in black were identified in elutions from strain J and 232 whole cell lysates. The fragment in grey was identified only in strain 232. The light grey bar indicates the inferred amino acid sequence of P55$_J$ based on its position on 2D immunoblots and approximate molecular mass on 1D SDS-PAGE. Coloured lines depict locations of putative heparin-binding sites. B. Computational prediction of helices, strands, loops and protein binding sections in disordered regions within P123$_J$ are shown (see key). Boxed regions within P123$_J$ depict putative heparin-binding domains comprising repetitive basic amino acids as noted in the key.

Identification of $P28_{J/232}$ in the eluent from the heparin-agarose column was considered unusual. Previously we reported that $F2_{P94\text{-}J}$ (amino acids 768-1069), which encompasses R1 and R2, bound heparin. However, $F3_{P94\text{-}J}$ (encompasses R1) and $F4_{P94\text{-}J}$ (encompasses R2) did not bind heparin and we concluded that both R1 and R2 are needed in the same molecule to bind heparin [41]. $F4_{P94\text{-}J}$ spans amino acids 935-1069 and lacks the C-terminal 23 amino acids of the cilium adhesin (Figure 4.5). For clarity, we have renamed it $F4_{P94\text{-}J/\Delta 23}$. It is conceivable that the C-terminal 23 amino acids from 1070-1092 that are absent in $F4_{P94\text{-}J/\Delta 23}$ may play a role in binding heparin given that we identified a putative heparin-binding motif (B-X-X-X-X-B-B-X-X-X-B-X-B) in the sequence ^{1065}K-S-G-D-P-K-K-S-S-L-K-V-K^{1077} and the remaining amino acids at the C-terminus of the molecule (^{1078}I-T-V-K-Q-S-N-N-N-Q-E-L-K-S-K^{1092}) contains several basic residues that may play a role in binding heparin. To examine the possibility that the C-terminal 23 amino acids of the cilium adhesin bind GAGs, a recombinant polyhistidine fusion protein ($F4_{97\text{-}J}$) spanning amino acid 935-1092 that included the C-terminal 23 amino acids (Figure 4.5) was purified by nickel-affinity chromatography. We compared the ability of $F4_{P97\text{-}J}$ to bind heparin with $F4_{P94\text{-}J/\Delta 23}$ using microscale thermophoresis. Consistent with our previous experiments, $F4_{P94\text{-}J/\Delta 23}$ did not bind heparin [41] but $F4_{P97\text{-}J}$ bound heparin with a physiologically significant K_D of 182.3 ± 49.64 nM (Figure S4.2).

To decipher the location of the heparin-binding domain in the C-terminal 23 amino acids, overlapping synthetic peptides (Figure 4.5) were synthesised commercially and assessed for their ability to bind heparin using a microtitre plate assay. Peptide 1 (23-mer) and peptides 8, 9 and 10 bound heparin. The shortest peptide that retained the ability to bind heparin had the sequence ^{1070}K-K-S-S-L-K-V-K-I-T-V-K^{1081} indicating

that a putative heparin-binding domain is encompassed within this peptide. These data provide an explanation for the inability of $F4_{P94J/\Delta 23}$, and the contrasting ability, of $P28_{J/232}$ to bind heparin.

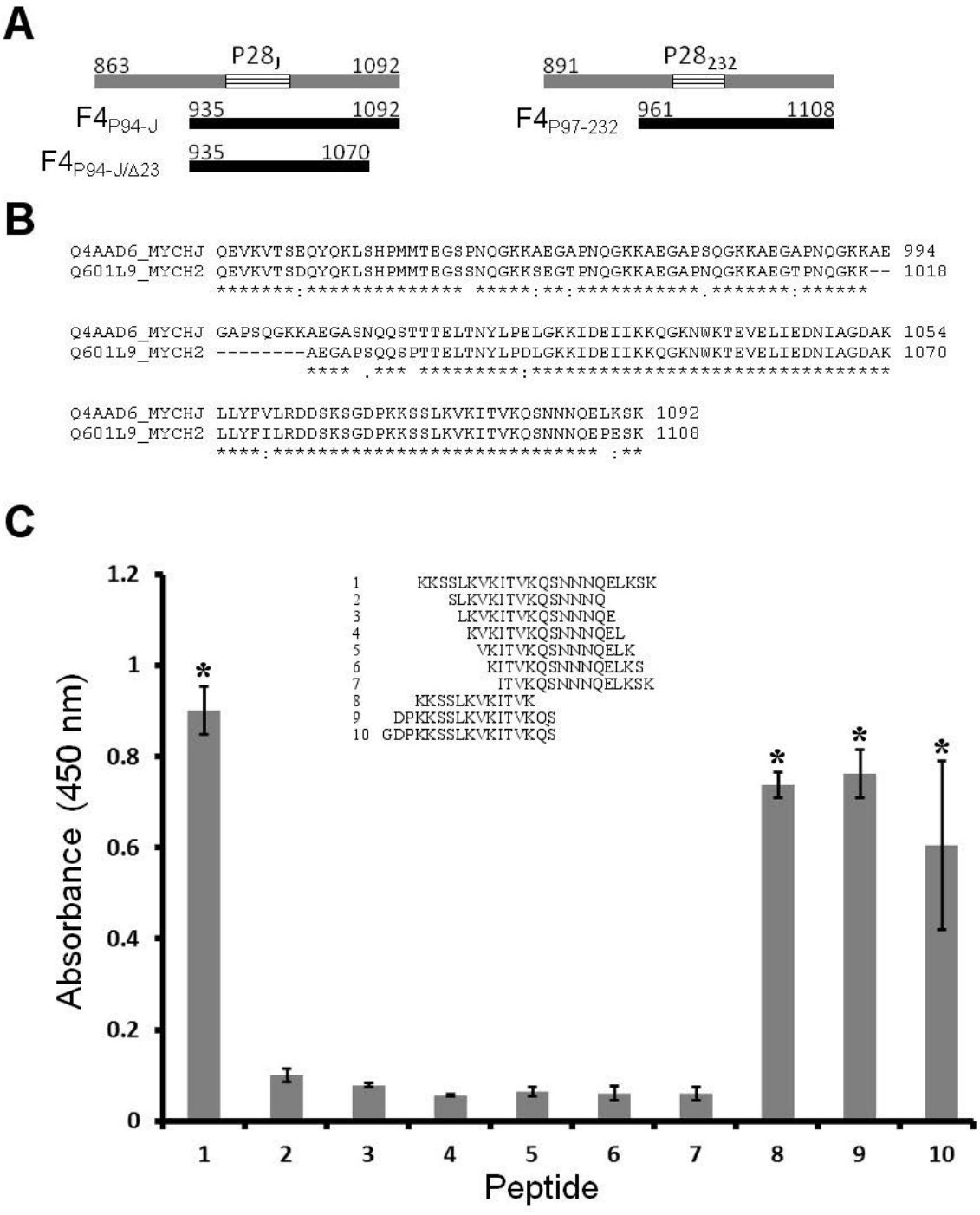

Figure 4.5: Comparative sequence analysis of the C-terminal region of $P123_J$ and $P125_{232}$ and recombinant fragments used to characterize the function of the C-terminus.

A) Schematic of $F4_{P97-232}$, $F4_{P94-J}$ and $F4_{P94-J/\Delta23}$. Amino acids encompassed by the recombinant fragments are noted. Horizontally hatched boxes represent the R2 region.

B) $F4_{P94\text{-}J}$ (Q4AAD6) and $F4_{P97\text{-}232}$ (Q601L9) show considerable sequence identity (asterisks) aside from one extra copy of a decapeptide repeat in R2 in $F4_{P94\text{-}J}$ and amino acids indicated by a dot. Double dots indicate amino acids that have a similar charge and structure. Absent amino acids are indicated by a single hyphen. C) Overlapping synthetic peptides spanning the C-terminal 23 amino acids of $P123_J$ and their ability to bind heparin by ELISA. The amino acid sequences of peptides 1-10 are shown. Peptides 1, 8, 9 and 10 bound heparin (asterisks). A t-test was performed between each peptide and the lowest binding peptide and any P score < 0.05 demonstrated a difference between those peptides which was deemed statistically significant.

4.3.4 The C-terminus of the mature cilium adhesin and the $P28_{232}$ cleavage fragment bind Plg

Previously, we determined that $P125_{232}$ paralog Mhp107 [8], P102 (Mhp182) [9] and P102 paralogs Mhp108 [7] and Mhp684 [2], and the aminopeptidase MHJ_0125 [145] are Plg-binding proteins that reside on the surface of *M. hyopneumoniae*. The C-terminus of $P97_{232}$/$P94_J$ comprises a C-terminal lysine residue, a feature of proteins that often confers an ability to interact with Plg [210]. C-terminal regions of $P97_{232}$ and $P94_J$ represented by $F4_{P97\text{-}232}$ and $F4_{P94\text{-}J}$ share strong amino acid identity varying by the presence of an extra decapeptide repeat in R2 of $P94_J$ and 13 single amino acid changes. We used surface plasmon resonance to determine if $F4_{P97\text{-}232}$ and an identical construct lacking the C-terminal lysine ($F4_{P97\text{-}232\Delta lys}$) bind Plg. $F4_{P97\text{-}232}$ and $F4_{P97\text{-}232\Delta lys}$ are recombinant polyhistidine fusion proteins purified by nickel-affinity chromatography from *E. coli* lysates. $F4_{P97\text{-}232}$ stably bound immobilised Plg with little evidence of dissociation. Binding saturated at low concentrations of $F4_{P97\text{-}232}$ with a physiologically relevant K_D of 13 ± 2 nM (Figure 4.6). When the C-terminal lysine was removed from

$F4_{P97-232}$ a higher concentration of protein was required to saturate binding, but the K_D value remained physiologically relevant (K_D = 49 ± 25 nM) (Figure 4.6), indicating that the C-terminal lysine is not critical for binding Plg.

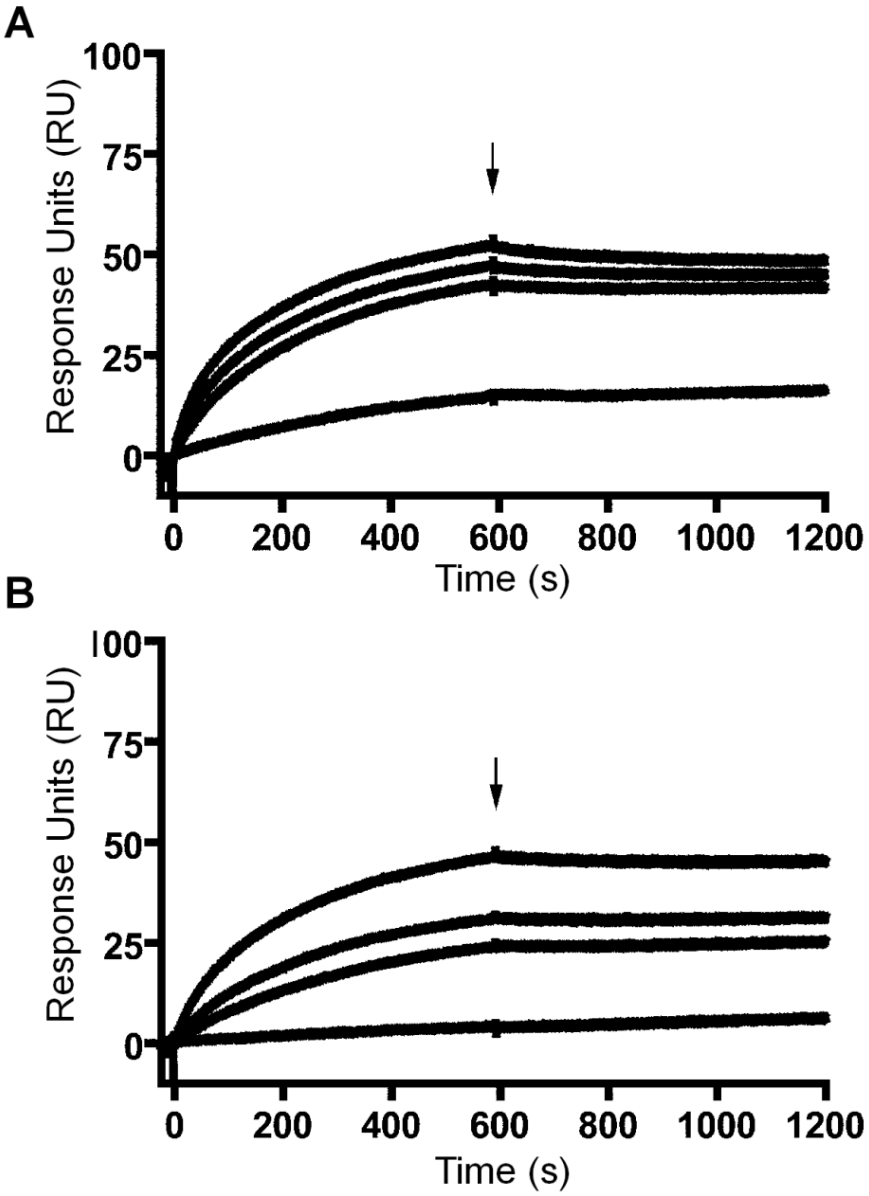

Figure 4.6: Surface plasmon resonance.

Surface plasmon resonance sensorgrams of $F4_{P97\text{-}232}$ (A) and $F4_{P97\text{-}232\Delta lys}$ (B) binding to immobilised porcine Plg. Proteins were injected over Plg at 10, 50, 100 and 200 nM for 600 s at 10 µL/min. The end of the injection period is indicated by an arrow. Following the injection period, dissociation of bound protein from Plg is observed.

4.3.5 The C-terminus of P28 binds Fn

Several adhesins including Mhp183 paralogs Mhp271 [5], Mhp107 [8], Mhp182 (P102) [9] and Mhp182 paralog Mhp108 [7] have been shown to bind Fn. Native cell lysates of *M. hyopneumoniae* strain J were screened for proteins that bind Fn by passing them through an affinity column containing biotinylated Fn immobilised on avidin agarose. Bound proteins were separated by 1D SDS-PAGE, digested in-gel with trypsin and analysed by LC-MS/MS. A peptide with the sequence ^{1040}T-E-V-E-L-I-E-D-N-I-A-G-D-A-K^{1054}, mapping to the C-terminus of $P94_J$, was identified among proteins migrating with a mass between 20-30 kDa (Figure S4.3), suggesting that the C-terminal cleavage fragment $P28_{J/232}$ may bind Fn. A microtitre plate assay was used to determine if $F4_{P97-232}$, $F4_{P94-J}$ and $F4_{P94-J\Delta23}$ bind Fn (Figure 4.7). $F4_{P97-232}$ and $F4_{P94-J}$ bound immobilised Fn in a dose-dependent and saturable manner with a physiologically relevant K_D of 29.3 ± 12.6 μM and 3.1 ± 0.7 μM, respectively. $F4_{P94-J/\Delta23}$ bound poorly to Fn suggesting that the C-terminal 23 amino acids of $P123_J$ are required for binding Fn.

Overlapping peptides (Figure 4.5) spanning the C-terminal 23 amino acids of $P94_J$ were tested for their ability to bind Fn. Peptides 1, 8, 9 and 10 bound Fn at levels significantly higher than the other peptides (Figure 4.7). The sequence ^{1070}K-K-S-S-L-K-V-K-I-T-V-K^{1081} which was encompassed in peptide 8 was common to all four of the peptides that bind Fn. Our data shows that the sequence represented by peptide 8 contains both a heparin (see Figure 4.7) and a Fn binding site.

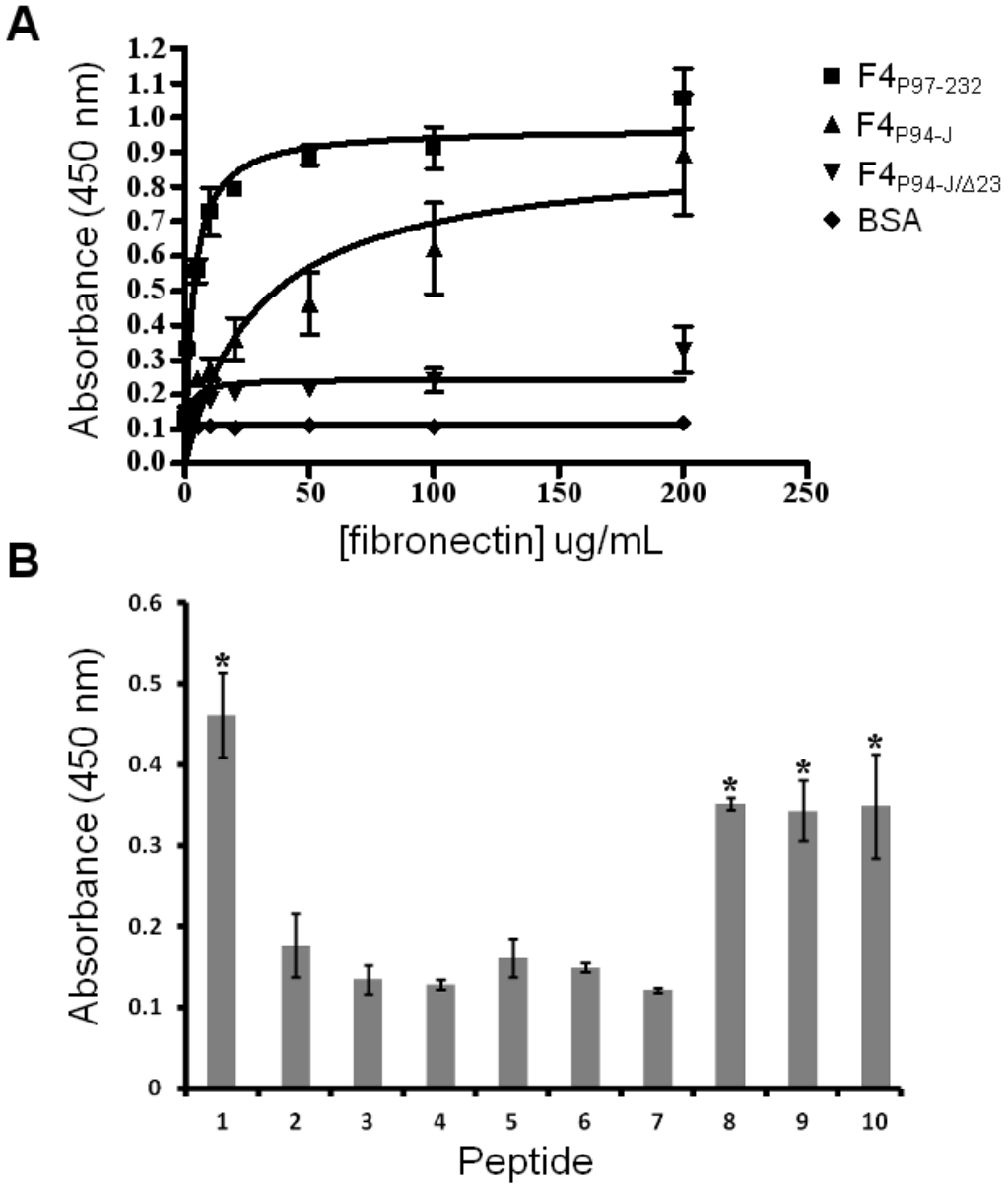

Figure 4.7: The C-terminus of P123$_J$ and P125$_{232}$ binds Fn.

A) Immobilised F4$_{P94-J}$ and F4$_{P97-232}$ bind Fn in a dose dependent and saturable manner in a microtitre plate binding assay. F4$_{P94-J}$ binds Fn with a higher affinity than F4$_{P97-232}$. F4$_{P94-J\Delta23}$ fails to bind Fn. BSA was used as a negative control. The data plotted here represents the averages from triplicate data and the corresponding standard deviations are shown. B) Microtitre plate binding assay showing the binding of overlapping synthetic peptides spanning the C-terminal 23 amino acids of P123$_J$ to soluble Fn. Peptide sequences can be found in Figure 4.5. Peptides that bound are denoted by an

asterisk. A t-test was performed between each peptide and the lowest binding peptide and any P score < 0.05 demonstrated a difference between those peptides which was deemed statistically significant.

4.3.6 Identifying cleavage fragments of $P123_J$ that adhere to PK-15 cell surface proteins

Eight tandem copies of the pentapeptide repeats in $P125_{232}$ are required to bind porcine epithelial cilia [207]. Here we employed an affinity chromatography procedure to identify cleavage fragments of $P123_J$ that adhere to surface proteins displayed by PK-15 cells. PK-15 monolayers have previously been established as the model system for monitoring *M. hyopneumoniae* adherence [215]. Proteins displayed on the surface of PK-15 cell monolayers were labelled with biotin, immobilised onto avidin agarose and exposed to a soluble *M. hyopneumoniae* strain J cell lysate. Proteins that bound were eluted, separated by 1D SDS-PAGE and identified by LC-MS/MS. Dominant cleavage fragments containing R1 were identified including $P94_J$ and $P66_J$. In addition, we identified a novel fragment of approximately 100 kDa (Fragment 10 in Figure 4.3) that generated tryptic peptides spanning $P22_J$ and $P66_J$.

4.3.7 *M. hyopneumoniae* co-localises with Fn when colonising PK-15 cell monolayers

Immunofluorescence microscopy (IFM) using anti- $F2_{P97}$ antibodies [41] was used to monitor the location of *M. hyopneumoniae* on PK-15 cell monolayers. Anti-Fn antibodies were also used to monitor the location of Fn on *M. hyopneumoniae*-infected PK-15 cell monolayers. CLSM showed Fn localising precisely where *M. hyopneumoniae* cells were colonising the surface of PK-15 cells (Figure 4.8). This finding was also consistent with studies using 3D-SIM showing the interaction between *M. hyopneumoniae* and PK-15 cells at higher resolution. 3D-SIM also revealed that Fn was not uniformly distributed around the *M. hyopneumoniae* cell surface suggesting that Fn-binding proteins were not uniformly distributed in the *M. hyopneumoniae* cell membrane (Figure 4.8).

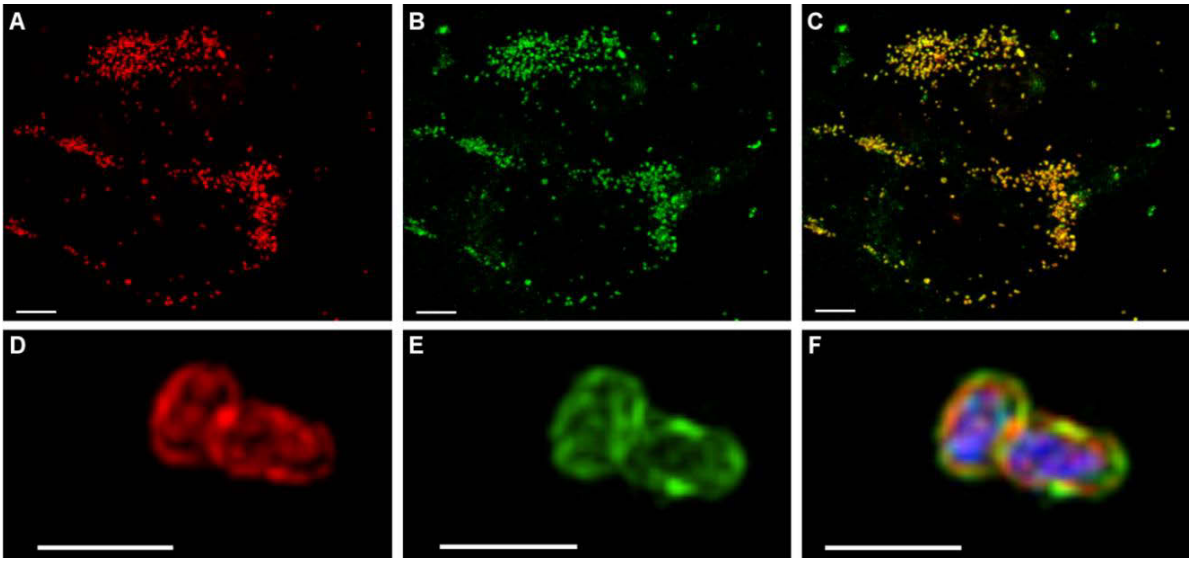

Figure 4.8: Fluorescence micrographs showing the distribution of Fn in *M. hyopneumoniae*-infected PK-15 monolayers.

A-C) CLSM images of *M. hyopneumoniae* cells colonising PK-15 monolayers. A. The location of *M. hyopneumoniae* cells on PK-15 cell monolayers were identified using rabbit anti-$F2_{P97}$ antibodies followed by goat anti-rabbit Ig conjugated to Alexa Fluor® (568 nm). B) The distribution of Fn on PK-15 cell monolayers was determined using goat anti-Fn antibodies followed by donkey anti-goat Ig antibodies conjugated with Alexa Fluor® (488 nm). C) A merge of *M. hyopneumoniae* cells and Fn showing their co-localisation. Scale bar is 10 µm. D-E) 3D-SIM images of *M. hyopneumoniae* cells bound to a PK-15 cell monolayer. D) Two *M. hyopneumoniae* cells adhering to the surface of a PK-15 cell showing the distribution of $P123_J$ cleavage fragments containing R1 and R2. E) The distribution of Fn on *M. hyopneumoniae* cells. F) Overlay of D-E. Merged image clearly depicts Fn co-localising on the surface of *M. hyopneumoniae* cells. DNA was stained with DAPI and appears blue. Scale bar is 1 µm.

In vitro studies show that *M. hyopneumoniae* can bind Fn in a dose-dependent manner and that P97/P102 adhesins are important Fn-binding proteins [5,7-9]. One of the circumstances in which Fn becomes available at the epithelial cell surface is from cellular damage caused by pathogenic bacteria [216,217]. To determine if Fn localises with *M. hyopneumoniae* during infection of the respiratory tract, immunohistochemical analysis of serial sections of lung tissue from pigs experimentally challenged with *M. hyopneumoniae* was undertaken. Lung scores for the lung images depicted in Figure 4.9 are listed in Table S4.2. *M. hyopneumoniae* cells were identified along the cilial border of the epithelium in sections of lung tissue taken from experimentally-infected pigs as expected (Figure 4.9). A serial lung section from the same pig (same area of tissue) stained with anti-Fn antibodies shows Fn staining along the cilial border (Figure 4.9) where *M. hyopneumoniae* cells adhere. Low levels of Fn were observed in the sub-epithelial layers (Figure 4.9) and also around the endothelium surrounding a blood vessel (Figure 4.9). Fn was never observed at the cilial borders of sections taken from uninfected pigs, which is consistent with Fn being expressed in connective tissue and at cellular junctions but not typically observed on the ciliated epithelial surface without evidence of tissue injury. Our data indicates that *M. hyopneumoniae* cells recruit Fn to the site of infection presumably by eliciting epithelial cell damage.

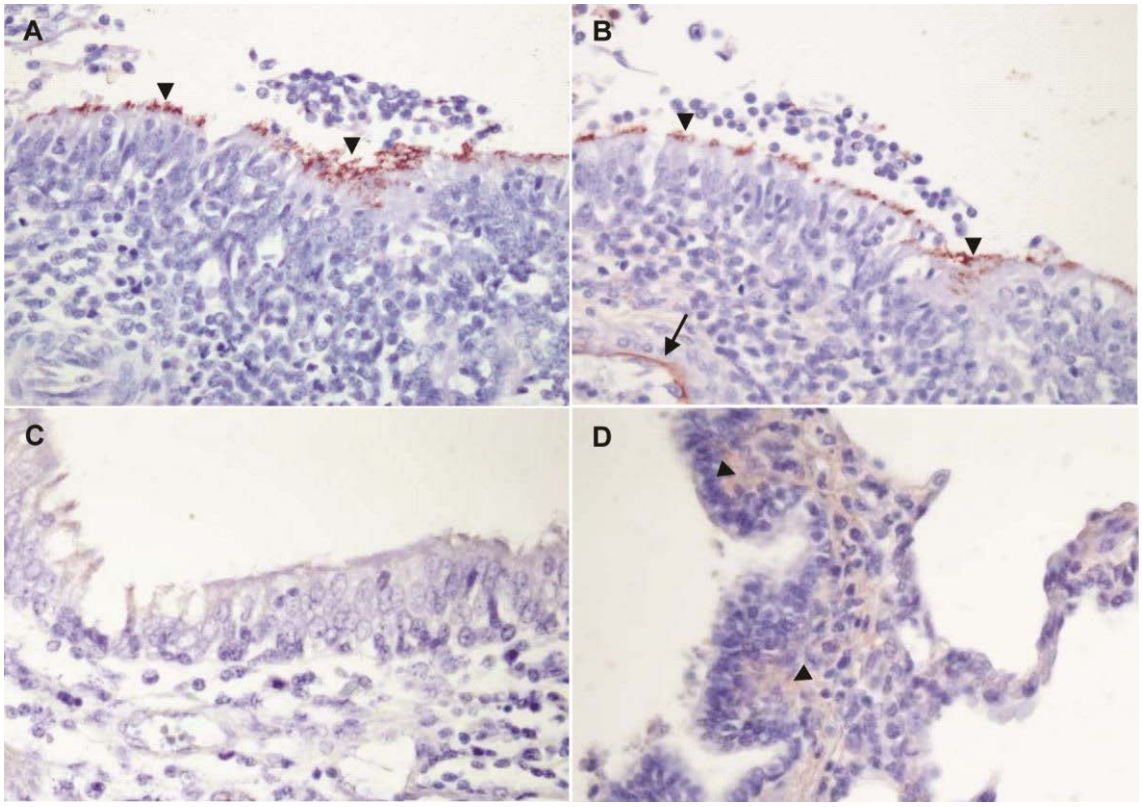

Figure 4.9: Mycoplasma cells and Fn co-localise in infected lung tissue.

A-B) Immunohistochemical staining of tracheal sections from a lung-homogenate inoculated pig stained with anti-$F2_{P97}$ and anti-Fn serum respectively. A. *M. hyopneumoniae* cells can be seen adhering to the tips of cilia (arrow). B) Fn observed at the tips of cilia (arrow) where *M. hyopneumoniae* cells adhere. The thin arrow denotes normal Fn distribution at the subepithelial layer. C) A section from an *M. hyopneumoniae*-infected pig, but stained with an irrelevant antibody, showing that the anti-ADH and anti-Fn reactivity seen in A and B is specific. D depicts the localisation of Fn in uninfected pig lung. Note diffuse staining depicted by arrows.

4.4 Discussion

During the early stages of colonisation of the porcine respiratory tract, *M. hyopneumoniae* targets GAGs on proteoglycans that decorate the surface of porcine epithelial cells and cilia. The inclusion of porcine heparin or fucoidan to assay buffers used for binding studies effectively blocks attachment of *M. hyopneumoniae* to cilia [154] and PK-15 monolayers [4] underscoring the biological importance of these interactions. GAGs on the surface of porcine respiratory tract cilia are sensitive to heparinase, indicating that heparin-binding proteins on the surface of *M. hyopneumoniae* are important adhesins needed to establish infection [40]. These observations indicated that heparin-agarose chromatography would be an effective method to recover cleavage fragments of $P123_J$ that display heparin-binding motifs. This approach identified $P22_J$, $P28_J$, $P55_J$ (novel fragment identified in this study), $P66_J$ and $P94_J$ as heparin binding cleavage fragments derived from the P123 preprotein. In our study we identified 12 cleavage fragments of P123. Of these only $P100_J$, $P94_J$, $P66_J$ and P50C retain the R1 cilium binding domain and P28 is the only fragment that contains R2 without R1. Only two fragments, $P94_J$ and P50C retain both R1 and R2 domains. Our data show that proteolytic cleavage of a large adhesin preprotein generates a sophisticated array of adhesion functions and is a versatile mechanism to generate multifunctional cell surface proteins.

mAb F2G5 reactive proteins recovered by affinity chromatography have been shown to be effective at blocking the adherence of *M. hyopneumoniae* cells to cilia [154]. In support of this, *M. hyopneumoniae* proteins that carry a minimum of three pentapeptide repeats (Mhp183, Mhp271 and Mhp385) were deemed to play a role in adherence to cilia, and these observations have been validated in subsequent studies [5,6]. $P94_J$, $P66_J$

and a novel 100 kDa cleavage fragment (Fragment 10) were shown to bind strongly to PK-15 surface proteins. These data indicate that R1 containing cleavage fragments are critical porcine epithelial cell adhesins.

Immunoblotting data generated using the adherence blocking mAbs F2G5 and F1B6 showed a complex banding profile indicating that the cilium adhesin preprotein $P123_J$ is a target of extensive endoproteolytic processing [54,154]. In a previous study, we identified $P22_J$, $P28_J$, $P66_J$ and $P94_J$ as *bona fide* cleavage fragments of the $P123_J$ cilium adhesin but indicated that processing of the molecule was likely to be more complex [54]. Processing is fundamental to the presentation of cilium adhesins on the surface of *M. hyopneumoniae* and cleavage fragments are the key effectors in binding interactions with host cells [2-10,43,44].

In this study, we have mapped both dominant and low abundance cleavage products of the cilium adhesin $P123_J$ and provide evidence that it is extensively processed generating a complex variety of cleavage fragments, all of which reside on the cell surface. Cleavage occurs at three S/T-X-F↓X-D/E sites (^{192}T-N-F↓A-D^{196} and ^{434}K-F-F↓A-D^{438}, and ^{604}S-Y-F↓Q-D^{608}) within acidic domains, consistent with studies of S/T-X-F↓X-D/E sites in other members of the P97 and P102 adhesin families [43,44]. The cleavage site within the sequence ^{192}T-N-F↓A-D^{196} at amino acid 195 is located within a long region of protein disorder, consistent with it being a dominant, high frequency cleavage site [2,3,6]. Notably, most cleavage sites generated fragments that were targets for further N-terminal aminopeptidase activity. We previously characterised a cell surface aminopeptidase in *M. hyopneumoniae* whose substrate specificity is consistent with cleavage at these sites [145]. In addition, the identification of several semi-tryptic

peptides with sequences ^{870}K↓P-V-A-A-K↓P-V-A-T-N-T^{862} and the peptide ^{863}N-T-N-T-G-F-S-L-T-N-K-P-K^{875} reconfirms the precise site of endoproteolysis in the dominant cleavage event at position 862 that generates $P66_J$ and $P28_J$. This cleavage site also resides in a long region of protein disorder. Data presented here and elsewhere [43,44,218] strongly suggests that *M. hyopneumoniae* possesses trypsin-like proteolytic activity on its cell surface. Our analysis of semi-tryptic peptides indicate that non-dominant cleavage occurs immediately after hydrophobic residues L (6 sites)/V (4 sites) /I (2 sites), an observation that corresponds with previous studies [6,43,44].

Functional analyses of the $P123_J/P125_{232}$ cilium adhesin have focussed on the role of the cilium binding R1 region [205,207].The identification of binding sites for Fn and heparin in the C-terminal 23 amino acids of $P123_J/P125_{232}$ is a seminal contribution of this study. The identification of $P28_J$ (amino acids 863 -1092) by LC-MS/MS in high salt eluates from heparin-agarose chromatography provided the first evidence that the C-terminus of $P123_J$ may bind heparin. Previously we showed that $F4_{P94\text{-}J}$ (renamed here $F4_{P94\text{-}J/\Delta23}$), which spans amino acids 935 – 1069, was unable to bind heparin [41]. Here, we have re-engineered the construct to include the C-terminal 23 amino acids ($F4_{P94\text{-}J}$) and showed that $F4_{P94\text{-}J}$ bound heparin (K_D of 182.3 ± 49.64 nM), while $F4_{P94\text{-}J/\Delta23}$ did not. In a separate series of experiments, we identified a peptide unique to $P123_J$ ^{1040}T-E-V-E-L-I-E-D-N-I-A-G-D-A-K^{1054} by LC-MS/MS in a tryptic digest of a gel slice containing proteins between 20-30 kDa that were retained on a column comprising biotinylated Fn bound to avidin-agarose. This peptide is located within $P28_J$'s amino acid sequence and our microtitre plate binding assays demonstrated that both $F4_{P97\text{-}232}$ and $F4_{P94\text{-}J}$ bound Fn with K_D's of 29.3 ± 12.6 and 3.1 ± 0.7 μM, respectively, suggesting that $P28_J$ binds Fn. $F4_{P94\text{-}J}$ contains an extra copy of the decapeptide repeat in

R2 compared with $F4_{P97-232}$ but it is unclear if this is the reason why $F4_{P94-J}$ binds Fn more strongly. Notably, $F4_{P94-J\Delta23}$ failed to bind Fn, suggesting that the C-terminal 23 amino acids plays a role in binding this ECM molecule. The presence of a C-terminal lysine residue in $P123_J$ and $P125_{232}$ indicated that the cilium adhesin may also bind Plg. Recombinants $F4_{P97-232}$ and $F4_{P97-232/\Delta lys}$ that were identical except for the loss of the terminal lysine were examined for their ability to bind Plg using surface plasmon resonance. Both constructs bound Plg with similar affinity, indicating that the C-terminal lysine of $P123_J/P125_{232}$ is not central to the ability of $P28_{232}$ to bind Plg. *In vitro* studies have previously shown that the binding of Plg to the surface of *M. hyopneumoniae* promotes activation to plasmin in the presence of tissue-specific activator (tPA) [9]. *M. hyopneumoniae* promotes the conversion of Plg to plasmin in the BALF bathing the respiratory tract of pigs. This is evidenced by elevated levels of plasmin in the BALF of pigs infected with *M. hyopneumoniae* when compared to BALF recovered from identical animals prior to experimental challenge [9,34] and by the significant correlation between bacterial load and plasmin activity in the BALF of experimentally challenged pigs [34]. Plasmin levels also correlate significantly with the levels of pro-inflammatory cytokines TNF-α, IL-1β and IL-6 in the BALF at 21 days post challenge with *M. hyopneumoniae* [34]. The sequestration of plasmin to the surface of *M. hyopneumoniae* arms the pathogen with a powerful host-derived endoprotease that degrades host ECM and has been linked with the ability of other bacteria to invade tissues sites distal to the initial site of colonisation [84]. *M. hyopneumoniae* has been cultured from the liver, spleen, kidneys and lymph nodes of infected swine suggesting that it capable of invading epithelial barriers and traversing to distal tissue sites [14-16]. The mechanism which *M. hyopneumoniae* utilises to disseminate to these distal tissue

sites is unknown however it is hypothesised to involve binding to glycosaminoglycans, Plg and Fn.

4.5 Conclusion

M. hyopneumoniae binds Fn in a dose-dependent manner and several paralogs of $P125_{232}$/$P123_J$ have been shown to bind Fn including Mhp271 [5], Mhp107 [8], and Mhp684 [2]. P102 (Mhp182) and Mhp108, a paralog of P102, have also been shown to bind Fn [7,9]. The biological significance of this interaction between *M. hyopneumoniae* and Fn has not been established. We show here that the distribution of Fn on the surface of porcine kidney epithelial-like cell correlates with the distribution of *M. hyopneumoniae* colonising the surface of the cell monolayer indicating that Fn is recruited to the site where *M. hyopneumoniae* cells are attached to PK-15 cells. Higher resolution images using 3D-SIM shows that Fn is non-uniformly attached to the surface of *M. hyopneumoniae* cells that are making contact with the membrane surface of the PK-15 cell monolayer. Immunohistochemical analysis of sections of lung tissue from pigs experimentally-infected with *M. hyopneumoniae* but not lung sections from healthy animals show the organism adhering to the ciliated epithelial lining in the lumen of the airways as expected. Anti-Fn antibodies clearly detected Fn localised to the ciliated epithelial lining of the *M. hyopneumoniae*-infected airways. These observations suggest that *M. hyopneumoniae* induces epithelial cell damage, which results in the recruitment of Fn.

Our observation that the C-terminal 23 amino acids of $P123_J$ binds heparin, and Fn allowed us to pinpoint the amino acids that play a key role in binding these important host molecules. A series of overlapping peptides were screened to find the shortest peptide that retained the ability to bind heparin and Fn. Other than the 23-mer peptide comprising the C-terminal 23 amino acids, peptides 8, 9 and 10 consistently bound Fn and heparin. The shortest peptide that retained the ability to bind heparin and Fn

comprised the sequence ^{1070}K-K-S-S-L-K-V-K-I-T-V-K^{1081}. BlastP analysis identified 100% sequence identity in P123 homologs from North American isolates (UniProt # Q6R518; Q6R510; Q6R514; Q6R5H9; Q6R5H7; Q6R5H8; Q6R5I6; **Q6R5I2**), two Chinese isolates (UniProt # E4QSB0; R4TYI6) [219] two Brazilian strains [208] (UniProt # Q4A8G7; S5FXB0), and an Australian strain [220] of *M. hyopneumoniae* (UniProt # Q56H18); indicating the importance of retaining this sequence in the cilium adhesin. Collectively, these data indicate that $P28_{J/232}$ is an adhesin that binds Fn, heparin and Plg.

Fn is a multidomain eukaryote adhesin with the ability to bind collagen, fibrin, actin (through β_1 integrins), DNA and heparin and other host molecules [46]. Fn is thought to function as a "bridging molecule" as it confers an additional adhesive property to Fn-binding proteins [46]. Bacterial Fn-binding proteins play a role in host cell invasion by interacting with β_1 integrins [51,221]. Pathogenic bacteria can utilise Fn as a bridging molecule to integrin β1 receptors, causing downstream signalling events leading to actin and microtubule rearrangement that facilitates internalisation [46]. Fn is also influenced by the fibrinolytic system; plasmin is able to degrade Fn [222] and Plg activators have been shown to degrade Fn in the absence of Plg [223]. Urokinase-type Plg activator and tPA have also been shown to promote the expression of Fn, and tPA can promote the assembly of Fn in the ECM [224]. Given that plasmin levels are upregulated in the BALF of *M. hyopneumoniae*-infected swine and that Fn is present on the ciliated epithelial border at the site of infection [9,34] plasmin(ogen) and tPA in the porcine lung likely play a dual role in the degradation of ECM proteins and in initiating increased expression of Fn.

Here we have shown that the C-terminus of P97 possesses the capacity to bind Fn, Plg and heparin; three molecules that meet at a number of biological crossroads and are involved in regulating several processes at the cellular level. Plasmin is a serine endoprotease with broad substrate specificity. Plasmin activates matrix metalloproteases initiating a proteolytic cascade that targets a wide range of host molecules [84]. These proteolytic events generate neo-N-termini and we hypothesized that these represent novel substrates for microbial cell surface aminopeptidases [145]. We have recently shown that a glutamyl aminopeptidase [145] and a leucine aminopeptidase (Jarocki *et al.,* unpublished results) are active as aminopeptidases on the surface of *M. hyopneumoniae*. These and other aminopeptidases are expected to digest neo N-termini generated by the endoproteolytic cascade described above, providing a supply of essential amino acids for growth.

Here we have shown that numerous cleavage fragments that are derived from a series of processing events in the cilium adhesin $P123_J/P125_{232}$ have a remarkable capacity to bind to a structurally diverse array of host molecules including Plg, glycosaminoglycans, and Fn. These host molecules play key roles in cell-cell communication and cellular integrity, innate immunity and inflammation and are often targeted by pathogens that seek to proliferate intracellularly with the host. Furthermore we show that *M. hyopneumoniae* co-localises with host Fn at the site of infection on the ciliated epithelium. Together, these attributes suggest that *M. hyopneumoniae* possesses the molecular armoury to influence key molecular communication pathways that are critical for host cell function. Further work is aimed at investigating how *M. hyopneumoniae* engages with host epithelial cell membranes and to determine if *M. hyopneumoniae* can penetrate and proliferate within porcine cells.

Chapter Five: (Paper IV) Global analysis of adhesins and host receptors, and biofilm formation in *M. hyopneumoniae*

Declaration

I declare that the following publication included in this thesis in lieu of a chapter meets the following:

- More than 50% of the content in the following publication included in this chapter has been planned, executed and prepared for publication by me
- The work presented here has been prepared for publication and will be submitted
- The initial draft of the work has been written by me and any subsequent changes in response to co-authors and editors reviews was performed by me
- The publication is not subject to any obligations or contractual agreements with a third party that would constrain its inclusion in the thesis.

Publication title: *Mycoplasma hyopneumoniae* forms biofilms on the surface of porcine epithelial cells and binds actin

Authors: Benjamin B.A. Raymond, Lynne Turnbull, Cynthia B. Whitchurch, Matthew P. Padula, and Steven P. Djordjevic

Candidate's contribution (%): above 50 %

Journal name: mBio

Volume/ page numbers:

Status: To be submitted

I declare that the publication above meets the requirements to be included in the thesis.

Candidate's name: Candidate's signature: Date (dd/mm/yy):

5.1 Introduction

Mycoplasmas evolved by a process of degenerative evolution, shedding genes for cell wall biosynthesis, nucleic acid and amino acid synthesis, and the tricarboxylic acid cycle. As such Mycoplasmas have lost many anabolic enzymatic functions and must form intimate interactions with their respective hosts to sequester essential biochemical reagents to survive and replicate. Mycoplasmas typically colonise and infect a restricted range of hosts and are not known to proliferate in the environment for extended periods but can survive in mucosal droplets and travel considerable distances on wind currents [225,226]. The inability of Mycoplasmas to synthesize a cell wall is thought to render them vulnerable to desiccation and osmotic stress and to membrane attack by both the innate and adaptive immune responses during infection. Nonetheless, Mycoplasmas are remarkably successful parasitic bacteria that typically induce a chronic infectious state in their respective hosts and cause significant economic losses to animals and plants of agricultural importance.

The Mycoplasmas are phylogenetically-related to the low G + C Firmicutes and have been assigned to five major and distinct clades based on whole genome comparisons: Clade I (*Ureaplasma* spp), Clade II (*Mycoplasma pulmonis*, *Mycoplasma mobil*e, *Mycoplasma arthritidis*, *Mycoplasma synoviae*, *Mycoplasma crocodyli* and *Mycoplasma agalactiae*); Clade III (*Mycoplasma hyopneumoniae*, *Mycoplasma conjunctivae* and *Mycoplasma hyorhinis*), Clade IV (*Mycoplasma capricolum* and *Mycoplasma mycoides*) and Clade V (*Mycoplasma pneumoniae*, *Mycoplasma genitalium*, *Mycoplasma gallisepticum* and *Mycoplasma penetrans*) [227]. The precise mechanisms employed by *Mycoplasma* spp. and other bacterial pathogens to achieve a persistent infectious state are not well understood but the ability to form biofilms is

considered significant [61,228,229]. Several mycoplasma species are known to form biofilms [61,64-66,73] including representatives associated with Clades II and IV and V. While many biofilm forming species belong to the subclade that synthesize a defined cytoskeletal tip structure (Clade V) [65], several species that form well defined biofilms do not possess this adhesive structure [61,63,66].

M. hyopneumoniae belongs to Clade III with other porcine mycoplasmal species and is widely considered to be a surface pathogen that attaches to the ciliated respiratory epithelium [17]. The P97 and P102 adhesin families play important roles in this regard. The P97 and P102 adhesin families i) are heavily expressed on the cell surface, ii) are subject to complex processing events that generate a large number of cleavage fragments and iii) bind glycosaminoglycans, fibronectin, plasminogen and PK-15 cell monolayers [2-10,41-44]. Our surfaceome analyses suggest that the surface of *M. hyopneumoniae* comprises over 150 protein species (Tacchi *et al.*, unpublished results) and the functional roles of many on the cell surface are not known. While it is clear that the extracellular matrix is targeted by adhesive cleavage fragments derived from the P97 and P102 families, knowledge of the identities of proteins that form protein-protein interactions when *M. hyopneumoniae* interfaces with porcine epithelial cell surface proteins is extremely limited.

M. hyopneumoniae is adept at adhering to epithelial cilia that line the airways in the upper respiratory tract of swine, causing ciliostasis and eventual epithelial cell death [1,22,179]. These pathological effects underpin the destruction of the mucociliary escalator and create a favourable microenvironment for infection by secondary bacterial and viral pathogens [25,26,179]. Several detailed ultrastructural studies depicting *M.*

hyopneumoniae interacting with porcine ciliated epithelium show microcolonies attaching along the length of cilia inducing cilial clumping and splitting but rarely to the surface of the epithelial cells [1,17,22,202,230].

Here, for the first time we describe *M. hyopneumoniae* forming biofilms on glass, on the surface of porcine epithelial cell monolayers and on epithelial cell surfaces in the porcine respiratory tract. We also show that in biofilms formed on abiotic surfaces, extracellular DNA (eDNA) appears to be concentrated at the base of the biofilm. We observed a pattern of colonisation by *M. hyopneumoniae* on epithelial cell monolayers that mimics the pattern of F-actin staining. Actin is known to reside on the cell surface of different eukaryote cell types [231-236] and our data suggests that *M. hyopneumoniae* interacts with cell surface actin. To investigate this we applied systems methodologies using proteins on the surface of *M. hyopneumoniae* as bait to identify surface proteins displayed by PK-15 porcine epithelial cells that are targeted by *M. hyopneumoniae*. We also performed the reverse analysis using PK-15 surface proteins as bait to identify interacting proteins on the surface of *M. hyopneumoniae*. These studies suggested that *M. hyopneumoniae* interacts with a wide range of cytoskeletal like proteins including actin. Microscale thermophoresis was used to show that several putative actin-binding proteins bind actin with physiologically relevant binding affinity. These complementary datasets provide new insight into the identities of proteins on the surface of *M. hyopneumoniae* that interact with proteins on the surface of porcine epithelial cells.

5.2 Materials and Methods

5.2.1 Bacterial strains and culturing of biofilms

Mycoplasma hyopneumoniae strain J was grown in modified Friis medium [182] as previously described [209]. Biofilm growth was encouraged by diluting a 48 h *M. hyopneumoniae* culture 1:100 in Friis media. Aliquots (1 ml) of the diluted culture were inoculated into 35 mm FluorDish's™ (World Precision Instruments) and incubated at 37°C. After an initial 48 h the spent Friis medium was replaced with new medium and this process was repeated every 24 h for a minimum of 12 d or until mature biofilms could be readily observed. This process was also performed in parallel with uninoculated Friis medium as a negative control.

5.2.2 Protein expression, purification and generation of antisera

Purified $P97_{232}$ fragments were expressed and purified as previously described [42]. Antiserum against $F2_{P94\text{-}J}$ was generated in a previous study and with titres determined empirically [41].

5.2.3 Live-cell imaging

Dishes were monitored daily using a Nikon Ti-E inverted microscope. This phase contrast system was used to image the dishes under 100 × oil immersed magnification. Images were captured using a Photometrics Cascade:1K EMCCD Imaging Camera (Coherent Scientific). These images were further processed using NIS Elements freeware (Nikon Instruments).

5.2.4 Biofilm formation on PK-15 monolayers

Porcine kidney epithelial-like monolayers (PK-15) were grown to semi-confluency and split into microtitre plates containing glass coverslips (13 mm, no. 1.5 thickness;

Gerhard Menzel GmbH, Braunschweig, Germany) at approximately 10^4 cells/ well and left to adhere overnight. A 48 h *M. hyopneumoniae* culture was washed twice in PBS and resuspended in 25 mM HEPES in DMEM containing 5% fetal bovine serum (infection medium) and incubated at 37°C for 2 h. *M. hyopneumoniae* cells were added to PK-15 cells so that 0.5 ml of the original 48 h *M. hyopneumoniae* culture was added to each well. *M. hyopneumoniae* cells were allowed to adhere overnight or for 6 days with medium refreshment every 24 h. After the different infection times samples were washed 3 × in PBS and fixed in 2% paraformaldehyde for 30 min at 4°C.

5.2.5 Immunofluorescence microscopy of infected monolayers

Cells were blocked in 2% BSA/ PBS for 1 h at RT. $F2_{P94\text{-}J}$ antisera was incubated at a dilution of 1:100 for 1 h at RT. A 1:1000 dilution of Alexa Fluor® 488 (Life Technologies) was incubated for 1 h at RT. Cells were permeabilised in 0.5% (v/v) Triton X-100 in PBS for 5 min, followed by extensive washing. DAPI was then added for 30 minutes at RT. Phalloidin conjugated to Alexa Fluor® 568 was then added for 30 min at RT. Coverslips were then mounted onto glass microscope slides in VECTASHIELD® (Vector Laboratories). Samples were imaged on a Nikon A1 CLSM. These samples were also imaged using super-resolution 3D-SIM on a V3 DeltaVision OMX 3D-SIM Imaging System (Applied Precision, GE Healthcare) as previously described [211].

5.2.6 Immunofluorescence microscopy of biofilms

All immunofluorescence steps conducted below were followed by washing 3 × with sterile PBS. All dilutions were made in 1% BSA/ PBS unless otherwise stated. Once mature biofilms were observed, the culture dish was washed 3 × with sterile PBS and fixed with ice cold 100% methanol for 30 s. Non-specific binding sites were blocked with 2% BSA in PBS for 1 h. Polyclonal rabbit antisera raised against the major surface and immunogenic P65 lipoprotein as well as PdhB and ribosomal protein L3 were diluted 1:100, added to the washed biofilms and incubated for 1 h. A 1:1000 dilution of anti-rabbit Alexa Fluor® 568 (Invitrogen, Life Technologies) or anti-rabbit CF™ 568 (Sigma-Aldrich) was then added and incubated for 1 h.

For the staining of eDNA and the live/dead composition of biofilms, *M. hyopneumoniae* cells were cultured in 35 mm FluorDish's™ for 30 days as described above. For eDNA staining, biofilms were washed 3 × with sterile PBS, followed by staining with the membrane-impermeant nucleic acid dye TOTO®-1 Iodide (Life Technologies) at a final concentration of 1μM for 1 h at RT. Excess TOTO®-1 was removed by washing 3 × with sterile PBS, followed by fixation in 2% paraformaldehyde for 1 h at RT. Excess aldehydes were quenched with 100 mM glycine for 5 min at RT, followed by blocking in 2% BSA from 1 h at RT. *M. hyopneumoniae* cells were labelled using polyclonal rabbit antisera raised against the R1 and R2 regions of $P94_J$ ($F2_{P94\text{-}J}$) [41] at a dilution of 1:100 for 1 h at RT. This was followed by adding a 1:1000 dilution of CF™ goat anti-rabbit 568 for 1 h at RT. Following extensive washing, the PBS was removed and replaced with VECTASHIELD®.

For live/dead staining of biofilms, a duplicate dish of the aforementioned FluorDish™ was washed 3 × with sterile PBS, followed by staining with the membrane-permeant

nucleic acid dye SYTO® 9, and the membrane-impermeant nucleic acid dye Ethidium Homodimer-1 (EthD-1) at a final concentration of 5 µM and 1 µM respectively, for 1 h at RT. Following washing in PBS, the FluoroDish™ was immediately imaged on a Nikon A1 CLSM.

5.2.7 Processing of immunofluorescence images

ND2 files generated by a Nikon A1 CLSM and those generated by the DeltaVision OMX were processed using Bitplane, Imaris Scientific 3D/4D image processing software to create Maximum Intensity Projection (MIP) and slices images.

5.2.8 Ruthenium red (RR) staining

A 24 h *M. hyopneumoniae* culture was diluted 1:100 in Friis medium and inoculated into a T75 culture flask. The culture was allowed to grow for 48 h before the medium was replaced with fresh Friis media. This was repeated every 24 h for a total of 30 d. Flasks were then washed 3 × in cacodylate buffer (0.1 M sodium cacodylate, 0.01 M $CaCl_2$, 0.01 M $MgCl_2$ and 0.09 M sucrose, pH 6.9) and fixed for 1 h in 2% glutaraldehyde in cacodylate buffer. Fixative was removed by washing 3 ×in cacodylate buffer followed by staining in RR (5 mg ml^{-1}) in cacodylate buffer for 2 h at RT. Excess stain was removed by washing 3 times in cacodylate buffer and then 5 ×in dH_2O.

5.2.9 Infection experiments for scanning electron microscopy

PK-15 cells were maintained in Dulbecco's modified eagle medium (DMEM, PAA Laboratories, Pasching, Austria) containing 10% foetal calf serum, 2 mM L-glutamine, 100 U/ml penicillin and 0.1 mg ml^{-1} streptomycin in culture dishes (9 cm in diameter, TPP, Trasadingen, Switzerland) at 37°C in 5% CO_2. Cells were harvested by

trypsinization, resuspended in DMEM with 5% FCS and 2 mM L-glutamine and seeded into 24-well plates containing sterile 12 mm glass cover slips at 1 x 10^5 cells/well. After growing overnight the medium was changed to infection medium (DMEM with 25 mM HEPES, 2 mM L-glutamine, 5% FCS) by adding 500 µl medium per well. 6 ml cultures of *M. hyopneumoniae* were harvested by centrifugation (14000 rpm for 5 min, Eppendorf, Hamburg) and resuspended in 1 ml fresh infection medium for 2 h at 37°C on a roller, centrifuged again and resuspended in 120 µl infection medium. 10 – 30 µl of the bacterial suspension were added per well and incubated at 37° in 5% CO_2 for 4-48 h for infection. After different infection times samples were washed once in infection medium in a beaker and subsequently fixed with 2% glutaraldehyde and 5% formaldehyde in cacodylate buffer (100 mM sodium dimethylarsenic acid, 10 mM $MgCl_2$, 10 mM $CaCl_2$, 90 mM sucrose, pH 6.9) for 1 h on ice. Samples were then washed with TE buffer (20 mM TRIS, 2 mM EDTA, pH 7.0), dehydrated in a graded acetone series (10, 30, 50, 70, 90, 100%) for 10 min each step on ice and critical-point dried using liquid CO_2. Samples were made conductive by sputter coating with a thin gold film. Samples were examined in a Zeiss field emission scanning electron microscope DSM982 Gemini at an acceleration voltage of 5 kV using the Everhart-Thornely SE-detector and the inlens SE-detector in a 50:50 ratio. Images were recorded on a MO-disk.

5.2.10 Scanning electron microscopy of tracheal sections

Tracheal sections from pigs euthanized 6 weeks post-infection with *M. hyopneumoniae* were harvested and prepared for SEM as previously described [20]. Sections were fixed in 2.5% glutaraldehyde for 2 d at 4 °C followed by washing 3 × in cacodylate buffer containing 0.1 M Sodium cacodylate, 0.01 M $CaCl_2$, 0.01M $MgCl_2$ and 0.09 M sucrose (pH 6.9). Samples were post-fixed in 1% osmium tetroxide (ProSciTech, Australia) in cacodylate buffer for 72 h at 4 °C. Cells were then dehydrated in a graded ethanol series; 20%, 30%, 50%, 70%, 80%, 90%, 96% for 5-15 min each and finally twice in 100% ethanol (15-30 min each). Further dehydration was carried out in a 1:1 solution of ethanol and hexamethyldisilazane (HMDS) [Sigma-Aldrich] for 5 min, followed by dehydration with 100% HMDS (10 min). To complete the dehydration process the cells were immersed once more in 100% HMDS for a minimum of 12 h in a fume cupboard. Sections were then placed on adhesive carbon covered specimen stubs and coated in a ~10 nm thick carbon coat using a MED 010 Balzers Union Carbon Coater and imaged on a Zeiss Supra 55VP in secondary electron mode at 1 kV.

5.2.11 Avidin Purification of Interacting Proteins

The purification of *M. hyopneumoniae* proteins that bind to proteins expressed on the surface of PK-15 cells was carried out as previously described [43].

The purification of porcine proteins from PK-15 monolayers that bind to proteins expressed on the surface of *M. hyopneumoniae* proteins was performed in reverse to the above procedure. *M. hyopneumoniae* cells from a 250 ml culture were pelleted, washed and resuspended in PBS containing 2 mM EZ-link Sulfo-NHS-Biotin for 30 s on ice. This ensured that *M. hyopneumoniae* cells did not lyse and any remaining biotin molecules were quenched in 100 mM glycine for 10 min at RT. Cells were washed

twice by centrifugation in PBS to remove excess glycine. Cells were gently lysed in 0.5% Triton X-100 in Tris-HCl pH 7.6, 150 mM NaCl with protease inhibitors on ice with vortexing and water bath sonication. Insoluble material was removed by centrifugation at 16 000 × *g* for 10 min. The cleared lysate was incubated with avidin agarose [Thermo Scientific] for 1 h at RT on a rotating wheel. The mixture was packed into a column and any unbound *M. hyopneumoniae* proteins were removed by thoroughly washing with PBS.

PK-15 cells were grown and harvested as previously described, without biotinylation [43]. The cleared protein lysate was incubated with the biotinylated-*M. hyopneumoniae*-avidin mixture overnight on a rotating wheel at 4 °C. The mixture was packed into a column and the procedure was performed as previously described [43].

5.2.12 Avidin Purification of Actin-binding Proteins

Actin from bovine muscle (Sigma-Aldrich) was solubilised in 8 M Urea/ 20 mM Triethylammonium bicarbonate pH 8.0. Cysteine residues were reduced and alkylated in 20 mM acrylamide monomers and 5 mM TBP for 90 min. Actin monomers were labelled with 20 × molar excess Sulfo-NHS-LC-Biotin for 3 h at RT. Removal of excess biotin and buffer exchange into PBS was performed using a PD-10 Desalting Column (GE Healthcare, Life Sciences). Biotinylated actin was incubated with avidin agarose (Thermo Scientific) on a rotating wheel for 5 h. The slurry was packed into a column and the flow through collected. Unbound actin was removed by thoroughly washing with PBS.

M. hyopneumoniae cells from a 250 ml culture were pelleted, washed with PBS, and gently lysed in 0.5% Triton X-100 in PBS. Insoluble material was removed by centrifugation at 16,000 × *g* for 10 min. The cleared lysate was incubated with biotinylated actin-avidin agarose mixture overnight on a rotating wheel at 4 ˚C. The mixture was packed into a column and the flow through collected. Unbound proteins were thoroughly washed and collected in PBS and interacting proteins were collected in 30% acetonitrile/ 0.4% trifluoroacetic acid. The elutions were concentrated in a 3000 Da cutoff filter and acetone precipitated at −20 °C for 30 min. Proteins were pelleted by centrifugation at 25, 000 × *g* at 4 °C for 30 min. Protein was resuspended in SDS sample buffer and separated by 1D SDS-PAGE. Proteins were in-gel trypsin digested and analyzed by LC−MS/MS.

5.2.13 Microscale thermophoresis

Actin monomers were fluorescently labelled with amine reactive NT-647 dye (NanoTemper) in a 3-fold molar excess for 30 min. Excess dye was removed using a desalting column (NanoTemper). Tween-20 (0.5%) was added to prevent aggregation of sample. The non-fluorescent $F1_{P97-232}$, $F3_{P97-232}$ and $F4_{P97-232}$ were titrated against 100 nM fluorescent actin in a 1:1 serial dilution starting from 30 µM for $F3_{P97-232}$ and $F4_{P97-232}$ and 11 µM for $F1_{P97-232}$. Samples were loaded into a Monolith NT.115™ (NanoTemper) in hydrophilic capillaries. Capillary scans were performed to confirm that no sample aggregation was occurring and that the fluorescence intensity was within the range of 80-1500 counts. The data presented here was generated at 40% MST laser power measuring the thermophoretic movement after the MST laser is switched off for 30 s. NanoTemper analysis software was used to analyse and generate the K_D values.

5.2.14 1D LC−MS/MS Using QTOF

Methods were performed as described previously with no modifications [43].

5.2.15 MS/MS Data Analysis

MS/MS data files were searched using Mascot as previously described [43] with slight modifications. Data files from avidin purification of interacting proteins were searched for both bacterial and mammalian proteins in order to identify the biotinylated "bait" proteins eluted in their respective experiments.

5.2.16 One- and Two-Dimensional Gel Electrophoresis and Ligand Blotting

1D and 2D SDS-PAGE was performed as previously described [43] with minor modifications. Once *M. hyopneumoniae* proteins were transferred to polyvinylidene fluoride (PVDF) membrane and blocked, biotinylated actin or biotinylated PK-15 lysate prepared as previously described [43] was incubated with the membrane overnight at 4 °C. Membranes were probed with a 1:2000 dilution of ExtrAvidin (Sigma-Aldrich) and developed with DAB (Sigma-Aldrich).

5.2.17 Biofilm Screening Assay

M. hyopneumoniae mutants were supplied to us by Prof Andrew Rycroft at the Royal Veterinary College. These mutants were generated using the hyperactive Himar1 transposase as previously described [161,237]. Each mutant was diluted 1:100 in Friis broth and added in duplicate to the wells of a black bottom 96-well plate, and incubated for 48 hours at 37 °C. Following this, the medium was replaced every 24 hours for 12 days after which wells were washed with PBS and fixed using 2% formaldehyde for 1 h at RT. After extensive washing, DAPI (Roche) was added at a final concentration of 1µg/ mL for 1 h at RT. Following extensive washing, plates were read at an excitation

and emission of 340 nm and 488 nm respectively. The background fluorescence of control wells were subtracted from the averaged values which were then graphed with the calculated standard errors.

5.2.18 Growth curves of ΔMhpX and ΔMhpY

10 µL of WT strain 232, ΔMhpX and ΔMhpY were diluted in 10 mL of Friis medium in triplicate and incubated at 37 °C. Every 24 h starting at time 0, an aliquot of each culture was diluted from $10^{0\,(neat)} - 10^{5}$ in PBS and plated onto 5cm^2 Friis agar plates. These plates contained 0.8% purified agar (Oxoid) and 0.01% DEAE-Dextran (Sigma) and were mixed with Friis broth prior to setting [181]. 10 µL of each dilution was spotted onto these plates and incubated at 37°C in 5% CO_2 for 10 days. Colonies (Figure S5.1) at each dilution (where colonies could be seen) were counted under a stereo microscope and values were analysed using GraphPad Prism. Values were plotted as the average of triplicate data with the calculated standard errors.

5.3 Results

5.3.1 *M. hyopneumoniae* forms biofilms on abiotic surfaces

Despite genome reduction, numerous *Mycoplasma* spp. belonging to different clades have been shown to produce biofilms [61]. *M. hyopneumoniae* has fastidious growth requirements and is routinely cultured as planktonic cells in Friis broth. *M. hyopneumoniae* has not previously been reported to form biofilms. Given the chronic nature of infections caused by *M. hyopneumoniae* in swine, we hypothesised that it may need to sequester host-derived biomolecules to facilitate adherence to abiotic and biotic surfaces prior to establishing a biofilm. To investigate this hypothesis *M. hyopneumoniae* cells grown in glass bottom culture dishes for 30 days with daily medium replenishment were monitored every 24 h by live-cell microscopy. Individual cells were observed to adhere to glass and interact with one another by day 5 (Figure 5.1). Discernible multilayered microcolonies < 10 μm in diameter and estimated to comprise 8-15 *M. hyopneumoniae* cells were observed 8-10 days post-inoculation (Figure 5.1). Not all cells appear to be in direct contact with one another suggesting that a matrix is formed around the cells of the growing microcolony. After 10 days, biofilms increased in size rapidly and were greater than 20 μm by day 13 (Figure 5.1). Mature biofilms expanded by subsuming smaller "satellite" microcolonies (Figure S5.2). This mechanism of growth most likely accounts for the rapid increase in the size of biofilms between days 10-12.

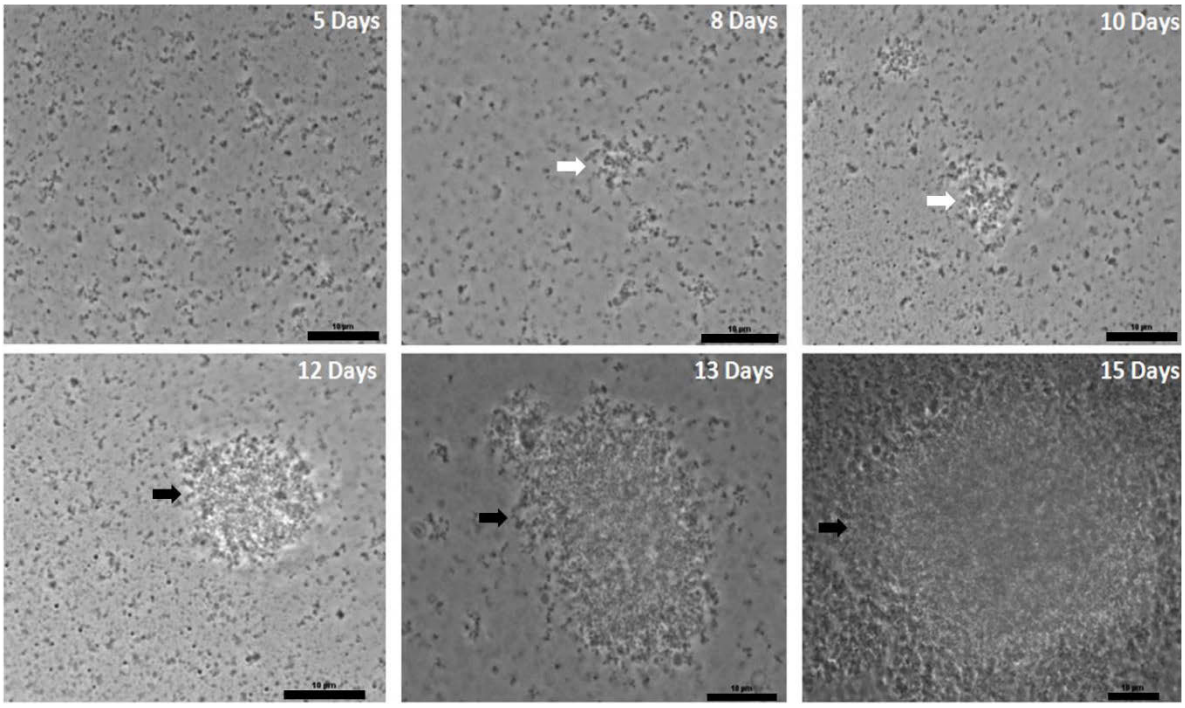

Figure 5.1: Biofilm formation of *M. hyopneumoniae* cells on glass over a time period of 15 days.

A) Within the first 5 days, only single *M. hyopneumoniae* cells can be seen adhering to the glass surface. Multilayered microcolonies were evident at 8 and 10 days post inoculation (white arrows). Biofilms > 20 µm in diameter were observed from day 12 (black arrows). Scale bar is 10 µm.

Prolonged incubation up to 30 days enabled biofilms to reach 100 μm in diameter (Figure 5.2). To observe these structures by CLSM, biofilms were exposed to polyclonal rabbit antibodies raised against an immunodominant surface lipoprotein P65 (Mhp677, Uniprot: Q5ZZN0) [238-240], the R1 and R2 regions of the P97 adhesin ($F2_{P97}$) [41], pyruvate dehydrogenase subunit B (PdhB), and 50S ribosomal protein L3 (rpL3). Antibodies against P65, a lipolytic enzyme that is attached to the external membrane surface of *M. hyopneumoniae*, localised to the core of biofilms while $F2_{P97}$, stained the entirety of the biofilm uniformly (Figure 5.2). $F2_{P97}$ antiserum has previously been demonstrated to routinely label the surface of *M. hyopneumoniae* cells [42] and so we chose to use this antibody for our studies. These data suggest that populations of *M. hyopneumoniae* cells react differently with P65 and PdhB antibodies at the periphery and centre of biofilms, while antibodies raised against $F2_{P97}$ and rpL3 stain uniformly.

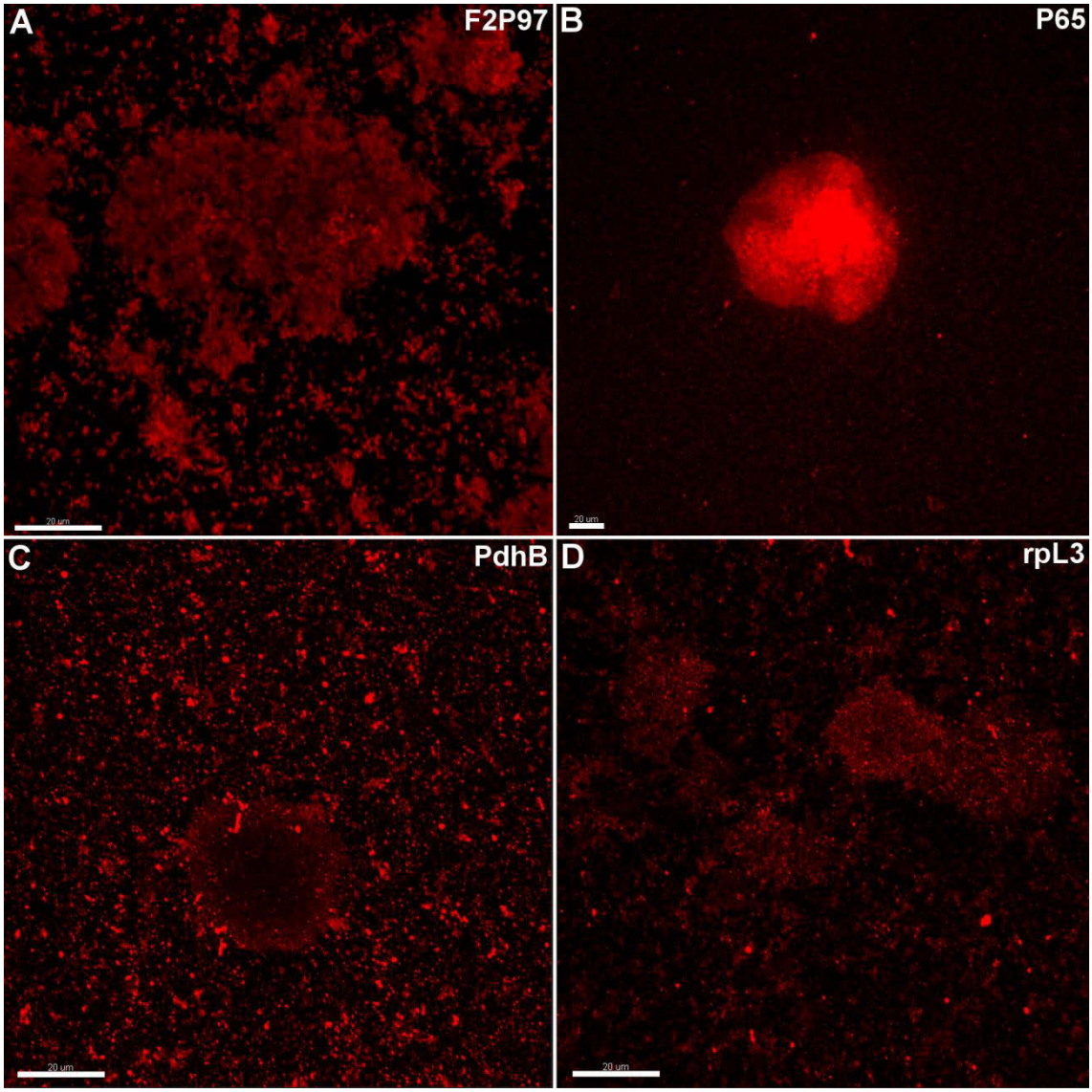

Figure 5.2: CLSM maximum intensity projections of 30 day *M. hyopneumoniae* biofilms forming on glass and stained with $F2_{P97}$ (A), P65 (B), PdhB (C), and rpL3 (D) antisera.

Rabbit antisera was conjugated to anti-rabbit CF™ 568 (A, C, D) or anti-rabbit Alexa Fluor® 568 (B). Biofilms are labelled intensely with $F2_{P97}$ and P65 antisera, with $F2_{P97}$ antisera also labelling the surrounding cells (A). P65 antiserum appears to label the cells in the middle of the biofilm more intensely than those residing at the exterior (B). C) PdhB antiserum can be seen to label numerous cells adhering at the periphery of the biofilm with little staining within the biofilm itself. Single cells adhering to the glass are

also labelled using this antiserum. D) rpL3 labelling was diffuse throughout the sample with even labelling within the biofilm and the peripherally adhering cells. Scale bar is 20 μm. Panels A, C and D were imaged at 100 X magnification while panel B was imaged at 60 X.

5.3.2 *M. hyopneumoniae* biofilms stain with ruthenium red

Ruthenium Red (RR) has typically been used to stain cellular extrapolymeric matrix comprising mucopolysaccharides [241] but more recent studies have shown that RR also binds to membrane proteins [242]. Figure 5.3 shows 30 day old biofilms at different stages of development stained with RR. Notably, very few of the surface attached single *M. hyopneumoniae* cells residing outside biofilms or clustered within small biofilms <150 μM in diameter stain with RR. *M. hyopneumoniae* cells residing in the core of mature biofilms ranging from sizes 400-600 μm in diameter bound strongly to RR. Our data suggests that molecules that interact with RR are selectively expressed inside the core of the biofilm.

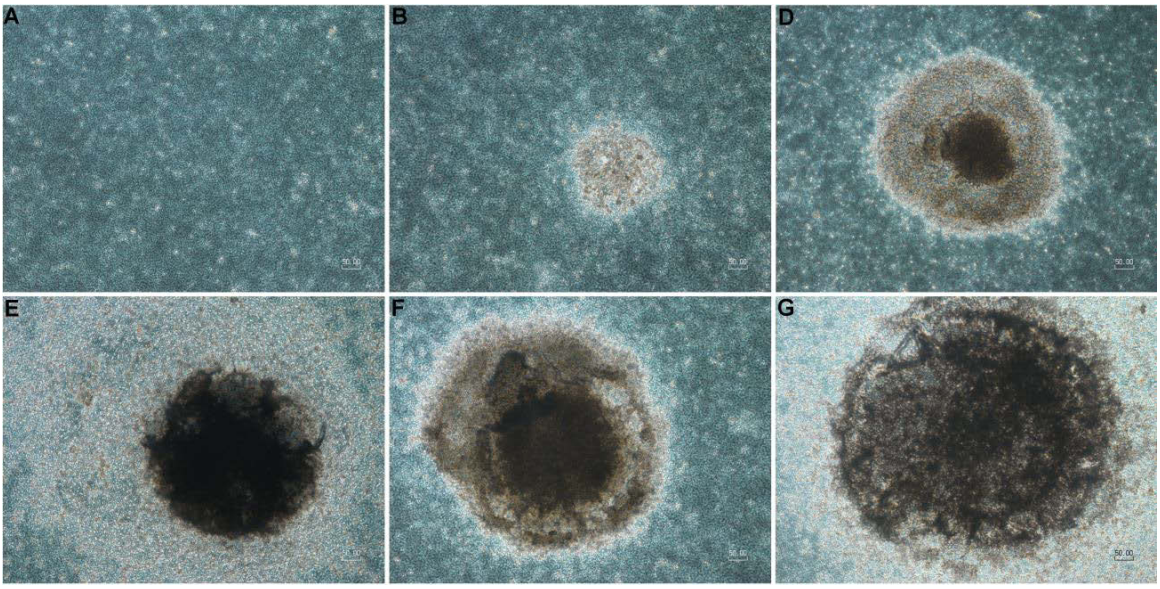

Figure 5.3: RR staining of *M. hyopneumoniae* biofilms.

Biofilms were grown for 30 days and stained with RR. Panel A depicts areas of the flask devoid of biofilms with only single cells adhering. A few scattered cells (arrowheads) stain with RR. Panel B depicts a small biofilm with a diameter of approximately 150 µm containing a significant number of cells that stain with ruthenium red (arrowheads). Panel C shows a large biofilm approximately 400 µm in diameter containing a central cluster of *M. hyopneumoniae* cells that stains heavily with RR. As the central core of a biofilm expands (panel D) so does the number of cells that stain with RR. Cells at the periphery of the biofilms that stain with RR (Panels E and F) eventually become subsumed into the biofilm core. Scale bar is 50 µm.

5.3.3 *M. hyopneumoniae* biofilms contain extracellular DNA

Extracellular DNA (eDNA) is an important structural component of bacterial biofilms [243] that has not previously been investigated in Mycoplasma biofilms. Here we stained a 30 day *M. hyopneumoniae* biofilm with TOTO-1, a cell-impermeant nucleic acid stain which we coupled with $F2_{P94\text{-}J}$ antisera in order to visualise the membrane of *M. hyopneumoniae* cells. We observed punctate TOTO-1 staining both within biofilms and in the surrounding area. This punctate staining was less than 1 μm indicating that these are dead/dying cells whose nucleic acids have become exposed to TOTO-1 due to membrane permeation. This is supported by the observation that these dead cells were not labelled by $F2_{P94\text{-}J}$ antisera. Closer inspection of the surrounding area around the biofilms revealed that there was abundant eDNA in the spaces between adhering *M. hyopneumoniae* cells (Figure 5.4). This eDNA appears to form a carpet-like layer on the surface of the glass that the *M. hyopneumoniae* cells and microcolonies are adhering to. This was most evident in the sections of large biofilms where a small mass of eDNA could be seen underneath the biofilm in the absence of $F2_{P94\text{-}J}$ labelling (Figure 5.4). These findings were supported by 3D-SIM images that demonstrated eDNA in the area of the glass adjacent to biofilms as well as at the base of mature biofilms (Figure 5.5). This eDNA appeared to be a product of cell lysis, being observed in areas where membrane remnants could also be seen (Figure 5.5). A number of cells could be seen staining with TOTO-1 as well as $F2_{P94\text{-}J}$ antisera (Figure 5.5) suggesting that they are in the process of lysing. From these images it appears that eDNA forms part of the conditioning material on the surface of the glass and may serve as the foundation of the biofilm.

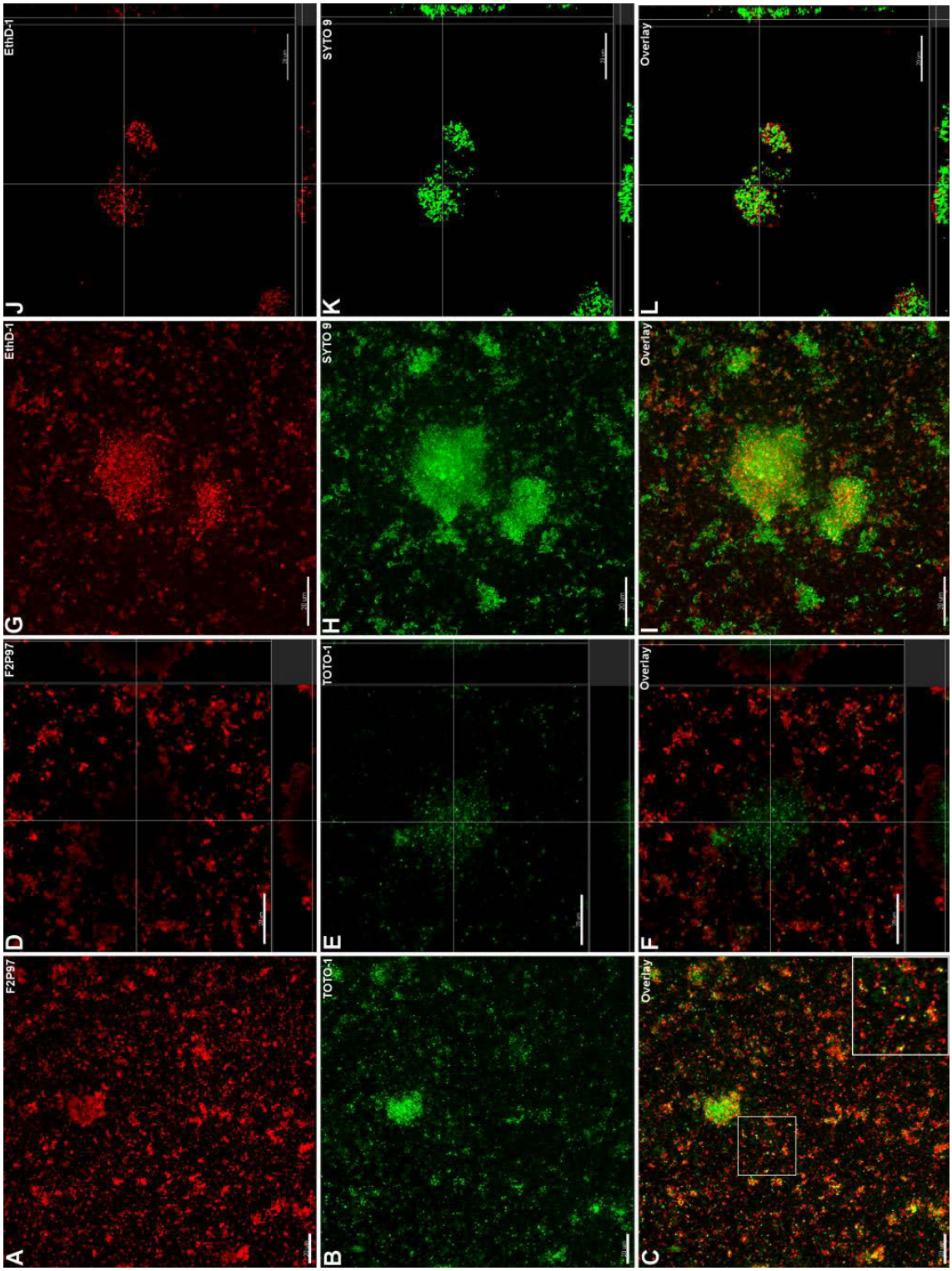

Figure 5.4: eDNA (A-F) and live/dead (G-L) staining of 30 day *M. hyopneumoniae* biofilms growing on glass coverslips.

A, D) *M. hyopneumoniae* cells have been labelled with rabbit $F2_{P94\text{-}J}$ antisera and anti-rabbit CF™ 568 and can be seen adhering to the surface of the dish and forming

biofilms. B, E) eDNA was stained using the membrane-impermeant nucleic acid dye TOTO-1. C) Overlay showing a *M. hyopneumoniae* biofilm that contains abundant eDNA. eDNA can also be seen in between the adhering *M. hyopneumoniae* cells and microcolonies. The zoomed in insert (boxed) demonstrates this eDNA in higher detail. D-F) Section of a large *M. hyopneumoniae* biofilm demonstrating that eDNA is most abundant at the bottom of the biofilm, with $F2_{P94\text{-}J}$ labelling localised on top of the eDNA. G) Dead/ dying cells have been stained with the membrane-impermeant dye EthD-1. H) Live cells have been stained with the membrane-permeant nucleic acid dye SYTO 9. I) Overlay showing the distribution of live and dead *M. hyopneumoniae* cells within the biofilm. The vast majority of cells appear to be live, with dead cells dispersed evenly throughout the biofilms. Small microcolonies do not seem to contain as many dead cells as the larger biofilms. The combined staining of SYTO 9 and EthD-1 appeared to also stain eDNA that had been deposited onto the coverslip; similarly to what was observed with TOTO-1. J-L) Section demonstrating the distribution of live and dead cells within a *M. hyopneumoniae* biofilm. The dead cells can be seen to reside within the spaces between clusters of live cells, with the vast majority of cells being live.

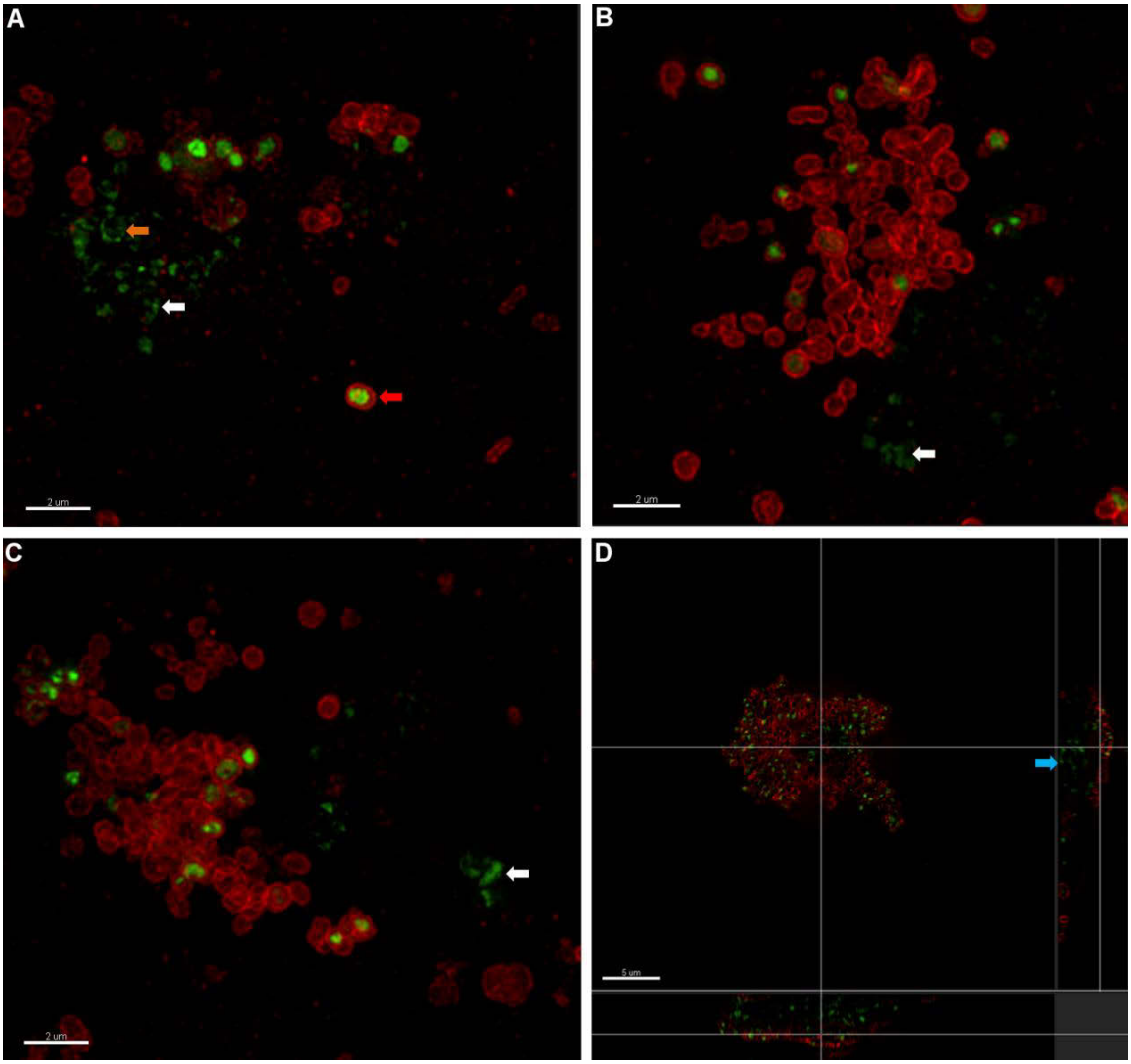

Figure 5.5: 3D-SIM images of *M. hyopneumoniae* biofilms grown on glass for 30 days.

M. hyopneumoniae cells were labelled using rabbit $F2_{P97}$ antisera conjugated to anti-rabbit CF™ 568 (red). Biofilms were also stained with TOTO-1 to visualise eDNA (green). A-C) Maximum intensity projections demonstrating the membranes of the *M. hyopneumoniae* cells residing within biofilms as well as the eDNA that has been released and deposited onto the glass (white arrows). This eDNA appears to have been released from lysed *M. hyopneumoniae* cells, demonstrated by the diffuse red fluorescence corresponding to membrane remnants labelled with $F2_{P97}$. A circular piece of eDNA can also be seen (orange arrow) which may represent eDNA that has just been

released from a lysed cell. TOTO-1 can also be seen staining the inside of a number of *M. hyopneumoniae* cells which appear to be in the process of lysis (red arrow). D) Section view of a *M. hyopneumoniae* biofilm demonstrating that the base of the biofilm is composed of eDNA/lytic cells (blue arrow) with the top of the biofilm consisting mainly of intact *M. hyopneumoniae* membranes labelled with $F2_{P97}$. Scale bars are 2 μm (A-C) and 5 μm (D).

5.3.4 Live/dead staining of *M. hyopneumoniae* biofilms

In order to better understand the cellular composition of these biofilms we sought out to examine the distribution of live and dead cells within 30 day biofilms formed by *M. hyopneumoniae*. For this we used the cell-permeant nucleic acid dye SYTO 9 in combination with the cell-impermeant nucleic acid dye EthD-1. When overlayed, live (green) and dead (red/yellow) cells could clearly be differentiated from one another. EthD-1 also appeared to stain eDNA that had been deposited onto the glass slide, similarly to what was observed using TOTO-1. Biofilms stained intensely with both SYTO 9 and EthD-1, although more so with the former (Figure 5.4). This indicated that the majority of the cells residing within these biofilms were viable. Dead cells could also be observed both within biofilms and in the surrounding area, although much more sparsely distributed. This was evident from a section of the middle of a biofilm where the dead cells can be seen within spaces, adjacent to aggregates of viable cells. Interestingly, little to no dead cells were observed in microcolonies and immature biofilms suggesting that the cell death is an event that occurs more frequently in mature biofilms.

5.3.5 *M. hyopneumoniae* adheres to and forms biofilms on PK-15 monolayers

Porcine kidney epithelial-like (PK-15) cells have been used as a model to study adherence by *M. hyopneumoniae* [4,5,7,8,10,215]. We sought to determine if *M. hyopneumoniae* can form biofilms on the surface of cell monolayers by using antiserum from rabbits immunised with $F2_{P94\text{-}J}$, a recombinant fragment that represents the C-terminal third of the cilium adhesion MHJ_0194, to detect *M. hyopneumoniae*, and phalloidin to stain cytoskeletal proteins. The monolayers were also stained with DAPI to detect the nucleus of PK-15 cells and the chromosome of *M. hyopneumoniae*. Small clusters of *M. hyopneumoniae* cells were observed on PK-15 monolayers after overnight incubations (data not shown). After 6 days *M. hyopneumoniae* cells formed biofilms on the surface of PK-15 cell monolayers (Figure 5.6) and reached a size (20 μm in diameter) comparable to biofilms on glass after 10-12 days growth. The application of a larger inoculum did not appear to accelerate biofilm production (data not shown). In control experiments uninfected PK-15 monolayers failed to stain with $F2_{P94\text{-}J}$ antisera (data not shown). Although we expected to observe individual *M. hyopneumoniae* cells growing on most glass surfaces after 6 days this was not the case except occasionally where *M. hyopneumonae* cells were in close proximity to actively growing PK-15 cells. This was unusual and suggested that *M. hyopneumoniae* preferred to adhere to PK-15 cells. SEM images of *M. hyopneumoniae* cells that appeared to be growing on glass show that cells are adhering to a matrix deposited on the glass surface that likely originated from secretions produced by the PK-15 cells (Figure 5.7). These data suggest that Friis medium components are required for *M. hyopneumoniae* to colonise glass or that medium used to culture PK-15 cells cannot provide the necessary components to promote growth of *M. hyopneumoniae* on glass. Panel A clearly shows that *M.*

hyopneumoniae adheres to the edges of PK-15 cells that often stain strongly with phalloidin.

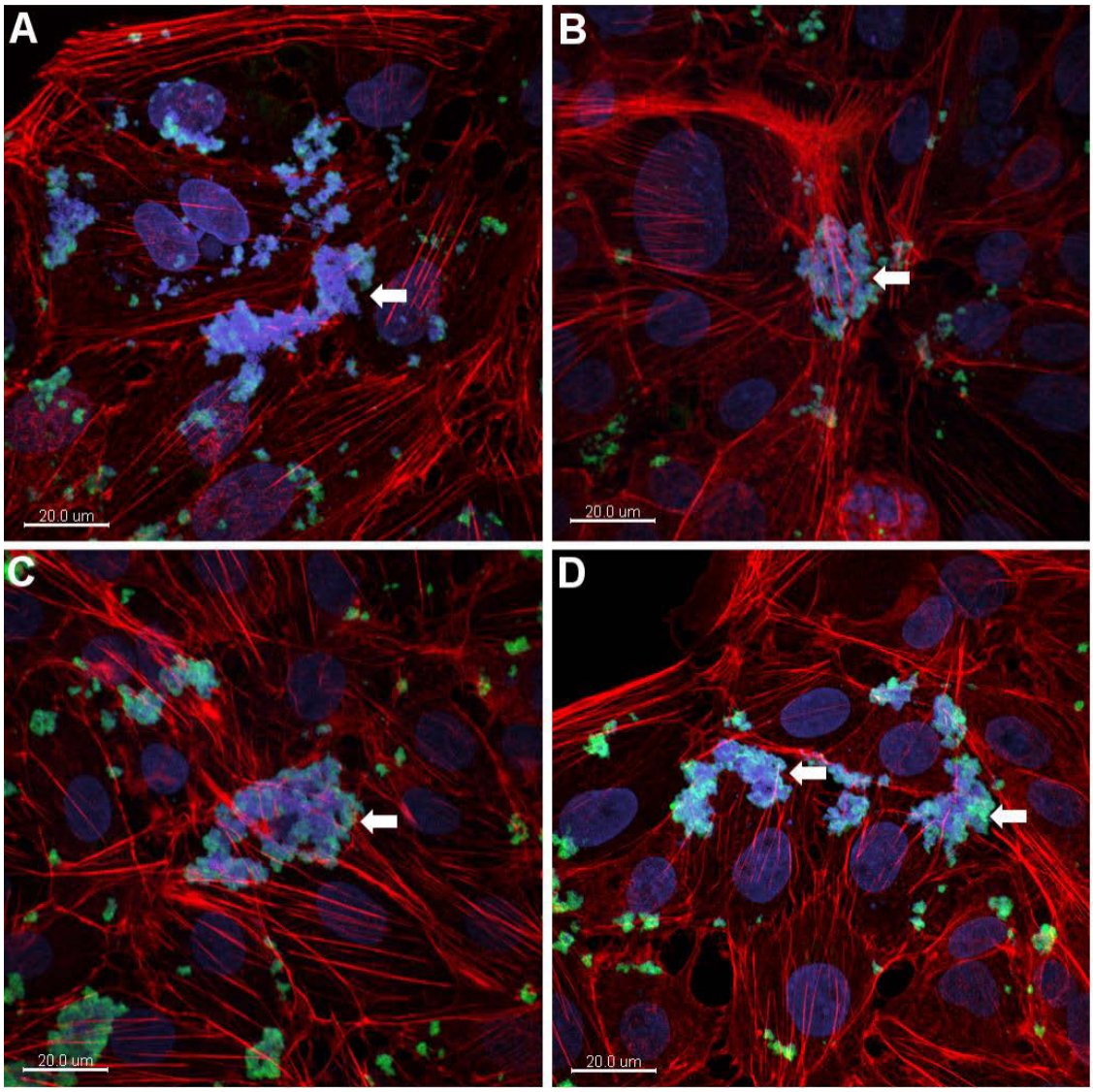

Figure 5.6: *M. hyopneumoniae* cells forming biofilms on PK-15 monolayers after 6 days.

PK-15 monolayers were permeabilised and stained with DAPI and Alexa Fluor® Phalloidin 568. *M. hyopneumoniae* cells were labelled with rabbit $F2_{P94\text{-}J}$ antisera that recognises the C-terminal third of cilium adhesin MHJ_0194 [41,42] on the surface of *M. hyopneumoniae*. Rabbit anti- $F2_{P94\text{-}J}$ antibodies were detected with anti-rabbit Alexa Fluor® 488 conjugate. DAPI was used to stain nucleic acids. Only large biofilms stained heavily with DAPI. Biofilms range in size from 5 – 45 μM (white arrows). Scale bar is 20 μm.

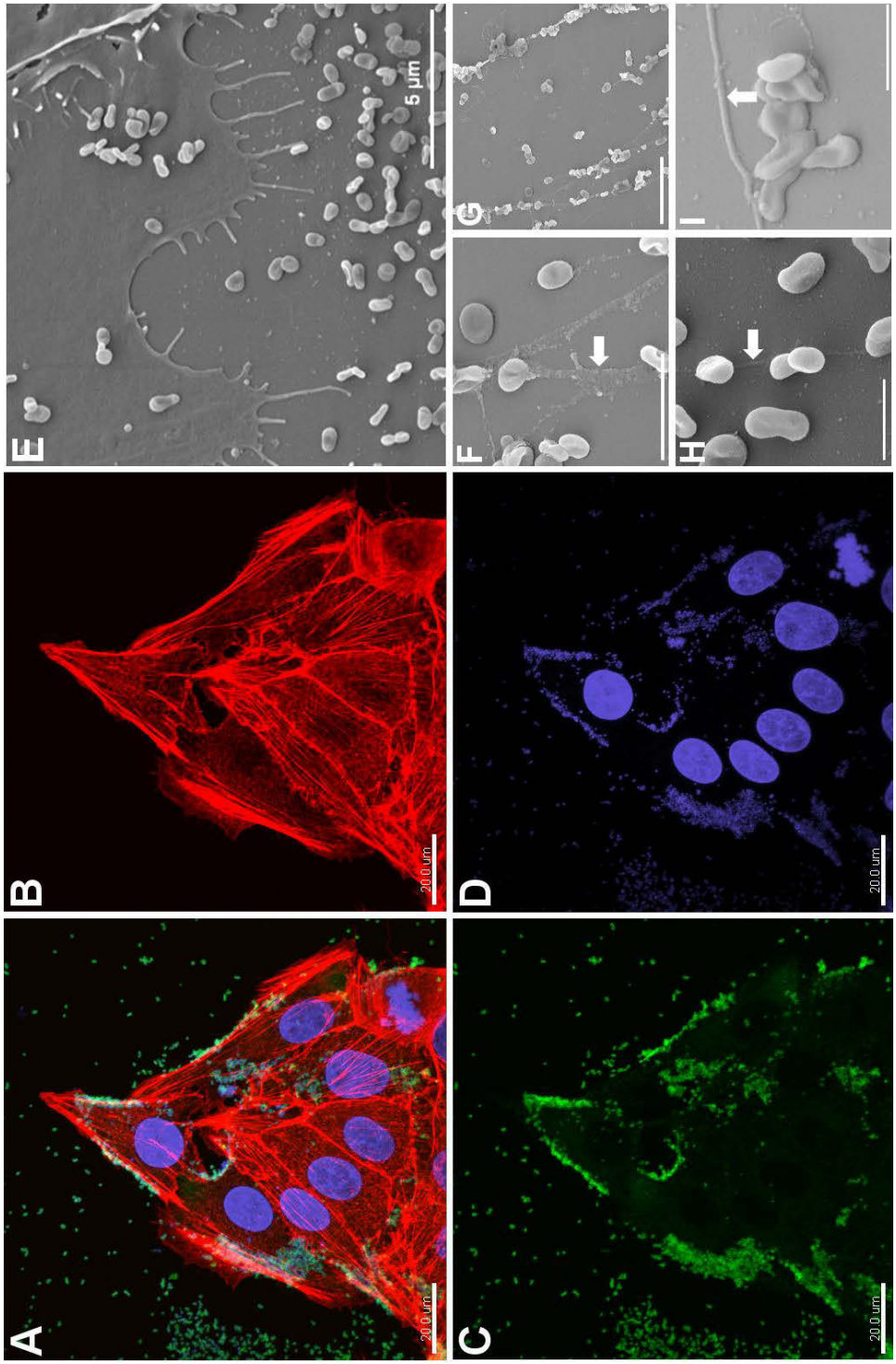

Figure 5.7: IFM and SEM of *M. hyopneumoniae*-infected PK-15 cell monolayers.

A) Overlay of the three channels showing *M. hyopneumoniae* cells adhering to the edges of the monolayer as well as the surrounding area of the coverslip void of PK-15 cells. B) PK-15 cells stained with phalloidin showing regions enriched in filamentous actin. C) Same region of PK-15 monolayer stained with rabbit anti- $F2_{P94\text{-}J}$ antibodies

followed by anti-rabbit Alexa Fluor® 488 conjugate. Image depicts *M. hyopneumoniae* cells as green rings on the surface of the monolayer. D) Same region of the PK15 monolayer stained with DAPI showing large blue nuclei of the PK-15 cells and *M. hyopneumoniae* chromosomes. Panels E-I show SEM images of *M. hyopneumoniae* cells adhering to PK-15 cells as well as extracellular material (white arrows) produced by the leading edge of the monolayer. A-D) Scale bar is 20 μm; E is 5 μm; F) is 2 μm and G-I) is 1 μm.

5.3.6 *M. hyopneumoniae* forms biofilms in the swine respiratory tract

M. hyopneumoniae form a chronic infectious state in swine and can be recovered from bronchial swabs up to 185 days post-challenge [18]. Pigs can become convalescent carriers for up to 200 days post-challenge and remain infectious during this period [19]. The ability to remain dormant within their host whilst still being infectious suggests that *M. hyopneumoniae* cells are capable of shielding themselves from the host immune system. We examined the trachea from pigs euthanised 6 weeks after endotracheal challenge with the Hillcrest strain of *M. hyopneumoniae* [20] and detected large biofilms approximately 100-150 μm in diameter on the surface of respiratory tract epithelium (Figure 5.8). The epithelium was completely denuded of cilia; a hallmark of *M. hyopneumoniae* infection [1].

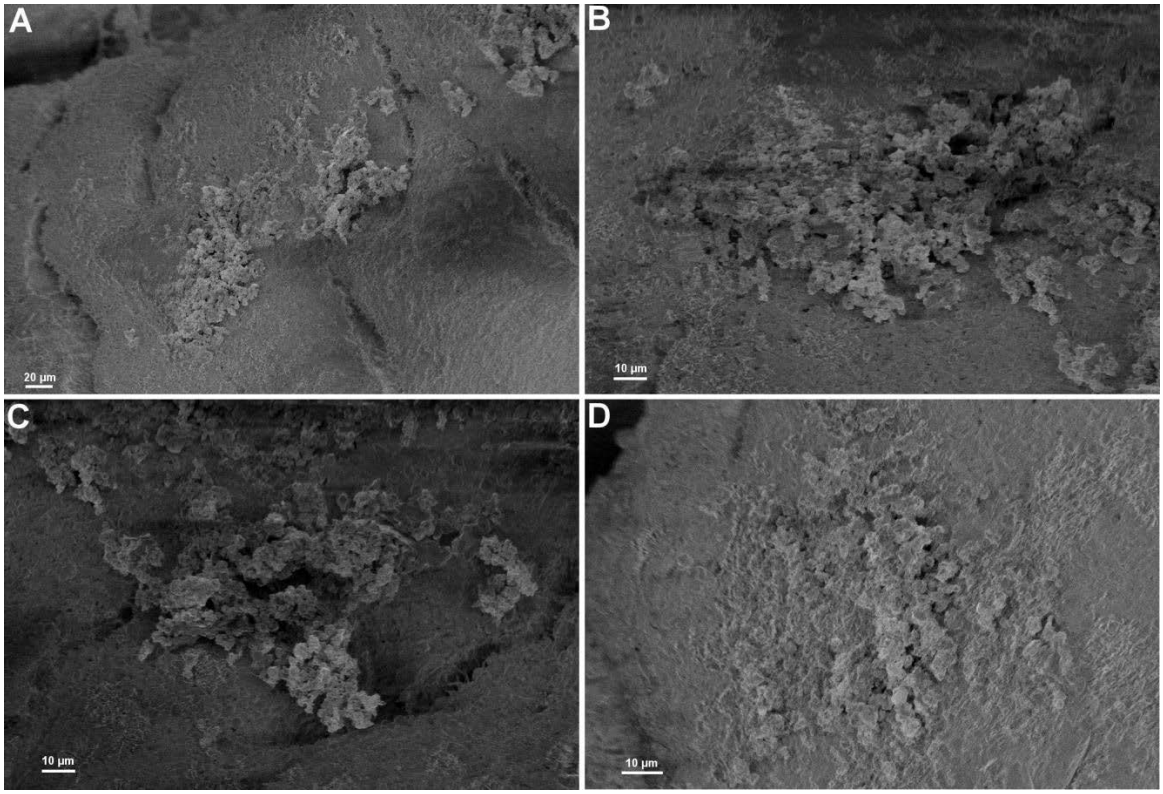

Figure 5.8: Scanning electron micrograph of tracheal epithelium from pigs experimentally infected with the Hillcrest strain of *M. hyopneumoniae*.

Biofilms approximately 100 µm in diameter on the surface of the epithelium denuded of cilia. All samples were imaged at 1kV. Magnifications: A) 600-fold; B-C) 2000-fold; D) 2500-fold.

5.3.7 *M. hyopneumoniae* surface adhesins bind PK-15 monolayers

Cleavage fragments of the P97 and P102 paralog families play an important role in facilitating adherence to cilia and epithelial cells in the respiratory tract of swine [2-10,41-44,154,205,206]. We undertook an unbiased, systems approach to determine the repertoire of *M. hyopneumoniae* proteins that bind PK-15 cell surface receptors by labelling accessible proteins on the surface of PK-15 cells with sulfo-NHS-LC-biotin, attaching them onto avidin agarose beads and incubating the beads with a native, whole cell lysate of *M. hyopneumoniae* strain J. After extensive washing to remove unbound proteins *M. hyopneumoniae* proteins that bound to the avidin beads were eluted using a two-stage protocol. The first elution (elution 1) used 2M NaCl to remove *M. hyopneumoniae* proteins from the PK-15 receptor proteins while the second (elution 2) used 0.4% trifluoroacetic acid to strip the PK-15 receptor proteins proteins from the avidin beads. Proteins recovered from both elution protocols were resolved by SDS-PAGE and identified by LC-MS/MS. We recovered 74 *M. hyopneumoniae* proteins in elution 1 (Table 5.1) including several adhesins belonging to the P97 and P102 families. Notably, 80% (59/74) of proteins detected by LC-MS/MS in elution 1 were also detected on the cell surface of *M. hyopneumoniae* (Table 5.1) in surfaceome studies including many proteins with well described functions in the cytosol [244] (Tacchi *et al.*, unpublished results). *M. hyopneumoniae* proteins identified in elution 2 included well described adhesins of *M. hyopneumoniae* including P97 (Q4AAD5), P102 (Q4AAD6) and their paralogs including Q4A925, Q4A926, Q4A9J2, Q4A9W4, Q9A4W5, Q4AAM4 and P159 (Q4A9J1) (Table 5.1) [2-6,9,41-44] . As expected, numerous porcine proteins were identified in elution 2 (data not shown).

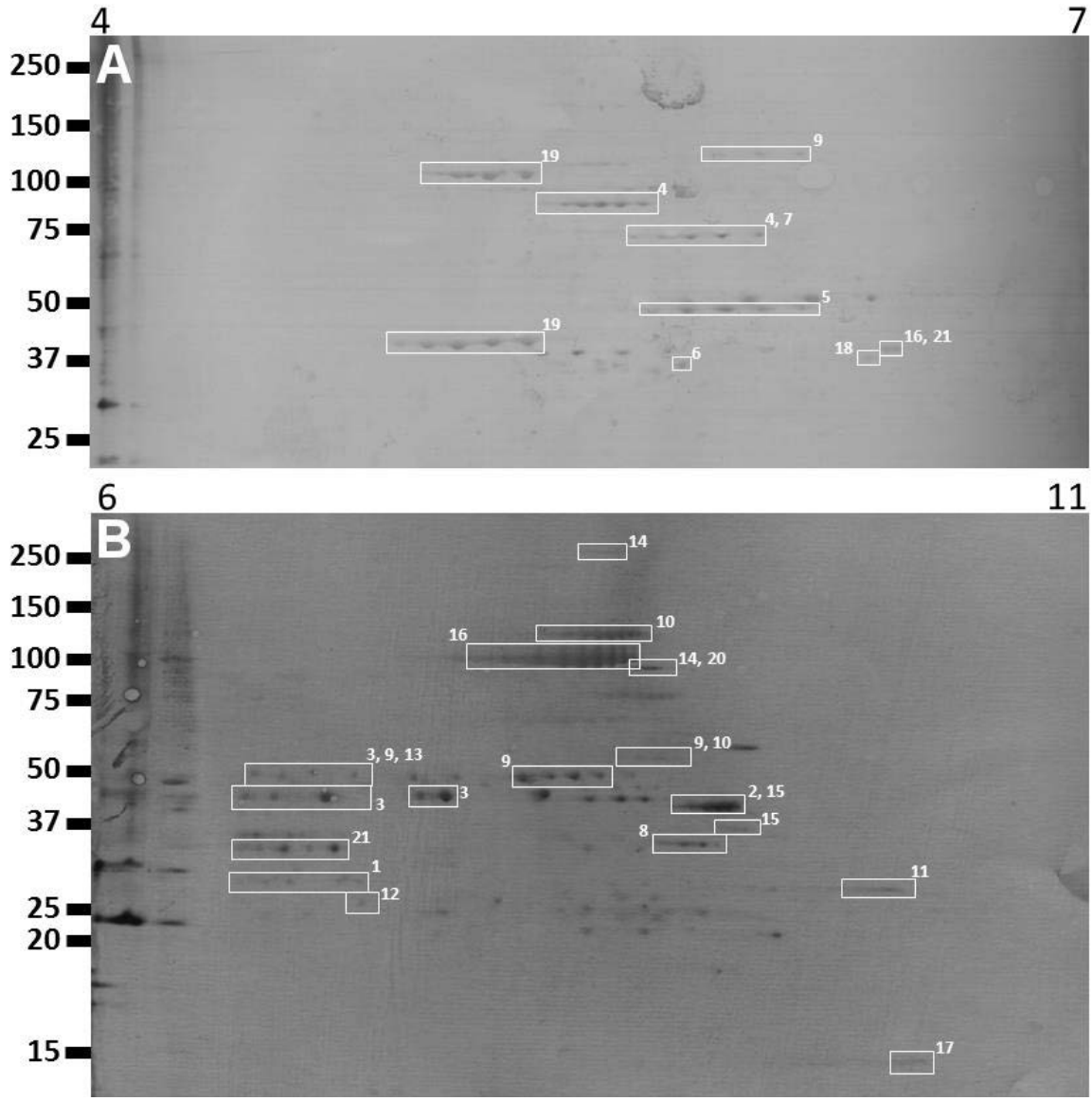

Figure 5.9: 2D ligand blot of *M. hyopneumoniae* proteins that bind to PK-15 cell surface receptors.

M. hyopneumoniae proteins were separated on 4-7 (A) and 6-11 (B) narrow range IPG strips, resolved by SDS-PAGE, transferred onto a PVDF membrane and probed with a biotinylated-PK-15 cell surface receptor proteins (1:2000). Proteins were identified by mapping them back to master gel images as described in the Materials and Methods.

The systems analysis is expected to recover *M. hyopneumoniae* proteins that bind directly with PK-15 surface proteins and indirectly via protein-protein interactions. To address this, we examined the ability of *M. hyopneumoniae* proteins to bind to PK-15 proteins using 2D ligand blotting (Figure 5.9). *M. hyopneumoniae* proteins were separated on 4-7 and 6-11 pH gradients and resolved by molecular mass in the second dimension using SDS-PAGE. Proteins were blotted onto PVDF membranes and probed with a lysate of biotinylated PK-15 proteins purified by avidin chromatography. Spots that bound to PK-15 cell surface proteins were mapped to reference 4-7 and 6-11 2D SDS-PAGE gels (Tacchi *et al.*, unpublished results) and identified by LC-MS/MS. The 2D ligand blotting studies identified 21 of the 74 proteins (28%) recovered in the affinity chromatography assays. Apart from P97 and P102 family adhesins, P159, P65 (lipoprotein), PdhA, PdhB, PdhC, PdhD, Ef-Tu, lactate dehydrogenase, glyceraldehyde-3-phosphate dehydrogenase, an uncharacterised hypothetical protein, phosphate acetyltransferase, and ribosomal proteins L1 and L21 were identified in 2D ligand studies (Table 5.1).

Table 5.1: *M. hyopneumoniae* proteins purified from Biotinylated PK-15 affinity column.

Accession	Protein Name	Elution*	Spot number**	Surface localisation
P0C0J3	L-lactate dehydrogenase	TFA	1	+
P0C0J8	P46	TFA		+
P0C0J9	30S ribosomal protein S15	Salt		+
Q4A925	P146	TFA	2	+
Q4A926	P135	Salt + TFA	3	+
Q4A932	Putative prolipoprotein P65	TFA	4	+
Q4A934	Ribose-phosphate pyrophosphokinase	Salt		
Q4A952	Probable tRNA threonylcarbamoyladenosine biosynthesis protein	TFA		
Q4A9B0	30S ribosomal protein S4	TFA		+
Q4A9G0	Lon Protease	Salt		+
Q4A9G1	Elongation factor Tu	TFA	5	+
Q4A9G3	Oligoendopeptidase F	Salt		+
Q4A9H0	Glucokinase	Salt		
Q4A9H9	Phosphate acetyltransferase	Salt	6	+
Q4A9I1	PdhD (Dihydrolipoamide dehydrogenase)	Salt	7	+
Q4A9I2	pdhC (Dihydrolipoamide acetyltransferase)	Salt + TFA	8	+
Q4A9J1	P159	Salt	9	+
Q4A9J2	P216	Salt + TFA	10	+
Q4A9J4	Mannnose-6 phosphate isomerase	Salt		
Q4A9J8	Phosphoglycerate kinase	TFA		+
Q4A9K9	ATP synthase alpha chain	TFA		+
Q4A9L2	Putative Uncharacterised Protein	Salt		
Q4A9L6	Phosphoenolpyruvate-protein phosphotransferase	TFA		+
Q4A9M8	50S ribosomal protein L11	TFA		
Q4A9M9	50S ribosomal protein L1	Salt + TFA	11	+
Q4A9N1	Neutrophil activating factor	Salt		+
Q4A9N8	Putative Uncharacterised Protein	Salt		
Q4A9T1	Protein MraZ	Salt		
Q4A9W4	Mhp385	Salt + TFA	12	+

Q4A9W5	Mhp384	Acid	13	+
Q4A9Y6	Putative Uncharacterised Protein	Acid		+
Q4AA43	30S ribosomal protein S6	Salt		+
Q4AA45	30S ribosomal protein S18	TFA		
Q4AA54	50S ribosomal protein L19	TFA		+
Q4AA88	Enolase	Salt + TFA		+
Q4AAA7	Myo-inositol catabolism protein	Salt		
Q4AAB8	Putative Uncharacterised Protein	TFA	14	+
Q4AAB9	Oligopeptide ABC transporter ATP-binding protein (oppF)	TFA		+
Q4AAC0	Oligopeptide ABC transporter ATP-binding protein (oppD)	TFA		
Q4AAD5	P102	Salt + TFA	15	+
Q4AAD6	P97	Salt + TFA	16	+
Q4AAE1	50S ribosomal protein L4	Salt		+
Q4AAE3	50S ribosomal protein L2	TFA		+
Q4AAE5	50S ribosomal protein L22	TFA		+
Q4AAE6	30S ribosomal protein S3	TFA		+
Q4AAE7	50S ribosomal protein L16	Salt		+
Q4AAE8	50S ribosomal protein L29	TFA		+
Q4AAE9	30S ribosomal protein S17	Salt		
Q4AAF1	50S ribosomal protein L24	Salt + TFA		+
Q4AAF2	50S ribosomal protein L5	Acid		+
Q4AAF4	30S ribosomal protein S8	Salt + TFA		+
Q4AAF6	50S ribosomal protein L18	Salt		+
Q4AAF7	30S ribosomal protein S5	Salt + TFA		
Q4AAF8	50S ribosomal protein L15	TFA		+
Q4AAG4	30S ribosomal protein S13	TFA		+
Q4AAG5	30S ribosomal protein S11	Salt + TFA		+
Q4AAG7	50S ribosomal protein L17	TFA		+
Q4AAI7	Putative Uncharacterised Protein	Salt		
Q4AAK1	50S ribosomal protein L27	Salt		+
Q4AAK2	50S ribosomal protein L21	Salt	17	+
Q4AAK8	Translation initiation factor IF-3	TFA		+
Q4AAL7	PdhB (Pyruvate dehydrogenase E1 component beta subunit)	Salt + TFA	18	+
Q4AAL8	PdhA (Pyruvate dehydrogenase E1-	Salt	19	+

	alpha subunit)			
Q4AAM4	Mhp271	Salt + TFA	20	+
Q4AAP9	NADH Oxidase	TFA		+
Q4AAQ5	30S ribosomal protein S7	TFA		+
Q4AAR2	Cytidylate kinase	Salt		
Q4AAR4	DnaK	Salt + TFA		+
Q4AAR6	Ribonuclease R	Salt		
Q4AAR8	Glyceraldehyde 3-phosphate	TFA	21	+
Q4AAS9	Putative ABC transporter ATP-binding protein	TFA		
Q4AAU3	Putative Uncharacterised Protein	Salt		
Q4AAV6	Protein RecA	TFA		
Q4AAW8	30S ribosomal protein S2	Salt		+

* Salt elution; 2M NaCl and acid elution; 0.4% Trifluoroacetic acid

** Spot numbers corresponding to Figure 5.9

5.3.8 Identification of target receptors on the surface of PK-15 monolayers

A similar systems approach was used to identify proteins on the surface of PK-15 cell that interact with proteins on the surface of *M. hyopneumoniae*. Native whole cell lysates of PK-15 cells were incubated with avidin beads containing biotinylated *M. hyopneumoniae* surface proteins as bait and washed extensively with PBS to remove unbound proteins. Proteins were recovered using 2M NaCl (elution 1) and 0.4% TFA (elution 2), separated by SDS-PAGE and identified by LC-MS/MS. 103 *Sus scrofa* (swine) proteins (Table 5.2) including many associated with the cytoskeleton such as actin, vimentin and keratin, tubulin, myosin and tropomyosin were identified. Other notable proteins identified in these analyses included cofilin (actin-binding protein), signalling molecules important to the organisation of the cytoskeleton such as calmodulin and GTPase-binding protein, and junction plakoglobin, which plays a role in linking the cytoskeleton with junction complexes by binding cadherins and desmosomal proteins. Proteins with well described functions in the cytosol of eukaryote cells were also detected in our analyses (Table 5.2).

Table 5.2: Porcine proteins purified by the biotinylated *M. hyopneumoniae* affinity column.

Accession	Protein Name	Elution
B2ZF46	ATP synthase subunit alpha	TFA
B3CL06	Serotransferrin	TFA
B6CVL5	High mobility group AT-hook 1 transcript variant 2	Salt
B7TJ03	Ribosomal protein L26-like 1	Salt
B9W5V0	Elongation factor 1-alpha	Salt + TFA
D5KJI2	High mobility group AT-hook protein 1	Salt
ENSSSCP00000018094	GTPase-activating protein-binding protein	Salt
F1RFI1	Elongation factor Tu	TFA
F1RFQ7	GTP-binding nuclear protein Ran	TFA
F1RGG1	40S ribosomal protein S19	Salt + TFA
F1RJS2	Clusterin	TFA
F1RPW2	Coagulation factor V light chain	Salt
F1RQ91	40S ribosomal protein S4, Y isoform 1	TFA
F1RTJ9	60S ribosomal protein L21	TFA
F1RUN2	Serum albumin	TFA
F1RUQ0	Immunoglobulin J	Salt + TFA
F1RY92	Serine/arginine-rich splicing factor 3	Salt
F1RYZ0	60S acidic ribosomal protein P2	TFA
F1RZ28	40S ribosomal protein S10	Salt + TFA
F1S0J8	Keratin19	TFA
F1S415	BAG family molecular chaperone regulator 3	TFA
F1S4M2	40S ribosomal protein S18	TFA
F1S6M7	Tubulin beta	Salt
F1S827	Isoform 3 of Plasminogen activator inhibitor 1 RNA-binding protein	TFA
F1S8L9	Heterogeneous nuclear ribonucleoprotein U	TFA
F1SA40	V-type proton ATPase subunit D	TFA
F1SAK6	ATP synthase subunit g, mitochondrial	TFA
F1SEY8	Polymeric immunoglobulin receptor	TFA
F1SFF4	Chromosome 14 open reading frame 166	TFA
F1SFI5	Histidine-rich glycoprotein	TFA
F1SGG2	Keratin8	TFA
F1SHC1	Tubulin alpha	Salt + TFA
F1SJQ6	60S ribosomal protein L14	TFA
F1SKJ1	Myosin 9	Salt
F1SLR1	NADH Dehydrogenase	Salt + TFA
F1SM14	Secreted phosphoprotein 24	TFA
F1SM78	Myosin regulatory light chain	Salt + TFA
F1SMZ7	Mitochondrial heat shock 60 kDa protein 1	TFA

F1SNY2	60S ribosomal protein L3	Salt + TFA
F1SPG1	Protein H1fx	Salt
F1SQ46	Cold shock domain protein A (DNA binding)	Salt
F1SRQ7	Single-stranded DNA-binding protein	Salt
F2Z522	Ribosomal protein L23a	Salt
F2Z539	40S ribosomal protein S20	Salt + TFA
F2Z546	60S ribosomal protein L19	TFA
F2Z554	Ribosomal protein L30	TFA
F2Z568	Ribosomal protein L38	TFA
F2Z571	Tubulin beta 2C chain	TFA
F2Z578	Histone H2B	TFA
F2Z5B6	Tropomyosin alpha-1 chain	Salt
F2Z5C7	40S ribosomal protein S3a-A	TFA
F2Z5E6	40S ribosomal protein S5	TFA
F2Z5F5	40S ribosomal protein S8	TFA
F2Z5G3	Calmodulin 2	Salt
F2Z5G8	40S ribosomal protein S25	TFA
F2Z5Q2	60S ribosomal protein L24	TFA
F2Z5Q6	40S ribosomal protein S6	TFA
F6Q5P0	40S ribosomal protein S13	TFA
G8ENL4	FUS RNA binding protein	Salt
I3L5B2	40S ribosomal protein S7	Salt + TFA
I3L6F1	60S ribosomal protein L18	TFA
I3LD74	60S ribosomal protein L11	Salt
I3LFH1	IgA heavy chian constant region	TFA
I3LI24	Guanine nucleotide-binding protein subunit beta-2-like 1	TFA
I3LJP6	40S ribosomal protein S24	TFA
I3LLG4	DnaJ	TFA
I3LNZ2	Histone H1.0	Salt
I3LPW0	NADH Dehydrogenase	TFA
I3LRH2	Nucleolin-related protein	Salt
I3LS16	NADH dehydrogenase [ubiquinone] 1 alpha subcomplex subunit 2	Salt
I3LS73	Mitochondrial import inner membrane translocase subunit Tim13	TFA
I3LSD3	60S ribosomal protein L13	TFA
I3LUP6	Putative nucleophosmin 1 variant 1	TFA
I7H541	Musashi homolog 2	TFA
K7GK75	Cofilin 1	Salt + TFA
K7GLT8	ATP synthase subunit beta	TFA
K7GNC6	Apolipoprotein O-like protein	TFA
K7GNZ3	Nascent polypeptide-associated complex subunit alpha	Salt
L8B0W9	IgG heavy chain	Salt + TFA

P02543	Vimentin	TFA
P18648	Apolipoprotein A-I	TFA
P60662	Myosin light polypeptide 6	Salt
P60662-2	Isoform Smooth muscle of Myosin light polypeptide 6	TFA
P62831	60S ribosomal protein L23	TFA
P62863	40S ribosomal protein S30	Salt
P62901	60S ribosomal protein L31	Salt
P63053	Ubiquitin-60S ribosomal protein L40	Salt
P67985	60S ribosomal protein L22	Salt + TFA
P80015	Azurocidin	TFA
Q0Z8U2	40S ribosomal protein S3	TFA
Q29201	40S ribosomal protein S16	TFA
Q2EN81	ATP synthase subunit O, mitochondrial	TFA
Q3YLA6	Serine/arginine-rich splicing factor 1	Salt
Q4TTS4	Histone H1.2-like protein	Salt
Q53DY5	Histone H1.3-like protein	Salt
Q5S1U1	Heat shock protein beta-1	Salt + TFA
Q6QAQ1	Actin, cytoplasmic 1	Salt + TFA
Q6QAS5	60S ribosomal protein L12	TFA
Q7M2W6	Alpha-crystallin B chain	TFA
Q8WNW3	Junction plakoglobin	Salt
Q95339	ATP synthase subunit f, mitochondrial	TFA
Q9GLP1	Coagulation factor V	TFA
Q9MYT8	ATP synthase subunit e, mitochondrial	TFA

Since the manner by which *M. hyopneumoniae* cells adhere to PK-15 cells often mimics phalloidin-staining patterns (see Figs. 6, 7 and 10) we investigated the hypothesis that *M. hyopneumoniae* interacts directly with cytoskeletal proteins. Several studies have identified actin on the surface of various cell types [231-236,245,246]. Consistent with this hypothesis we repeatedly identified monomeric actin by LC-MS/MS analysis of biotinylated PK-15 proteins recovered by avidin chromatography (Mascot Scores of 371 and 310 with 25% and 28% sequence coverage respectively) (Figure S5.3). Notably, we also identified actin at molecular masses ranging from approximately 5 kDa to 400 kDa suggesting that multimeric or filamentous forms of actin are present on the cell surface and that actin may be a target of ectodomain shedding.

5.3.9 Global analysis of actin-binding proteins

Actin is an important structural and functional component of all mammalian cells. Invasive bacterial pathogens typically trigger cytoskeletal rearrangements as part of their arsenal to commandeer the host cell [49,50,247,248]. We used CLSM and 3D-Structured Illumination Microscopy (3D-SIM) to monitor the distribution of *M. hyopneumoniae* cells on PK-15 monolayers that were stained with phalloidin. 3D-SIM images clearly depict *M. hyopneumoniae* cells in direct contact with F-actin suggesting that *M. hyopneumoniae* displays actin-binding proteins on its cell surface (Figure 5.10).

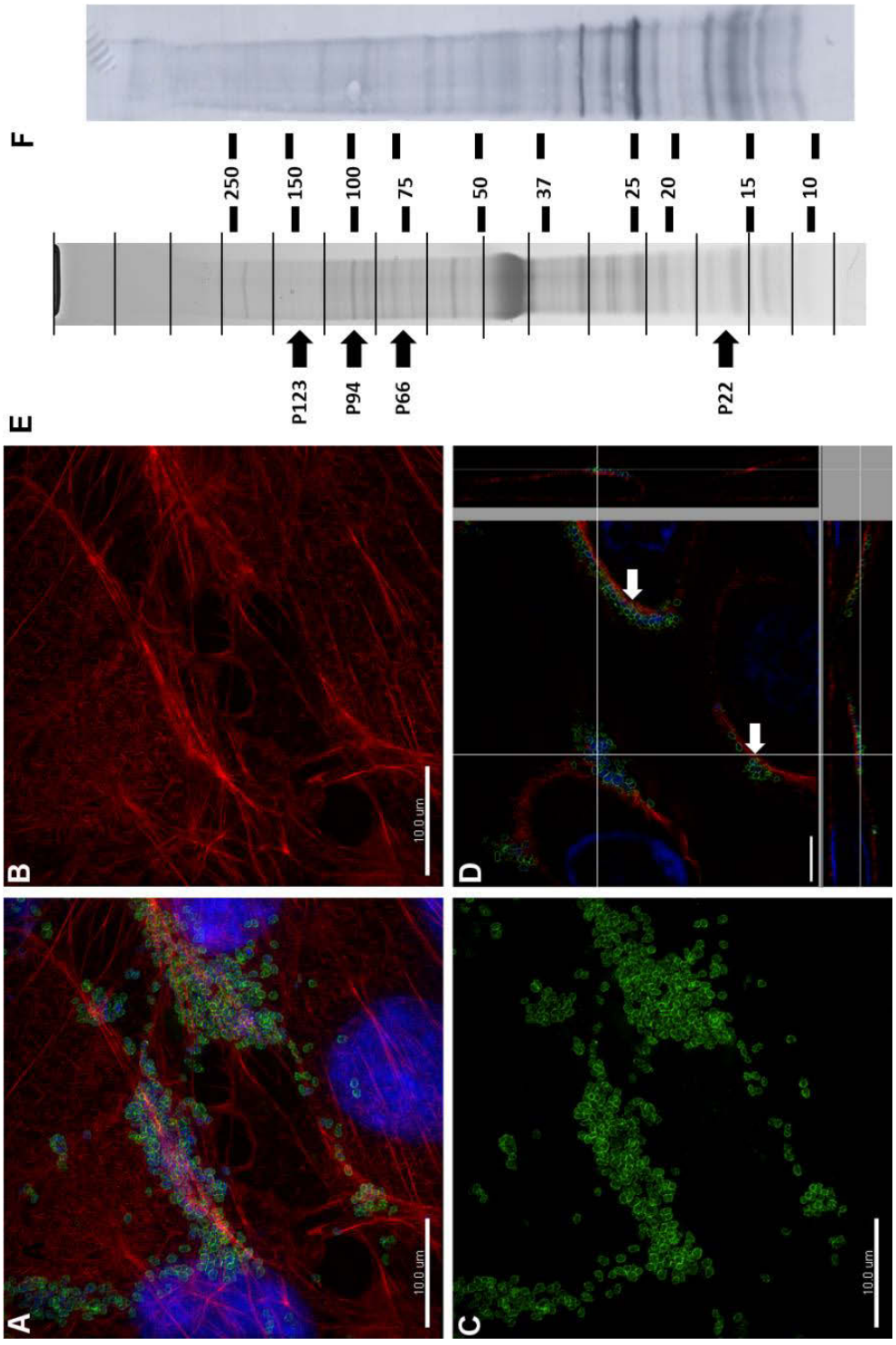

Figure 5.10: *M. hyopneumoniae* interacts with actin.

A-D) 3D-SIM images depicting *M. hyopneumoniae* cells adhering to PK-15 cells along cellular junctions where F-actin is prominent. A) *M. hyopneumoniae* cells were allowed to adhere to PK-15 monolayers overnight, followed by labelling with rabbit $F2_{P94\text{-}J}$ antisera and anti-rabbit Alexa Fluor® 488 conjugate (green). B) Monolayers were

permeabilised and stained with Alexa Fluor® 568 Phalloidin to visualise F-actin (red). Infected PK-15 monolayers were also stained with DAPI (blue) in order to visualise their nucleus as well as the nucleic acid present in *M. hyopneumoniae* cells. C) An overlay of all three channels showing *M. hyopneumoniae* cells adhering along the lengths of actin filaments. D) Slices view of the central area of Panel C depicting *M. hyopneumoniae* cells in close proximity to F-actin; cells can be seen in almost direct contact (white arrows). E) SDS-PAGE profile of *M. hyopneumoniae* proteins that elute from avidin column containing biotinylated actin as bait. Proteins in each of the 16 slices were digested with trypsin (in gel) and analysed by LC-MS/MS. P123J and cleavage fragments of P123J identified by LC-MS/MS are indicated by arrows. Molecular mass markers (kDa) are shown on the right. F) Ligand blot depicting *M. hyopneumoniae* whole cell lysate separated by SDS-PAGE and probed with biotinylated monomeric/G-actin.

To investigate the interaction between *M. hyopneumoniae* proteins and actin we immobilised biotinylated G-actin on avidin agarose beads and incubated them with a cell lysate of *M. hyopneumoniae*. No proteins were recovered in elution 1 (2M NaCl) suggesting that interactions between proteins from *M. hyopneumoniae* and actin are strong. Proteins recovered from elution 2 (0.4% TFA) were separated by SDS-PAGE and analysed by LC-MS/MS. We identified 143 proteins in elution 2. Notably, 51 (36%) of the 143 proteins also bound biotinlyated PK-15 surface proteins (Table 5.3). We identified most members of the P97 and P102 adhesin families including, for the first time, the P102 paralog Mhp275. Consistent with results from affinity chromatography experiments a large number of protein bands were detected on ligand blots containing *M. hyopneuoniae* cell lysates probed with biotinylated actin including a

number of strongly-staining proteins with masses from 10-35 kDa. On a cautionary note, many of the 143 proteins identified by LC-MS/MS have ATP-binding motifs. Each actin monomer contains an ATP molecule and it is possible that a proportion of these actin-binding proteins are exploiting the interaction with ATP. Further studies are needed to verify the biological relevance of these observations.

Table 5.3: Putative actin-binding proteins of *M. hyopneumoniae*

Accession	Protein Name	Binds to PK-15 surface proteins
P0C0J3	L-lactate dehydrogenase	+
P0C0J8	46 kDa surface antigen	+
P0C0J9	30S ribosomal protein S15	+
Q4A915	Putative uncharacterized protein	
Q4A925	Putative adhesin like-protein P146	
Q4A926	P135/Mhp683 (P102 paralog)	+
Q4A931	Chromosome partition protein	
Q4A932	Putative prolipoprotein P65	+
Q4A937	50S ribosomal protein L13	
Q4A938	30S ribosomal protein S9	
Q4A941	Leucine--tRNA ligase	
Q4A943	50S ribosomal protein L9	
Q4A947	Cysteine--tRNA ligase	
Q4A951	Transcription antitermination protein	
Q4A952	Probable tRNA threonylcarbamoyladenosine biosynthesis protein	+
Q4A967	50S ribosomal protein L10	
Q4A980	Putative sugar ABC transporter ATP-binding protein	
Q4A981	Putative Uncharacterised Protein	
Q4A982	Inorganic pyrophosphatase	
Q4A995	Putative ATP-binding protein	
Q4A998	Threonine--tRNA ligase	
Q4A9A0	Pullulanase	
Q4A9A2	Translation initiation factor IF-2	
Q4A9A3	Ribosome-binding factor A	
Q4A9A8	DNA glycosylase	
Q4A9B0	30S ribosomal protein S4	+
Q4A9E7	Putative uncharacterized protein	
Q4A9E9	Uridylate kinase	
Q4A9F7	Deoxyribose-phosphate aldolase	
Q4A9F8	Uracil phosphoribosyltransferase	
Q4A9G1	Elongation factor Tu	+
Q4A9H3	Xylose ABC transporter ATP-binding protein	
Q4A9I0	Acetate kinase	
Q4A9J1	Putative p76 membrane protein	
Q4A9J2	Putative P216 surface protein	
Q4A9J8	Phosphoglycerate kinase	+
Q4A9K0	Putative uncharacterized protein	
Q4A9K9	ATP synthase alpha chain	+
Q4A9L9	Putative ABC transporter atp-binding protein	
Q4A9M8	50S ribosomal protein L11	+
Q4A9M9	50S ribosomal protein L1	+
Q4A9N3	FMN-dependent NADH-azoreductase	
Q4A9N6	Putative ABC transporter ATP-binding protein	
Q4A9N9	Probable GTP-binding protein	

Q4A9Q0	Hexulose-6-phosphate isomerase	
Q4A9Q2	Putative Uncharacterised Protein	
Q4A9R9	ATP-dependent helicase PcrA	
Q4A9S1	Asparagine--tRNA ligase	
Q4A9S4	Ribonuclease 3	
Q4A9S6	Methionyl-tRNA synthetase	
Q4A9V2	Proline--tRNA ligase	
Q4A9V4	Putative ABC transporter ATP-binding protein	
Q4A9W4	Mhp385	+
Q4A9W5	Mhp384	+
Q4A9X1	Putative lipoprotein	
Q4A9X8	Glycerol kinase	
Q4A9Y6	Putative uncharacterized protein (P80)	+
Q4AA33	ABC transporter ATP binding protein	
Q4AA35	Glycerophosphoryl diester phosphodiesterase	
Q4AA39	Putative uncharacterized protein	
Q4AA43	30S ribosomal protein S6	+
Q4AA45	30S ribosomal protein S18	+
Q4AA52	30S ribosomal protein S16	
Q4AA54	50S ribosomal protein L19	+
Q4AA58	CTP synthetase	
Q4AA61	Putative Uncharacterised Protein	
Q4AA64	Phenylalanine--tRNA ligase beta subunit	
Q4AA66	Mhp107	
Q4AA67	Mhp108	
Q4AA74	Energy-coupling factor transporter ATP-binding protein EcfA 2	
Q4AA75	Energy-coupling factor transporter ATP-binding protein EcfA 1	
Q4AA76	Hypoxanthine phosphoribosyltransferase	
Q4AA88	Enolase	+
Q4AA93	30S ribosomal protein S20	
Q4AA95	Aspartyl-tRNA synthetase	
Q4AAA5	Ribose ABC transport ATP-binding protein	
Q4AAB5	Ribonucleoside-diphosphate reductase	
Q4AAB8	Putative Uncharacterised Protein	+
Q4AAC0	Oligopeptide ABC transporter ATP-binding protein	+
Q4AAD3	Alanine--tRNA ligas	
Q4AAD5	P102	+
Q4AAD6	P97 Adhesin	+
Q4AAE0	50S ribosomal protein L3	
Q4AAE1	50S ribosomal protein L4	+
Q4AAE2	50S ribosomal protein L23	
Q4AAE3	50S ribosomal protein L2	+
Q4AAE5	50S ribosomal protein L22	+
Q4AAE6	30S ribosomal protein S3	+
Q4AAE7	50S ribosomal protein L16	+
Q4AAE8	50S ribosomal protein L29	+
Q4AAE9	30S ribosomal protein S17	+

Q4AAF0	50S ribosomal protein L14	
Q4AAF1	50S ribosomal protein L24	+
Q4AAF2	50S ribosomal protein L5	+
Q4AAF4	30S ribosomal protein S8	+
Q4AAF5	50S ribosomal protein L6	
Q4AAF6	50S ribosomal protein L18	+
Q4AAF7	30S ribosomal protein S5	+
Q4AAF8	50S ribosomal protein L15	+
Q4AAG0	Adenylate kinase	
Q4AAG4	30S ribosomal protein S13	+
Q4AAG5	30S ribosomal protein S11	+
Q4AAG7	50S ribosomal protein L17	+
Q4AAJ3	Glutamate--tRNA ligase	
Q4AAJ6	Putative uncharacterised protein	
Q4AAK1	50S ribosomal protein L27	+
Q4AAK2	50S ribosomal protein L21	+
Q4AAK7	Pyruvate Kinase	
Q4AAK8	Translation initiation factor IF-3	+
Q4AAL1	50S ribosomal protein L28	
Q4AAL7	pdhB (Pyruvate dehydrogenase E1-beta subunit)	+
Q4AAL9	Adenine phosphoribosyltransferase	
Q4AAM2	6-phosphofructokinase	
Q4AAM3	DNA gyrase subunit B	
Q4AAM4	Mhp271	+
Q4AAM9	ATP-dependent protease binding protein	
Q4AAN0	Putative Uncharacterised Protein	
Q4AAN3	Prolipoprotein diacylglyceryl transferase	
Q4AAN4	Thiol peroxidase	
Q4AAP5	Protein translocase subunit SecA	
Q4AAP7	Purine-nucleoside phosphorylase	
Q4AAP8	Thymidine phosphorylase	
Q4AAP9	NADH Oxidase	+
Q4AAQ5	30S ribosomal protein S7	+
Q4AAQ8	Elongation factor 4	
Q4AAR0	Bacterial nucleoid DNA-binding protein	
Q4AAR3	Heat shock protein DnaJ	
Q4AAR4	Chaperone protein dnaK	+
Q4AAR8	Glyceraldehyde 3-phosphate	+
Q4AAR9	Topoisomerase IV subunit B	
Q4AAS1	Isoleucine--tRNA ligase	
Q4AAS9	ABC transporter ATP binding protein	+
Q4AAT0	Putative ABC transporter ATP-binding protein	
Q4AAT9	Heat-inducible transcription repressor HrcA	
Q4AAU7	DNA polymerase III beta subunit	
Q4AAV6	Protein RecA	+
Q4AAV7	ATP synthase subunit beta	
Q4AAW5	Glycyl-tRNA synthetase	
Q4AAW6	Signal recognition particle protein	

Q4AAW8	30S ribosomal protein S2	+
Q4AAX2	Putative uncharacterized protein	
Q4AAX3	Tyrosine--tRNA ligase	
Q600K9	MhpX	
Q601C7	Mhp275 (No J homolog)	

5.3.10 Domains within P97 bind actin

Cleavage fragments representing different regions of the multifunctional adhesin $P123_J$ were among the highest abundance proteins recovered from affinity chromatography experiments using biotinylated actin as bait. The cilium adhesin $P123_J$ is endoproteolytically processed [42,54] and $P22_J$, $P66_J$, $P94_J$ and $P28_J$ are the major cleavage fragments that bind host molecules [41,42,54]. We identified $P22_J$, $P66_J$, $P94_J$ and $P123_J$ but not $P28_J$ in our 0.4% TFA elution (Figure 5.10) indicating that the C-terminal, R2-containing region does not bind actin. Microscale thermophoresis was employed to test the ability of recombinant fragments $F1_{P97\text{-}232}$ (amino acids 106-758), $F3_{P97\text{-}232}$ (amino acids 768-938) and $F4_{P97\text{-}232}$ (amino acids 961-1107) to bind actin [41,42]. $F1_{P97\text{-}232}$ and $F3_{P97\text{-}232}$ bound actin with K_D's of 34.2 nM and 1.79 μM respectively while $F4_{P97\text{-}232}$ did not bind (Figure S5.3). $F1_{P97\text{-}232}$ and $F3_{P97\text{-}232}$ span the N-terminal regions of P97 that were identified in actin affinity chromatography while $F4_{P97\text{-}232}$ represents the C-terminal cleavage fragment $P28_J$ that was not identified. These findings show that the N-terminus of P97/P22 represented by $F1_{P97\text{-}232}$ possesses at least one actin-binding domain with nanomolar binding affinity and has a stronger affinity for actin than the region represented by $F3_{P97\text{-}232}$. This is the first study to investigate the binding affinities of a bacterial adhesin to mammalian actin.

[**The section below is preliminary data for a planned patent application and not included in the manuscript. Gene names have been excluded for copyright purposes**]

5.3.11 Screening for Biofilm-Deficient Mutants

The ability to link phenotype to genotype in *M. hyopneumoniae* has been hampered by the inability to genetically modify this organism. Recent advances have led to the successful transposon mutagenesis of *M. hyopneumoniae* strain 232 [161,237]. With access to this transposon mutant library we sought to screen for biofilm-deficient mutants. We devised a nucleic acid-specific assay that utilised DAPI for the quantification of *M. hyopneumoniae* biofilms grown in a 96-well plate. We compared biofilm growth in mutants containing a transposon in MhpX, MhpY and another gene MhpZ to WT strain 232 as well as strain J in duplicate. Mutations in MhpX, MhpY and MhpZ had a profound effect on biofilm formation (Figure 5.13). Multiple mutations in the MhpY gene displayed a similar phenotypic effect on biofilm formation (Figure 5.13), suggesting that it is a true biofilm-associated gene. It is important to note that MhpX and MhpY are too large to complement and so we are unable to observe whether or not complementation can restore the biofilm phenotype. MhpZ is a newly identified biofilm deficient mutant and work is being undertaken to characterise this gene.

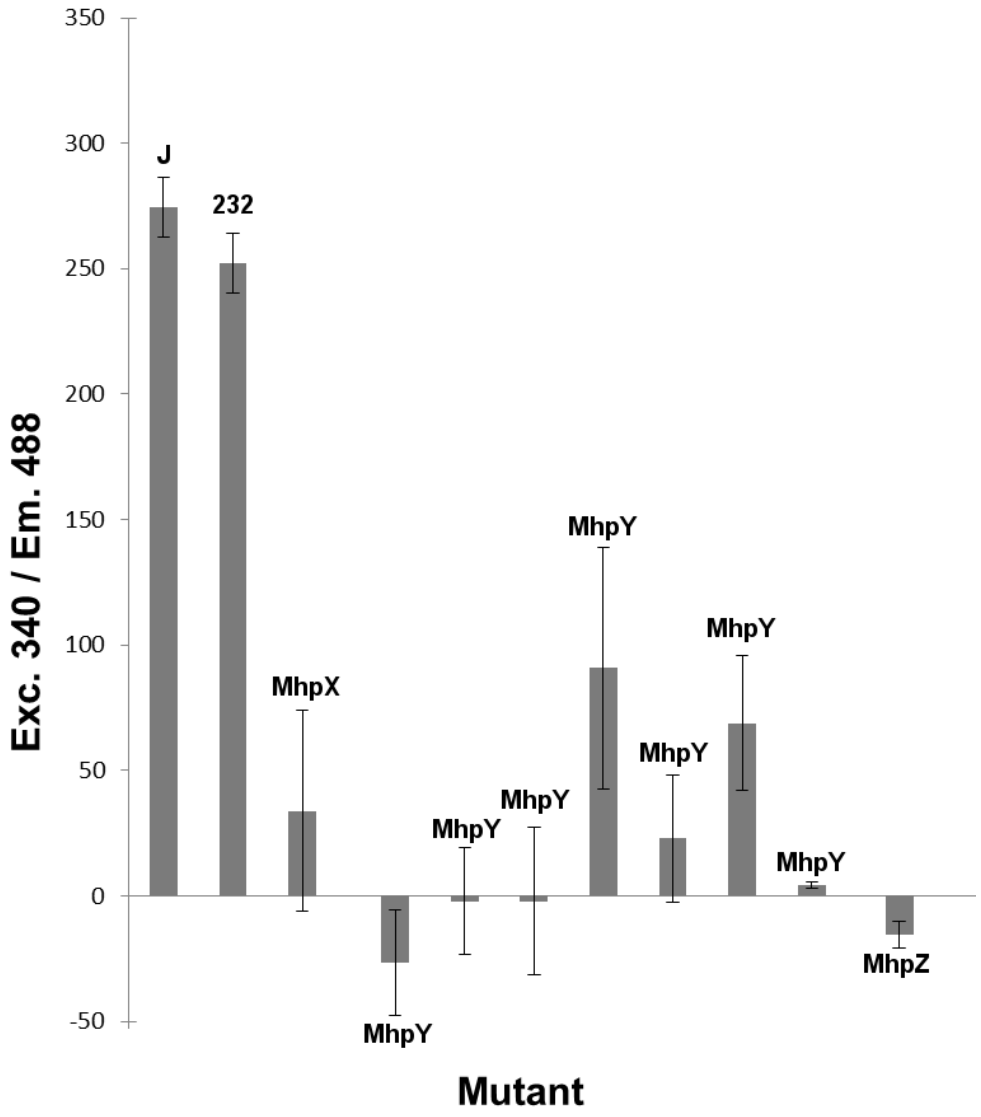

Figure 5.11: Biofilm screen of *M. hyopneumoniae* transposon mutants.

Results are presented as the average of duplicate experiments with standard error bars added. WT strain 232 and strain J are labelled. It can be seen that transposons in MhpX, MhpY and MhpZ form less biofilms.

5.3.12 Growth Curve of ΔMhpX, ΔMhpY and WT

In order to examine whether or not the observed decrease in biofilm formation was due to a decrease in growth rate we compared the growth rates of WT, ΔMhpX and ΔMhpY. A broth culture of WT, ΔMhpX and ΔMhpY was set up in triplicate for 96 hours, where an aliquot was taken and plated in a dilution series every 24 hours onto Friis agar. The resulting growth curve demonstrated that WT, ΔMhpX and ΔMhpY had similar starting numbers and growth rates, with WT having approximately 10-fold fewer cells than ΔMhpX and ΔMhpY at 96 hours (end of log phase) (Figure 5.14). This would suggest that not only do ΔMhpX and ΔMhpY grow slightly faster than WT but their diminished ability to form biofilms is not a growth-rate effect. Notably, ΔMhpY appeared to exist in log phase for much longer than ΔMhpX and Mhp232 and we were unable to observe stationary phase. Laboratory strains of *M. hyopneumoniae* are typically not cultured for more than 48 h, due to the suspected short log phase. These data now suggest that we are harvesting cells that are in early log phase and will aid us in future experiments. It is important to note that this is the first growth curve for *M. hyopneumoniae* and demonstrates that the doubling time of *M. hyopneumoniae* strain 232 is approximately 5 hours.

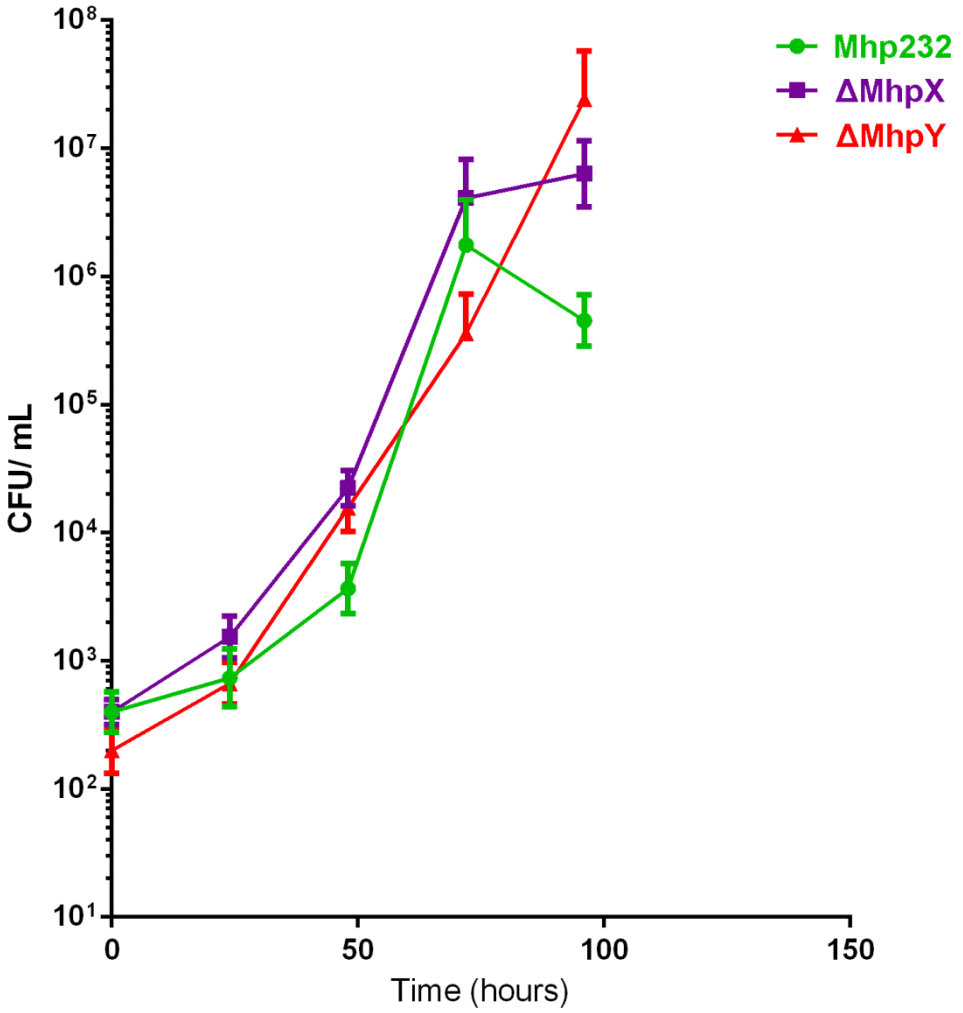

Figure 5.12: Growth Curve of ΔMhpX, ΔMhpY and WT.

Mhp232, ΔMhpX and ΔMhpY were grown in Friis broth culture, in triplicate, for a total of 96 hours. The data presented here are the averages of triplicate data with the calculated standard error bars presented. Lag phase appears to occur between 0 – 25 h with log phase starting at approximately 50 h. Stationary phase occurs at approximately 70 h for Mhp232 and ΔMhpX. Mhp232 does not appear to exhibit much of a stationary phase, quickly progressing to death phase after log phase.

5.4 Discussion

Infection of the lungs of pigs with *M. hyopneumoniae* has been estimated to reduce the percentage of intact healthy cilia to less than 20% [1]. While *M. hyopneumoniae* may initially reduce ciliary beat frequency prior to binding ciliated airways, the ability of *M. hyopneumoniae* to form microcolonies is considered an important step to the process of crosslinking cilia and inducing ciliostasis. Detailed analyses of the binding functions of all members of the P97 and P102 adhesin families [2-10,41,42,44], P159 [4,43] and several surface accessible aminopeptidases [145,155] implicate the importance of interactions between *M. hyopneumoniae* cell surfaces and extracellular matrix and circulatory host molecules during the colonisation process. The P97 and P102 adhesin families are constitutively expressed during growth *in vitro* [2-10,42-44,249,250] and in the respiratory tract of *M. hyopneumoniae*-infected pigs [52]. Adhesin family members are barely detectable as full length gene products and perform their functions as cleavage fragments that are bound to the *M. hyopneumoniae* cell surface [2-10,42-44,250] or shed into the extracellular milieu where they associate with cilial surfaces distal to the cells that produced them [52]. Adhesin cleavage fragments [41,250], metabolic enzymes that moonlight on the cell surface (Unpublished Data) and aminopeptidases [145,155] are all capable of forming homopolymeric interactions and may play important roles in promoting microcolony formation. Microcolonies of *M. hyopneumoniae* represent a focal region of microbial metabolic activity and the by-products of these processes are likely to influence ciliostasis and epithelial cell death [17,202]. *In vivo*, microbial communities are likely to contain mixed bacterial and viral species [179] and the ability to form biofilms is advantageous to initiating chronic infections and evading host immune responses. Here we outline a time course of events depicting *M. hyopneumoniae* forming biofilms on glass. Formation of biofilms on glass

occurs only after prolonged incubation (8-10 days) suggesting that *M. hyopneumoniae* is unable to adhere without a conditioning phase where medium components sourced from serum supplements are deposited onto the glass surface. The requirement for lengthy growth conditions likely explains why *M. hyopneumoniae* has not been shown to form biofilms in previous studies. Biofilms grew rapidly after 12-15 days exceeding 100 μm in diameter and do so by subsuming microcolonies in the path of the advancing growth zone. The formation of biofilms in other Mycoplasma species offers protection from antimicrobial compounds and the host immune response [61,73]. Our *in vitro* studies suggest that *M. hyopneumoniae* can adopt an alternate lifestyle in the lungs of pigs that plays an important role in initiating a chronic infectious state; a hallmark of infections caused by this pathogen. Consistent with this hypothesis we demonstrated for the first time large biofilms (> 150 μm) on epithelial cells denuded of cilia in the lungs of pigs experimentally-infected with *M. hyopneumoniae*. These studies show that biofilms are not a curiosity of *in vitro* culture and are likely to be important to the ability of *M. hyopneumoniae* to form chronic infections in swine.

IFM showed that the core of the mature biofilms that form on glass comprise *M. hyopneumoniae* cells that are capable of expressing the lipolytic lipoprotein P65. At the perimeter of mature biofilms, there are fewer *M. hyopneumoniae* cells expressing P65. The pattern of expression of P65 is non-uniform and is concentrated in random pockets at the periphery of expanding and mature biofilms (Figure 5.2). These observations suggest that subpopulations of *M. hyopneumoniae* on the perimeter of biofilms fail to or weakly express P65. $F2_{P97}$ antiserum on the other hand labels these biofilms uniformly, suggesting that the majority of cells are expressing the P97 adhesin. Significant progress has been made in determining how surface lipoproteins that undergo size variation by

the gain or loss of tandem repeats influence biofilm formation [55,61]. During replication, slip-strand DNA mispairing can lead to stochastic changes in the length of surface expressed lipoproteins by variation in the number of tandem-repeat regions [251]. In *M. pulmonis*, cells producing either long or short variable surface lipoproteins display differences in their ability to i) adhere to pulmonary epithelial cells and form biofilms [55], ii) interact with components of complement [58] and iii) bind to red blood cells [59]. Notably, lipoproteins expressed by *M. hyopneumoniae* are not known to display phase variation or vary in size by the gain or loss of tandem repeats [156]. Further studies are required to determine the mechanism(s) by which *M. hyopneumoniae* forms biofilms.

Ruthenium red (RR) has been shown to bind to amorphous capsular matrix (approximately 20 – 40 μm in diameter) that surrounds the perimeter of *M. hyopneumoniae* cells and to long filamentous projections that emanate from the surface of cells that attach to neighbouring *M. hyopneumoniae* cells, cilia and microvillae [230]. Here we show that biofilms of *M. hyopneumoniae* grown in tissue culture flasks for 30 days produce an extrapolymeric matrix that binds RR. Cells that stain with RR are localised to the centre of the biofilms and sporadically at the periphery of the growing core. Outside of the biofilm core, RR staining patterns are unpredictable. *M. hyopneumoniae* cells residing outside of biofilms also stain sporadically with RR. Our data suggests that the molecules that directly interact with RR are differentially expressed. RR was originally thought to stain mucopolysaccharides but recent evidence indicates that it also binds to membrane proteins [242] and as such it cannot be used to reliably predict the expression of extracellular polysaccharides (EPS). EPS are synthesized by some *Mycoplasma* spp. and are known to play a role in the structure of

biofilms and how Mycoplasmas interface with host cells and the environment. Mutants of *M. pulmonis* defective in exopolysaccharide production adhere poorly to pulmonary epithelial cells yet retain the ability to adhere strongly to abiotic surfaces and colonise the respiratory tract of mice [55,59,62,252]. *M. pulmonis* forms a glycocalyx that protects cells from complement and phagocytosis and modulates adherence to host cells [39,55,253,254]. Other than *M. hyopneumoniae*, RR has been used to stain the capsules of different mycoplasma species including *Mycoplasma dispar* [255], *Mycoplasma synoviae* [256], *Mycoplasma meleagridis* [257], *Ureaplasma urealyticum* [258] and *Mycoplasma pneumoniae* [259]. It is not known if *M. hyopneumoniae* produces EPS. Additionally, we used TOTO-1 to stain for the presence of eDNA and showed that it appears to form the basis of *M. hyopneumoniae* biofilms formed on glass. eDNA is an important component of the extrapolymeric matrix of microbial biofilms and aids in cellular adhesion within biofilms [60,260,261]. The mechanism of eDNA release has not been examined in Mycoplasma species, however here it appears to be produced as a bi-product of cellular lysis. eDNA could be observed in areas where remnants of *M. hyopneumoniae* membranes (stained with $F2_{P97}$) could be seen, and a number of apparently intact cells stained with TOTO-1; suggesting that their membrane integrity has become compromised and they are undergoing lysis (Figure 5.5). Using 3D-SIM we observed circular eDNA that may have just been released from the lysis of a *M. hyopneumoniae* cell (Figure 5.5). Further work will be required to examine how eDNA is released from *M. hyopneumoniae* cells and how much of the biofilm matrix it comprises.

Studies of the mechanisms of pathogenesis of *M. hyopneumoniae* have primarily focused on characterising the P97 and P102 adhesin families and several proteases and

their roles in binding to glycosaminoglycans, fibronectin and plasminogen [2,3,5-9,42-44,54,145,155,244,249]. *M. hyopneumoniae* is not restricted to colonising cilia and is capable of localising to organs distal to the respiratory tract including the spleen, liver and kidneys [14-16] indicating that *M. hyopneumoniae* is adept at colonising a range of different cell types. To gain further insight into the adhesive capabilities of surface proteins produced by *M. hyopneumoniae* we developed a series of affinity matrices comprising biotinylated PK-15 cell surface proteins (bait proteins) to identify interacting proteins produced by *M. hyopneumoniae*. Experiments using biotinylated surface proteins from *M. hyopneumoniae* as bait to identify proteins that interact with PK-15 cell surface proteins were also undertaken. We identified 74 *M. hyopneumoniae* proteins that may interact directly to PK-15 cell surface proteins. Of the 74 proteins from *M. hyopneumoniae*, 59 (80%) have been detected on the surface of *M. hyopneumoniae* in surfaceome analyses (Tacchi *et al.*, unpublished results) and include most members of the P97 and P102 adhesin families, lipoproteins and various conserved and unique hypothetical proteins. Notably, a significant proportion of the 74 putative cell adhesins are glycolytic enzymes including glyceraldehyde 3-phosphate dehydrogenase, l-lactate dehydrogenase and pyruvate dehydrogenase components A – D. While these proteins are known to moonlight as adhesins on the surface of bacterial pathogens including various Mycoplasma species and bind fibronectin and plasminogen [143,170,262,263], we show here that many of these proteins also reside on the surface of *M. hyopneumoniae* and potentially bind actin. There have only been a few reports of bacterial proteins that bind actin [264,265]. Our studies suggest that the many bacterial proteins may display the ability to bind actin. Further studies are needed to confirm these binding interactions. We also demonstrated that antisera raised against these putative moonlighting proteins labelled *M. hyopneumoniae* biofilms grown on glass for

30 days (Figure 5.2). PdhB antisera appeared to label the exterior of the biofilm while rpL3 antisera appeared to label the entirety of the biofilm (Figure 5.2) PdhB was identified in the salt and acid elutions from our PK-15 pulldowns (Table 5.1) as well as our actin pulldowns (Table 5.3), while L3 was only identified from our actin pulldown experiments (Table 5.3). This suggests that these putative moonlighting proteins are either expressed on the surface of cells residing within the biofilm, or are secreted into the biofilm. The extracellular matrix of biofilms formed by *Staphylococcus aureus* are comprised of cytoplasmic proteins [266]. Proteomic examination of extracellular proteins contained within biofilms demonstrated that 50S ribosomal protein L3 was one of the proteins present in high abundance [266]. The diffuse staining pattern of rpL3 in *M. hyopneumoniae* biofilms appears different to that of $F2_{P97}$, suggesting that what we are observing here may be secreted rpL3. Further work will be needed to investigate this.

Recent breakthroughs in the mutagenesis of *M. hyopneumoniae* [161,237] have allowed us to screen for genes associated with biofilm formation. We utilised a 96-well plate assay that measured biofilm formation by quantifying for total nucleic acids present using DAPI. From this assay we identified 3 putative biofilm associated genes that we have denoted ΔMhpX, ΔMhpY and ΔMhpZ. These 3 mutants formed little to no biofilms (Figure 5.13). In order to investigate whether or not the diminished biofilm formation was due to a reduced growth rate we compared the growth rates of ΔMhpX and ΔMhpY as they were of the most interest to us. The growth rates of these mutants were almost identical, if not faster, than the WT strain (Figure 5.14). This suggests that the diminished biofilm formation was not correlated with growth rate and that these mutants are unable to form biofilms. Notably, MhpX was identified in our actin

pulldowns, suggesting that it may be an actin-binding protein. Neither of these genes share homology with any other bacterial protein and so future work will be required to investigate their function(s).

We identified 103 porcine (*Sus* scrofa) proteins that may interact directly with proteins on the surface of *M. hyopneumoniae* including the cytoskeletal-like proteins actin, tubulin, myosin and keratin. Furthermore, using G actin as a bait protein we identified 143 putative actin-binding proteins from *M. hyopneumoniae*. CLSM and 3D-SIM were used to observe *M. hyopneumoniae* cells associating with the surface of PK-15 monolayers. The pattern of colonisation of *M. hyopneumoniae* on the surface of PK-15 cells is often predicted by regions that stain heavily with phalloidin suggesting that PK-15 cells secrete actin onto their cell surface. Consistent with this hypothesis we identified actin by LC-MS/MS in our surface biotinylation studies of PK-15 cells (Figure S5.3). Actin has been identified on the surface of a wide variety of eukaryote cells including catecholaminergic, endothelial and lymphocytic cells [231-236]. We investigated the notion that *M. hyopneumoniae* may display surface proteins that target actin on the surface of PK-15 cells. Among the most abundant *M. hyopneumoniae* proteins identified in affinity experiments using actin as bait were cleavage fragments of the multifunctional cilium adhesin $P123_J$. $P22_J$ (amino acids 1-194), $P66_J$ (amino acids 195-862), $P94_J$ (amino acids 195-1092) and $P123_J$ (amino acids 1-1092) were recovered from an avidin column containing biotinylated actin as bait. These data suggested that actin-binding domains are associated with sequences that reside with the N-terminal half of the $P123_J$ pre-protein because we did not recover $P28_J$ (amino acids 863-1092). To test this hypothesis we utilised microscale thermophoresis to assess the ability of different regions of $P123_J$ to bind actin using recombinant fragments spanning the

cilium adhesin [41,42]. $F1_{P97\text{-}232}$ (amino acids 106-758) and $F3_{P97\text{-}232}$ (amino acids 765 – 914) bound actin with K_D's of 34.2 nM and 1.79 μM respectively while $F4_{P97\text{-}232}$ (amino acids 961 –1108) failed to bind actin. $F1_{P97\text{-}232}$ spans P22 and P66 but does not contain the R1 pentapeptide repeat in the C-terminus of P66 that is important for binding porcine cilia [207]. Because $F1_{P97\text{-}232}$ and $F3_{P97\text{-}232}$ do not share sequences we can assume that at least two actin-binding sites exist in P123J (UniProt # Q4AAD6). P22 spans amino acids 1- 194 and bound strongly to actin-coated avidin beads indicating that an actin-binding domain exists within this region of the adhesin. A second actin-binding domain resides between amino acids 765- 914 in the $P123_J$ pre-protein. Thus $P94_J$ carries at least two actin-binding domains. A BLAST of amino acids 106-194, reflecting the start site of $F1_{P97\text{-}232}$ and the ^{192}T-N-F↓A-D^{196} cleavage site did not yield any significant matches outside of a few *Mycoplasma* spp suggesting that the actin-binding domain is unique to the phylogenetic clade that *M. hyopneumoniae* belongs to. $F3_{P97\text{-}232}$ bound actin with micromolar affinity 50-fold lower than $F1_{P97\text{-}232}$ suggesting that the actin-binding domain in this region binds weakly with actin. BLASTP analysis of this region identified significant homology to collagen type VI (72.3% identity) belonging to *Sus scrofa* (Uniprot: I3LUR7) at amino acids 2889 – 2935. Collagen VI is part of the extracellular matrix of skeletal muscle which may explain why this region binds to actin [267].

Only a handful of bacterial actin-binding proteins have been reported to date [264,265]. The actin cytoskeleton is the major target of most bacterial effector molecules that are introduced into target host cells. Here we have identified numerous putative actin-binding proteins on the surface of *M. hyopneumoniae* and confirmed that one of these, the cilium adhesin MHJ_0194 contains two actin-binding domains that reside in

different regions of the molecule. Recently we have shown that *M. hyopneumoniae* is capable of invading PK-15 cells where it resides within lysosomal-like vacuoles (Raymond *et al.*, unpublished results). During the process of internalisation, *M. hyopneumoniae* clearly induces cytoskeletal rearrangements at the point of contact on the epithelial cell surface facilitating entry into a vacuole. The presence of actin-binding proteins on the surface of *M. hyopneumoniae* has important ramifications for deciphering how this bacterial pathogen influences host cytoskeletal rearrangements. We also identified actin on the surface of PK-15 cells suggesting that actin may be another receptor targeted by *M. hyopneumoniae* during colonisation of the epithelial-cell surface. How cell surface actin on PK-15 cells interacts with intracellular actin fibres, if at all, is not understood. Recently we have shown that *M. hyopneumoniae* induces the expression of fibronectin at the point of contact with PK-15 epithelial cells [42]. Microbial fibronectin-binding proteins often function as bridging molecule to membrane exposed integrin β1 receptors on target host cells and binding initiates downstream signalling events leading to actin and microtubule rearrangement that facilitate internalisation [49,50]. Further studies are needed to unravel these complex molecular mechanisms.

5.5 Conclusion

M. hyopneumoniae forms a chronic respiratory disease by colonising the ciliated epithelium of the swine respiratory tract where it causes ciliostasis and eventual cilial death [1]. It has been previously demonstrated that adhesins on the surface of *M. hyopneumoniae* bind to glycosaminoglycans, Plg and Fn [2-9,41-44] and that host cellular responses are elicited in conjunction with these molecules [9,42]. Here we have shown for the first time that *M. hyopneumoniae* forms prolific biofilms on abiotic surfaces, host cell monolayers, and on the denuded epithelium of the swine respiratory tract. We have shown that these biofilms contain eDNA that appears to be a produced by cell lysis, with a number of lytic cells present in the biofilms. Our affinity chromatography experiments and 3D-SIM images demonstrated that *M. hyopneumoniae* targets actin on the surface of PK-15 monolayers and that it utilises a number of putative moonlighting proteins to do so. A number of these proteins appear to be unevenly distributed throughout *M. hyopneumoniae* biofilms, suggesting that they may be differentially expressed. This is the first study to investigate biofilm formation in *M. hyopneumoniae*, and the first to identify the full repertoire of adhesins as well as the receptors that it targets on PK-15 monolayers. These methodologies have allowed us to create a subset of novel virulence factors and mechanisms that can be targeted as vaccine candidates in the future.

Chapter Six: (Paper V) *M. hyopneumoniae* is an invasive pathogen that escapes lysosomes

Declaration

I declare that the following publication included in this thesis in lieu of a chapter meets the following:

- More than 50% of the content in the following publication included in this chapter has been planned, executed and prepared for publication by me
- The work presented here has been prepared for publication and will be submitted
- The initial draft of the work has been written by me and any subsequent changes in response to co-authors and editors reviews was performed by me
- The publication is not subject to any obligations or contractual agreements with a third party that would constrain its inclusion in the thesis.

Publication title: *Mycoplasma hyopneumoniae* invades epithelial cells and escapes lysosomes

Authors: Benjamin B.A. Raymond, Manfred Rohde, Tracey Kuit, Ina Schleicher, Cord Uphoff, G.S. Chhatwal, Lynne Turnbull, Cynthia B. Whitchurch, Matthew P. Padula, and Steven P. Djordjevic

Candidate's contribution (%): above 50 %

Journal name: Infection and Immunity

Volume/ page numbers:

Status: To be Submitted

I declare that the publication above meets the requirements to be included in the thesis.

Candidate's name: Candidate's signature: Date (dd/mm/yy):

6.1 Introduction

Bacterial invasion is a highly complex process employed by both obligate and non-professional intracellular pathogens, providing protection from host immune defences and a niche for persistent bacteria to replicate. The process of engulfing foreign material such as bacteria is referred to as endocytosis, and this term can be subdivided into phagocytosis, macropinocytosis and pinocytosis [268]. Phagocytosis is one of the most well understood endocytic mechanisms, and is employed by macrophages and dendritic cells to engulf opsonised foreign particles [268]. Macropinocytosis involves the ruffling of cell membranes resulting in its invagination and the formation of lamellipodia which engulf and seal off the internalised particles within vacuoles [269]. These vacuoles fuse with endosomes and later lysosomes for degradation. Two important forms of pinocytosis are clathrin mediated and caveolae dependent endocytosis [268]. Clathrin is a receptor-mediated form of endocytosis which involves internalisation into clathrin-coated vesicles which are pinched off into early endosomes destined for lysosomal degradation [268,270]. Caveolae dependent endocytosis involves caveolins and cholesterol on the cell membrane which lead to invagination and vesicle formation [268]. This method is frequently exploited by bacterial pathogens as it does not result in lysosomal fusion [271-273]. This pathway is thus an optimal target for non-professional intracellular pathogens as it requires less specialised mechanisms to subvert.

The genome-reduced Mycoplasmas have generally been regarded as extracellular pathogens and so the pathways that any Mycoplasma species uses to gain access to the cytoplasm have not been characterised, although a number of species have been reported to possess intracellular stages [274-278]. *M. hyopneumoniae* is a swine pathogen that binds to the ciliated epithelium that lines the respiratory tract, where it

induces cilial clumping, tangling and eventual death [1]. *M. hyopneumoniae* has not been reported to internalise within host cells although reports of the isolation of *M. hyopneumoniae* from tissue sites distal to the respiratory ciliated epithelium including liver, spleen, kidneys and bronchial lymph nodes have been noted [14-16]. It is not known how *M. hyopneumoniae* traffics to these sites. *M. hyopneumoniae* does however possess an arsenal of surface adhesins that can bind Fn and Plg [2,3,5-9,42-44]. Fn binding is crucial to the internalisation of both Gram positive and Gram negative pathogens [49,51] and these pathogens utilise Fn-binding proteins on their cell surface to bind Fn that acts as a bridging molecule to bind β integrins that cause signalling cascades that facilitate the uptake of the bacteria [49,51]. *M. hyopneumoniae* has been shown to recruit Fn to its cell surface and co-localise with Fn at the site of adherence on PK-15 monolayers [42]. Plg is a fibrinolytic component that is bound to the *M. hyopneumoniae* cell surface and converted to its active form plasmin in the presence of specific activators [7-9,145,279]. When bound to the cell surface it retains its proteolytic activity, evidenced by its ability to degrade fibrinogen [9]. Notably, plasmin levels in the BALF of swine are significantly elevated after infection with *M. hyopneumoniae* [9]. In Leptospira, plasmin activity has been associated with the degradation of cadherins [95] that comprise cellular junctions and are crucial to the ability of bacteria to transmigrate across cellular barriers [114]. It is not known if *M. hyopneumoniae* utilises Fn or Plg to disseminate to distal tissue sites. In this work, we have investigated the invasive potential of *M. hyopneumoniae* using a PK-15 cell monolayer infection model. Invasion of epithelial cells was demonstrated using IFM, SEM, and TEM. Mechanisms of invasion were also investigated by staining for lysosomal and endosomal markers by IFM and demonstrated that *M. hyopneumoniae* escapes lysosomes and resides within the cytoplasm.

6.2 Materials and Methods

6.2.1 Bacterial strains

Mycoplasma hyopneumoniae strain J was grown in modified Friis medium [182] as previously described [209].

6.2.2 Infection of PK-15 monolayers

Porcine kidney epithelial-like monolayers (PK-15) were grown to semi-confluency and split into microtitre plates containing glass coverslips (13 mm, no. 1.5 thickness; Gerhard Menzel GmbH, Braunschweig, Germany) at approximately 1 x 10^4 cells/ well and left to adhere overnight. A 48 h *M. hyopneumoniae* culture was washed twice in PBS and resuspended in 25 mM HEPES in DMEM containing 5% fetal bovine serum (infection medium) and incubated at 37°C for 2 h. *M. hyopneumoniae* cells were added to PK-15 cells so that 0.5 ml of the original 48 h *M. hyopneumoniae* culture was added to each well. *M. hyopneumoniae* cells were allowed to adhere overnight. After the different infection times samples were washed 3 × in PBS and fixed in 2% paraformaldehyde for 30 min at 4°C.

6.2.3 Immunofluorescence microscopy

Cells were blocked in 2% BSA/ PBS for 1 h at RT. Polyclonal rabbit antisera raised against the R1 and R2 regions of $P94_J$ ($F2_{P94\text{-}J}$) [41] was incubated at a dilution of 1:100 for 1 h at RT. A 1:1000 dilution of anti-rabbit Alexa Fluor® 488 (Life Technologies) was incubated for 1 h at RT. Cells were permeabilised in 0.5% (v/v) Triton X-100 in PBS for 5 min, followed by extensive washing. DAPI was then added for 30 minutes at RT. Phalloidin conjugated to Alexa Fluor® 568 was then added for 30 min at RT. For the visualisation of lysosomes, mouse LAMP1 antisera (Abcam) was incubated at a dilution of 1:200 for 1 h at RT. A 1:1000 dilution of anti-mouse CF™ 568 (Sigma-

Aldrich) was incubated for 1 h at RT. Coverslips were then mounted onto glass microscope slides in VECTASHIELD® (Vector Laboratories). Samples were imaged on a Nikon A1 CLSM. These samples were also imaged using super-resolution 3D-SIM on a V3 DeltaVision OMX 3D-SIM Imaging System (Applied Precision, GE Healthcare) as previously described [211].

6.2.4 Processing of immunofluorescence images

ND2 files generated by a Nikon A1 CLSM and those generated by the DeltaVision OMX were processed using Bitplane, Imaris Scientific 3D/4D image processing software to create Maximum Intensity Projection (MIP) and slices images.

6.2.5 Transmission electron microscopy

Samples were fixed in a fixation solution containing 5% formaldehyde and 2% glutaraldehyde in cacodylate buffer (0.1M cacodylate, 0.01 M $CaCl_2$, 0.01 M $MgCl_2$, 0.09 M sucrose, pH 6.9) and washed with cacodylate buffer. Samples were then osmificated with 1% aqueous osmium for 1 h at RT, washed and pellets of the samples were embedded in 2% water agar and cut into small cubes. Dehydration was achieved with a graded series of acetone (10%, 20%, 50%) for 30 min on ice followed by contrasting with 2% uranyl acetate in 70% acetone for overnight at 4° C and further dehydrated with 90% and 100% acetone. Samples in 100% acetone were allowed to reach RT and were infiltrated with epoxy resin according to Spurr's formular for a medium resin [280]; 1 part 100% acetone/1 part resin for overnight, 1 part 100% acetone/2 parts resin for 8 h, pure resin for overnight and several changes the following 2 days. Samples were then transferred to resin filled gelatine capsules and polymerized for 8 h at 75° C. Ultrathin sections were cut with a diamond knife, picked up with

formvar-coated copper grids (300 mesh) and counterstained with 2% aqeuous uranyl acetate and lead citrate. After air-drying samples were examined in a Zeiss transmission electron microscope TEM910 at an acceleration voltage of 80 kV. Images were recorded digitally with a Slow-Scan CCD-Camera (ProScan, 1024x1024, Scheuring, Germany) with ITEM-Software (Olympus Soft Imaging Solutions, Münster, Germany). Brightness and contrast were adjusted with Adobe Photoshop CS4.

6.2.6 Field emission scanning electron microscopy

For morphological studies, samples were fixed in 5% formaldehyde and 2% glutaraldehyde in cacodylate buffer (0.1M cacodylate, 0.01 M $CaCl_2$, 0.01 M $MgCl_2$, 0.09 M sucrose, pH 6.9) for 1 h on ice and washed with cacodylate buffer and subsequently washed with TE-buffer (20 mM TRIS, 1 mM EDTA, pH 6,9) before dehydrating in a graded series of acetone (10, 30, 50, 70, 90, 100%) on ice for 15 min for each step. Samples in the 100% acetone step were allowed to reach RT before another change in 100% acetone. Samples were then subjected to critical-point drying with liquid CO_2 (CPD 30, Bal-Tec, Liechtenstein). Dried samples were covered with a gold film by sputter coating (SCD 500, Bal-Tec, Liechtenstein) before examination in a field emission scanning electron microscope Zeiss DSM 982 Gemini using the Everhart Thornley SE detector and the inlens detector in a 50:50 ratio, at an acceleration voltage of 5 kV at calibrated magnifications.

6.3 Results

6.3.1 Scanning Electron Microscopy of *M. hyopneumoniae* cells adhering to, and invading PK-15 monolayers

The isolation of *M. hyopneumoniae* from distal tissue sites such as the liver, spleen, kidneys, and lymph nodes led us to investigate the invasive potential of this genome-reduced pathogen. The ability of *M. hyopneumoniae* cells to adhere to PK-15 monolayers has been extensively studied [4,42,215], and so we have opted to use this cell line to assess the invasive potential of *M. hyopneumoniae*. SEM was used to observe *M. hyopneumoniae* cells adhering to PK-15 monolayers after 4 h incubation. *M. hyopneumoniae* cells readily adhere to the surface of PK-15 monolayers as individual cells and small aggregated groups (Figure 6.1). A small proportion of cells could be seen interacting with areas of the PK-15 membrane that appear to be ruffled surrounding and encapsulating the *M. hyopneumoniae* cell(s) (Figure 6.1). At the site of engulfment the surface of the monolayer can be seen forming sheet-like extensions around the *M. hyopneumoniae* cells (Figure 6.1). Microvilli/filopodia can also be seen at the site of entry, likely due to the cytoskeletal rearrangement induced during the process of engulfment. The engulfment of *M. hyopneumoniae* cells is reminiscent of macropinocytosis where membrane extensions internalise foreign particles. Complete, engulfment of a *M. hyopneumoniae* cell can also be seen (Figure 6.1), suggesting that the events observed here are involved in the internalisation of *M. hyopneumoniae* cells. From these images it is not possible to examine what cellular compartments the engulfed *M. hyopneumoniae* cells localise to or if they survive intracellularly.

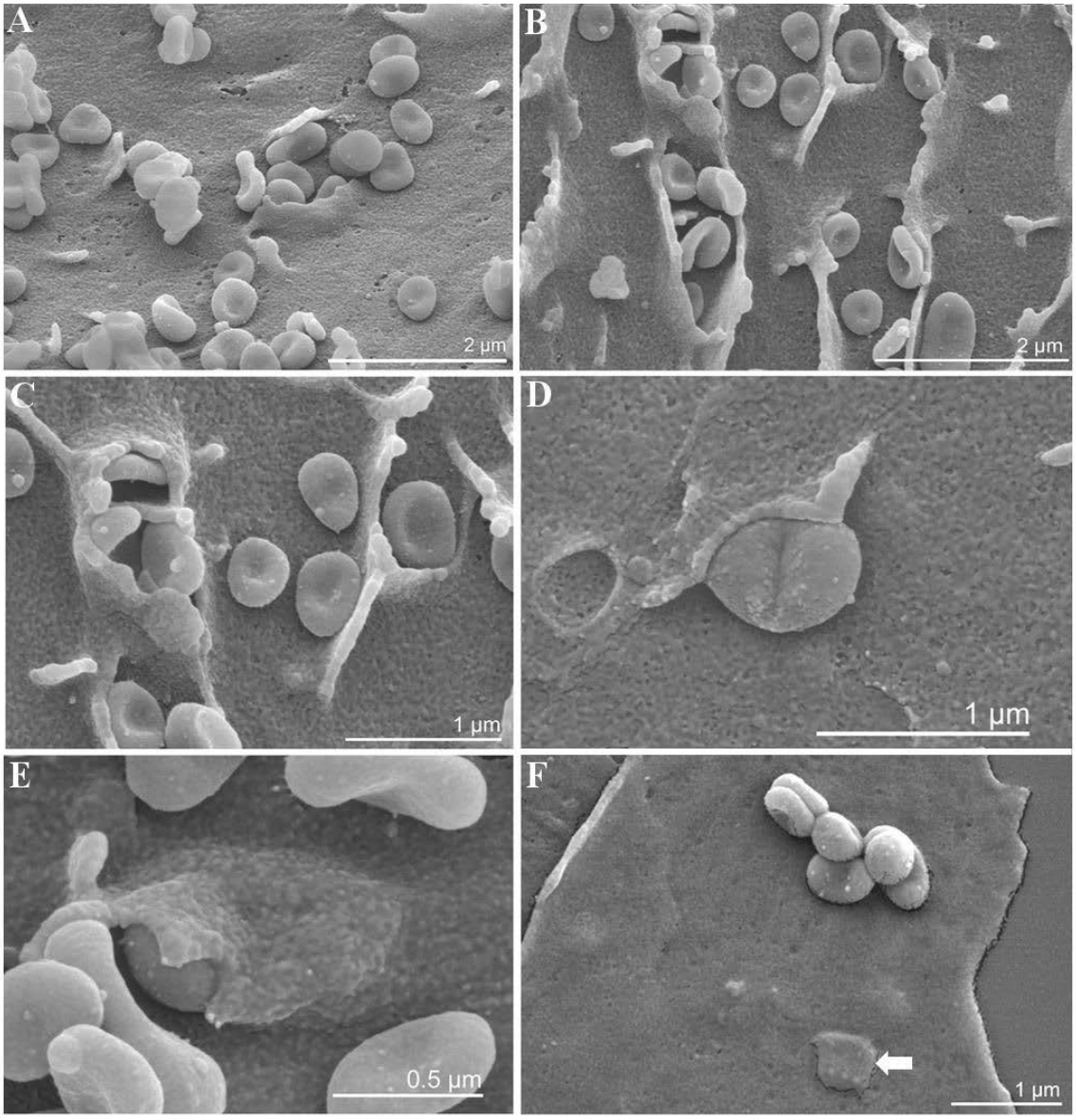

Figure 6.1: Scanning electron micrograph of *M. hyopneumoniae* cells interacting with and invading PK-15 monolayers.

A-E) *M. hyopneumoniae* cells being engulfed by PK-15 cells. Microvilli/filopodia appear to be interacting with the *M. hyopneumoniae* cells and forming sheet-like projections over the cells. F) *M. hyopneumoniae* cells adhering to the monolayer and one cell which has become completely engulfed (white arrow).

Further investigation by SEM revealed that *M. hyopneumoniae* cells appear to be associated with small invaginations in the surface of the PK-15 monolayers. These round invaginations are reminiscent of caveolae. Caveolae are membrane invaginations that are involved in endocytosis and have been shown to facilitate the internalisation of group A streptococci [273]. Here we show that the distribution of caveolae is positively correlated with the presence of adhering *M. hyopneumoniae* cells (Figure 6.2). In some areas where caveolae are highly concentrated, filopodia can be seen starting to engulf *M. hyopneumoniae* cells into the growing invagination (Figure 6.2).

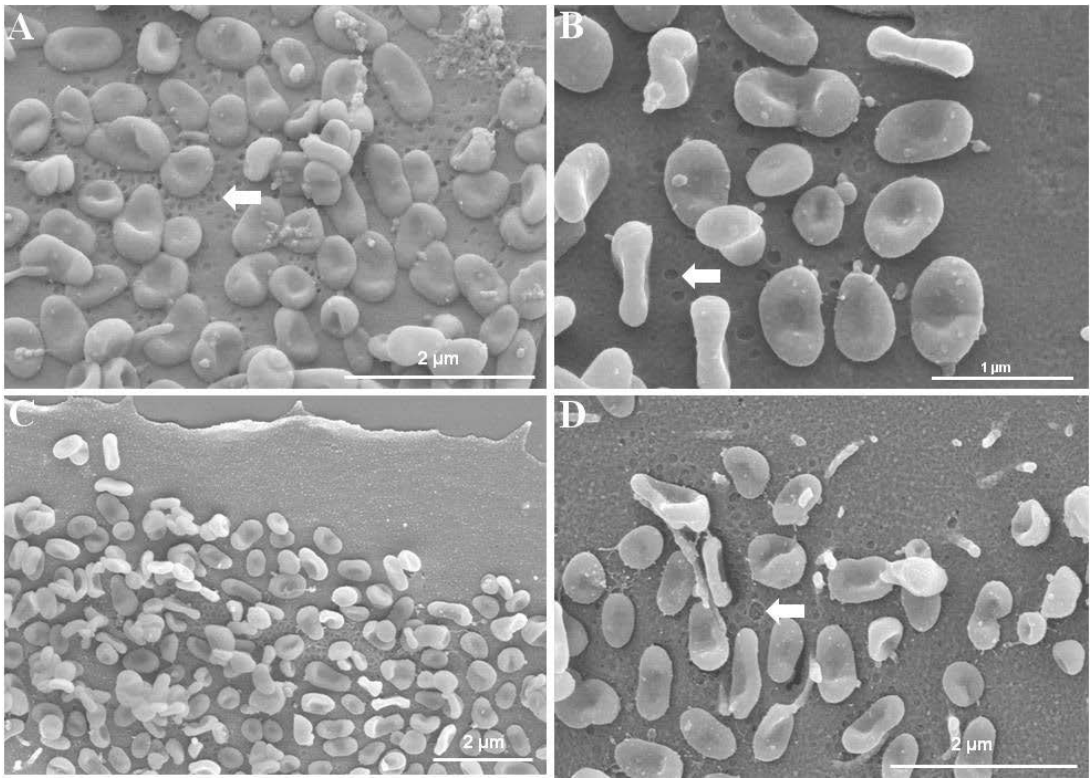

Figure 6.2: *M. hyopneumoniae* cells adhering to PK-15 monolayers with what appear to be caveolin-like structures.

The *M. hyopneumoniae* cells adhere to the PK-15 epithelial surface. In close proximity to these cells, small invaginations in the PK-15 membrane can be seen (white arrows). These structures are 50 -100 nm in size and are reminiscent of caveolae.

6.3.2 Immunofluorescence microscopy of *M. hyopneumoniae* cells adhering to and invading PK-15 monolayers

SEM is unable to visualise *M. hyopneumoniae* cells that have become fully engulfed by the PK-15 monolayers and so we sought out to use IFM to track where they traffic to. Differential fluorescent staining in combination with triton X-100 permeabilisation was used to visualise *M. hyopneumoniae* cells residing within PK-15 monolayers. Those cells appearing green-blue represent the overlay of the labelling of anti-$F2_{P97}$ with CF™ 488 pre-permeabilisation and DAPI post-permeabilisation (Figure 6.3). These cells are adhering extracellularly and are highly abundant. *M. hyopneumoniae* is unable to adhere to glass, although cells can clearly be seen adhering to the surrounding glass around the leading edge of the PK-15 monolayer. As it has been shown by SEM (Chapter V), the leading edge of PK-15 monolayer appears to deposit a fibrous like network of proteins that does not stain with phalloidin that it utilises for migration. *M. hyopneumoniae* cells adhere to this material giving the impression that they can adhere to glass. Staining of F-actin with phalloidin provided an enhanced view of the landscape in which these cells are adhering and it can be seen that the *M. hyopneumoniae* cells are adhering where the F-actin is most prominent; at the leading edge of the monolayer. Those cells which appear blue represent internalized cells that have only been stained after permeabilisation (Figure 6.3). These invasive cells were low in abundance but present in almost all fields of view. Invasive cells were singular suggesting that those cells adhering in large aggregates are non-invasive. The punctate DAPI staining suggests that these cells are free within the cytoplasm. Further studies are required to confirm this.

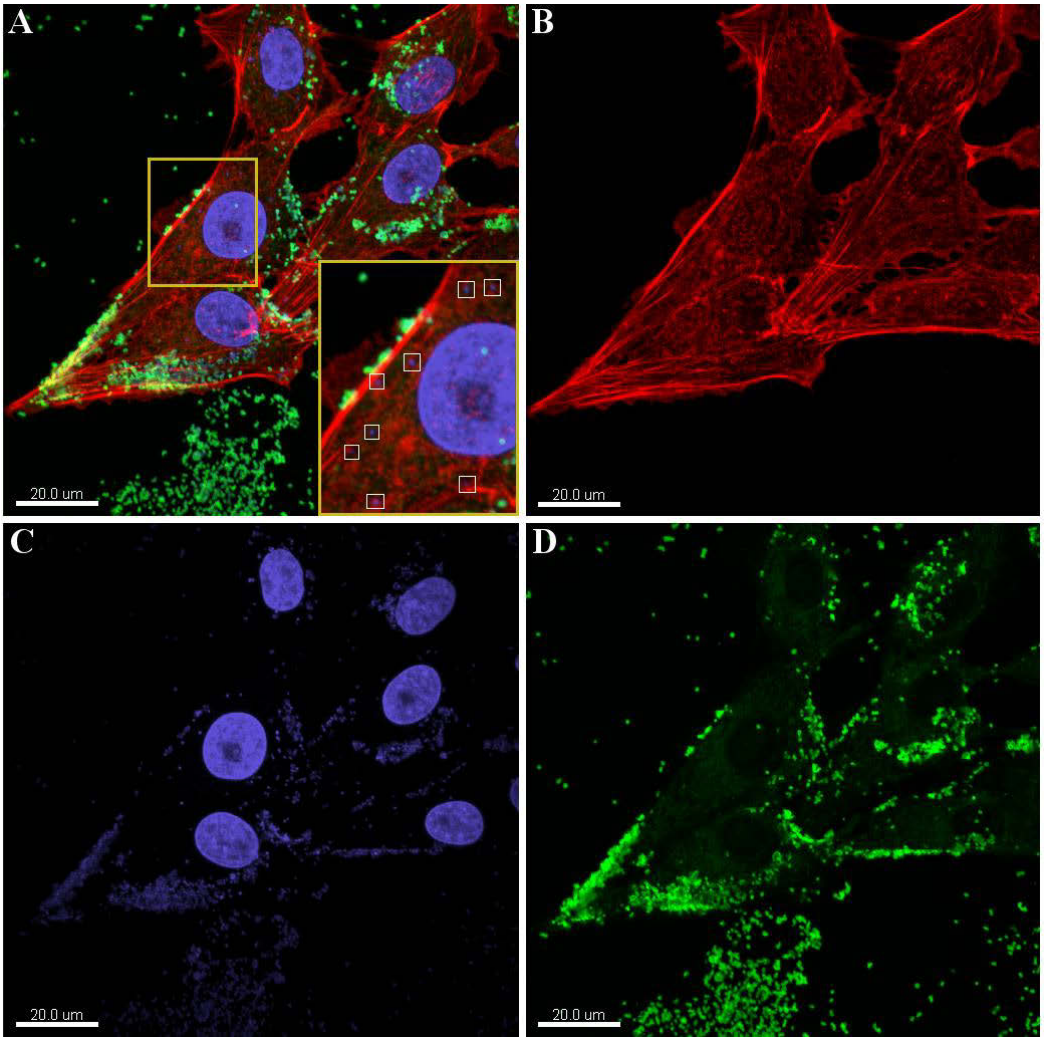

Figure 6.3: *M. hyopneumoniae* cells internalised within PK-15 cells.

M. hyopneumoniae cells were labelled with $F2_{P97}$ antisera conjugated to Alexa Fluor 488 (green). Post-permeabilisation, intracellular *M. hyopneumoniae* cells were stained with DAPI (blue). Filamentous actin of the PK-15 cells was stained using Phalloidin. A) Overlay of the three channels showing *M. hyopneumoniae* cells adhering to the edges of the monolayer as well as the surrounding area of the coverslip void of PK-15 cells. Internalised *M. hyopneumoniae* cells appear blue due to the permeabilisation process. These cells are boxed and shown in the zoomed in panel. B) Filamentous actin of the PK-15 cytoskeleton. C) Nucleic acid of the PK-15 cells (large blue nuclei) and *M. hyopneumoniae* cells. D) *M. hyopneumoniae* cells appearing as green rings, representing the surface bound P97 labelled with anti-$F2_{P97}$.

6.3.3 Transmission Electron Microscopy of *M. hyopneumoniae* invading PK-15 monolayers and porcine tracheal epithelia

In order to gain better spatial resolution of the process of internalisation, particularly the localisation of *M. hyopneumoniae* cells within the cytoplasm, we employed TEM. As was expected we could readily observe *M. hyopneumoniae* cells adhering closely to the surface of the PK-15 monolayer (Figure 6.4). Some of these cells can be seen associating with what appear to be microvilli/filopodia; similarly to what was observed by SEM. In cells that can be seen becoming engulfed by the PK-15 monolayer, these microvilli/filopodia appear to be directly involved; they are most likely associated with the membrane ruffling that was observed by SEM (Figure 6.1). The subsequent complete internalisation of intact internalised *M. hyopneumoniae* cells could be observed, and these cells appear to reside within electron-lucent vacuole-like structures (Figure 6.4). Previous electron microscopy studies have reported that vacuoles appear electron-lucent under TEM [281,282] and this observation supports our hypothesis that *M. hyopneumoniae* cells become endocytosed into autophagic vacuoles that are destined for lysosomal fusion. A number of these electron-lucent vacuoles harbour what appear to be lysed *M. hyopneumoniae* cells (Figure 6.4) suggesting that not all cells survive the process of endocytosis. Additionally, numerous apparent intact *M. hyopneumoniae* cells appear to reside free within the cytoplasm (Figure 6.4), potentially due to them escaping from the observed vacuole-like structures. Electron-lucent vacuoles can be observed in the same field of view, supporting the notion that these particular *M. hyopneumoniae* cells are not contained within these structures.

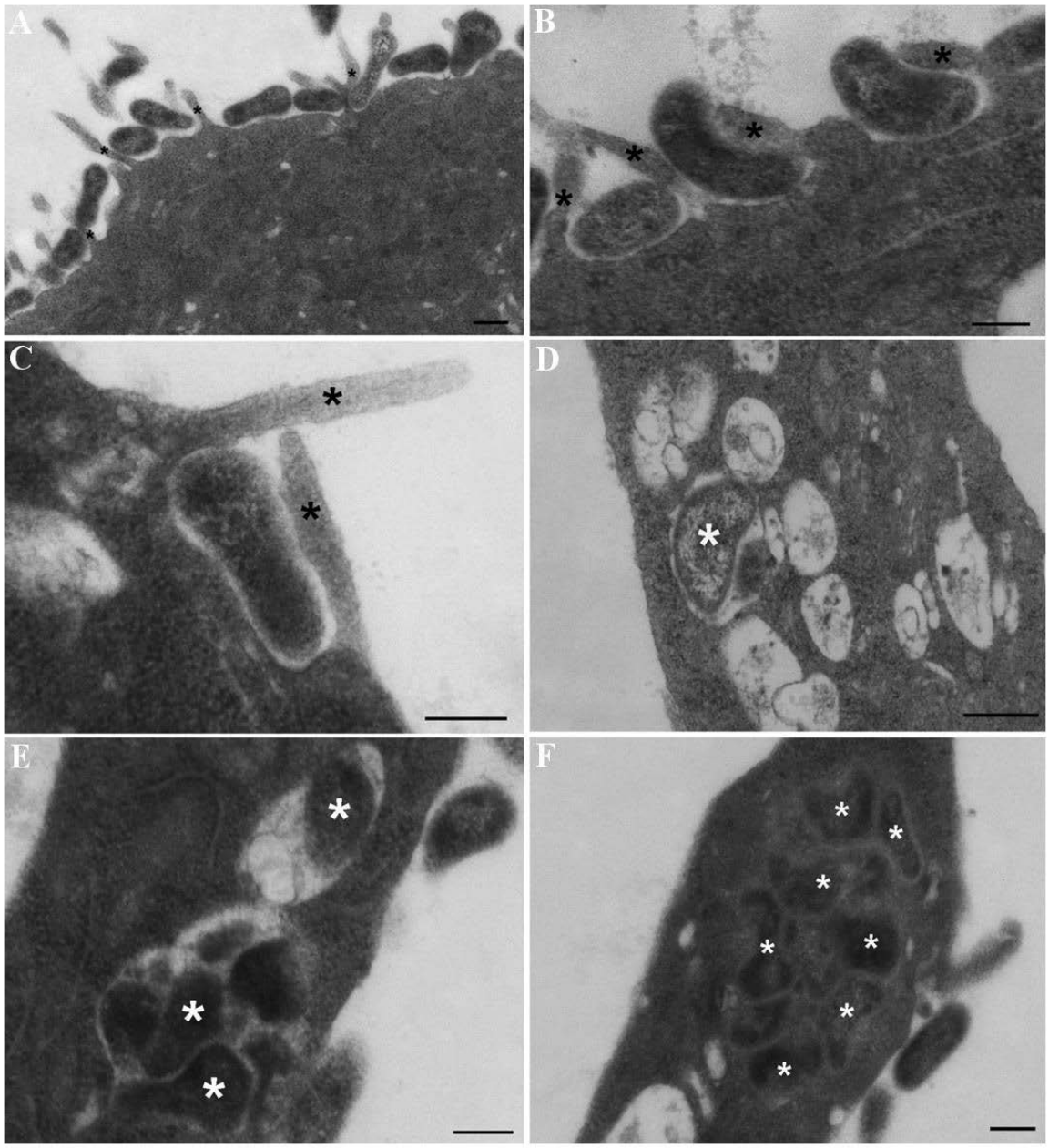

Figure 6.4: Transmission electron micrograph of *M. hyopneumoniae* cells becoming internalised by PK-15 monolayers.

A-C) Black asterisks represent microvilli/filopodia engulfing the invading *M. hyopneumoniae* cells. Abundant *M. hyopneumoniae* cells can be seen adhering to the surface of the PK-15 monolayer. D-E) White asterisks represent *M. hyopneumoniae* cells which have become internalised and appear to be residing within electron-lucent vacuole-like structures. Some of these vacuoles appear to contain remnants of lysed *M.*

hyopneumoniae cells. F) *M. hyopneumoniae* cells (white asterisks) residing within the cytoplasm of PK-15 monolayers. These cells do not appear to be contained within vacuoles and have potentially escaped to reside free within the cytoplasm. Scale bars are 200 nm (A-E) and 400 nm (F).

We have shown that *M. hyopneumoniae* binds to the surface of PK-15 monolayers, induces membrane ruffling, becomes engulfed in vacuole-like structures and appears to escape these structures (Figure 6.4). Thus, we sought to investigate whether this phenomenon occurred *in vivo*. TEM of the ciliated epithelium from the trachea of infected swine showed abundant cilia on the epithelial surface with what appear to be internalised *M. hyopneumoniae* cells residing within the cytoplasm (Figure 6.5). These electron-dense cells appear to be intact, and do not seem to be associated with any vacuole-like structures as was observed in PK-15 cells. This is however, the first instance describing the *in vivo* internalisation of *M. hyopneumoniae*.

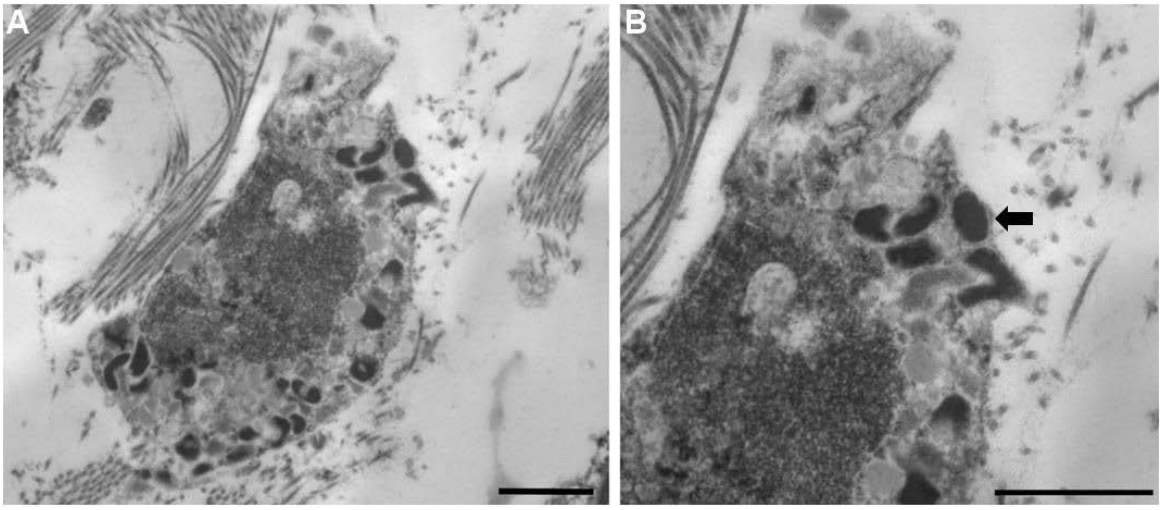

Figure 6.5: Transmission electron micrograph of tracheal sections taken from the respiratory tract of a pig infected with *M. hyopneumoniae*.

A) Arrows indicate *M. hyopneumoniae* cells which appear to have become engulfed by the respiratory epithelium (black arrow). Cilia can also be seen among the epithelium. B) A higher magnification of panel A. Scale bar is 2 μm.

6.3.4 Co-localisation LAMP1 with *M. hyopneumoniae* cells

To determine the role of the endocytic pathways in the internalisation of *M. hyopneumoniae* cells, we investigated co-localisation of *M. hyopneumoniae* cells with the lysosomal marker LAMP1. Once foreign material is taken up inside the cell within endosomes, they mature to late endosomes that fuse with lysosomes. This process delivers hydrolytic enzymes into the vacuole that degrades foreign material. *M. hyopneumoniae* cells adhering extracellularly to PK-15 cells were labelled with rabbit $F2_{P97}$ antisera while internalised cells were stained with DAPI. *M. hyopneumoniae* cells which have become internalised by the PK-15 monolayers were not labelled with the $F2_{P97}$ antisera pre-permeabilisation and appear blue.

LAMP1 labelling demonstrated the presence of abundant lysosomes within the cytoplasm of PK-15 monolayers. These lysosomes were approximately 2 μm in diameter and were only present in areas abundant in intracellular *M. hyopneumoniae* cells (Figure 6.6). A small number of internalised *M. hyopneumoniae* cells could be seen residing within the LAMP1 labelled lysosomes by CLSM (Figure 6.6). Internalised cells can also be seen in the immediate vicinity but not within, LAMP1 labelled lysosomes (Figure 6.6). These cells are abundant and appear intact, suggesting that they have escaped the lysosome. Interestingly, groups of intracellular *M. hyopneumoniae* cells can be seen in PK-15 cells completely devoid of lysosomes, suggesting that they may have become internalised via a different pathway such as caveolae-mediated endocytosis. 3D-SIM images demonstrated the presence of lysosomes in super resolution whereby intracellular *M. hyopneumoniae* cells can be seen residing within the lysosomes (Figure 6.7). It is important to note that these intracellular bacteria appear to be less than 500 nm in diameter and this is because the true size of the *M.*

hyopneumoniae cell is underrepresented when only stained for nucleic acids using DAPI as opposed to labelling the cell surface. However, small remnants of nucleic acid can be seen in some lysosomes (Figure 6.7); suggesting that some of the intracellular *M. hyopneumoniae* cells succumb to the lytic effects of the lysosome.

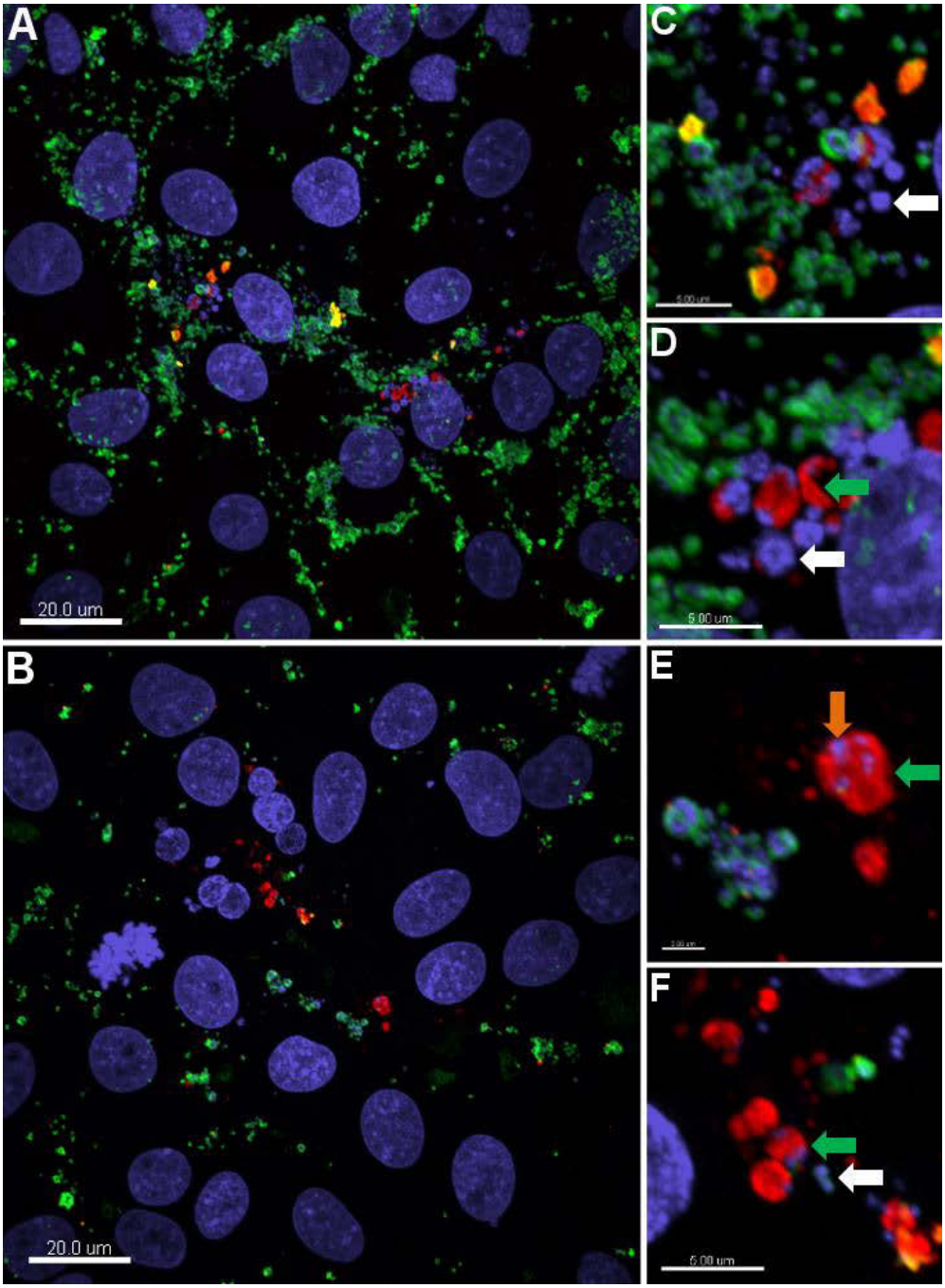

Figure 6.6: Association of intracellular *M. hyopneumoniae* cells with lysosomes.

A-B) CLSM of *M. hyopneumoniae* cells adhering to PK-15 monolayers. Lysosomes were labelled with LAMP1 antisera conjugated to CF™ 568 (red). Internalised *M. hyopneumoniae* cells were labelled with DAPI (blue) and can be seen associating with the lysosomes. Extracellularly adhering *M. hyopneumoniae* cells were labelled with $F2_{P97}$ antisera conjugated to CF™ 488 (green) and could be seen in all fields of view. C-

D, E-F) zoomed in image of panels A and B respectively. Intracellular *M. hyopneumoniae* cells can be seen residing within the lysosomes (orange arrow). A large number of intracellular *M. hyopneumoniae* cells appear to have escaped the lysosomes and are free within the cytoplasm (white arrows).

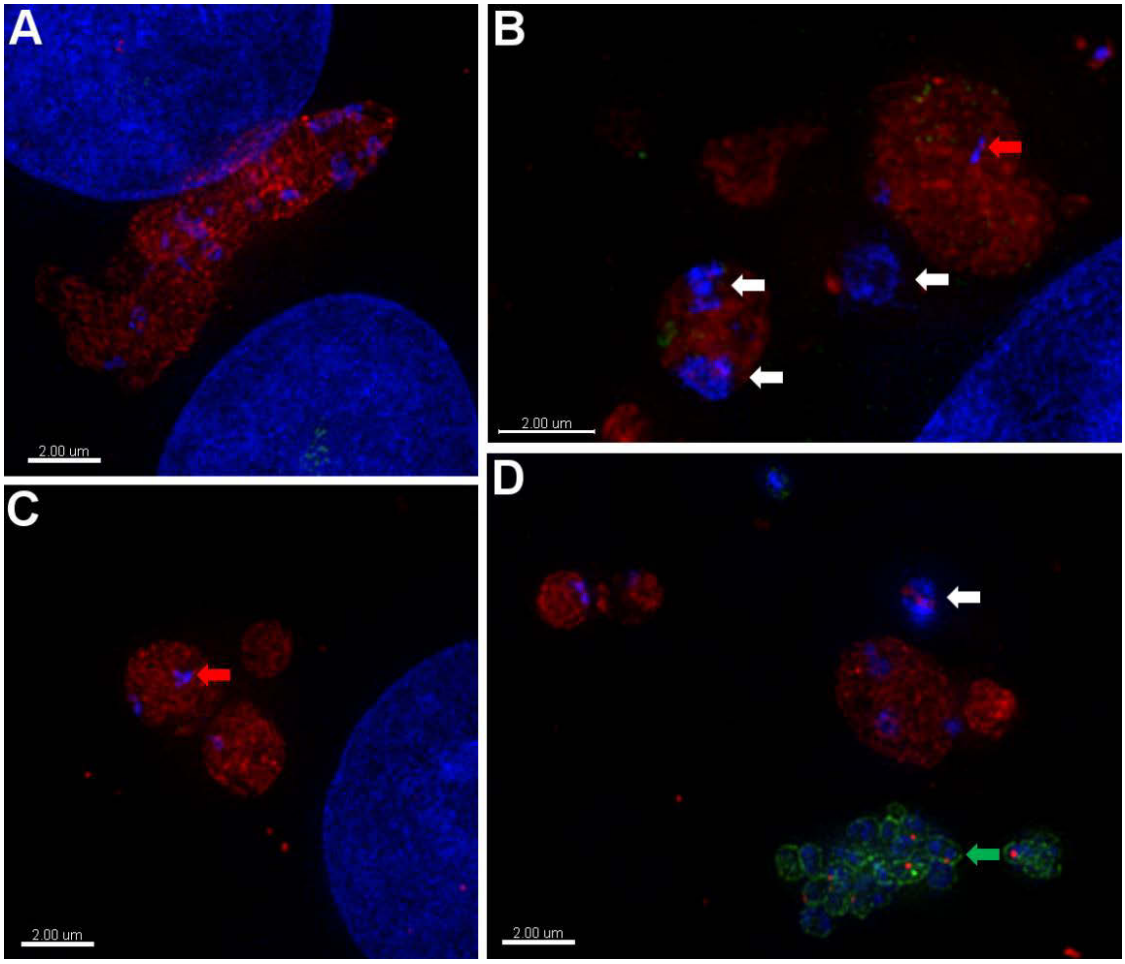

Figure 6.7: 3D-SIM images of intracellular *M. hyopneumoniae* cells associating with lysosomes.

3D-SIM images of the sample shown in Figure 6.6. Lysosomes were labelled using LAMP1 antisera conjugated to CF™ 568 and appear red. These lysosomes are approximately 2 μm in diameter. Intracellular *M. hyopneumoniae* cells were stained using DAPI and appear blue. These intracellular cells are labelled with white arrows. Remnants of cells that appear to have been lysed can also be seen (red arrows). Extracellularly adhering *M. hyopneumoniae* cells that have been labelled with $F2_{P97}$ antisera (green arrow) can also be seen.

Further examination by 3D-SIM revealed that there are areas where there seem to be lysosomal breakdown with intracellular *M. hyopneumoniae* cells existing free in the cytoplasm. In these images no intact lysosomes could be as observed; with only small remnants of the lysosomal membrane present (Figure 6.8). In these areas intracellular *M. hyopneumoniae* cells were abundant suggesting that they are replicating within the cytoplasm of the PK-15 cell. Collectively these data indicate that internalised *M. hyopneumoniae* cells become associated with lysosomes which a proportion of bacteria can escape. These events appear to trigger the breakdown of the lysosome and intracellular survival of the *M. hyopneumoniae* cells.

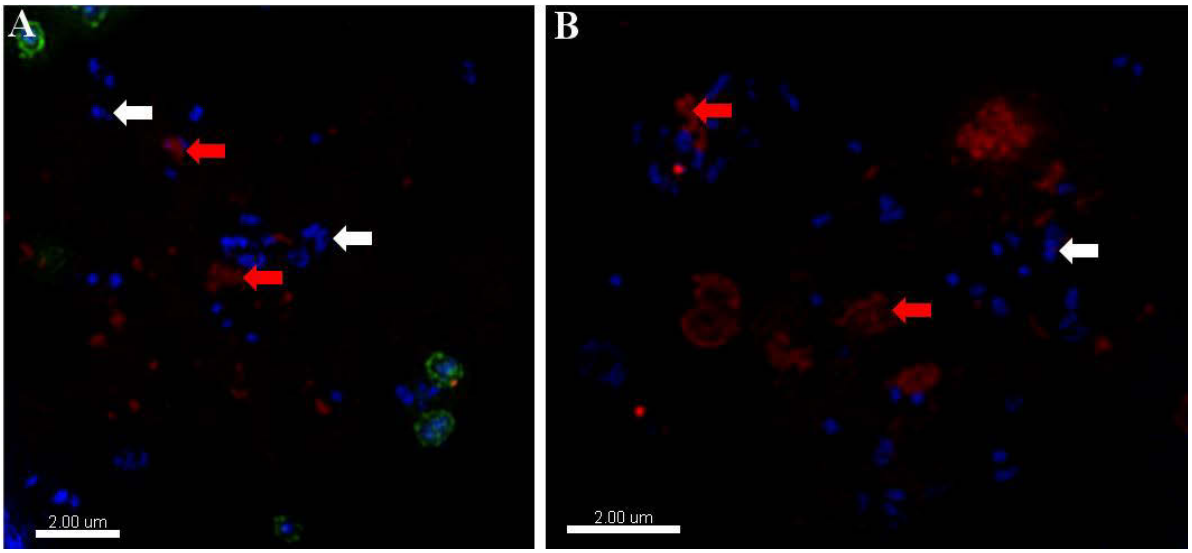

Figure 6.8: Super-resolution microscopy of intracellular *M. hyopneumoniae* cells that appear to have escaped from lysosomes.

The intracellular *M. hyopneumoniae* cells (blue) can be seen free in the cytoplasm (white arrows) in the proximity of lysosomal membrane remnants (red arrows) that have been labelled with LAMP1 antisera (red). A number of extracellular *M. hyopneumoniae* cells labelled with $F2_{P97}$ antisera can be seen (green).

6.4 Discussion

M. hyopneumoniae is a colonizer of the swine respiratory tract where it adheres to the rapidly beating cilia [17,22]. The earliest images of *M. hyopneumoniae* cells adhering to tracheal and bronchial cells show them adhering to cilia as well as the underlying epithelium denuded of cilia [17]. Upon infection, cilial loss is prevalent [1] due to a combination of microbial load, the release of metabolic products and the effects of the host immune response. While some studies have detected *M. hyopneumoniae* cells in the respiratory tract up to 16 weeks P.I. [22] porcine mycoplasmal pneumonia is usually cleared by at least 13 weeks P.I. [283]. However, experimentally infected pigs have been found to remain infectious for up to 200 days P.I. without displaying any symptoms [19]. It appears that *M. hyopneumoniae* possesses mechanisms in which it can remain dormant within pigs but is still able to gain access to the respiratory tract to be disseminated to the exterior environment. We have hypothesised that *M. hyopneumoniae* achieves this by forming biofilms (Chapter V) and internalising within host cells (presented here). These are substantial advances because they indicate that *M. hyopneumoniae* has the armoury to adopt different lifestyles which are likely to be critical to its ability to colonise pigs and form persistent and chronic infectious states. *M. hyopneumoniae* cells have been isolated from the liver, spleen, kidneys and bronchial lymph nodes >20 days P.I. [15,16], suggesting that *M. hyopneumoniae* cells have the ability to transmigrate across epithelial barriers, gain access to the bloodstream, and disseminate to distal tissue sites. *M. hyopneumoniae* binds plasmin(ogen) to its cell surface where it promotes its activation to its active form plasmin [7-9,279]. Plasmin is a serine protease that is capable of degrading a number of substrates such as ECM and junction components [84]. The acquisition of plasmin activity on the surface of bacterial pathogens has been shown to aid in transmigration and internalisation [84,172,279]. We

believe that the sequestration of plasmin(ogen) to the *M. hyopneumoniae* cell surface may aid in its ability to disseminate to distal tissue sites. Fn is another eukaryote protein that is exploited by bacterial pathogens to facilitate internalisation by host cells [49,50]. *M. hyopneumoniae* expresses a number of adhesins on its cell surface that are capable of binding and recruiting Fn to the cell surface [5,7-9,42], and *in vivo* Fn is present at the ciliary border in infected pigs where *M. hyopneumoniae* cells are adhering [42]. *M. hyopneumoniae* therefore possesses the molecular mechanisms necessary to invade host cells. Here we have investigated the internalisation of *M. hyopneumoniae* using four complementary high resolution microscopy techniques that have allowed us to visualise the uptake and cytoplasmic survival of *M. hyopneumoniae*.

Here we have demonstrated for the first time, the ability of *M. hyopneumoniae* to become engulfed by epithelial cells, localise to vacuole-like structures, and escape the lytic effects of lysozymes and persist within the cytosol. We observed that while adhering to PK-15 monolayers, *M. hyopneumoniae* cells adhere singularly and in small groups. In some areas, abundant small invaginations, reminiscent of caveolae could be seen where *M. hyopneumoniae* cells were adhering. These structures are identical to the caveolae that group A streptococci exploit to gain entry into host cells [273]. Caveolae-mediated endocytosis is a mechanism of endocytosis that does not result in lysosomal fusion and is employed by Gram positive pathogens such as *Streptococcus pyogenes* and *Streptococcus uberis* to exploit intracellular trafficking [272,284]. The process of internalisation seems to involve ruffling of the epithelial membrane with microvilli/filopodia appearing to engulf the *M. hyopneumoniae* cells into the growing invagination. These microvilli/filopodia could clearly be seen under TEM ushering the *M. hyopneumoniae* cells that are becoming engulfed across the membrane. In order for

membrane ruffling and invagination to occur, significant cytoskeletal rearrangement must be stimulated. The Gram-negative pathogens *Salmonella typhimurium* and *Campylobacter jejuni* influence signalling molecules such as Rho GTPases involved in cytoskeletal maintenance leading to a similar membrane ruffling that we have observed here in *M. hyopneumoniae* [285-287]. The *M. hyopneumoniae* cells seem to be ushered across the membrane where they localise to *M. hyopneumoniae*-containing electron-lucent vacuoles akin to macropinocytosis. In the process of internalisation, foreign particles are taken up into what are called 'autophagosomes' or autophagic vacuoles, which are destined for endosomal and lysosomal fusion. Under TEM it did appear that some of the vacuole-like structures contained cellular debris that were likely lysed *M. hyopneumoniae* cells (Figure 6.4). We observed internalised *M. hyopneumoniae* cells both localised within, and exterior to LAMP1 labelled lysosomes. These lysosomes were approximately 2 μm in diameter and were found to harbour what appeared to be intact as well as potentially lysed intracellular *M. hyopneumoniae* cells. In some areas, there appears to be lysosomal remnants with abundant intracellular *M. hyopneumoniae* cells in the surrounding environment; indicating that these cells may have escaped from lysosomes. The observation that these cells may possess the capability to escape lysosomes suggests that *M. hyopneumoniae*, like other pathogens, possesses mechanisms to survive lysosomal fusion. We also observed intracellular *M. hyopneumoniae* cells which do not appear to have associated with lysosomes, suggesting that multiple mechanisms of internalisation may be occurring; such as caveolae-mediated endocytosis. Finally, we showed that internalised *M. hyopneumoniae* cells could be observed in the ciliated tracheal epithelial taken from an *M. hyopneumoniae* infected pig. Internalisation seems to be infrequent with only a subset

of cells becoming internalised, however the presence of internalised *M. hyopneumoniae* cells *in vivo* suggests that it has the ability to survival within the cytoplasm of host cells.

6.5 Conclusion

M. hyopneumoniae has historically been regarded as an extracellular pathogen that exclusively binds to the ciliated epithelium that lines the swine respiratory tract. *M. hyopneumoniae* is responsible for causing porcine enzootic pneumonia; a chronic respiratory disease that can leave pigs infectious for up to 200 days [19]. Given that *M. hyopneumoniae* cells have been isolated from distal tissue sites >20 days P.I. [14-16], it was our hypothesis that *M. hyopneumoniae* cells become invasive as the severity of lung lesions decrease, allowing for recovery and possible re-dissemination to the respiratory tract and providing a mechanism to evade the host immune response. Here we have shown that *M. hyopneumoniae* cells become internalised by PK-15 monolayers and ciliated epithelial cells, and that they escape lysosomes to reside free within the cytoplasm. Given the difficulty that arises in trying to prevent the transmission of *M. hyopneumoniae*, this genome-reduced pathogen must possess mechanisms in which it can survive dormant within its host. Invasion is likely a pre-emptive adaptation to the changing nature of the porcine respiratory tract upon infection with *M. hyopneumoniae*. Further work will be required in order to elucidate the exact pathways that *M. hyopneumoniae* becomes internalised by and trafficked within the cell so that these can be used as potential therapeutic targets.

Chapter Seven: Final Summary and Future Directions

The overarching aim of this thesis was to investigate the interactions between the swine pathogen *M. hyopneumoniae* and its host. This has been achieved by investigating the functional domains of a number of surface adhesins (**AIMS 1 & 2)** as well as the ability of *M. hyopneumoniae* to form biofilms (**AIM 3)** and internalise within host cells (**AIM 4)**. The combined contributions of these findings have added significant amounts of knowledge to the field of Mycoplasmology and how these genome-reduced organisms evade the host immune system and cause disease in their host. As a preface to my results chapters (chapter 2), I have reviewed one of the recurring topics in veterinary Mycoplasmology; the exploitation of the fibrinolytic system. The exploitation of plasmin(ogen) by the Mycoplasma species has been shown to enhance adherence and invasion, as well as influencing the proinflammatory response. This is the first review [279] to consolidate the interaction of veterinary pathogens with plasmin(ogen) and highlights the need to investigate how veterinary pathogens such as *M. hyopneumoniae* interact with and exploit host systems.

7.1. The extent of proteolytic processing in the adhesins P159 and P97 and the cleavage sites present in these molecules

The first topic covered in this thesis was a survey of the surface proteome of *M. hyopneumoniae*; focusing on the investigation of endoproteolytic processing in a number of surface proteins. The comprehensive surface proteome of *M. hyopneumoniae* is part of a manuscript under revision (Tacchi *et al.*) for which I am second author. Modification of the cell surface protein architecture is a mechanism by which mycoplasmal pathogens such as *M. pulmonis* evade the host immune response and interact with cells [55-59]. Varying levels of endoproteolytic processing have been characterised in a number of *M. hyopneumoniae* adhesins [2,3,5-9,42-44,54]. Our lab has further shown that members of the P97 and P102 adhesin families undergo what we refer to as efficient and inefficient cleavage events; the former being more stringent than the latter [2,3,5-9,42-44]. The full length pre-proteins of these adhesins are rarely observed except for instances where we have enriched for these proteins [42-44], indicating the functional necessity of proteolytic processing. This work has shown for the first time, the ability of the P102 paralog P159 to undergo extensive endoproteolytic processing (Chapter III) [43]. Previously it was shown that P159 undergoes two dominant cleavage events; generating P27, P110 and P52 [4]. In this work, the exact cleavage sites that generate these fragments were only speculated upon [4]. Here the cleavage sites ^{233}F↓Q^{234} and ^{981}F↓Q^{982} that generate these fragments were identified, as well as the less-efficient cleavage site ^{738}L-K-V↓G-A-A^{743} that generates P76 and P35 [43]. In addition to identifying these cleavage motifs, it was observed that P159 is further processed in a manner reminiscent of ectodomain shedding in eukaryotes [43]. 23 additional minor cleavage fragments were identified that ranged in size from ~15 – 100 kDa [43]. These fragments were initially detected by 2D-immunoblotting studies of

proteins resolved in the 4 – 7 and 6 – 11 pI ranges (Figure 3.3) [4]. The majority of these fragments were low abundance fragments and were only identified from methodologies that enriched for these proteins such as avidin purification of biotinylated proteins, heparin-agarose chromatography and PK-15-agarose chromatography [43]. This work presented semi-tryptic peptides from shotgun proteomic data of surface enriched proteins that were used to identify novel cleavage sites [43]. These events produce small fragments that are predicted to play roles in binding host ECM components as well as acting as decoy molecules against host defences.

Following from this, this work sought out to investigate more deeply the P97 cilium adhesin; the first *M. hyopneumoniae* adhesin characterised [154]. P97 consists of a repeat region (R1) that binds to swine cilia and a second repeat region (R2) whose function is unknown [206]. Subsequent studies demonstrated that the R1 and R2 regions are both required for heparin binding [41]. In addition to showing that multiple regions of P97 bind heparin, it was demonstrated, for the first time, in chapter 4 that a recombinant protein ($F4_{P94\text{-}J}$) that mimics the C-terminal cleavage product P28 binds heparin [42]. This fragment lacks the R1 region and was previously reported to not bind heparin [41]. Notable, the original $F4_{P94\text{-}J/\Delta 23}$ construct was engineered without the last 23 amino acid residues from the P97 sequence [41]. Here it was demonstrated that these amino acids were crucial to not only bind heparin but also Fn [42]. Bioinformatic analysis using ScanProsite revealed that a putative heparin-binding motif was present within amino acid residues 1064 – 1077 [42], whereas the original $F4_{P94\text{-}J/\Delta 23}$ construct ends at amino acid 1070. The thermophoresis binding data presented in chapter 4 confirmed that the predicted heparin binding motif is a true heparin binding domain that

allows *M. hyopneumoniae* to bind heparin with nanomolar affinity [42]. This was confirmed by testing the ability of overlapping peptides to bind heparin which suggested that a Lys-Lys-Ser region was responsible for binding heparin [42]. Using this same strategy of overlapping peptides, this region was found to also be responsible for Fn but not Plg binding [42].

7.2. The interaction of *M. hyopneumoniae* with host molecules such as Fn and actin and the cellular responses the interaction elicits in its host

Many *M. hyopneumoniae* adhesins have been reported to bind Fn [5,7-9,42], however the biological significance of this phenomena has not been investigated. Chapter 4 reports the investigation of the interaction of *M. hyopneumoniae* and Fn in the context of Mycoplasma cells adhering to PK-15 monolayers [42]. It was shown that *M. hyopneumoniae* not only co-localises with Fn at the site of adherence but that these cells recruit Fn onto their cell surface (Figure 4.8) [42]. Examination of lung tissue from *M. hyopneumoniae*-infected and uninfected pigs showed that Fn was present at the ciliary border where *M. hyopneumoniae* cells were adhering (Figure 4.9) [42]. No Fn was observed on the ciliary border of uninfected pigs and indicates that *M. hyopneumoniae* induces Fn release; likely by damage to the airway epithelium [42]. The Fn-binding protein FlpA from *C. jejuni* has been shown to increase adherence to intestinal epithelial cells [48] and although this has not been investigated in *M. hyopneumoniae*, it is likely that Fn plays a role in its ability to adhere to host cells. Further work will be required to investigate how *M. hyopneumoniae* exploits Fn. The availability of a transposon mutant library [161] will allow for the screening of mutants that are unable to bind Fn and observe what effect this has on the virulence of these mutants.

Aside from Fn, Plg and glycosaminoglycans [2-9,32,42-44], no other host receptor molecules for *M. hyopneumoniae* have been identified. Given the plethora of knowledge we have gained from understanding its interactions with Plg and Fn (presented in chapter 4), it is not unreasonable to assume that the discovery of novel interacting partners will drastically change the way in which we approach *M. hyopneumoniae* driven research. In order to non-biasedly investigate additional receptors that *M. hyopneumoniae* targets an affinity chromatography method was devised to purify these proteins. From this methodology a number of novel receptors that *M. hyopneumoniae* has the ability to bind were identified. Notably, a number of proteins that are associated with the cytoskeleton, specifically cytoplasmic actin were identified. This was remarkable considering that actin is not thought to be surface exposed. Actin was consistently identified from the examination of PK-15 surface proteins by biotinylation; suggesting that *M. hyopneumoniae* may be targeting the surface exposed actin. This was the first study to demonstrate actin on the surface of epithelial cells. Infection experiments with *M. hyopneumoniae* demonstrated that cells adhered along cellular junctions where F-actin was most prominent (Figure 5.10). Affinity chromatography using actin as the bait molecule captured over 100 *M. hyopneumoniae* proteins (Table 5.3). In order to validate these findings this work focused on the P97 adhesin which was identified in high abundance from these pulldowns. It was found that recombinant fragments representing the N-terminus and R1 region of P97 bound actin with nanomolar and micromolar affinity respectively (Figure S5.3). Thus it appears that *M. hyopneumoniae* binds to actin exposed on the surface of PK-15 monolayers. Further work will be required to examine the importance of this interaction. I hypothesise that the action of actin and Fn are involved in the internalisation of *M. hyopneumoniae* as it

has been previously shown that bacterial pathogens exploit both these molecules for their uptake into host cells [49,50].

7.3. The ability of *M. hyopneumoniae* to form biofilms on abiotic and host cells

In chapter 5 it was demonstrated that *M. hyopneumoniae* has the ability to form biofilms *in vitro*, on host cells, as well as *in vivo*. Biofilm formation has long been postulated in *M. hyopneumoniae* however there has been no previous example of its ability to do so. Biofilm formation was promoted on abiotic surfaces by prolonging growth with medium refreshment. Biofilm formation occurred after approximately 12 days suggesting that there is a conditioning phase whereby non-adherent cells are continuously washed away and host components are sequestered from the medium and into the growing biofilm by adherent cells. Further investigation demonstrated that eDNA is present in these biofilms, particularly at the base of the biofilms (Figure 5.4), suggesting that eDNA forms the foundation of these biofilms. The effect of DNase will need to be assessed in order to investigate the role of eDNA in biofilm formation. Live/dead staining demonstrated that the bulk of the biofilms consist of live cells with dead cells distributed amongst them (Figure 5.4). Biofilm formation was significantly more rapid when *M. hyopneumoniae* cells were incubated with PK-15 monolayers (Figure 5.6). Biofilms formed in half the amount of time than on abiotic surfaces and reinforced the notion that *M. hyopneumoniae* requires host derived molecules for growth and proliferation. Investigation of tracheal sections from *M. hyopneumoniae*-infected pigs showed that large biofilms were present on the denuded epithelium (Figure 5.8). This is the first evidence demonstrating biofilms forming on the epithelial surface of the swine respiratory tract.

A *M. hyopneumoniae* transposon mutant library was screened using a 96-well plate assay in order to identify biofilm-associated genes. It was found that mutations in three genes denoted MhpX, MhpY and MhpZ caused significant disruptions to the ability of *M. hyopneumoniae* to form biofilms when compared with the wild-type (WT) strain (Figure 5.11). The proteins that are encoded by these genes do not share homology to any previously characterised proteins and are therefore of interest to us. MhpX was identified in our actin pulldowns which suggests that it may play a role as an adhesin. This is the first ever study to link phenotype to genotype in regards to biofilm formation in a Mycoplasma species and is thus ground-breaking in this aspect. Future work stemming from this project will focus on the complementation of those genes that have been identified as putative biofilm-associated genes in the hopes that they restore the biofilm phenotype. Pig trials will also be performed to observe whether or not these biofilm-deficient mutants are able to cause chronic disease.

7.4 Internalisation and cytoplasmic life of *M. hyopneumoniae*

Historically, the scientific literature has treated *M. hyopneumoniae* as an extracellular pathogen and thus no work has been performed to target potential virulence factors that may play a role in intracellular survival. Numerous studies have isolated viable *M. hyopneumoniae* cells from distal tissue sites such as the liver, spleen, kidneys and lymph nodes [14-16]. This would suggest that *M. hyopneumoniae* has the capacity to cross the epithelial lining of the swine respiratory tract and disseminate to these distal tissue sites. Chapter 6 showed by three different microscopy techniques that *M. hyopneumoniae* internalises within PK-15 monolayers and localises to vacuole-like structures. 3D-SIM demonstrated that not only do internalised *M. hyopneumoniae* cells associate with lysosomes (Figure 6.7) but they seem to escape from these lytic vesicles

and reside free within the cytoplasm (Figure 6.8). Cells residing within vacuole-like structures could be observed in tracheal sections from *M. hyopneumoniae*-infected pigs (Figure 6.5); suggesting that *M. hyopneumoniae* cells are internalised *in vivo*. As was described in Chapter II, *M. hyopneumoniae* binds Plg to its cell surface and promotes its activation to the serine protease plasmin. This plasmin is capable of degrading a number of ECM and junction components and has been shown in other bacterial pathogens to aid in transmigration and internalisation [84,114]. Future work will be required to investigate whether or not the host-derived plasmin plays a role in invasion. Further work will also be needed to examine the mechanisms by which *M. hyopneumoniae* becomes endocytosed, escapes lysosomes, and resides within the cytoplasm. Further to this point, the ability to replicate within the cytoplasm and undergo exocytosis back into the extracellular environment needs to be investigated.

7.5 Concluding remarks

This thesis has sought to address a number of issues concerning the swine pathogen *M. hyopneumoniae* and the ways in which it colonises the swine respiratory tract and causes disease. *M. hyopneumoniae* is responsible for significant economic losses to the livestock industry mainly due to its ability to elicit chronic respiratory disease. There are currently no efficacious vaccines that prevent the transmission of *M. hyopneumoniae* and so novel vaccine targets are required. The work presented in this thesis has investigated a number of previously uncharacterised lifestyles of *M. hyopneumoniae* as well as the proteins that may be involved. It has been shown that proteins expressed by *M. hyopneumoniae* not only bind host components and elicit host responses but they play a role in biofilm formation.

The examination of the surface proteome of *M. hyopneumoniae* demonstrated that the adhesins P97 and P159 undergo extensive endoproteolytic processing events in a process referred to as ectodomain shedding; a process by which diverse cleavage fragments are secreted into the extracellular milieu as immune decoy molecules. I have demonstrated for the first time that *M. hyopneumoniae* forms biofilms (chapter 5) and internalises freely within cells (chapter 6) of the swine respiratory tract *in vivo*. These two bacterial lifestyles are used by pathogens to evade the immune response and protect it from the lytic effects of antimicrobial compounds. Prior to this work, *M. hyopneumoniae* was thought of as a strict extracellular pathogen that bound only to the respiratory cilia [17,22,202]. Extending from the results and insights generated in this work, future work can aim to target the genes involved in these processes in the hopes of developing vaccines that prevent the transmission and progression of the chronic disease caused by *M. hyopneumoniae*. The topics presented in this thesis have greatly

expanded our understanding of the host-pathogen interactions involved in the pathogenesis of *M. hyopneumoniae*.

Appendix

Chapter 3 (Paper II)

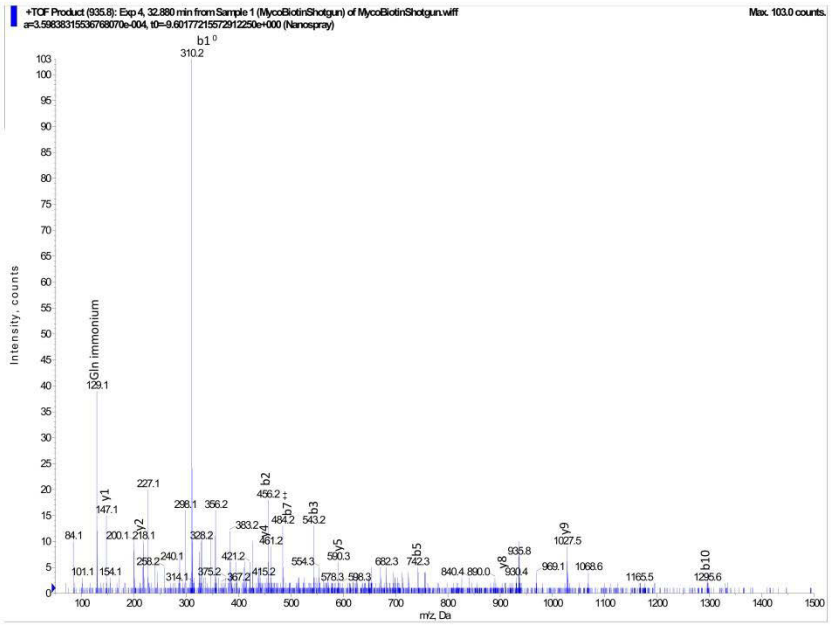

Figure S3.1a: Annotated LC-MS/MS spectrum of the P159 semi-tryptic peptide ^{741}GAAAANSIFSSEIR^{755}

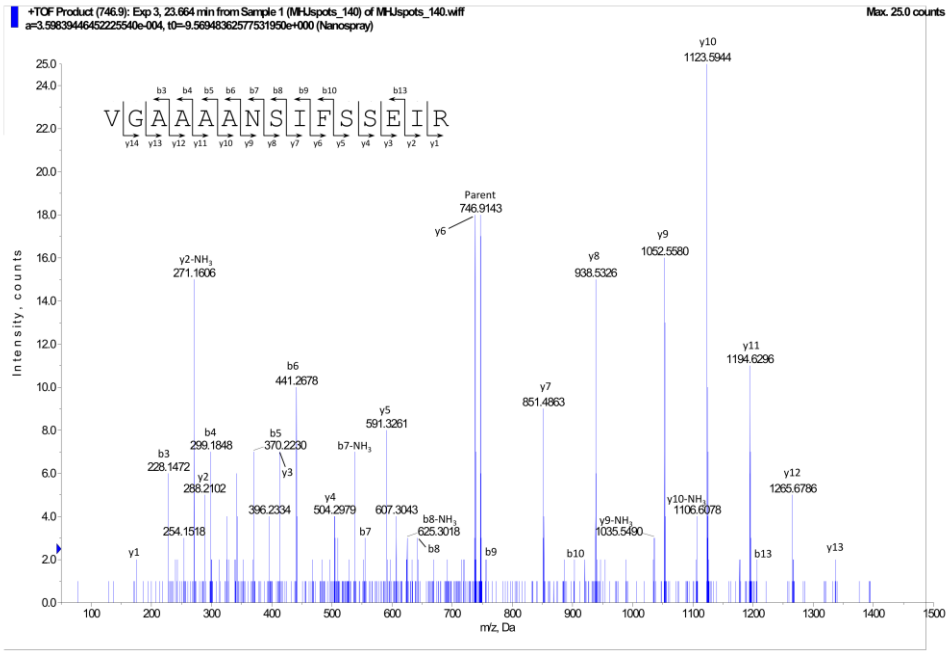

Figure S3.1b: Annotated LC-MS/MS spectrum of the P159 tryptic peptide ^{740}VGAAAANSIFSSEIR^{755}

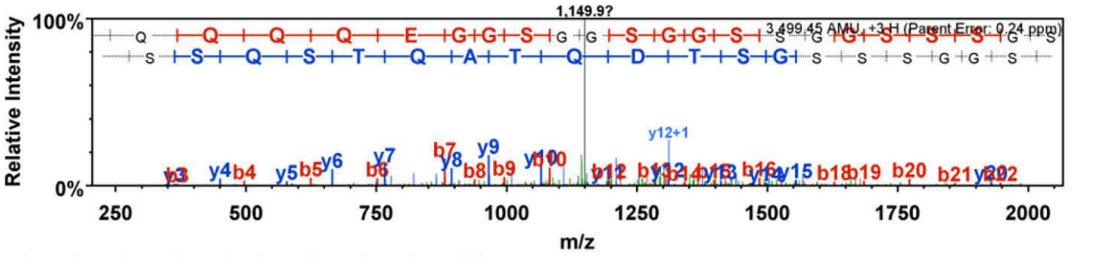

B	B Ions	B+2H	B-NH3	B-H2O	AA	Y Ions	Y+2H	Y-NH3	Y-H2O	Y
1	112.0		95.0		Q-17	3,500.5	1,750.7	3,483.4	3,482.4	37
2	240.1		223.1		Q	3,389.4	1,695.2	3,372.4	3,371.4	36
3	368.2		351.1		Q	3,261.4	1,631.2	3,244.3	3,243.4	35
4	496.2		479.2		Q	3,133.3	1,567.2	3,116.3	3,115.3	34
5	624.3		607.2		Q	3,005.2	1,503.1	2,988.2	2,987.2	33
6	752.3	376.7	735.3		Q	2,877.2	1,439.1	2,860.2	2,859.2	32
7	881.4	441.2	864.3	863.4	E	2,749.1	1,375.1	2,732.1	2,731.1	31
8	938.4	469.7	921.4	920.4	G	2,620.1	1,310.5	2,603.1	2,602.1	30
9	995.4	498.2	978.4	977.4	G	2,563.1	1,282.0	2,546.0	2,545.1	29
10	1,082.4	541.7	1,065.4	1,064.4	S	2,506.0	1,253.5	2,489.0	2,488.0	28
11	1,139.5	570.2	1,122.4	1,121.5	G	2,419.0	1,210.0	2,402.0	2,401.0	27
12	1,196.5	598.8	1,179.5	1,178.5	G	2,362.0	1,181.5	2,345.0	2,344.0	26
13	1,283.5	642.3	1,266.5	1,265.5	S	2,305.0	1,153.0	2,287.9	2,287.0	25
14	1,340.5	670.8	1,323.5	1,322.5	G	2,217.9	1,109.5	2,200.9	2,199.9	24
15	1,397.6	699.3	1,380.5	1,379.6	G	2,160.9	1,081.0	2,143.9	2,142.9	23
16	1,484.6	742.8	1,467.6	1,466.6	S	2,103.9	1,052.4	2,086.9	2,085.9	22
17	1,571.6	786.3	1,554.6	1,553.6	S	2,016.9	1,008.9	1,999.8	1,998.8	21
18	1,628.7	814.8	1,611.6	1,610.6	G	1,929.8	965.4	1,912.8	1,911.8	20
19	1,685.7	843.3	1,668.6	1,667.7	G	1,872.8	936.9	1,855.8	1,854.8	19
20	1,772.7	886.9	1,755.7	1,754.7	S	1,815.8	908.4	1,798.8	1,797.8	18
21	1,859.7	930.4	1,842.7	1,841.7	S	1,728.8	864.9	1,711.7	1,710.7	17
22	1,946.8	973.9	1,929.7	1,928.8	S	1,641.7	821.4	1,624.7	1,623.7	16
23	2,003.8	1,002.4	1,986.8	1,985.8	G	1,554.7	777.8	1,537.7	1,536.7	15
24	2,090.8	1,045.9	2,073.8	2,072.8	S	1,497.7	749.3	1,480.6	1,479.7	14
25	2,191.9	1,096.4	2,174.8	2,173.9	T	1,410.6	705.8	1,393.6	1,392.6	13
26	2,306.9	1,154.0	2,289.9	2,288.9	D	1,309.6	655.3	1,292.6	1,291.6	12
27	2,435.0	1,218.0	2,417.9	2,416.9	Q	1,194.6	597.8	1,177.5	1,176.5	11
28	2,536.0	1,268.5	2,519.0	2,518.0	T	1,066.5	533.8	1,049.5	1,048.5	10
29	2,607.0	1,304.0	2,590.0	2,589.0	A	965.5	483.2	948.4	947.4	9
30	2,735.1	1,368.1	2,718.1	2,717.1	Q	894.4	447.7	877.4	876.4	8
31	2,836.1	1,418.6	2,819.1	2,818.1	T	766.4	383.7	749.3	748.3	7
32	2,923.2	1,462.1	2,906.2	2,905.2	S	665.3	333.2	648.3	647.3	6
33	3,051.2	1,526.1	3,034.2	3,033.2	Q	578.3		561.3	560.3	5
34	3,138.3	1,569.6	3,121.2	3,120.3	S	450.2		433.2	432.2	4
35	3,225.3	1,613.2	3,208.3	3,207.3	S	363.2		346.2	345.2	3
36	3,354.3	1,677.7	3,337.3	3,336.3	E	276.2		259.1	258.1	2
37	3,500.5	1,750.7	3,483.4	3,482.4	K	147.1		130.1		1

Figure S3.1c: Annotated LC-MS/MS spectrum of the P159 semi-tryptic peptide ^{234}QQQQQEGG/24/SSEK^{270}. Zoomed view above.

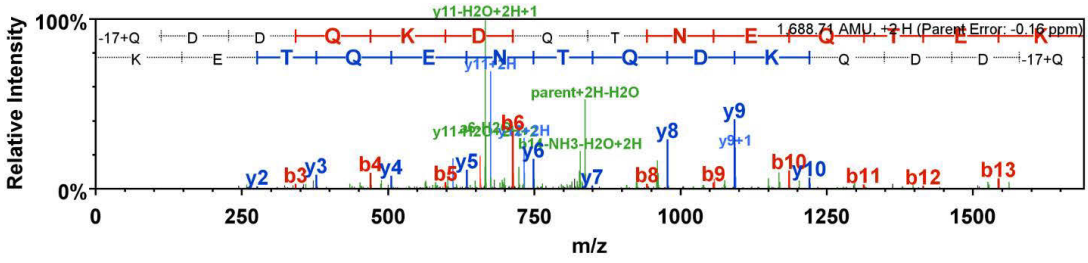

B	B Ions	B+2H	B-NH3	B-H2O	AA	Y Ions	Y+2H	Y-NH3	Y-H2O	Y
1	112.0		95.0		Q-17	1,689.7	845.4	1,672.7	1,671.7	14
2	227.1		210.0	209.1	D	1,578.7	789.8	1,561.7	1,560.7	13
3	342.1		325.1	324.1	D	1,463.7	732.3	1,446.6	1,445.7	12
4	470.2		453.1	452.1	Q	1,348.6	674.8	1,331.6	1,330.6	11
5	598.2	299.6	581.2	580.2	K	1,220.6	610.8	1,203.5	1,202.6	10
6	713.3	357.1	696.2	695.3	D	1,092.5	546.7	1,075.5	1,074.5	9
7	841.3	421.2	824.3	823.3	Q	977.5	489.2	960.4	959.4	8
8	942.4	471.7	925.4	924.4	T	849.4	425.2	832.4	831.4	7
9	1,056.4	528.7	1,039.4	1,038.4	N	748.3	374.7	731.3	730.3	6
10	1,185.5	593.2	1,168.4	1,167.5	E	634.3		617.3	616.3	5
11	1,313.5	657.3	1,296.5	1,295.5	Q	505.3		488.2	487.3	4
12	1,414.6	707.8	1,397.5	1,396.6	T	377.2		360.2	359.2	3
13	1,543.6	772.3	1,526.6	1,525.6	E	276.2		259.1	258.1	2
14	1,689.7	845.4	1,672.7	1,671.7	K	147.1		130.1		1

Figure S3.1d: Annotated LC-MS/MS spectrum of the P159 semi-tryptic peptide ^{982}QDDQKDQTNEQTEK^{995}

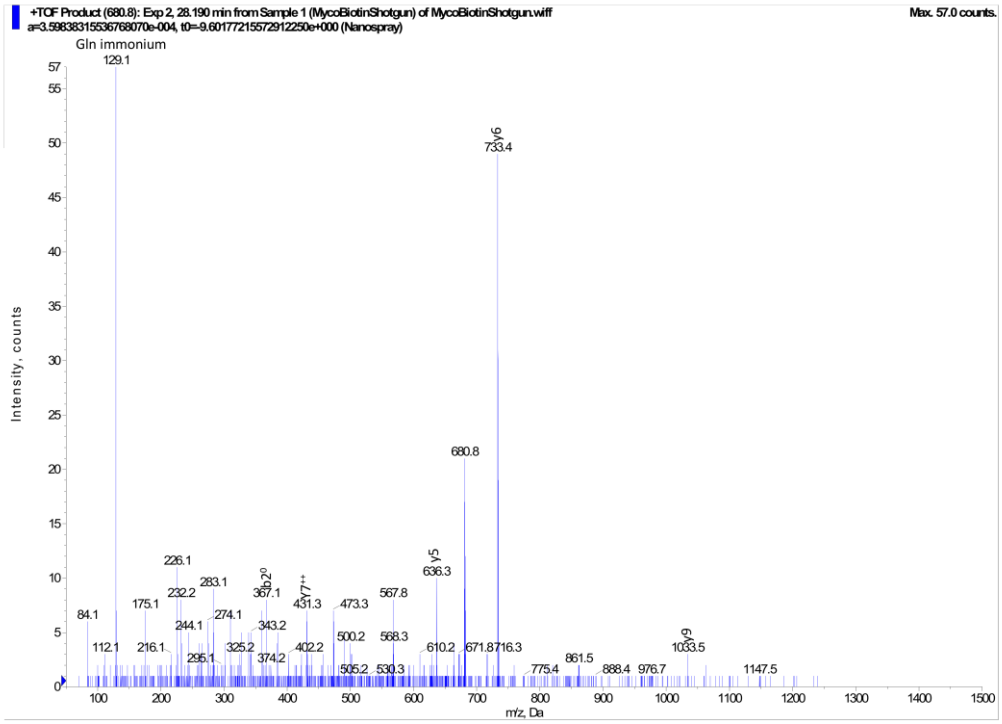

Figure S3.2a: Annotation of MS/MS spectra for the P159 semi-tryptic peptide TGDKPYLQGR.

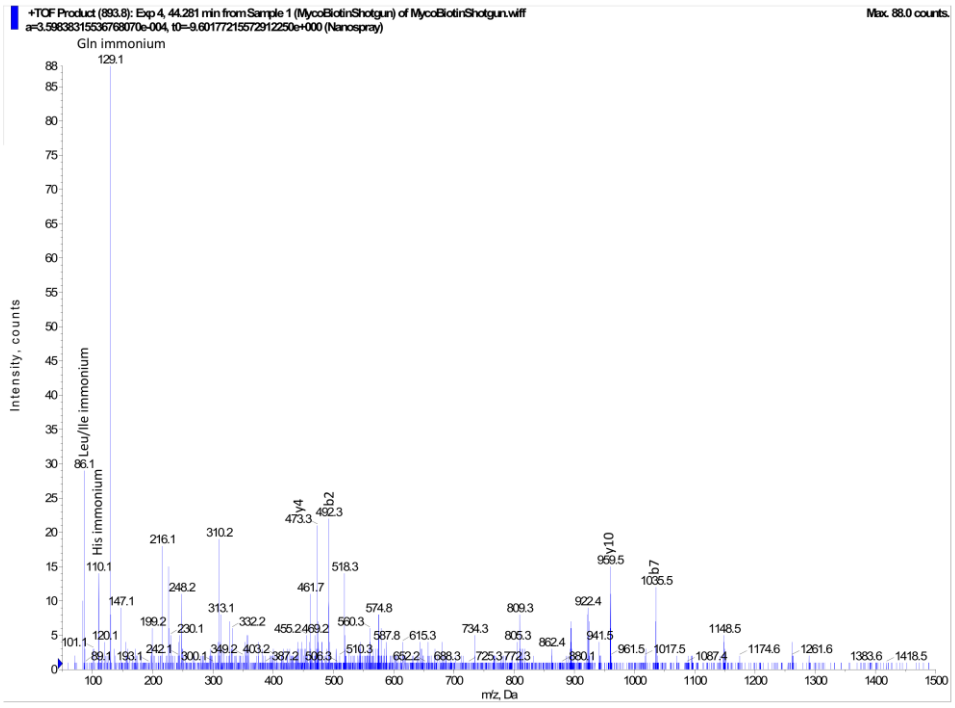

Figure S3.2b: Annotation of MS/MS spectra for the P159 semi-tryptic peptide HKSTEIILLEDSKPGASSSPQTK.

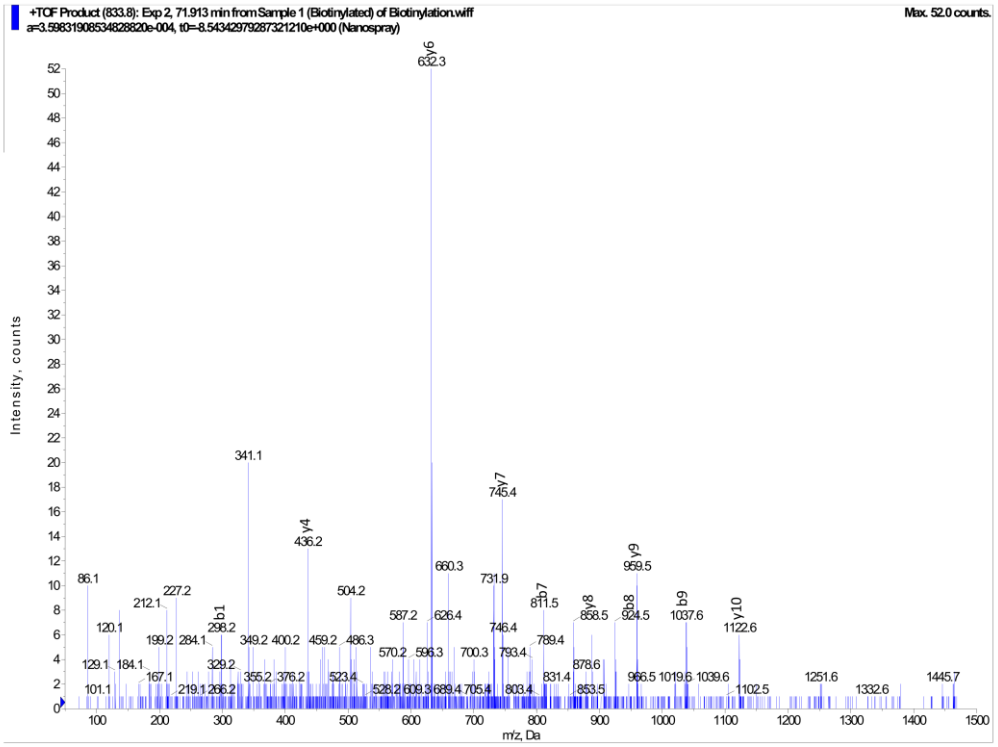

Figure S3.2c: Annotation of MS/MS spectra for the P159 semi-tryptic peptide AASGLQGLLPNEYTLLPVSSDK.

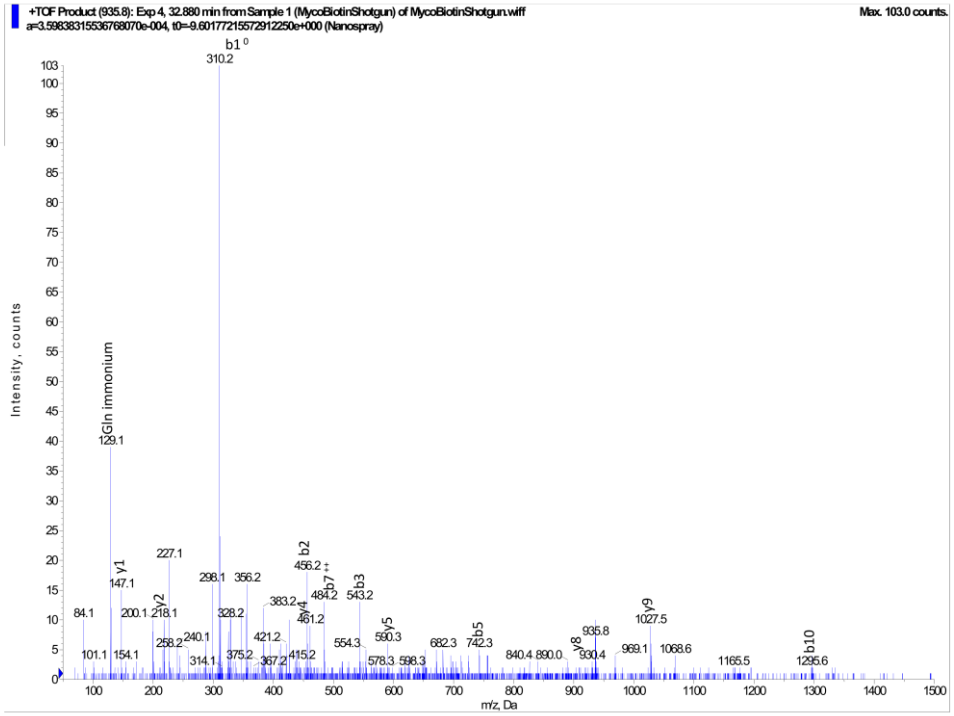

Figure S3.2d: Annotation of MS/MS spectra for the P159 semi-tryptic peptide TKSQAKPEAKPEEKPINLEDQAK.

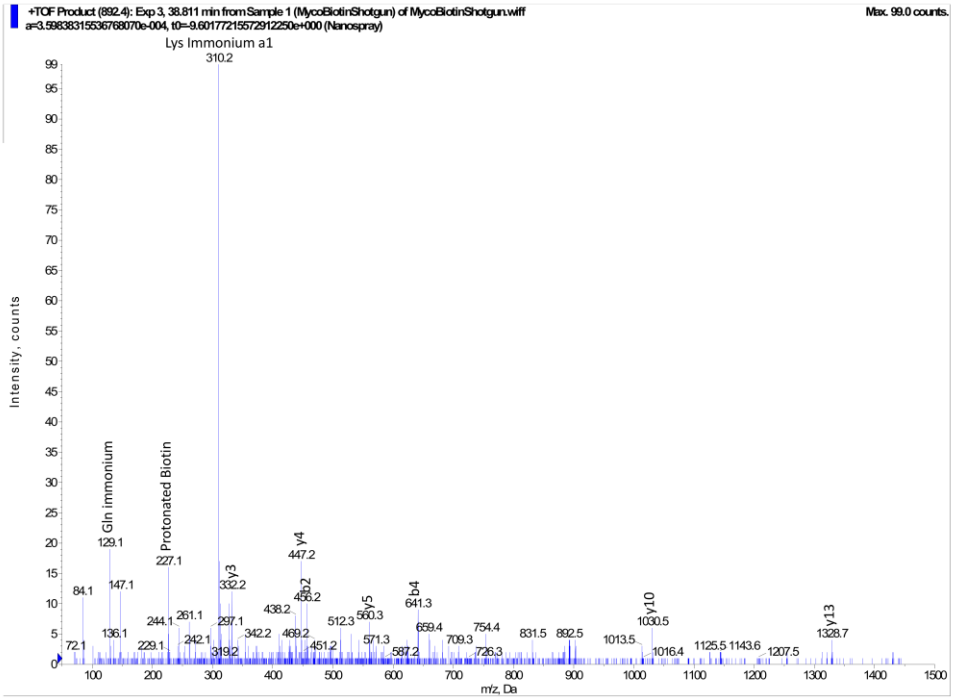

Figure S3.2e: Annotation of MS/MS spectra for the P159 semi-tryptic peptide KTGQIQAGDVIDANK.

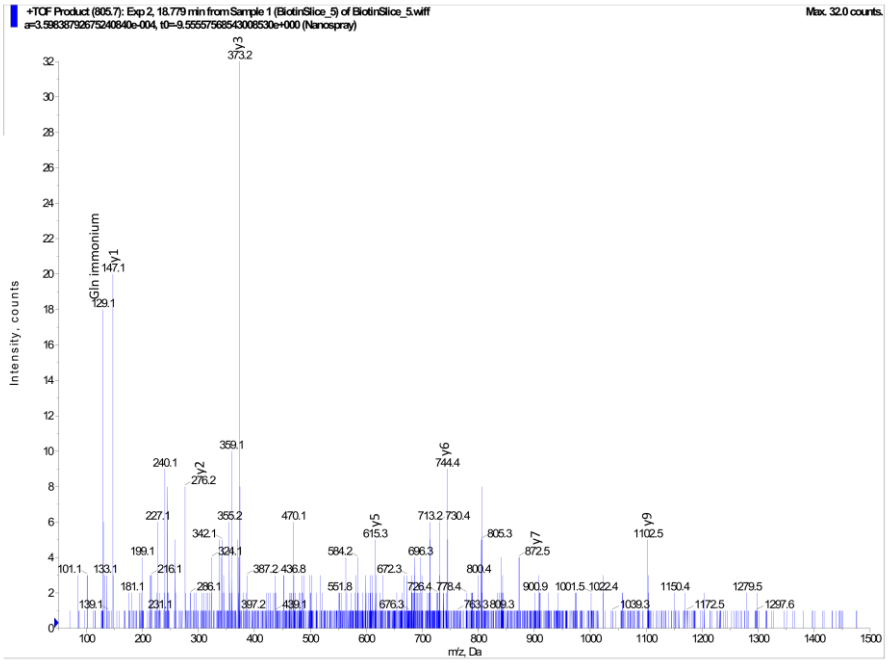

Figure S3.3: Annotation of MS/MS spectra for the P159 semi-tryptic peptide QKDQTNEQTEKEIEPEK.

Table S3.1: Ingredients for 1L of Friis broth.

Hanks A (500 mL stock)	**15.2 mL**	**Autoclaved**
Sodium Chloride	80g	
Potassium Chloride	4g	
Magnesium Sulphate heptahydrate	1g	
Magnesium Chloride hexahydrate	1g	
Calcium chloride	1.4g	
Hanks B (500 mL stock)	**15.2 mL**	
disodium Hydrogen Orthophosphate	1.5g	
Potassium diHydrogen Orthophosphate	0.6g	
Brain Heart Infusion (Difco)	**4.9g**	
PPLO without crystal violet (Difco)	**5.25g**	
0.5% Phenol Red	**2.6 mL**	
MilliQ water	**827 mL**	
Aqueous solution containing 2.5 % Bacitracin and Ampicillin	**5.7 mL**	
Pig Serum	**50 mL**	
Horse Serum	**50 mL**	
Yeast Extract	**34 mL**	

Chapter 4 (Paper III)

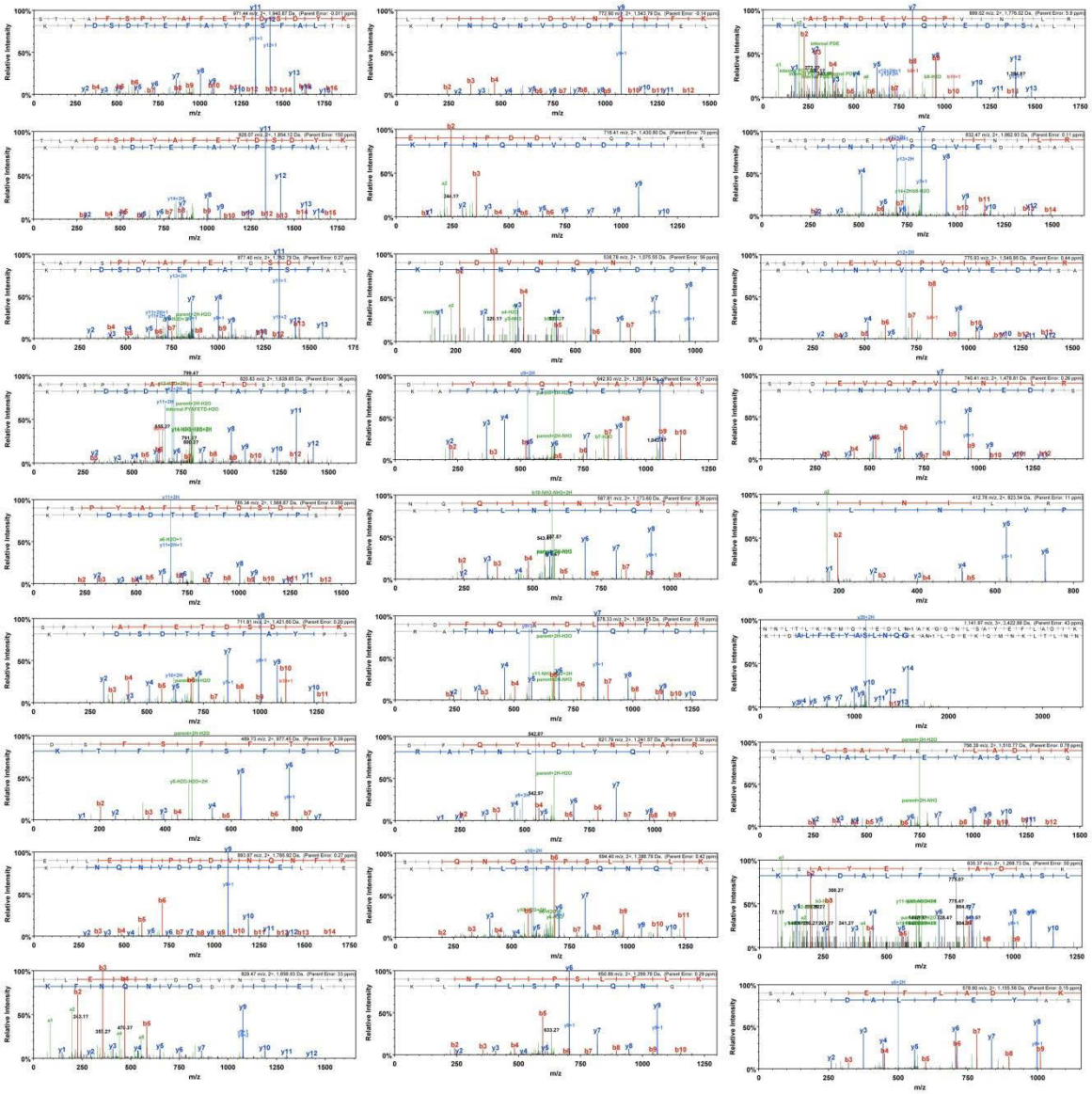

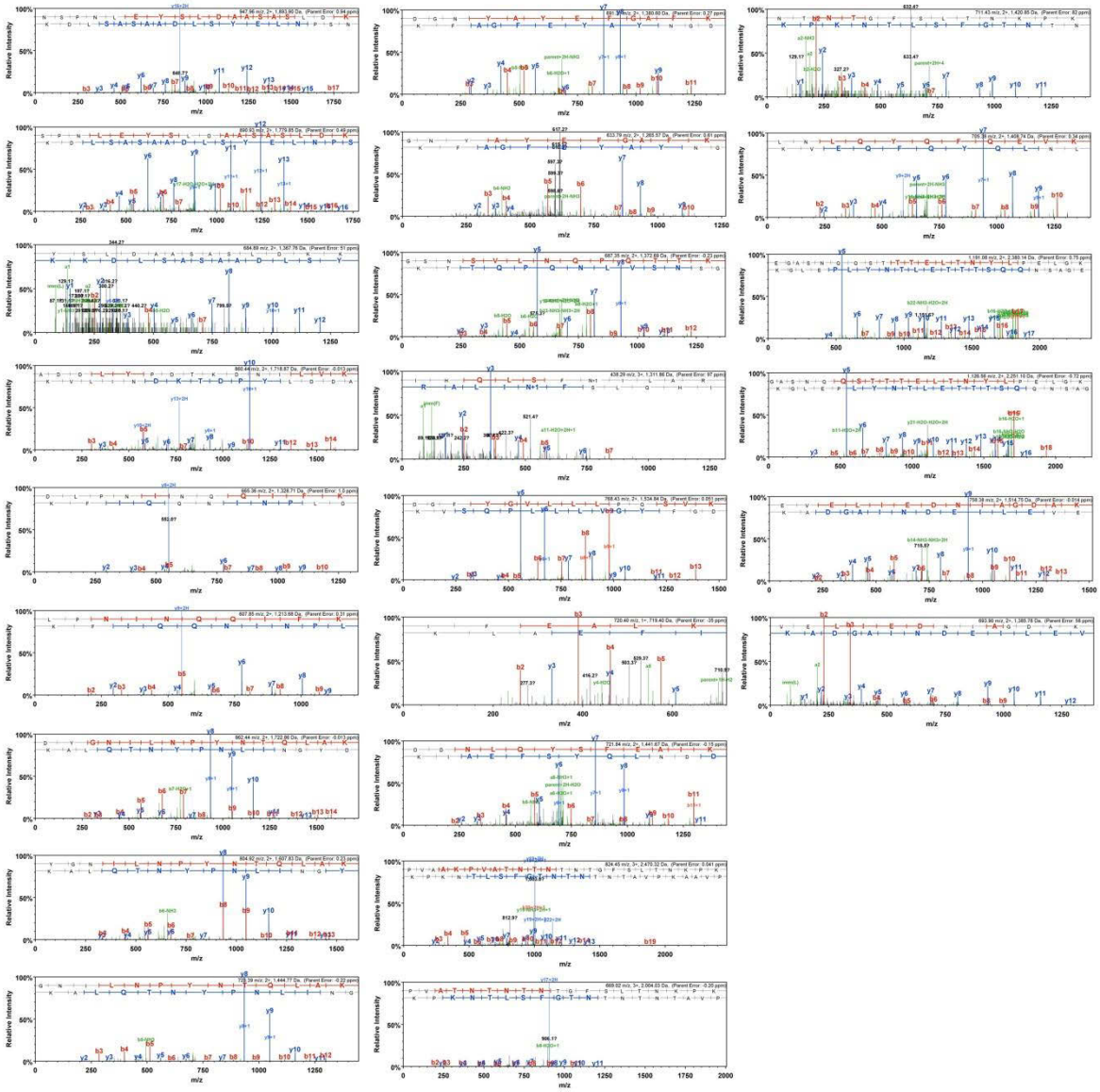

Figure S4.1: Spectra of the semi-tryptic peptides mapping to P123$_J$. Spectra were analysed by Scaffold (Proteome Software). A, B, Y and Z ions are labelled above their respective peaks.

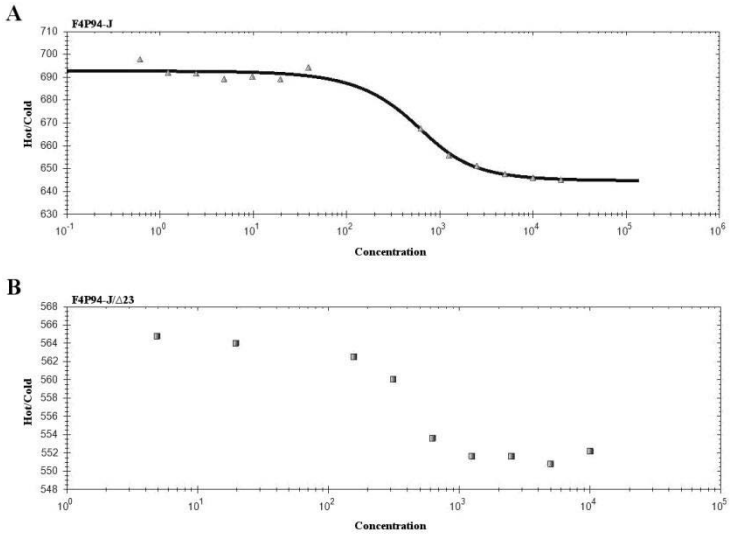

Figure S4.2: Thermophoretic output of the interaction between $F4_{P94\text{-}J}$ (A) and $F4_{P94\text{-}J/\Delta23}$ (B) and heparin. Concentration of the non-fluorescence molecule (heparin) is plotted against the thermophoretic movement of the fluorescent molecule ($F4_{P94\text{-}J}$ or $F4_{P94\text{-}J/\Delta23}$). $F4_{P94\text{-}J}$ bound heparin with a K_D of 182.3 ± 49.64 nM. A K_D could not be assigned to $F4_{P94\text{-}J/\Delta23}$ suggesting that the apparent binding observed in panel B is not indicative of a true binding event.

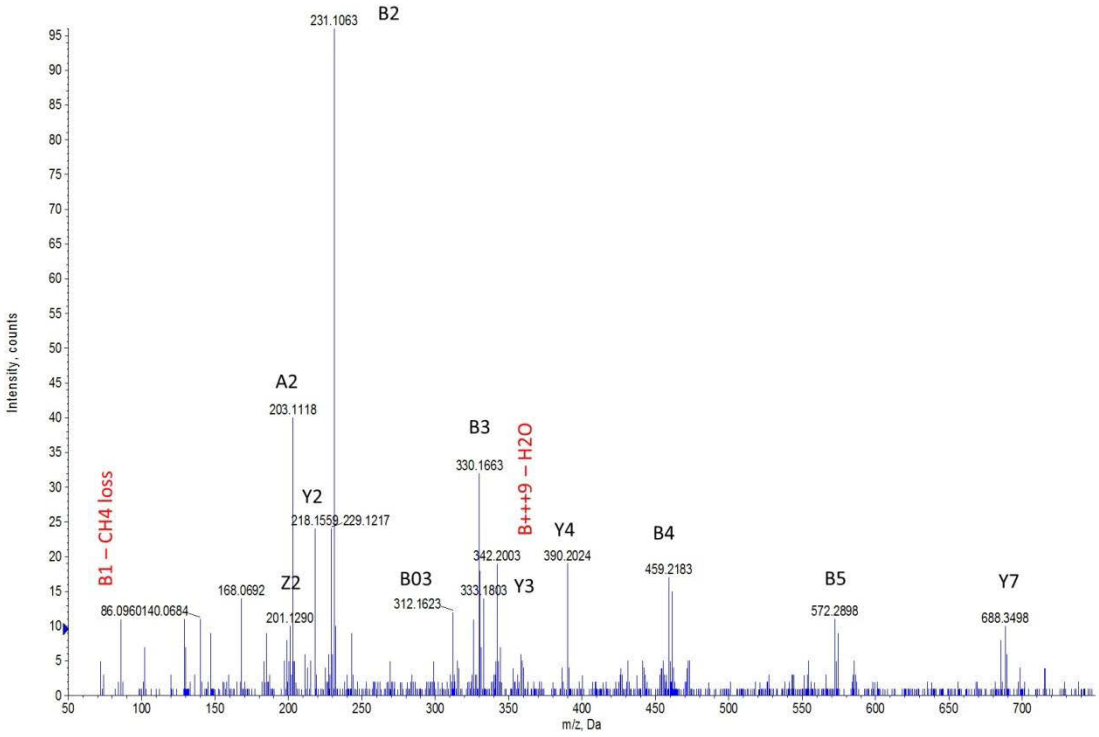

Figure S4.3: Spectra for the peptide ^{1040}T-E-V-E-L-I-E-D-N-I-A-G-D-A-K^{1054} belonging to P28$_J$. The mascot score for this peptide was 76.0. All major peaks from the MS/MS fragmentation pattern are accounted for (A, B, Y and Z ions)

Table S4.1: Semi-tryptic peptides identified in this study. Each peptide is shown in the first column while the method by which it was identified is shown in the second column. The Mascot scores are shown in parentheses.

Peptide Sequence	Method (Mascot Score)
PDDVNQNFK	SCX Mudpit QSTAR (62.4)
STLAFSPYAFETDSDYK	FTICR shotgun (92.2)
TLAFSPYAFETDSDYK	LTQ (75.5)
LAFSPYAFETDSDYK	FTICR shotgun (67.8)
AFSPYAFETDSDYK	LTQ (59.0)
FSPYAFETDSDYK	FTICR shotgun (44.1)
SPYAFETDSDYK	FTICR shotgun (79.1)
DSFSFFTK	FTICR shotgun (55.7)
EILEIIPDDVNQNFK	FTICR shotgun (44.6)
ILEIIPDDVNQNFK	Mudpit (45.4)
LEIIPDDVNQNFK	FTICR shotgun (34.4)
EIIPDDVNQNFK	SCX Mudpit QSTAR (53.6)
PDDVNQNFK	QSTAR (44.5)
DIYEQTVAFAK	FTICR shotgun (63.9)
NQQIENLSTK	FTICR shotgun (46.0)
IDFQYDLNTAR	FTICR shotgun (70.9)
DFQYDLNTAR	FTICR shotgun (37.5)
SIQNQIPSLFLK	FTICR shotgun (52.9)
IQNQIPSLFLK	FTICR shotgun (40.8)
ILASPDEVQPVINILR	Mudpit (86.0)
LASPDEVQPVINILR	FTICR shotgun (37.2)
ASPDEVQPVINILR	FTICR shotgun (74.0)
SPDEVQPVINILR	FTICR shotgun (67.3)
PVINILR	QSTAR (45.7)
NNLTLKNMQKEDLNAKGQNLSAYEFLADIK	LTQ (50.5)
QNLSAYEFLADIK	FTICR shotgun (73.9)
LSAYEFLADIK	Mudpit (48.4)
SAYEFLADIK	FTICR shotgun (67.9)
NSPNLEYSLDAASASLDK	FTICR shotgun (93.2)
SPNLEYSLDAASASLDK	FTICR shotgun (110.2)
YSLDAASASLDKK	Mudpit (68.3)
ADDLYPDTKDNILVK	FTICR shotgun (26.6)
DLPNINQIFK	FTICR shotgun (33.9)
LPNINQQIFK	FTICR shotgun (62.8)
DYGNILNPYNTQLAK	FTICR shotgun (82.0)
YGNILNPYNTQLAK	FTICR shotgun (71.7)
GNILNPYNTQLAK	FTICR shotgun (47.7)
DGNYAYEFGAFK	FTICR shotgun (73.5)
GNYAYEFGAFK	FTICR shotgun (34.7)
GSNSVLNQPQTTK	FTICR shotgun (62.0)
IHQLSFN	Mudpit (30.7)
DGFYGVLLLPQSVK	FTICR shotgun (68.2)
IFEALK	LTQ (32.8)
DDNLQYSFEAIK	FTICR shotgun (71.4)

PVAAKPVATNTNTNTGFSLTNKPK	FTICR shotgun (61.7)
PVATNTNTNTGFSLTNKPK	FTICR shotgun (67.8)
NTNTGFSLTNKPK	QSTAR (63.9)
LNLQYQFQEVK	FTICR shotgun (61.4)
EGASNQQSTTTELTNYLPELGK	FTICR shotgun (83.9)
GASNQQSTTTELTNYPELGK	FTICR shotgun (77.7)
EVELIEDNIAGDAK	FTICR shotgun (86.6)
VELIEDNIAGDAK	Mudpit (73.6)

Table S4.2: Lung scores of lung tissue-homogenates shown in Figure 4.8. Scores for A, B, C and D correspond with each of the respective panels. A lung score of zero indicates that no lesions were present, while lung scores above this indicate the varying levels of lesions observed, consistent with *M. hyopneumoniae* infection.

Sample	Lung Score
A (Infected)	6
B (Infected)	6
C (Infected)	12
D (Uninfected)	0

Chapter 5 (Paper IV)

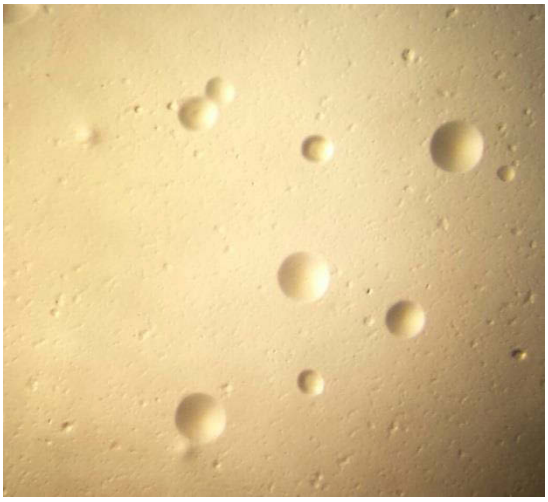

Figure S5.1: *M. hyopneumoniae* colonies grown on Friis agar for approximately 10 days. Colonies were visualised under a stereo microscope and the smooth, slightly raised circular colonies can be seen on the surface of the agar.

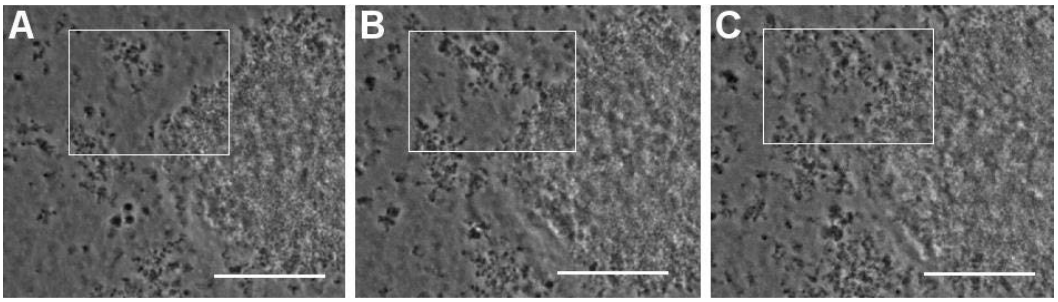

Figure S5.2: Timelapse microscopy of a *M. hyopneumoniae* biofilm 12 d of age over the course of 24 h. A small microcolony (boxed) can be seen being incorporated into a large biofilm. A) "cellular-bridge" can be seen forming at 15 h (B) which becomes incorporated in the biofilm (C). Scale bar is 10 μm.

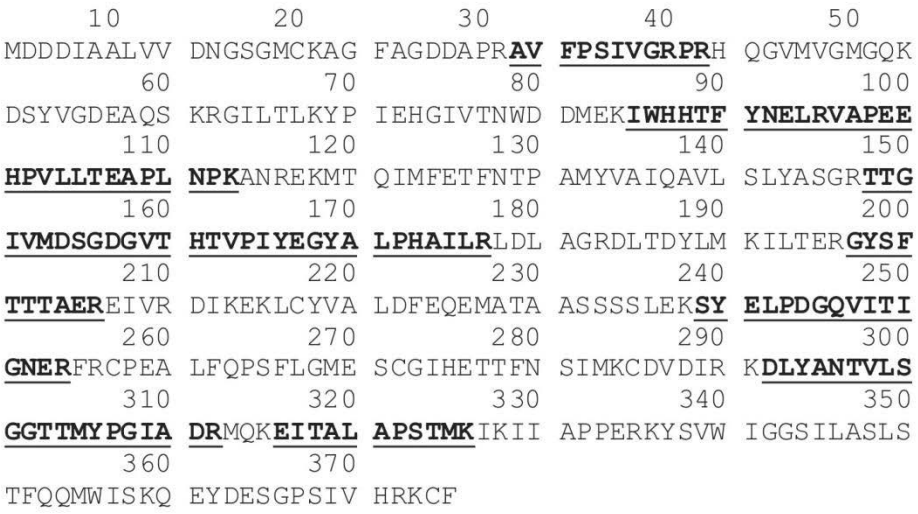

Figure S5.3: Peptide coverage of surface exposed actin (Q6QAQ1) recovered from the surface of PK-15 epithelial-like cells (*Sus scrofa*). Biotinylated PK-15 surface proteins were incubated with avidin agarose and purified by elution using low pH. These proteins were separated by SDS PAGE and analysed by LC-MS/MS. The peptide coverage presented here was obtained from an area of the gel at approximately 40 kDa.

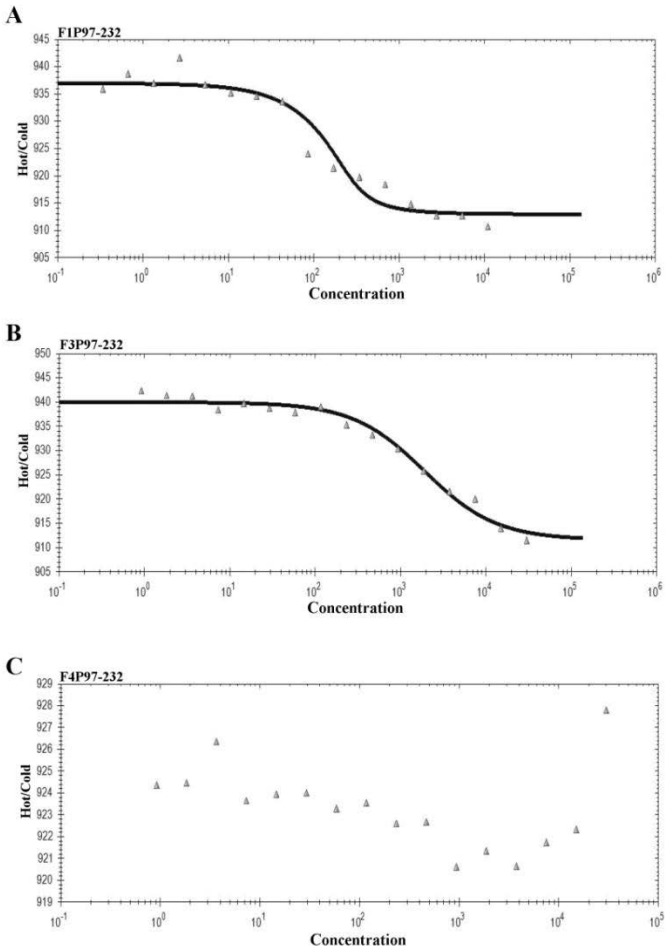

Figure S5.3: Thermophoretic output of the interaction between $F1_{P97-232}$ (A), $F3_{P97-232}$ (B) and $F4_{P97-232}$ (C) and actin. Concentration of the non-fluorescence molecule is plotted against the thermophoretic movement of the fluorescent molecule (actin). $F1_{P97-232}$ and $F3_{P97-232}$ bound actin with a K_D of 34.2 nM and 1.79 µM respectively. A K_D could not be assigned to $F4_{P97-232}$ suggesting that it does not bind actin.

References

1. DeBey MC, Ross RF (1994) Ciliostasis and loss of cilia induced by Mycoplasma hyopneumoniae in porcine tracheal organ cultures. Infect Immun 62: 5312-5318.
2. Bogema DR, Deutscher AT, Woolley LK, Seymour LM, Raymond BB, et al. (2012) Characterization of cleavage events in the multifunctional cilium adhesin Mhp684 (P146) reveals a mechanism by which Mycoplasma hyopneumoniae regulates surface topography. MBio 3.
3. Bogema DR, Scott NE, Padula MP, Tacchi JL, Raymond BB, et al. (2011) Sequence TTKF ↓ QE defines the site of proteolytic cleavage in Mhp683 protein, a novel glycosaminoglycan and cilium adhesin of Mycoplasma hyopneumoniae. J Biol Chem 286: 41217-41229.
4. Burnett TA, Dinkla K, Rohde M, Chhatwal GS, Uphoff C, et al. (2006) P159 is a proteolytically processed, surface adhesin of Mycoplasma hyopneumoniae: defined domains of P159 bind heparin and promote adherence to eukaryote cells. Mol Microbiol 60: 669-686.
5. Deutscher AT, Jenkins C, Minion FC, Seymour LM, Padula MP, et al. (2010) Repeat regions R1 and R2 in the P97 paralogue Mhp271 of Mycoplasma hyopneumoniae bind heparin, fibronectin and porcine cilia. Mol Microbiol 78: 444-458.
6. Deutscher AT, Tacchi JL, Minion FC, Padula MP, Crossett B, et al. (2012) Mycoplasma hyopneumoniae Surface proteins Mhp385 and Mhp384 bind host cilia and glycosaminoglycans and are endoproteolytically processed by proteases that recognize different cleavage motifs. J Proteome Res 11: 1924-1936.
7. Seymour LM, Deutscher AT, Jenkins C, Kuit TA, Falconer L, et al. (2010) A processed multidomain mycoplasma hyopneumoniae adhesin binds fibronectin, plasminogen, and swine respiratory cilia. J Biol Chem 285: 33971-33978.
8. Seymour LM, Falconer L, Deutscher AT, Minion FC, Padula MP, et al. (2011) Mhp107 is a member of the multifunctional adhesin family of Mycoplasma hyopneumoniae. J Biol Chem 286: 10097-10104.
9. Seymour LM, Jenkins C, Deutscher AT, Raymond BB, Padula MP, et al. (2012) Mhp182 (P102) binds fibronectin and contributes to the recruitment of plasmin(ogen) to the Mycoplasma hyopneumoniae cell surface. Cell Microbiol 14: 81-94.
10. Wilton J, Jenkins C, Cordwell SJ, Falconer L, Minion FC, et al. (2009) Mhp493 (P216) is a proteolytically processed, cilium and heparin binding protein of Mycoplasma hyopneumoniae. Mol Microbiol 71: 566-582.
11. Choi C, Kwon D, Jung K, Ha Y, Lee YH, et al. (2006) Expression of inflammatory cytokines in pigs experimentally infected with Mycoplasma hyopneumoniae. J Comp Pathol 134: 40-46.
12. Lorenzo H, Quesada O, Assuncao P, Castro A, Rodriguez F (2006) Cytokine expression in porcine lungs experimentally infected with Mycoplasma hyopneumoniae. Vet Immunol Immunopathol 109: 199-207.
13. Redondo E, Masot AJ, Fernandez A, Gazquez A (2009) Histopathological and immunohistochemical findings in the lungs of pigs infected experimentally with Mycoplasma hyopneumoniae. J Comp Pathol 140: 260-270.
14. Le Carrou J, Laurentie M, Kobisch M, Gautier-Bouchardon AV (2006) Persistence of Mycoplasma hyopneumoniae in experimentally infected pigs after marbofloxacin treatment and detection of mutations in the parC gene. Antimicrob Agents Chemother 50: 1959-1966.
15. Marois C, Le Carrou J, Kobisch M, Gautier-Bouchardon AV (2007) Isolation of Mycoplasma hyopneumoniae from different sampling sites in experimentally infected and contact SPF piglets. Vet Microbiol 120: 96-104.
16. Woolley LK, Fell S, Gonsalves JR, Walker MJ, Djordjevic SP, et al. (2012) Evaluation of clinical, histological and immunological changes and qPCR detection of Mycoplasma

hyopneumoniae in tissues during the early stages of mycoplasmal pneumonia in pigs after experimental challenge with two field isolates. Vet Microbiol 161: 186-195.
17. Mebus CA, Underdahl NR (1977) Scanning electron microscopy of trachea and bronchi from gnotobiotic pigs inoculated with Mycoplasma hyopneumoniae. Am J Vet Res 38: 1249-1254.
18. Fano E, Pijoan C, Dee S (2005) Dynamics and persistence of Mycoplasma hyopneumoniae infection in pigs. Can J Vet Res 69: 223-228.
19. Pieters M, Pijoan C, Fano E, Dee S (2009) An assessment of the duration of Mycoplasma hyopneumoniae infection in an experimentally infected population of pigs. Vet Microbiol 134: 261-266.
20. Woolley LK, Fell SA, Gonsalves JR, Raymond BB, Collins D, et al. (2014) Evaluation of recombinant Mycoplasma hyopneumoniae P97/P102 paralogs formulated with selected adjuvants as vaccines against mycoplasmal pneumonia in pigs. Vaccine 32: 4333-4341.
21. Razin S, Yogev D, Naot Y (1998) Molecular biology and pathogenicity of mycoplasmas. Microbiol Mol Biol Rev 62: 1094-1156.
22. Underdahl NR, Kennedy GA, Ramos AS, Jr. (1980) Duration of Mycoplasma hyopneumoniae infection in gnotobiotic pigs. Can Vet J 21: 258-261.
23. Livingston CW, Jr., Stair EL, Underdahl NR, Mebus CA (1972) Pathogenesis of mycoplasmal pneumonia in swine. Am J Vet Res 33: 2249-2258.
24. DeBey MC, Jacobson CD, Ross RF (1992) Histochemical and morphologic changes of porcine airway epithelial cells in response to infection with Mycoplasma hyopneumoniae. Am J Vet Res 53: 1705-1710.
25. Thacker EL, Halbur PG, Ross RF, Thanawongnuwech R, Thacker BJ (1999) Mycoplasma hyopneumoniae potentiation of porcine reproductive and respiratory syndrome virus-induced pneumonia. J Clin Microbiol 37: 620-627.
26. Thacker EL, Thacker BJ, Janke BH (2001) Interaction between Mycoplasma hyopneumoniae and swine influenza virus. J Clin Microbiol 39: 2525-2530.
27. Park SC, Yibchok-Anun S, Cheng H, Young TF, Thacker EL, et al. (2002) Mycoplasma hyopneumoniae increases intracellular calcium release in porcine ciliated tracheal cells. Infect Immun 70: 2502-2506.
28. Salathe M (2007) Regulation of mammalian ciliary beating. Annu Rev Physiol 69: 401-422.
29. Salathe M, Bookman RJ (1999) Mode of Ca2+ action on ciliary beat frequency in single ovine airway epithelial cells. J Physiol 520 Pt 3: 851-865.
30. Praetorius HA, Praetorius J, Nielsen S, Frokiaer J, Spring KR (2004) Beta1-integrins in the primary cilium of MDCK cells potentiate fibronectin-induced Ca2+ signaling. Am J Physiol Renal Physiol 287: F969-978.
31. Joki S, Saano V (1994) Ciliary beat frequency at six levels of the respiratory tract in cow, dog, guinea-pig, pig, rabbit and rat. Clin Exp Pharmacol Physiol 21: 427-434.
32. Zhang Q, Young TF, Ross RF (1994) Microtiter plate adherence assay and receptor analogs for Mycoplasma hyopneumoniae. Infect Immun 62: 1616-1622.
33. Kim CH, Oh Y, Han K, Seo HW, Kim D, et al. (2012) Expression of secreted and membrane-bound mucins in the airways of piglets experimentally infected with Mycoplasma hyopneumoniae. Vet J 192: 120-122.
34. Woolley LK, Fell SA, Djordjevic SP, Eamens GJ, Jenkins C (2013) Plasmin activity in the porcine airways is enhanced during experimental infection with Mycoplasma hyopneumoniae, is positively correlated with proinflammatory cytokine levels and is ameliorated by vaccination. Vet Microbiol 164: 60-66.
35. Sarradell J, Andrada M, Ramirez AS, Fernandez A, Gomez-Villamandos JC, et al. (2003) A morphologic and immunohistochemical study of the bronchus-associated lymphoid

tissue of pigs naturally infected with Mycoplasma hyopneumoniae. Vet Pathol 40: 395-404.
36. Rodriguez F, Ramirez GA, Sarradell J, Andrada M, Lorenzo H (2004) Immunohistochemical labelling of cytokines in lung lesions of pigs naturally infected with Mycoplasma hyopneumoniae. J Comp Pathol 130: 306-312.
37. Henderson AJ (1994) Bronchoalveolar lavage. Arch Dis Child 70: 167-169.
38. Bartlett JA, Albertolle ME, Wohlford-Lenane C, Pezzulo AA, Zabner J, et al. (2013) Protein composition of bronchoalveolar lavage fluid and airway surface liquid from newborn pigs. Am J Physiol Lung Cell Mol Physiol 305: L256-266.
39. Bolland JR, Simmons WL, Daubenspeck JM, Dybvig K (2012) Mycoplasma polysaccharide protects against complement. Microbiology 158: 1867-1873.
40. Erlinger R (1995) Glycosaminoglycans in porcine lung: an ultrastructural study using cupromeronic blue. Cell Tissue Res 281: 473-483.
41. Jenkins C, Wilton JL, Minion FC, Falconer L, Walker MJ, et al. (2006) Two domains within the Mycoplasma hyopneumoniae cilium adhesin bind heparin. Infect Immun 74: 481-487.
42. Raymond BB, Jenkins C, Seymour LM, Tacchi JL, Widjaja M, et al. (2015) Proteolytic processing of the cilium adhesin MHJ_0194 (P123J) in Mycoplasma hyopneumoniae generates a functionally diverse array of cleavage fragments that bind multiple host molecules. Cell Microbiol 17: 425-444.
43. Raymond BB, Tacchi JL, Jarocki VM, Minion FC, Padula MP, et al. (2013) P159 from Mycoplasma hyopneumoniae binds porcine cilia and heparin and is cleaved in a manner akin to ectodomain shedding. J Proteome Res 12: 5891-5903.
44. Tacchi JL, Raymond BB, Jarocki VM, Berry IJ, Padula MP, et al. (2014) Cilium adhesin P216 (MHJ_0493) is a target of ectodomain shedding and aminopeptidase activity on the surface of Mycoplasma hyopneumoniae. J Proteome Res 13: 2920-2930.
45. Zhang Q, Young TF, Ross RF (1994) Glycolipid receptors for attachment of Mycoplasma hyopneumoniae to porcine respiratory ciliated cells. Infect Immun 62: 4367-4373.
46. Henderson B, Nair S, Pallas J, Williams MA (2011) Fibronectin: a multidomain host adhesin targeted by bacterial fibronectin-binding proteins. FEMS Microbiol Rev 35: 147-200.
47. Sabatelli P, Bonaldo P, Lattanzi G, Braghetta P, Bergamin N, et al. (2001) Collagen VI deficiency affects the organization of fibronectin in the extracellular matrix of cultured fibroblasts. Matrix Biol 20: 475-486.
48. Konkel ME, Larson CL, Flanagan RC (2010) Campylobacter jejuni FlpA binds fibronectin and is required for maximal host cell adherence. J Bacteriol 192: 68-76.
49. Boehm M, Krause-Gruszczynska M, Rohde M, Tegtmeyer N, Takahashi S, et al. (2011) Major host factors involved in epithelial cell invasion of Campylobacter jejuni: role of fibronectin, integrin beta1, FAK, Tiam-1, and DOCK180 in activating Rho GTPase Rac1. Front Cell Infect Microbiol 1: 17.
50. Krause-Gruszczynska M, Boehm M, Rohde M, Tegtmeyer N, Takahashi S, et al. (2011) The signaling pathway of Campylobacter jejuni-induced Cdc42 activation: Role of fibronectin, integrin beta1, tyrosine kinases and guanine exchange factor Vav2. Cell Commun Signal 9: 32.
51. Sinha B, Francois PP, Nusse O, Foti M, Hartford OM, et al. (1999) Fibronectin-binding protein acts as Staphylococcus aureus invasin via fibronectin bridging to integrin alpha5beta1. Cell Microbiol 1: 101-117.
52. Adams C, Pitzer J, Minion FC (2005) In vivo expression analysis of the P97 and P102 paralog families of Mycoplasma hyopneumoniae. Infect Immun 73: 7784-7787.
53. Pendarvis K, Padula MP, Tacchi JL, Petersen AC, Djordjevic SP, et al. (2014) Proteogenomic mapping of Mycoplasma hyopneumoniae virulent strain 232. BMC Genomics 15: 576.

54. Djordjevic SP, Cordwell SJ, Djordjevic MA, Wilton J, Minion FC (2004) Proteolytic Processing of the Mycoplasma hyopneumoniae Cilium Adhesin. Infection and Immunity 72: 2791-2802.
55. Bolland JR, Dybvig K (2012) Mycoplasma pulmonis Vsa proteins and polysaccharide modulate adherence to pulmonary epithelial cells. FEMS Microbiol Lett 331: 25-30.
56. Shaw BM, Simmons WL, Dybvig K (2012) The Vsa shield of Mycoplasma pulmonis is antiphagocytic. Infect Immun 80: 704-709.
57. Shen X, Gumulak J, Yu H, French CT, Zou N, et al. (2000) Gene rearrangements in the vsa locus of Mycoplasma pulmonis. J Bacteriol 182: 2900-2908.
58. Simmons WL, Denison AM, Dybvig K (2004) Resistance of Mycoplasma pulmonis to complement lysis is dependent on the number of Vsa tandem repeats: shield hypothesis. Infect Immun 72: 6846-6851.
59. Simmons WL, Dybvig K (2003) The Vsa Proteins Modulate Susceptibility of Mycoplasma pulmonis to Complement Killing, Hemadsorption, and Adherence to Polystyrene. Infection and Immunity 71: 5733-5738.
60. Flemming HC, Wingender J (2010) The biofilm matrix. Nat Rev Microbiol 8: 623-633.
61. McAuliffe L, Ellis RJ, Miles K, Ayling RD, Nicholas RA (2006) Biofilm formation by mycoplasma species and its role in environmental persistence and survival. Microbiology 152: 913-922.
62. Simmons WL, Bolland JR, Daubenspeck JM, Dybvig K (2007) A stochastic mechanism for biofilm formation by Mycoplasma pulmonis. J Bacteriol 189: 1905-1913.
63. McAuliffe L, Ayling RD, Ellis RJ, Nicholas RA (2008) Biofilm-grown Mycoplasma mycoides subsp. mycoides SC exhibit both phenotypic and genotypic variation compared with planktonic cells. Vet Microbiol 129: 315-324.
64. Simmons WL, Dybvig K (2009) Mycoplasma biofilms ex vivo and in vivo. FEMS Microbiol Lett 295: 77-81.
65. Kornspan JD, Tarshis M, Rottem S (2011) Adhesion and biofilm formation of Mycoplasma pneumoniae on an abiotic surface. Arch Microbiol 193: 833-836.
66. Chen H, Yu S, Hu M, Han X, Chen D, et al. (2012) Identification of biofilm formation by Mycoplasma gallisepticum. Vet Microbiol 161: 96-103.
67. Simmons WL, Daubenspeck JM, Osborne JD, Balish MF, Waites KB, et al. (2013) Type 1 and type 2 strains of Mycoplasma pneumoniae form different biofilms. Microbiology 159: 737-747.
68. Mah TF, O'Toole GA (2001) Mechanisms of biofilm resistance to antimicrobial agents. Trends Microbiol 9: 34-39.
69. Sitaraman R, Denison AM, Dybvig K (2002) A unique, bifunctional site-specific DNA recombinase from Mycoplasma pulmonis. Mol Microbiol 46: 1033-1040.
70. Simmons WL, Zuhua C, Glass JI, Simecka JW, Cassell GH, et al. (1996) Sequence analysis of the chromosomal region around and within the V-1-encoding gene of Mycoplasma pulmonis: evidence for DNA inversion as a mechanism for V-1 variation. Infect Immun 64: 472-479.
71. Bhugra B, Voelker LL, Zou N, Yu H, Dybvig K (1995) Mechanism of antigenic variation in Mycoplasma pulmonis: interwoven, site-specific DNA inversions. Mol Microbiol 18: 703-714.
72. Simmons WL, Dybvig K (2003) The Vsa proteins modulate susceptibility of Mycoplasma pulmonis to complement killing, hemadsorption, and adherence to polystyrene. Infect Immun 71: 5733-5738.
73. Simmons WL, Dybvig K (2007) Biofilms protect Mycoplasma pulmonis cells from lytic effects of complement and gramicidin. Infect Immun 75: 3696-3699.
74. Cesarman-Maus G, Hajjar KA (2005) Molecular mechanisms of fibrinolysis. Br J Haematol 129: 307-321.

75. Trexler M, Vali Z, Patthy L (1982) Structure of the omega-aminocarboxylic acid-binding sites of human plasminogen. Arginine 70 and aspartic acid 56 are essential for binding of ligand by kringle 4. J Biol Chem 257: 7401-7406.
76. Castellino FJ, Ploplis VA (2005) Structure and function of the plasminogen/plasmin system. Thromb Haemost 93: 647-654.
77. Violand BN, Castellino FJ (1976) Mechanism of the urokinase-catalyzed activation of human plasminogen. J Biol Chem 251: 3906-3912.
78. Wiman B (1973) Primary structure of peptides released during activation of human plasminogen by urokinase. Eur J Biochem 39: 1-9.
79. Wiman B, Wallen P (1973) Activation of human plasminogen by an insoluble derivative of urokinase. Structural changes of plasminogen in the course of activation to plasmin and demonstration of a possible intermediate compound. Eur J Biochem 36: 25-31.
80. Gong Y, Kim SO, Felez J, Grella DK, Castellino FJ, et al. (2001) Conversion of Glu-plasminogen to Lys-plasminogen is necessary for optimal stimulation of plasminogen activation on the endothelial cell surface. J Biol Chem 276: 19078-19083.
81. Law RH, Caradoc-Davies T, Cowieson N, Horvath AJ, Quek AJ, et al. (2012) The X-ray crystal structure of full-length human plasminogen. Cell Rep 1: 185-190.
82. Mosher DF (1975) Cross-linking of cold-insoluble globulin by fibrin-stabilizing factor. J Biol Chem 250: 6614-6621.
83. Wang Y, Reheman A, Spring CM, Kalantari J, Marshall AH, et al. (2014) Plasma fibronectin supports hemostasis and regulates thrombosis. J Clin Invest 124: 4281-4293.
84. Lahteenmaki K, Edelman S, Korhonen TK (2005) Bacterial metastasis: the host plasminogen system in bacterial invasion. Trends Microbiol 13: 79-85.
85. Pancholi V, Fischetti VA (1992) A major surface protein on group A streptococci is a glyceraldehyde-3-phosphate-dehydrogenase with multiple binding activity. J Exp Med 176: 415-426.
86. Lishko VK, Novokhatny VV, Yakubenko VP, Skomorovska-Prokvolit HV, Ugarova TP (2004) Characterization of plasminogen as an adhesive ligand for integrins alphaMbeta2 (Mac-1) and alpha5beta1 (VLA-5). Blood 104: 719-726.
87. Ho E, Dagnino L (2012) Epidermal growth factor induction of front-rear polarity and migration in keratinocytes is mediated by integrin-linked kinase and ELMO2. Mol Biol Cell 23: 492-502.
88. Ho E, Irvine T, Vilk GJ, Lajoie G, Ravichandran KS, et al. (2009) Integrin-linked kinase interactions with ELMO2 modulate cell polarity. Mol Biol Cell 20: 3033-3043.
89. Nakrieko KA, Welch I, Dupuis H, Bryce D, Pajak A, et al. (2008) Impaired hair follicle morphogenesis and polarized keratinocyte movement upon conditional inactivation of integrin-linked kinase in the epidermis. Mol Biol Cell 19: 1462-1473.
90. Sayedyahossein S, Nini L, Irvine TS, Dagnino L (2012) Essential role of integrin-linked kinase in regulation of phagocytosis in keratinocytes. FASEB J 26: 4218-4229.
91. Massey RC, Kantzanou MN, Fowler T, Day NP, Schofield K, et al. (2001) Fibronectin-binding protein A of Staphylococcus aureus has multiple, substituting, binding regions that mediate adherence to fibronectin and invasion of endothelial cells. Cell Microbiol 3: 839-851.
92. Banerjee A, Kim BJ, Carmona EM, Cutting AS, Gurney MA, et al. (2011) Bacterial Pili exploit integrin machinery to promote immune activation and efficient blood-brain barrier penetration. Nat Commun 2: 462.
93. Mu R, Kim BJ, Paco C, Del Rosario Y, Courtney HS, et al. (2014) Identification of a group B streptococcal fibronectin binding protein, SfbA, that contributes to invasion of brain endothelium and development of meningitis. Infect Immun 82: 2276-2286.
94. Siemens N, Patenge N, Otto J, Fiedler T, Kreikemeyer B (2011) Streptococcus pyogenes M49 plasminogen/plasmin binding facilitates keratinocyte invasion via integrin-

integrin-linked kinase (ILK) pathways and protects from macrophage killing. J Biol Chem 286: 21612-21622.
95. Attali C, Durmort C, Vernet T, Di Guilmi AM (2008) The interaction of Streptococcus pneumoniae with plasmin mediates transmigration across endothelial and epithelial monolayers by intercellular junction cleavage. Infect Immun 76: 5350-5356.
96. Jobin MC, Brassard J, Quessy S, Gottschalk M, Grenier D (2004) Acquisition of host plasmin activity by the Swine pathogen Streptococcus suis serotype 2. Infect Immun 72: 606-610.
97. Mathew AG, Cissell R, Liamthong S (2007) Antibiotic resistance in bacteria associated with food animals: a United States perspective of livestock production. Foodborne Pathog Dis 4: 115-133.
98. Silbergeld EK, Graham J, Price LB (2008) Industrial food animal production, antimicrobial resistance, and human health. Annu Rev Public Health 29: 151-169.
99. Amara U, Rittirsch D, Flierl M, Bruckner U, Klos A, et al. (2008) Interaction between the coagulation and complement system. Adv Exp Med Biol 632: 71-79.
100. Barthel D, Schindler S, Zipfel PF (2012) Plasminogen is a complement inhibitor. J Biol Chem 287: 18831-18842.
101. Walport MJ (2001) Complement. First of two parts. N Engl J Med 344: 1058-1066.
102. Walport MJ (2001) Complement. Second of two parts. N Engl J Med 344: 1140-1144.
103. (1999) Leptospirosis worldwide, 1999. Wkly Epidemiol Rec 74: 237-242.
104. McBride AJ, Athanazio DA, Reis MG, Ko AI (2005) Leptospirosis. Curr Opin Infect Dis 18: 376-386.
105. Lilenbaum W, Martins G (2014) Leptospirosis in cattle: a challenging scenario for the understanding of the epidemiology. Transbound Emerg Dis 61 Suppl 1: 63-68.
106. Barbosa AS, Abreu PA, Vasconcellos SA, Morais ZM, Goncales AP, et al. (2009) Immune evasion of leptospira species by acquisition of human complement regulator C4BP. Infect Immun 77: 1137-1143.
107. Meri T, Murgia R, Stefanel P, Meri S, Cinco M (2005) Regulation of complement activation at the C3-level by serum resistant leptospires. Microb Pathog 39: 139-147.
108. Cinco M, Banfi E, Soranzo MR (1981) Studies on the interaction between macrophages and leptospires. J Gen Microbiol 124: 409-413.
109. Banfi E, Cinco M, Bellini M, Soranzo MR (1982) The role of antibodies and serum complement in the interaction between macrophages and leptospires. J Gen Microbiol 128: 813-816.
110. Cinco M, Cini B, Perticarari S, Presani G (2002) Leptospira interrogans binds to the CR3 receptor on mammalian cells. Microb Pathog 33: 299-305.
111. Li L, Ojcius DM, Yan J (2007) Comparison of invasion of fibroblasts and macrophages by high- and low-virulence Leptospira strains: colonization of the host-cell nucleus and induction of necrosis by the virulent strain. Arch Microbiol 188: 591-598.
112. Schulz F, Horn M (2015) Intranuclear bacteria: inside the cellular control center of eukaryotes. Trends Cell Biol.
113. Barocchi MA, Ko AI, Reis MG, McDonald KL, Riley LW (2002) Rapid translocation of polarized MDCK cell monolayers by Leptospira interrogans, an invasive but nonintracellular pathogen. Infect Immun 70: 6926-6932.
114. Evangelista K, Franco R, Schwab A, Coburn J (2014) Leptospira interrogans binds to cadherins. PLoS Negl Trop Dis 8: e2672.
115. Martinez-Lopez DG, Fahey M, Coburn J (2010) Responses of human endothelial cells to pathogenic and non-pathogenic Leptospira species. PLoS Negl Trop Dis 4: e918.
116. Fraga TR, Barbosa AS, Isaac L (2011) Leptospirosis: aspects of innate immunity, immunopathogenesis and immune evasion from the complement system. Scand J Immunol 73: 408-419.

117. Pangburn MK (2000) Host recognition and target differentiation by factor H, a regulator of the alternative pathway of complement. Immunopharmacology 49: 149-157.
118. Siqueira GH, Atzingen MV, Alves IJ, de Morais ZM, Vasconcellos SA, et al. (2013) Characterization of three novel adhesins of Leptospira interrogans. Am J Trop Med Hyg 89: 1103-1116.
119. Domingos RF, Vieira ML, Romero EC, Goncales AP, de Morais ZM, et al. (2012) Features of two proteins of Leptospira interrogans with potential role in host-pathogen interactions. BMC Microbiol 12: 50.
120. Verma A, Hellwage J, Artiushin S, Zipfel PF, Kraiczy P, et al. (2006) LfhA, a novel factor H-binding protein of Leptospira interrogans. Infect Immun 74: 2659-2666.
121. Wolff DG, Castiblanco-Valencia MM, Abe CM, Monaris D, Morais ZM, et al. (2013) Interaction of leptospira elongation factor tu with plasminogen and complement factor h: a metabolic leptospiral protein with moonlighting activities. PLoS One 8: e81818.
122. Stevenson B, Choy HA, Pinne M, Rotondi ML, Miller MC, et al. (2007) Leptospira interrogans endostatin-like outer membrane proteins bind host fibronectin, laminin and regulators of complement. PLoS One 2: e1188.
123. Castiblanco-Valencia MM, Fraga TR, Silva LB, Monaris D, Abreu PA, et al. (2012) Leptospiral immunoglobulin-like proteins interact with human complement regulators factor H, FHL-1, FHR-1, and C4BP. J Infect Dis 205: 995-1004.
124. Choy HA (2012) Multiple activities of LigB potentiate virulence of Leptospira interrogans: inhibition of alternative and classical pathways of complement. PLoS One 7: e41566.
125. Souza NM, Vieira ML, Alves IJ, de Morais ZM, Vasconcellos SA, et al. (2012) Lsa30, a novel adhesin of Leptospira interrogans binds human plasminogen and the complement regulator C4bp. Microb Pathog 53: 125-134.
126. Domingos R, Fernandes L, Romero E, de Morais Z, Vasconcellos S, et al. (2015) The novel Leptospira interrogans protein Lsa32 is expressed during infection and binds laminin and plasminogen. Microbiology.
127. Fernandes LG, Vieira ML, Kirchgatter K, Alves IJ, de Morais ZM, et al. (2012) OmpL1 is an extracellular matrix- and plasminogen-interacting protein of Leptospira spp. Infect Immun 80: 3679-3692.
128. Oliveira TR, Longhi MT, Goncales AP, de Morais ZM, Vasconcellos SA, et al. (2010) LipL53, a temperature regulated protein from Leptospira interrogans that binds to extracellular matrix molecules. Microbes Infect 12: 207-217.
129. Ito T, Yanagawa R (1987) Leptospiral attachment to extracellular matrix of mouse fibroblast (L929) cells. Vet Microbiol 15: 89-96.
130. Barbosa AS, Abreu PA, Neves FO, Atzingen MV, Watanabe MM, et al. (2006) A newly identified leptospiral adhesin mediates attachment to laminin. Infect Immun 74: 6356-6364.
131. Evangelista KV, Hahn B, Wunder EA, Jr., Ko AI, Haake DA, et al. (2014) Identification of cell-binding adhesins of Leptospira interrogans. PLoS Negl Trop Dis 8: e3215.
132. Verma A, Brissette CA, Bowman AA, Shah ST, Zipfel PF, et al. (2010) Leptospiral endostatin-like protein A is a bacterial cell surface receptor for human plasminogen. Infect Immun 78: 2053-2059.
133. Vieira ML, Vasconcellos SA, Goncales AP, de Morais ZM, Nascimento AL (2009) Plasminogen acquisition and activation at the surface of leptospira species lead to fibronectin degradation. Infect Immun 77: 4092-4101.
134. Vieira ML, Atzingen MV, Oliveira TR, Oliveira R, Andrade DM, et al. (2010) In vitro identification of novel plasminogen-binding receptors of the pathogen Leptospira interrogans. PLoS One 5: e11259.

135. Vieira ML, Alvarez-Flores MP, Kirchgatter K, Romero EC, Alves IJ, et al. (2013) Interaction of Leptospira interrogans with human proteolytic systems enhances dissemination through endothelial cells and protease levels. Infect Immun 81: 1764-1774.
136. Vieira ML, de Morais ZM, Vasconcellos SA, Romero EC, Nascimento AL (2011) In vitro evidence for immune evasion activity by human plasmin associated to pathogenic Leptospira interrogans. Microb Pathog 51: 360-365.
137. Agarwal V, Hammerschmidt S, Malm S, Bergmann S, Riesbeck K, et al. (2012) Enolase of Streptococcus pneumoniae binds human complement inhibitor C4b-binding protein and contributes to complement evasion. J Immunol 189: 3575-3584.
138. Koch TK, Reuter M, Barthel D, Bohm S, van den Elsen J, et al. (2012) Staphylococcus aureus proteins Sbi and Efb recruit human plasmin to degrade complement C3 and C3b. PLoS One 7: e47638.
139. Yavlovich A, Rechnitzer H, Rottem S (2007) Alpha-enolase resides on the cell surface of Mycoplasma fermentans and binds plasminogen. Infect Immun 75: 5716-5719.
140. Song Z, Li Y, Liu Y, Xin J, Zou X, et al. (2012) alpha-Enolase, an adhesion-related factor of Mycoplasma bovis. PLoS One 7: e38836.
141. Yavlovich A, Rottem S (2007) Binding of host extracellular matrix proteins to Mycoplasma fermentans and its effect on adherence to, and invasion of HeLa cells. FEMS Microbiol Lett 266: 158-162.
142. Bower K, Djordjevic SP, Andronicos NM, Ranson M (2003) Cell surface antigens of Mycoplasma species bovine group 7 bind to and activate plasminogen. Infect Immun 71: 4823-4827.
143. Thomas C, Jacobs E, Dumke R (2013) Characterization of pyruvate dehydrogenase subunit B and enolase as plasminogen-binding proteins in Mycoplasma pneumoniae. Microbiology 159: 352-365.
144. Furnkranz U, Siebert-Gulle K, Rosengarten R, Szostak MP (2013) Factors influencing the cell adhesion and invasion capacity of Mycoplasma gallisepticum. Acta Vet Scand 55: 63.
145. Robinson MW, Buchtmann KA, Jenkins C, Tacchi JL, Raymond BB, et al. (2013) MHJ_0125 is an M42 glutamyl aminopeptidase that moonlights as a multifunctional adhesin on the surface of Mycoplasma hyopneumoniae. Open Biol 3: 130017.
146. Bao S, Guo X, Yu S, Ding J, Tan L, et al. (2014) Mycoplasma synoviae enolase is a plasminogen/fibronectin binding protein. BMC Vet Res 10: 223.
147. Yavlovich A, Higazi AA, Rottem S (2001) Plasminogen binding and activation by Mycoplasma fermentans. Infect Immun 69: 1977-1982.
148. Manso-Silvan L, Vilei EM, Sachse K, Djordjevic SP, Thiaucourt F, et al. (2009) Mycoplasma leachii sp. nov. as a new species designation for Mycoplasma sp. bovine group 7 of Leach, and reclassification of Mycoplasma mycoides subsp. mycoides LC as a serovar of Mycoplasma mycoides subsp. capri. Int J Syst Evol Microbiol 59: 1353-1358.
149. Kleinschmidt S, Spergser J, Rosengarten R, Hewicker-Trautwein M (2013) Long-term survival of Mycoplasma bovis in necrotic lesions and in phagocytic cells as demonstrated by transmission and immunogold electron microscopy in lung tissue from experimentally infected calves. Vet Microbiol 162: 949-953.
150. van der Merwe J, Prysliak T, Perez-Casal J (2010) Invasion of bovine peripheral blood mononuclear cells and erythrocytes by Mycoplasma bovis. Infect Immun 78: 4570-4578.
151. Diaz-Ramos A, Roig-Borrellas A, Garcia-Melero A, Lopez-Alemany R (2012) alpha-Enolase, a multifunctional protein: its role on pathophysiological situations. J Biomed Biotechnol 2012: 156795.

152. Bergmann S, Rohde M, Chhatwal GS, Hammerschmidt S (2001) alpha-Enolase of Streptococcus pneumoniae is a plasmin(ogen)-binding protein displayed on the bacterial cell surface. Mol Microbiol 40: 1273-1287.
153. Chen H, Yu S, Shen X, Chen D, Qiu X, et al. (2011) The Mycoplasma gallisepticum alpha-enolase is cell surface-exposed and mediates adherence by binding to chicken plasminogen. Microb Pathog 51: 285-290.
154. Zhang Q, Young TF, Ross RF (1995) Identification and characterization of a Mycoplasma hyopneumoniae adhesin. Infect Immun 63: 1013-1019.
155. Jarocki VM, Santos J, Tacchi JL, Raymond BB, Deutscher AT, et al. (2015) MHJ_0461 is a multifunctional leucine aminopeptidase on the surface of Mycoplasma hyopneumoniae. Open Biol 5.
156. Minion FC, Lefkowitz EJ, Madsen ML, Cleary BJ, Swartzell SM, et al. (2004) The genome sequence of Mycoplasma hyopneumoniae strain 232, the agent of swine mycoplasmosis. J Bacteriol 186: 7123-7133.
157. Sanderson-Smith ML, Dowton M, Ranson M, Walker MJ (2007) The plasminogen-binding group A streptococcal M protein-related protein Prp binds plasminogen via arginine and histidine residues. J Bacteriol 189: 1435-1440.
158. Andrade-Gordon P, Strickland S (1989) Anticoagulant low molecular weight heparin does not enhance the activation of plasminogen by tissue plasminogen activator. J Bi ol Chem 264: 15177-15181.
159. Vinazzer H, Stemberger A, Haas S, Blumel G (1982) Influence of heparin; of different heparin fractions and of a low molecular weight heparin-like substance on the mechanism of fibrinolysis. Thromb Res 27: 341-352.
160. Liang JF, Li Y, Yang VC (2000) The potential mechanism for the effect of heparin on tissue plasminogen activator-mediated plasminogen activation. Thromb Res 97: 349-358.
161. Maglennon GA, Cook BS, Deeney AS, Bosse JT, Peters SE, et al. (2013) Transposon mutagenesis in Mycoplasma hyopneumoniae using a novel mariner-based system for generating random mutations. Vet Res 44: 124.
162. Bin L, Luping D, Bing S, Zhengyu Y, Maojun L, et al. (2014) Transcription analysis of the porcine alveolar macrophage response to Mycoplasma hyopneumoniae. PLoS One 9: e101968.
163. Burysek L, Syrovets T, Simmet T (2002) The serine protease plasmin triggers expression of MCP-1 and CD40 in human primary monocytes via activation of p38 MAPK and janus kinase (JAK)/STAT signaling pathways. J Biol Chem 277: 33509-33517.
164. Syrovets T, Tippler B, Rieks M, Simmet T (1997) Plasmin is a potent and specific chemoattractant for human peripheral monocytes acting via a cyclic guanosine monophosphate-dependent pathway. Blood 89: 4574-4583.
165. Li Q, Laumonnier Y, Syrovets T, Simmet T (2007) Plasmin triggers cytokine induction in human monocyte-derived macrophages. Arterioscler Thromb Vasc Biol 27: 1383-1389.
166. Syrovets T, Jendrach M, Rohwedder A, Schule A, Simmet T (2001) Plasmin-induced expression of cytokines and tissue factor in human monocytes involves AP-1 and IKKbeta-mediated NF-kappaB activation. Blood 97: 3941-3950.
167. Kassam G, Choi KS, Ghuman J, Kang HM, Fitzpatrick SL, et al. (1998) The role of annexin II tetramer in the activation of plasminogen. J Biol Chem 273: 4790-4799.
168. Kassam G, Le BH, Choi KS, Kang HM, Fitzpatrick SL, et al. (1998) The p11 subunit of the annexin II tetramer plays a key role in the stimulation of t-PA-dependent plasminogen activation. Biochemistry 37: 16958-16966.
169. Jericho KW (1986) Pathogenesis of mycoplasma pneumonia of swine. Can J Vet Res 50: 136-137.

170. Henderson B, Martin A (2011) Bacterial virulence in the moonlight: multitasking bacterial moonlighting proteins are virulence determinants in infectious disease. Infect Immun 79: 3476-3491.
171. Pancholi V, Chhatwal GS (2003) Housekeeping enzymes as virulence factors for pathogens. Int J Med Microbiol 293: 391-401.
172. Sanderson-Smith ML, De Oliveira DM, Ranson M, McArthur JD (2012) Bacterial plasminogen receptors: mediators of a multifaceted relationship. J Biomed Biotechnol 2012: 272148.
173. Candela M, Bergmann S, Vici M, Vitali B, Turroni S, et al. (2007) Binding of human plasminogen to Bifidobacterium. J Bacteriol 189: 5929-5936.
174. Candela M, Turroni S, Centanni M, Fiori J, Bergmann S, et al. (2011) Relevance of Bifidobacterium animalis subsp. lactis plasminogen binding activity in the human gastrointestinal microenvironment. Appl Environ Microbiol 77: 7072-7076.
175. Centanni M, Bergmann S, Turroni S, Hammerschmidt S, Chhatwal GS, et al. (2012) Tumor necrosis factor alpha modulates the dynamics of the plasminogen-mediated early interaction between Bifidobacterium animalis subsp. lactis and human enterocytes. Appl Environ Microbiol 78: 2465-2469.
176. Haesebrouck F, Pasmans F, Chiers K, Maes D, Ducatelle R, et al. (2004) Efficacy of vaccines against bacterial diseases in swine: what can we expect? Vet Microbiol 100: 255-268.
177. Maes D, Segales J, Meyns T, Sibila M, Pieters M, et al. (2008) Control of Mycoplasma hyopneumoniae infections in pigs. Vet Microbiol 126: 297-309.
178. Madsen ML, Nettleton D, Thacker EL, Edwards R, Minion FC (2006) Transcriptional profiling of Mycoplasma hyopneumoniae during heat shock using microarrays. Infect Immun 74: 160-166.
179. Thacker EL, Thacker BJ, Young TF, Halbur PG (2000) Effect of vaccination on the potentiation of porcine reproductive and respiratory syndrome virus (PRRSV)-induced pneumonia by Mycoplasma hyopneumoniae. Vaccine 18: 1244-1252.
180. Kobisch M, Blanchard B, Le Potier MF (1993) Mycoplasma hyopneumoniae infection in pigs: duration of the disease and resistance to reinfection. Vet Res 24: 67-77.
181. Friis NF (1975) Some recommendations concerning primary isolation of Mycoplasma suipneumoniae and Mycoplasma flocculare a survey. Nord Vet Med 27: 337-339.
182. Scarman AL, Chin JC, Eamens GJ, Delaney SF, Djordjevic SP (1997) Identification of novel species-specific antigens of Mycoplasma hyopneumoniae by preparative SDS-PAGE ELISA profiling. Microbiology 143 (Pt 2): 663-673.
183. Nunomura K, Nagano K, Itagaki C, Taoka M, Okamura N, et al. (2005) Cell surface labeling and mass spectrometry reveal diversity of cell surface markers and signaling molecules expressed in undifferentiated mouse embryonic stem cells. Mol Cell Proteomics 4: 1968-1976.
184. Szczepanek SM, Frasca S, Jr., Schumacher VL, Liao X, Padula M, et al. (2010) Identification of lipoprotein MslA as a neoteric virulence factor of Mycoplasma gallisepticum. Infect Immun 78: 3475-3483.
185. Kyhse-Andersen J (1984) Electroblotting of multiple gels: a simple apparatus without buffer tank for rapid transfer of proteins from polyacrylamide to nitrocellulose. J Biochem Biophys Methods 10: 203-209.
186. Chen B, Zhang A, Xu Z, Li R, Chen H, et al. (2011) Large-scale identification of bacteria-host crosstalk by affinity chromatography: capturing the interactions of Streptococcus suis proteins with host cells. J Proteome Res 10: 5163-5174.
187. Wilkins MR, Gasteiger E, Bairoch A, Sanchez JC, Williams KL, et al. (1999) Protein identification and analysis tools in the ExPASy server. Methods Mol Biol 112: 531-552.
188. Lupas A, Van Dyke M, Stock J (1991) Predicting coiled coils from protein sequences. Science 252: 1162-1164.

189. Obradovic Z, Peng K, Vucetic S, Radivojac P, Dunker AK (2005) Exploiting heterogeneous sequence properties improves prediction of protein disorder. Proteins 61 Suppl 7: 176-182.
190. Su HC, Hutchison CA, 3rd, Giddings MC (2007) Mapping phosphoproteins in Mycoplasma genitalium and Mycoplasma pneumoniae. BMC Microbiol 7: 63.
191. Wilton J, Jenkins C, Cordwell SJ, Falconer L, Minion CF, et al. (2009) Mhp493 (P216) is a proteolytically processed, cilium and heparin binding protein of *Mycoplasma hyopneumoniae* Molecular Microbiology 71: 17.
192. Righetti PG (2006) Real and imaginary artefacts in proteome analysis via two-dimensional maps. J Chromatogr B Analyt Technol Biomed Life Sci 841: 14-22.
193. Cardin AD, Weintraub HJ (1989) Molecular modeling of protein-glycosaminoglycan interactions. Arteriosclerosis 9: 21-32.
194. Horiuchi K (2013) A brief history of tumor necrosis factor alpha--converting enzyme: an overview of ectodomain shedding. Keio J Med 62: 29-36.
195. Arribas J, Massague J (1995) Transforming growth factor-alpha and beta-amyloid precursor protein share a secretory mechanism. J Cell Biol 128: 433-441.
196. Yamagishi S, Hampel F, Hata K, Del Toro D, Schwark M, et al. (2011) FLRT2 and FLRT3 act as repulsive guidance cues for Unc5-positive neurons. EMBO J 30: 2920-2933.
197. Sanderson-Smith M, Batzloff M, Sriprakash KS, Dowton M, Ranson M, et al. (2006) Divergence in the plasminogen-binding group a streptococcal M protein family: functional conservation of binding site and potential role for immune selection of variants. J Biol Chem 281: 3217-3226.
198. Stoeck A, Keller S, Riedle S, Sanderson MP, Runz S, et al. (2006) A role for exosomes in the constitutive and stimulus-induced ectodomain cleavage of L1 and CD44. Biochem J 393: 609-618.
199. Scott NE, Marzook NB, Deutscher A, Falconer L, Crossett B, et al. (2010) Mass spectrometric characterization of the Campylobacter jejuni adherence factor CadF reveals post-translational processing that removes immunogenicity while retaining fibronectin binding. Proteomics 10: 277-288.
200. Cole JN, Ramirez RD, Currie BJ, Cordwell SJ, Djordjevic SP, et al. (2005) Surface analyses and immune reactivities of major cell wall-associated proteins of group a streptococcus. Infect Immun 73: 3137-3146.
201. Baskerville A, Wright CL (1973) Ultrastructural changes in experimental enzootic pneumonia of pigs. Res Vet Sci 14: 155-160.
202. Blanchard B, Vena MM, Cavalier A, Le Lannic J, Gouranton J, et al. (1992) Electron microscopic observation of the respiratory tract of SPF piglets inoculated with Mycoplasma hyopneumoniae. Vet Microbiol 30: 329-341.
203. Villarreal I, Vranckx K, Calus D, Pasmans F, Haesebrouck F, et al. (2012) Effect of challenge of pigs previously immunised with inactivated vaccines containing homologous and heterologous Mycoplasma hyopneumoniae strains. BMC Vet Res 8: 2.
204. Wilton JL, Scarman AL, Walker MJ, Djordjevic SP (1998) Reiterated repeat region variability in the ciliary adhesin gene of Mycoplasma hyopneumoniae. Microbiology 144 (Pt 7): 1931-1943.
205. Hsu T, Artiushin S, Minion FC (1997) Cloning and functional analysis of the P97 swine cilium adhesin gene of Mycoplasma hyopneumoniae. J Bacteriol 179: 1317-1323.
206. Hsu T, Minion FC (1998) Identification of the cilium binding epitope of the Mycoplasma hyopneumoniae P97 adhesin. Infect Immun 66: 4762-4766.
207. Minion FC, Adams C, Hsu T (2000) R1 region of P97 mediates adherence of Mycoplasma hyopneumoniae to swine cilia. Infect Immun 68: 3056-3060.

208. Vasconcelos AT, Ferreira HB, Bizarro CV, Bonatto SL, Carvalho MO, et al. (2005) Swine and poultry pathogens: the complete genome sequences of two strains of Mycoplasma hyopneumoniae and a strain of Mycoplasma synoviae. J Bacteriol 187: 5568-5577.
209. Bereiter M, Young TF, Joo HS, Ross RF (1990) Evaluation of the ELISA and comparison to the complement fixation test and radial immunodiffusion enzyme assay for detection of antibodies against Mycoplasma hyopneumoniae in swine serum. Vet Microbiol 25: 177-192.
210. Andronicos NM, Ranson M, Bognacki J, Baker MS (1997) The human ENO1 gene product (recombinant human alpha-enolase) displays characteristics required for a plasminogen binding protein. Biochim Biophys Acta 1337: 27-39.
211. Strauss MP, Liew AT, Turnbull L, Whitchurch CB, Monahan LG, et al. (2012) 3D-SIM super resolution microscopy reveals a bead-like arrangement for FtsZ and the division machinery: implications for triggering cytokinesis. PLoS Biol 10: e1001389.
212. Peng K, Radivojac P, Vucetic S, Dunker AK, Obradovic Z (2006) Length-dependent prediction of protein intrinsic disorder. BMC Bioinformatics 7: 208.
213. Rost B, Sander C (1993) Prediction of protein secondary structure at better than 70% accuracy. J Mol Biol 232: 584-599.
214. Dosztanyi Z, Meszaros B, Simon I (2009) ANCHOR: web server for predicting protein binding regions in disordered proteins. Bioinformatics 25: 2745-2746.
215. Zielinski GC, Young T, Ross RF, Rosenbusch RF (1990) Adherence of Mycoplasma hyopneumoniae to cell monolayers. Am J Vet Res 51: 339-343.
216. Herard AL, Pierrot D, Hinnrasky J, Kaplan H, Sheppard D, et al. (1996) Fibronectin and its alpha 5 beta 1-integrin receptor are involved in the wound-repair process of airway epithelium. Am J Physiol 271: L726-733.
217. Herard AL, Zahm JM, Pierrot D, Hinnrasky J, Fuchey C, et al. (1996) Epithelial barrier integrity during in vitro wound repair of the airway epithelium. Am J Respir Cell Mol Biol 15: 624-632.
218. Moitinho-Silva L, Kondo MY, Oliveira LC, Okamoto DN, Paes JA, et al. (2013) Mycoplasma hyopneumoniae in vitro peptidase activities: identification and cleavage of kallikrein-kinin system-like substrates. Vet Microbiol 163: 264-273.
219. Liu W, Feng Z, Fang L, Zhou Z, Li Q, et al. (2011) Complete genome sequence of Mycoplasma hyopneumoniae strain 168. J Bacteriol 193: 1016-1017.
220. Chen AY, Fry SR, Forbes-Faulkner J, Daggard G, Mukkur TK (2006) Evaluation of the immunogenicity of the P97R1 adhesin of Mycoplasma hyopneumoniae as a mucosal vaccine in mice. J Med Microbiol 55: 923-929.
221. Dziewanowska K, Patti JM, Deobald CF, Bayles KW, Trumble WR, et al. (1999) Fibronectin binding protein and host cell tyrosine kinase are required for internalization of Staphylococcus aureus by epithelial cells. Infect Immun 67: 4673-4678.
222. Wachtfogel YT, Abrams W, Kucich U, Weinbaum G, Schapira M, et al. (1988) Fibronectin degradation products containing the cytoadhesive tetrapeptide stimulate human neutrophil degranulation. J Clin Invest 81: 1310-1316.
223. Quigley JP, Gold LI, Schwimmer R, Sullivan LM (1987) Limited cleavage of cellular fibronectin by plasminogen activator purified from transformed cells. Proc Natl Acad Sci U S A 84: 2776-2780.
224. De Petro G, Tavian D, Marchina E, Barlati S (2002) Induction of fibronectin mRNA by urokinase- and tissue-type plasminogen activator in human skin fibroblasts: differential role of u-PA and t-PA at the fibronectin protein level. Biol Chem 383: 177-187.
225. Otake S, Dee S, Corzo C, Oliveira S, Deen J (2010) Long-distance airborne transport of infectious PRRSV and Mycoplasma hyopneumoniae from a swine population infected with multiple viral variants. Vet Microbiol 145: 198-208.

226. Dee S, Otake S, Oliveira S, Deen J (2009) Evidence of long distance airborne transport of porcine reproductive and respiratory syndrome virus and Mycoplasma hyopneumoniae. Vet Res 40: 39.
227. Liu W, Fang L, Li M, Li S, Guo S, et al. (2012) Comparative genomics of Mycoplasma: analysis of conserved essential genes and diversity of the pan-genome. PLoS One 7: e35698.
228. Costerton JW (1999) Introduction to biofilm. Int J Antimicrob Agents 11: 217-221; discussion 237-219.
229. Wolcott RD, Rhoads DD (2008) A study of biofilm-based wound management in subjects with critical limb ischaemia. J Wound Care 17: 145-148, 150-142, 154-145.
230. Tajima M, Yagihashi T (1982) Interaction of Mycoplasma hyopneumoniae with the porcine respiratory epithelium as observed by electron microscopy. Infect Immun 37: 1162-1169.
231. Dudani AK, Ganz PR (1996) Endothelial cell surface actin serves as a binding site for plasminogen, tissue plasminogen activator and lipoprotein(a). Br J Haematol 95: 168-178.
232. Miles LA, Andronicos NM, Baik N, Parmer RJ (2006) Cell-surface actin binds plasminogen and modulates neurotransmitter release from catecholaminergic cells. J Neurosci 26: 13017-13024.
233. Moroianu J, Fett JW, Riordan JF, Vallee BL (1993) Actin is a surface component of calf pulmonary artery endothelial cells in culture. Proc Natl Acad Sci U S A 90: 3815-3819.
234. Owen MJ, Auger J, Barber BH, Edwards AJ, Walsh FS, et al. (1978) Actin may be present on the lymphocyte surface. Proc Natl Acad Sci U S A 75: 4484-4488.
235. Pardridge WM, Nowlin DM, Choi TB, Yang J, Calaycay J, et al. (1989) Brain capillary 46,000 dalton protein is cytoplasmic actin and is localized to endothelial plasma membrane. J Cereb Blood Flow Metab 9: 675-680.
236. Sanders SK, Craig SW (1983) A lymphocyte cell surface molecule that is antigenically related to actin. J Immunol 131: 370-377.
237. Maglennon GA, Cook BS, Matthews D, Deeney AS, Bosse JT, et al. (2013) Development of a self-replicating plasmid system for Mycoplasma hyopneumoniae. Vet Res 44: 63.
238. Schmidt JA, Browning GF, Markham PF (2004) Mycoplasma hyopneumoniae p65 surface lipoprotein is a lipolytic enzyme with a preference for shorter-chain fatty acids. J Bacteriol 186: 5790-5798.
239. Wise KS, Kim MF (1987) Identification of intrinsic and extrinsic membrane proteins bearing surface epitopes of Mycoplasma hyopneumoniae. Isr J Med Sci 23: 469-473.
240. Wise KS, Kim MF (1987) Major membrane surface proteins of Mycoplasma hyopneumoniae selectively modified by covalently bound lipid. J Bacteriol 169: 5546-5555.
241. Borucki MK, Peppin JD, White D, Loge F, Call DR (2003) Variation in biofilm formation among strains of Listeria monocytogenes. Appl Environ Microbiol 69: 7336-7342.
242. DeCaen PG, Delling M, Vien TN, Clapham DE (2013) Direct recording and molecular identification of the calcium channel of primary cilia. Nature 504: 315-318.
243. Whitchurch CB, Tolker-Nielsen T, Ragas PC, Mattick JS (2002) Extracellular DNA required for bacterial biofilm formation. Science 295: 1487.
244. Reolon LA, Martello CL, Schrank IS, Ferreira HB (2014) Survey of surface proteins from the pathogenic Mycoplasma hyopneumoniae strain 7448 using a biotin cell surface labeling approach. PLoS One 9: e112596.
245. Chen LB, Murray A, Segal RA, Bushnell A, Walsh ML (1978) Studies on intercellular LETS glycoprotein matrices. Cell 14: 377-391.
246. Jones PA, Scott-Burden T, Gevers W (1979) Glycoprotein, elastin, and collagen secretion by rat smooth muscle cells. Proc Natl Acad Sci U S A 76: 353-357.

247. Francis CL, Starnbach MN, Falkow S (1992) Morphological and cytoskeletal changes in epithelial cells occur immediately upon interaction with Salmonella typhimurium grown under low-oxygen conditions. Mol Microbiol 6: 3077-3087.
248. Kadurugamuwa JL, Rohde M, Wehland J, Timmis KN (1991) Intercellular spread of Shigella flexneri through a monolayer mediated by membranous protrusions and associated with reorganization of the cytoskeletal protein vinculin. Infect Immun 59: 3463-3471.
249. Pinto PM, Chemale G, de Castro LA, Costa AP, Kich JD, et al. (2007) Proteomic survey of the pathogenic Mycoplasma hyopneumoniae strain 7448 and identification of novel post-translationally modified and antigenic proteins. Vet Microbiol 121: 83-93.
250. Djordjevic SP, Cordwell SJ, Djordjevic MA, Wilton J, Minion FC (2004) Proteolytic processing of the Mycoplasma hyopneumoniae cilium adhesin. Infect Immun 72: 2791-2802.
251. Citti C, Rosengarten R (1997) Mycoplasma genetic variation and its implication for pathogenesis. Wien Klin Wochenschr 109: 562-568.
252. Daubenspeck JM, Bolland JR, Luo W, Simmons WL, Dybvig K (2009) Identification of exopolysaccharide-deficient mutants of Mycoplasma pulmonis. Mol Microbiol 72: 1235-1245.
253. Jordan DS, Daubenspeck JM, Dybvig K (2013) Rhamnose biosynthesis in mycoplasmas requires precursor glycans larger than monosaccharide. Mol Microbiol 89: 918-928.
254. Shaw BM, Daubenspeck JM, Simmons WL, Dybvig K (2013) EPS-I polysaccharide protects Mycoplasma pulmonis from phagocytosis. FEMS Microbiol Lett 338: 155-160.
255. Almeida RA, Rosenbusch RF (1991) Capsulelike surface material of Mycoplasma dispar induced by in vitro growth in culture with bovine cells is antigenically related to similar structures expressed in vivo. Infect Immun 59: 3119-3125.
256. Ajufo JC, Whithear KG (1978) Evidence for a ruthenium red-staining extracellular layer as the haemagglutinin of the WVU 1853 strain of Mycoplasma synoviae. Aust Vet J 54: 502-504.
257. Green F, 3rd, Hanson RP (1973) Ultrastructure and capsule of Mycoplasma meleagridis. J Bacteriol 116: 1011-1018.
258. Robertson J, Smook E (1976) Cytochemical evidence of extramembranous carbohydrates on Ureaplasma urealyticum (T-strain Mycoplasma). J Bacteriol 128: 658-660.
259. Wilson MH, Collier AM (1976) Ultrastructural study of Mycoplasma pneumoniae in organ culture. J Bacteriol 125: 332-339.
260. Vilain S, Pretorius JM, Theron J, Brozel VS (2009) DNA as an adhesin: Bacillus cereus requires extracellular DNA to form biofilms. Appl Environ Microbiol 75: 2861-2868.
261. Yang L, Barken KB, Skindersoe ME, Christensen AB, Givskov M, et al. (2007) Effects of iron on DNA release and biofilm development by Pseudomonas aeruginosa. Microbiology 153: 1318-1328.
262. Kainulainen V, Korhonen TK (2014) Dancing to another tune-adhesive moonlighting proteins in bacteria. Biology (Basel) 3: 178-204.
263. Balasubramanian S, Kannan TR, Hart PJ, Baseman JB (2009) Amino acid changes in elongation factor Tu of Mycoplasma pneumoniae and Mycoplasma genitalium influence fibronectin binding. Infect Immun 77: 3533-3541.
264. Zhou D, Mooseker MS, Galan JE (1999) An invasion-associated Salmonella protein modulates the actin-bundling activity of plastin. Proc Natl Acad Sci U S A 96: 10176-10181.
265. Zhou D, Mooseker MS, Galan JE (1999) Role of the S. typhimurium actin-binding protein SipA in bacterial internalization. Science 283: 2092-2095.
266. Foulston L, Elsholz AK, DeFrancesco AS, Losick R (2014) The extracellular matrix of Staphylococcus aureus biofilms comprises cytoplasmic proteins that associate with the cell surface in response to decreasing pH. MBio 5: e01667-01614.

267. Merlini L, Angelin A, Tiepolo T, Braghetta P, Sabatelli P, et al. (2008) Cyclosporin A corrects mitochondrial dysfunction and muscle apoptosis in patients with collagen VI myopathies. Proc Natl Acad Sci U S A 105: 5225-5229.
268. Mercer J, Greber UF (2013) Virus interactions with endocytic pathways in macrophages and dendritic cells. Trends Microbiol 21: 380-388.
269. Steinman RM, Swanson J (1995) The endocytic activity of dendritic cells. J Exp Med 182: 283-288.
270. Antonescu CN, Aguet F, Danuser G, Schmid SL (2011) Phosphatidylinositol-(4,5)-bisphosphate regulates clathrin-coated pit initiation, stabilization, and size. Mol Biol Cell 22: 2588-2600.
271. Almeida RA, Dunlap JR, Oliver SP (2010) Binding of Host Factors Influences Internalization and Intracellular Trafficking of Streptococcus uberis in Bovine Mammary Epithelial Cells. Vet Med Int 2010: 319192.
272. Almeida RA, Oliver SP (2006) Trafficking of Streptococcus uberis in bovine mammary epithelial cells. Microb Pathog 41: 80-89.
273. Rohde M, Muller E, Chhatwal GS, Talay SR (2003) Host cell caveolae act as an entry-port for group A streptococci. Cell Microbiol 5: 323-342.
274. Yavlovich A, Katzenell A, Tarshis M, Higazi AA, Rottem S (2004) Mycoplasma fermentans binds to and invades HeLa cells: involvement of plasminogen and urokinase. Infect Immun 72: 5004-5011.
275. Winner F, Rosengarten R, Citti C (2000) In vitro cell invasion of Mycoplasma gallisepticum. Infect Immun 68: 4238-4244.
276. Tully JG, Rose DL, Baseman JB, Dallo SF, Lazzell AL, et al. (1995) Mycoplasma pneumoniae and Mycoplasma genitalium mixture in synovial fluid isolate. J Clin Microbiol 33: 1851-1855.
277. Lo SC, Hayes MM, Kotani H, Pierce PF, Wear DJ, et al. (1993) Adhesion onto and invasion into mammalian cells by mycoplasma penetrans: a newly isolated mycoplasma from patients with AIDS. Mod Pathol 6: 276-280.
278. Taylor-Robinson D, Davies HA, Sarathchandra P, Furr PM (1991) Intracellular location of mycoplasmas in cultured cells demonstrated by immunocytochemistry and electron microscopy. Int J Exp Pathol 72: 705-714.
279. Raymond BB, Djordjevic S (2015) Exploitation of plasmin(ogen) by bacterial pathogens of veterinary significance. Vet Microbiol.
280. Spurr AR (1969) A low-viscosity epoxy resin embedding medium for electron microscopy. J Ultrastruct Res 26: 31-43.
281. Suzuki T, Yamazaki N, Sada Y, Oguni I, Moriyasu Y (2003) Tissue distribution and intracellular localization of catechins in tea leaves. Biosci Biotechnol Biochem 67: 2683-2686.
282. Shimono M, Hashimoto S, Abiko Y, Hamano H, Chen SH (1991) Vacuoles and vesicles in the rat junctional epithelium: a study with serial ultrathin sections. J Periodontal Res 26: 85-90.
283. Irigoyen LF, Van Alstine W, Turek J, Clark LK (1998) Ultrastructural observation of the airways of recovered and susceptible pigs after inoculation with *Mycoplasma hyopneumoniae*. PESQUISA VETERINARIA BRASILEIRA 18: 1-7.
284. Molinari G, Rohde M, Guzman CA, Chhatwal GS (2000) Two distinct pathways for the invasion of Streptococcus pyogenes in non-phagocytic cells. Cell Microbiol 2: 145-154.
285. Hanisch J, Ehinger J, Ladwein M, Rohde M, Derivery E, et al. (2010) Molecular dissection of Salmonella-induced membrane ruffling versus invasion. Cell Microbiol 12: 84-98.
286. Hardt WD, Chen LM, Schuebel KE, Bustelo XR, Galan JE (1998) S. typhimurium encodes an activator of Rho GTPases that induces membrane ruffling and nuclear responses in host cells. Cell 93: 815-826.

287. Eucker TP, Konkel ME (2012) The cooperative action of bacterial fibronectin-binding proteins and secreted proteins promote maximal Campylobacter jejuni invasion of host cells by stimulating membrane ruffling. Cell Microbiol 14: 226-238.